Redundant Unilaterally Actuated Kinematic Chains: Modeling and Analysis

UNIVERSITÀ DEGLI STUDI DI GENOVA

Vishal RAMADOSS

Department of Mechanical Engineering

University of Genoa, Italy

This dissertation is submitted for the degree of

Doctor of Philosophy

December 21, 2019

Acknowledgements

Firstly, I would like to thank Prof. Dimiter Zlatanov for being my thesis supervisor, always providing continuous support for the research work. His insights and advice have significantly improved my technical writing skills and developed my overall critical thinking process.

I would like to acknowledge Prof. Matteo Zoppi and Prof. Rezia Molfino for giving me the opportunity to participate in different activities related to my research. I am particularly grateful to Prof. Darwin Lau from Chinese University of Hong Kong, who provided me the technical guidance to carry forward my research.

I would like to express my gratitude to my fellow laboratory mates Lugo, Sadiq, Cuong, Ahmad and Giorgio for their friendship and support during my stay. In particular, my sincere thanks to Keerthi and Michal for the technical support. I would like to thank my family for being supportive all these years. I am grateful for the sacrifices they have made to provide me with opportunities.

I appreciate the support, the space and funding of the PMAR Robotics Group, Department of Mechanical Engineering from the University of Genoa.

Abstract

Unilaterally Actuated Robots (UAR)s are a class of robots defined by an actuation that is constrained to a single sign. Cable robots, grasping, fixturing and tensegrity systems are certain applications of UARs. In recent years, there has been increasing interest in robotic and other mechanical systems actuated or constrained by cables. In such systems, an individual constraint is applied to a body of the mechanism in the form of a pure force which can change its magnitude but cannot reverse its direction. This uni-directional actuation complicates the design of cable-driven robots and can result in limited performance.

Cable Driven Parallel Robot (CDPR)s are a class of parallel mechanisms where the actuating legs are replaced by cables. CDPRs benefit from higher payload to weight ratio and increased rigidity. There is growing interest in the cable actuation of multibody systems. There are potential applications for such mechanisms where low moving inertia is required. Cable Driven Serial Kinematic Chain (CDSKC) are mechanisms where the rigid links form a serial kinematic chain and the cables are arranged in parallel configuration. CDSKC benefits from the dexterity of the serial mechanisms and the actuation advantages of cable-driven manipulators.

Firstly, the kinematic modeling of CDSKC is presented, with focus on different types of cable routings. A geometric approach based on convex cones is utilized to develop novel cable actuation schemes. The cable routing scheme and architecture has a significant effect on the performance of the robot resulting in limited workspace and high cable forces required to perform a desired task. A novel cable routing scheme is proposed to reduce the number of actuating cables. The internal routing scheme is where, in addition to being externally routed, the cable can be re-routed internally within the link. This type of routing can be considered as the most generalized form of the multi-segment pass-through routing scheme where a cable segment can be attached within the same link. Secondly, the analysis for CDSKCs require extensions from single link CDPRs to consider different routings. The

conditions to satisfy wrench-closure and the workspace analysis of different multi link unilateral manipulators are investigated. Due to redundant and constrained actuation it is possible for a motion to be either infeasible or the desired motion can be produced by infinite number of different actuation profiles. The motion generation of the CDSKCs with minimal number of actuating cables is studied. The static stiffness evaluation of CDSKCs with different routing topologies and isotropic stiffness conditions were investigated. The dexterity and wrench based metrics were evaluated throughout the mechanism's workspace.

Through this thesis, the fundamental tools required in studying cable driven serial kinematic chains have been presented. The results of this work highlight the potential of using CDSKCs in bio-inspired systems and tensegrity robots.

Contents

List of Figures

List of Tables

List of Abbreviations

CDLE Cable driven lower limb exoskeleton. 14

CDPR Cable Driven Parallel Robot. ii, 3, 5, 6, 10–13, 16, 32–35, 37, 40, 41, 43, 83, 92, 95

CDSKC Cable Driven Serial Kinematic Chain. ii, iii, 2, 4, 6, 7, 9, 12, 13, 34, 43, 84, 92

DOF Degree Of Freedom. 3, 11, 12, 43, 84, 108

EOM Equations of Motion. 42

ID Inverse dynamics. 42

IK Inverse kinematics. 40

MCDPR Mobile cable driven parallel robot. 13

RCDPR Reconfigurable cable driven parallel robot. 13

TF Tension factor. 35, 42

UAR Unilaterally Actuated Robots. ii, 13, 36, 37

UD Unilateral dexterity. 36, 37

UF Unilateral maximum force amplification. 37

UMQI Unilateral Manipulability Quality Indices. 37

WCC Wrench closure condition. 34–36

WCW Wrench Closure Workspace. 34, 35, 85, 95, 97, 151

WFW Wrench Feasible Workspace. 34, 92

Chapter 1

Introduction

1.1 Motivation

In recent years, a class of robotic systems that has been a topic of interest is cable-driven robots [1, 5, 6]. Cable-driven robots are often considered an attractive solution for a range of applications such as building construction [5, 7], assistive exoskeletons [8], aircraft testing, haptic and rehabilitation devices [9], motion simulators and bio-inspired mechanisms [8, 10]. The important feature of a cable-driven system is that cables can only provide unilateral actuation. Cable-driven parallel mechanisms (CDPMs) are a class of parallel mechanisms [11] where the actuating legs are replaced by cables. CDPMs benefit from higher payload to weight ratio and increased rigidity. There is growing interest in the cable actuation of multibody systems. Cable-driven serial kinematic chain (CDSKC) are mechanisms where the rigid links form a serial kinematic chain and the cables are arranged in parallel configuration. CDSKC benefits from the dexterity of the serial mechanisms and the actuation advantages of cable-driven manipulators. There is often a need to control a rigid kinematic chain such as a prosthetic limb in the field of rehabilitation robotics [12]. The two primary approaches towards rehabilitation are end-point devices and exoskeletons. Some of them include CAREX [8], STRINGMAN [9] and CDWRR [13]. Wearable exoskeletons are targeted directly at each human joint although have a greater mechanical complexity.

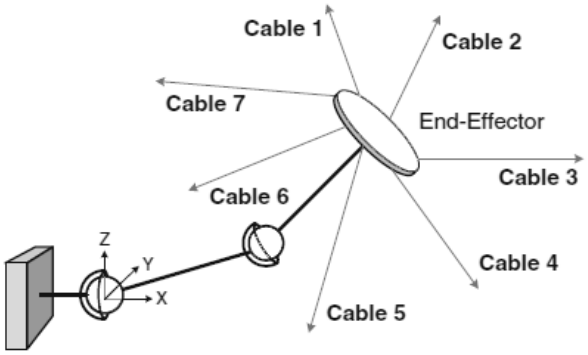

Figure 1.1: End-effector with actuated cables [1]

The cable driven system eliminates the need of rigid linkages and joints making the system lightweight. They also reduce the external constraints on the user as cables are flexible. As cable actuators [10] provide only unilateral constraints, it is required that to control a n-dof system at least $n+1$ cables are necessary [14, 15]. A revolute joint can be fixed using two unilateral constraint forces that are not reciprocal to the hinge rotation. Similarly, it is possible to find four independent unilateral forces that will fix a ball joint and transmit a force through its center. It can be useful to know the geometrical properties of the convex cones and conic spans of wrenches [4]. The cable-driven manipulators are being developed to assist individuals and others who need assistance in performing mundane tasks.

The CDSKC comprises of serially articulated rigid links and preserves the advantages associated with cable driven parallel mechanisms. The proposed design, as shown in Fig. 1.2 differs from many existing mechanisms with a single end-effector platform. This design allows arbitrary cable routing through serial links which is similar to the unilaterally actuated muscles in the human arm. Fig. 1.1 shows the multilink serial chain actuated at the end-effector with cables. This multi-link structure in Fig. 1.2 with multiple routing poses a great challenge in kinematic modeling and the definition of Jacobian matrix compared to single link mechanisms.

In such systems, forces acting on each rigid body of the mechanism are constrained to be unidirectional. Similar situations occur in grasping and problems of fixturing. Consequently, the total wrench applied to each body must stay within

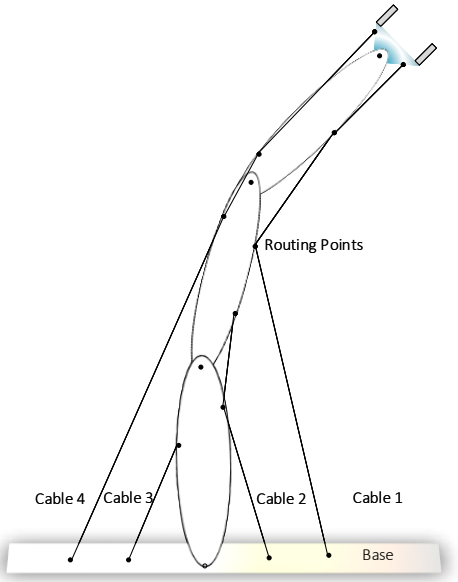

Figure 1.2: Base with fully routed actuated cables

a convex cone of pure-forces [4]. Due to the unilateral driving property of the cables, maintaining positive cable tension is essential in controlling the moving platform. As a result, the number of actuators must be more than the number of degrees of freedom (DOF) of the moving platform to obtain force-closure [16]. Force closure refers to the ability for a CDPR to produce arbitrary wrenches in all Degree Of Freedom (DOF)s. There has been numerous efforts in force-closure analysis of cable-driven platforms [1] and more recently of cable-driven multibody systems with open and closed structures [14, 17, 18]. The ability of a system to maintain the equilibrium with a set of positive cable tension (force-closure) is a vital tool in workspace analysis and minimization of actuators. For cable driven serial kinematic chain, one of the key design element is the cable routing, which defines the structure matrix, of the multi-link unilateral manipulator(MULM). This structure matrix defines the torque and force produced by the serial chain based on the cable tensions. The number of cables used in the design is crucial to the design of the structure matrix, and using minimal number of cables has the advantage of reducing the number of cables and actuators thereby reducing

the weight, size and complexity of the serial chain. The problem of isotropic force transmission characteristics based on structure matrix has been studied. The distribution of maximal tensions across cables is an important factor and is known to have a significant effect on force-production capabilities. By using cable routing between links, re-routing and cable bundles, it is possible to actuate any serial kinematic chain. It has to be ensured that all cables remain in tension for a functional cable-driven system. To the best of the author's knowledge, limited studies address the modeling and design problems of minimally routed CDSKCs, especially, when the redundancy and routing optimization problems are introduced, the kinematics and dynamics modeling becomes more challenging.

This thesis will introduce contributions which solve the aforementioned problems for CDSKCs with multiple links in order to increase their dexterity and actuation advantages. To develop and implement these contributions, this thesis focuses on CDSKCs, including modeling, analysis, and performance evaluation.

1.2 Research Background

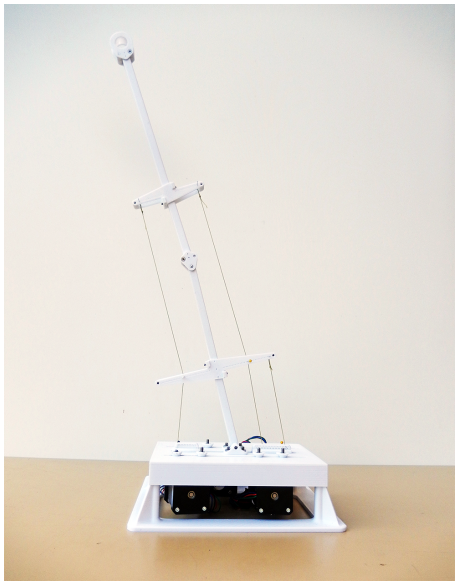

Figure 1.3: Unilaterally actuated two link robot with 3 externally routed cables

Most robotic manipulators have been designed to possess anthropomorphic

structures, such as the human arm, structured and articulated. The role of the articulated mechanical structure is to place the end-effector at a given location (position and orientation) with a desired velocity and acceleration. The mechanical structure is composed of a kinematic chain of articulated rigid links. One end of the chain is fixed and is called the base. The end-effector is fixed to the free extremity of the chain. This chain may be serial (simple open chain), tree structured or closed. The last two structures are termed complex chains since they contain at least one link with more than two joints. The advantages of serial chain include high dexterity, compactness and large achievable workspace compared to their size. They are capable of manipulating relatively low effective load. Each link carries the weight of the links and actuators of its child links. Due to the serial arrangement, each link is prone to significant bending moment and hence decreases in stiffness as the link is further from the base. Compared with serial chains, closed kinematic chains distribute the load over multiple links. The overall stiffness is increased as the actuated links support the end-effector in a parallel topology. The payload to wright ratio is higher. The positional accuracy of the end-effector is generally higher as the errors in the links of manipulators do not accumulate and amplify. Owing to their importance in practical applications and the complexity of conceptual problems, parallel manipulators have been extensively studied over the last decades.

A new class of parallel robots have appeared in recent years, replacing the rigid connections with wires. This class of manipulators has been commonly referred to as cable-driven parallel manipulators (CDPMs), cable-driven parallel robots (CDPRs), or simply cable / wire robots. The legs of conventional rigid link parallel manipulators can provide both tension and compression forces. In CDPRs, the cable actuators only provide positive tension force constraint to the end-effector. Due to the unilateral force constraint, CDPRs require actuation redundancy to produce motion in all degrees of freedom. The analysis of such manipulators becomes challenging due to the positive force constraint and redundancy in actuation. Secondly, the type of cables used influences the modeling of manipulator dynamics. The bone and muscle-tendon networks of biomechanical systems have structural similarities with rigid links and cables of CDPRs.

Most of the robots that have been studied are single link CDPRs, where a

single body is actuated by cables driven from the base. Another class of cable actuated manipulators is cable driven multibody mechanisms or (CDSKCs). This is a general form of capstan mechanisms where cables are routed through capstan pulleys and drive the mechanism. The rigid bodies are actuated by cables in parallel and the cables are arbitrarily routed through one or more links in CDSKCs. The advantage of such manipulators include the compactness of serial chains, the actuation and reconfigurability of cable driven manipulators. CDSKCs are more anthropomorphic in nature, where the rigid bodies and cables are structurally analogous to bones and muscles, respectively. An unilaterally actuated two link robot driven by 3 cables is shown in Fig. 1.3.

In summary, the study of CDSKCs is necessary as there are new challenges in modeling, routing schemes and analysis compared to the single link CDPRs. CDSKCs can be applied in bio inspired mechanisms and in the analysis of biomechanical systems, such as the human limb, human arm exoskeletons and neck.

1.3 Objectives

The primary objective of this thesis is to develop analytical models for cable driven serial kinematic chains with arbitrary routing topologies and thereby perform analysis on CDSKC model for applications in bio-engineered and tensegrity systems. The following research questions are considered in this thesis to accomplish the primary research motive:

1. How can CDSKCs be modelled for different combinations in cable routing?.
2. How can the analysis of single link cable-driven manipulators be extended to multi link unilateral manipulators?
3. How to immobilize(and therefore actuate) any n-dof serial chain with n+1 cables?
4. What are the effects of cable routing and number of cables on workspace, tension and stiffness?

5. How can analysis methods developed for CDSKC systems be applied to bioengineered/ tensegrity systems?

1.4 Thesis contributions

In this thesis, the study on modeling and analysis of redundant unilaterally actuated kinematic chains is presented. In particular, modeling of cable driven serial kinematic chains with different routing topologies are investigated. In studying the proposed objectives, this thesis makes the following major contributions:

1. A systematic and analytical approach for modeling and force-closure analysis of CDSKCs is proposed.

2. A recursive procedure of constructing conic frames that finds the axes and directions of n+1 cables which will immobilize an otherwise unactuated n-dof serial chain.

3. A fully routed actuation scheme is proposed by investigating arbitrary cable routing schemes and minimal cable requirement for general case to achieve force-closure is presented.

4. The kinematic and workspace analysis for CDSKCs is extended to bio-inspired systems by allowing arbitrary cable routing.

The contributions of the thesis can be applied in the study of CDSKCs in the fields of robotics, biomechanics, tensegrity systems and soft robotics. In the field of robotics, the analytical formulation of different CDSKC architectures would allow this class of systems to be studied in systematic manner. The workspace analysis of CDSKCs (which can be regarded as anthropomorphic in nature) can be applied to study the musculoskeletal systems. These computational tools are particularly beneficial in applications such as rehabilitation robotics and human-inspired subsystems (the head, spine, neck, legs and arm). In summary, this thesis contributes to the fundamental knowledge of cable-driven manipulators with motivation and application in both robotics and bio-tensegrity systems.

1.5 Structure of the Thesis

The thesis contains 7 chapters organized into 2 parts to present the contributions towards the five identified research objectives. It is worth to note that each chapter contains relevant content that has been already accepted for publications and oral presentations in international events. This thesis is organized as follows.

Chapter 2: This chapter details the state-of-the art works that are relevant to the contributions of this thesis.

Chapter 3: This section presents the modeling of single body cable driven robots. It presents the methodology to evaluate the cable robot performance with a workspace analysis procedure and a cable tension analysis approach combined together to assess the performance of cable robot architecture. It discusses the modeling of CDPR, one joint kinematic chain and spherical chain driven by $n+1$ cables. The presented examples motivate the need for extending the concepts for CDSKCs.

Chapter 4: This chapter introduces convex cone theory and recursive algorithm based on convex cones to actuate a serial chain subject to unilateral constraint forces. The procedure to construct conic frames for different CDSKCs is illustrated with examples. The kinematics and tensionablity conditions for different cable driven serial kinematic chains are presented.

Chapter 5: This chapter introduces novel cable routing topologies and investigates the kinematic models of two link multi link unilateral manipulators. The workspace, motion generation capablities and stiffness characteristics of two link cable/ tendon driven serial kinematic chains are presented. A methodology for reducing actuator requirements in multi link planar and spatial unilaterally actuated robots through optimized cable routing is presented. This chapter demonstrates how highly coupled fully routed crossing cable configurations can reduce number of actuators and actuator torque requirements in serial kinematic chains while maintaining force closure and workspace reachability.

Chapter 6: An introduction for applications related to minimal fully routed and bundled actuation in bioinspired mechanisms. Simulations of stacked unilateral manipulator for designing large moving range shoulder mechanism are performed.

Chapter 7: Finally, this section summarizes the results observed during the development of this project. The description of the ongoing work is given with a possible future research direction.

Appendix A: This is a short chapter providing the analytical expressions used for workspace evaluation of different CDSKCs.

Appendix B: This annex provides the description of the components used in the prototype and mechanism.

Appendix C: Publications related to this thesis are briefly reported.

Chapter 2

State of the art and theoretical background

2.1 Overview of Cable-Driven Robots

A cable-driven robot [19] is actuated by adjusting cable lengths and tensions instead of rotary motors or linear actuators attached to the rigid bodies of the system. Such robots are generally categorized as parallel or serial robots. The cable actuators are only able to provide unilateral positive force constraint to the end-effector. Due to the unique unilateral driving property cables can carry payloads only when in tension. This dissertation would lay out basic tools for systematic modeling and analysis of such multi link unilateral manipulators, including kinematic analysis, workspace-related analysis, design optimization and stiffness modeling.

2.1.1 Parallel Robots

Much of the research has focused on (CDPRs) [5, 20–24] which have multiple cables connected to a single platform as shown in Fig. 2.1. The design of CDPR is not compact as the stationary frame must fully cover the desired workspace of the manipulator. The parallel configuration allows to effectively distribute the load over multiple links forming closed kinematic chains. Considerable amount of research into CDPR has resulted in these robots being well utilized in a variety

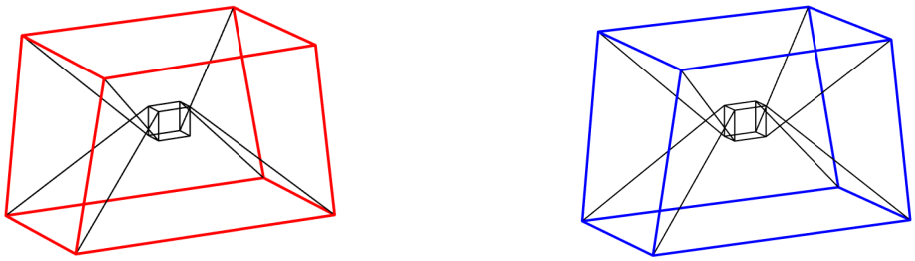

(a) CDPR with n+1 cable configuration **(b)** CDPR with n+2 cable configuration

Figure 2.1: 6-DOF Spatial CDPR

of applications, ranging from logistics [25] and cargo handling, construction [7], painting tasks [26], aircraft maintenance [5] to aerial camera technology [22] in stadiums. CDPR is mainly composed of winches, cables, pulleys, platform where the cables and tool is anchored, controller and drives. The pulleys permit the cable to be routed from the winch to the desired output point. They can be directly mounted on the building or on a dedicated frame. The cable lengths are controlled in order to provide the desired motion of the platform in the Cartesian space. The exact cable routing, sagging and elongation for a better positioning accuracy needs to be modeled and implemented on the controller. The management of actuation redundancy and integration of robot's dynamics is taken care by the controller. The light weight of the cables, the compact size while enabling a large working space and the reconfigurabilitiy of the system performing different tasks are the benefits in using the cable legs instead of rigid ones. Higuchi and Ming [16] proposed the concept of 3 DOF planar and spatial manipulator wire crane for use in building construction. The NIST RoboCrane [5] allows manipulation of both translational and rotational motions of the crane.

The number of cables that actuate the system is used in classifying CDPRs. Due to the unilateral force constraint, an n DoF CDPR requires minimum of $n+1$ number of cables to produce force closure in all DOFs. A n DOF CDPR with m actuating cables is incompletely restrained when $m < n+1$, completely restrained

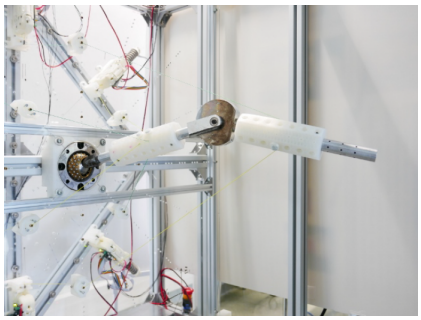

(a) Two link Bio Muscular Arm [27]

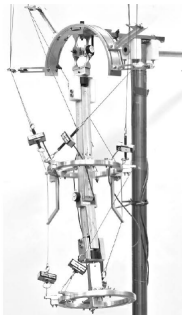

(b) CAREX [8] mounted on an anthropomorphic arm

Figure 2.2: Cable Driven Multibody Chain

for $m = n + 1$ and redundantly restrained if $m > n + 1$ [16]. For example, the manipulators shown in Fig. 2.1(a-b) is actuated by 7 and 8 cables respectively, and hence regarded as a 6 DOF redundantly restrained spatial CDPR. The theoretical problems related to various aspects of CDPRs have been well studied. The existing theoretical contributions will be utilized and extended for modeling and analysis of CDSKCs.

2.1.2 Serial Robots

Cable-driven serial kinematic chains [14, 17, 23] use cables to actuate a series of connected rigid bodies as shown in Fig. 2.2. The use of cables allows the motors and gearboxes to be moved from the dynamic parts to the base frame of the robot, resulting in a decrease in the mass and inertia of the moving components. This change results in a more flexible robot that can accelerate more quickly and allow the robot to be designed with smaller, less expensive motors and fewer materials due to decreased loads. An important are of application is rehabilitation robotics, where there is often a need to control a rigid-body kinematic chain [15] such as an exoskeletal system or prosthetic limb. The legged locomotion of agile mobile robots utilized CDSKCs by actuating the leg remotely using cables. Cable-driven exoskeletons can be designed to use the existing upper/lower limb of human as the main structure and provide actuation to the biological limbs using cables. This allows to avoid the joint alignment issues and customized device setup in contrast to the conventional bulky exoskeletons. The uni-directional nature of cable

actuation results in redundancy of actuation and limits the operational workspace. Also, the geometric relationship between the cable routing and mounting points on the frame and robot rigid bodies, influences the wrenches on the robot. Cable-cable interference and collisions can limit the range of motion of the device. The performance of the CDSKC depends on the particular arrangement of cables and optimal cable routing [28] choice. The generalized model of multi link cable driven serial manipulators is investigated using cable routing matrix in [6,18,27,29]. The primary challenge in modeling such UARs is the complexity involved in the cable routing. Cable routing [30–37] refers to the path in which a cable is connected to the links of the manipulator. *Arbitrary cable routing* refers to the complete set of possible cable routings. Depending on the particular routing arrangement, the performance of the robot varies. Therefore, it is important to identify the set of customizable design parameters that encapsulates the cable routing for the robot along with possible configuration values for each parameter.

2.1.3 Hybrid Robots

Hybrid cable driven robot(HCDR) is a hybrid structure of CDPR(s) and serial robot(s). Gouttefarde developed CoGiRo CDPR with onboard Yasakawa-Motoman SIA20 robot arm for painting and metal cutting operations. This is shown in Fig. 2.3(a). CUHK C3 Robotics Laboratory introduced SpiderArm robot, a CDPR with the onboard UR3 robot arm as shown in Fig. 2.3(b). The literature shows existing research to utilize the CDPR platform and mainly control the robot while treating the serial arm as a manipulation tool rather than a whole system. The development of kinematic and dynamic models, stiffness optimization for HCDRs was studied in [38].

A major disadvantage in CDPR is having a fixed cable configuration and the potential collisions between cables and the environment thereby reducing the workspace significantly. Cable robots that allow change in their configuration/ geometric structure is known as reconfigurable CDPR [41](RCDPR). Works on Mobile CDPRs(MCDPRs) [2] led to autonomous reconfigurability of Reconfigurable cable driven parallel robot (RCDPR)s. The targeted application for such Mobile cable driven parallel robot (MCDPR) is logistics and it was built in the

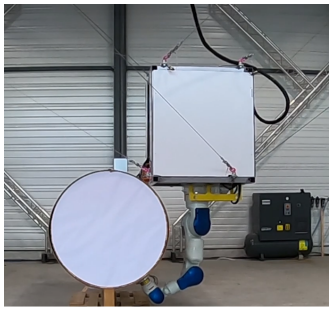

(a) CoGiRo CSPR with the onboard Yaskawa-Motoman SIA20 robot arm [39]

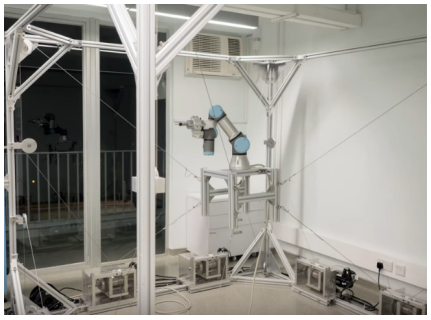

(b) SpiderArm robot [40]

Figure 2.3: Some existing HCDRs

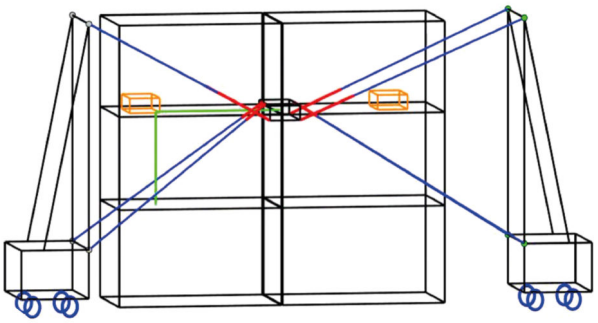

Figure 2.4: Colloborative and mobile CDPR [2]

context of FASTKIT project as shown in Fig. 2.4.

2.1.4 Bioinspired Robots

Robotic systems are being used for gait rehabilitation and the efficacy of a rehabilitation paradigm depends on the human robot interaction. A cable driven lower limb exoskeleton (CDLE) use actuated cables to apply external joint torques on human leg. Due to the actuation redundancy there are multiple ways to exert a particular force which makes control of these systems difficult. In order to ensure positive tension in each cable, numerical optimization problems are constructed. Workspace and stiffness analysis of such Cable driven lower limb exoskeleton (CDLE) are studied in [42–45]. The stiffness modulation in an elastic articulated-cable leg-orthosis emulator for gait training is investigated in [46]. Human lower

extremity comprises of pelvis, thigh, shank and foot segments which are connected by hip, knee and ankle joints. These segments are comprised of muscles and bones. The signals from central nervous system lets the muscles contract and try to pull the bone to which they are connected and result in limb movement. Muscles have unilateral force property and are modeled as cables. The cable in a cable-driven system acts as an ideal force generator such that positive tension values that are independent of manipulator poses and are in a given range are generated. However, muscle force in a musculoskeletal system depends on the muscle length and the contraction velocity. Hill-type muscle model [47] is used to model the state-dependency of muscle as an actuator. The muscle comprises of two elements, an active element capable of generating force and a passive element that always produces force, depend on state parameters like muscle activation level, muscle instantaneous length, muscle contraction velocity and optimum muscle fiber length and maximum isometric muscle force. The lower limb musculoskeletal system as a cable-driven serial chain system from OpenSim [48, 49] software is shown in Fig. 2.5(a). Fig. 2.5(b) shows the OpenSim shoulder model [51] which

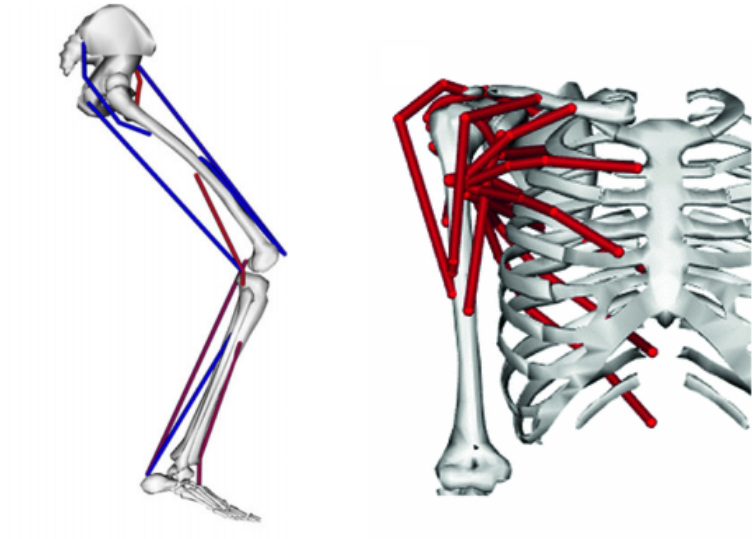

(a) Open Sim model of human leg [50]

(b) Open Sim model of human shoulder [51]

Figure 2.5: Musculoskeletal model of human lower limb and upper arm

is comprised of three major bones: the clavicle, the scapula and the humerus

bones and one major joint: the glenohumeral joint. The humerus bone can be regarded as the end-effector of the system and is connected to base through the glenohumeral joint. The musculoskeletal static workspace for human shoulder was studied in [52]. The musculoskeletal static workspace was formulated by extending from conventional CDPR static workspace analysis and incorporating state dependent force generators as the cables within the system. The ability to computationally study musculoskeletal systems as CDPRs is beneficial for a wide range of biomechanics and rehabilitation applications.

2.1.5 Tensegrity Robots

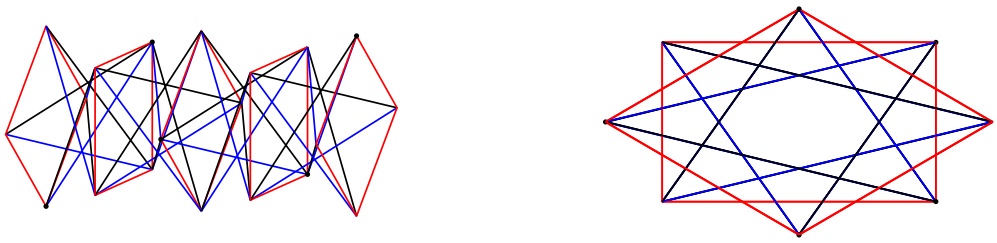

(a) Cylindrical Tensegrity **(b)** Top view

Figure 2.6: Stacked Cylindrical Tensegrity Mechanism

Tensegrity systems [53–57] have the unique ability to be flexible in all DoFs, lightweight and independent of heavy hardware setups. Ideal tensegrity structures consist of rigid compressive elements (rods) held together in tension network (cables) such that no two rigid bodies touch each other. A stacked cylindrical tensegrity mechanism is shown in Fig. 2.6. Without rigid contact, ideal systems have no flexture and thus compressive elements can be thinner. The structures passively distribute forces through the tension network, contrary to concentrating moment arms at mechanical joints. Robot designs [58–60] using tensegrity structures are a relatively new concept. The word tensegrity [57] was introduced by Fuller to describe assemblies of axially loaded members with tensile or compressive forces. In comparison to CDPR, tensegrity robots avoid the need to encompass their moving platform with cables in order to achieve wrench-closure without

Figure 2.7: DuCTT Tensegrity Robot [3]

relying on gravitational forces. Snelson's X-shaped [61] tensegrity system has inspired many planar and spatial tensegrity robots. The computation of workspace for tensegrity robots are investigated in [62–66]. It is interesting to note that the tensegrity structure exists in musculoskeletal system of most vertebrates [55,67–69]. The structural elements (bones) are compressed, supported by tendons and actuated by muscles. Using compression elements suspended in a network of tension elements creates an inherently flexible structure, which most conventional robots lack. Bio-inspired tensegrity manipulators [70–73] could potentially be significantly more dexterous than a conventional rigid manipulator and carry more load than an entirely soft robot. The interlocked tetrahedron tensegrity structure [71] is inspired by a biotensegrity model of a vertebrate spinal column and also has a striking resemblance to that of a human shoulder. A lightweight compliant robot capable of exploring duct systems DuCTT [3, 74] utilized such biotensegrity [73] models, is shown in Fig. 2.7.

2.2 Fundamental concepts and definitions

2.2.1 Wrenches, Twists and Screws

Definition 1. A *vector space* (or *linear space*) consists of a set V over the field* $\mathbb{R}$ and two operations

1. An operation called *vector addition* takes two vectors $v, w \in V$, and produces a third vector, $v + w \in V$
2. An operation called *scalar multiplication* that takes a scalar $c \in \mathbb{R}$ and a vector $v \in V$, and produces a new vector, written $cv \in V$.

which satisfy certain axioms such as associativity of vector addition, existence of zero vector, existence of negatives, associativity of multiplication, distributivity and unitarity. A vector space must be closed under vector addition [75].
The system of forces are external action on a system of particles B: $\{\vec{f}_P \mid P \in B\}$. The system of forces at O acting on a rigid body is mathematically denoted as Φ_O=$\{\varphi_O, \mu_O\}$, where φ_O is the force through O with intensity and direction $\vec{f}$ and μ_O is the couple with moment $\vec{m}_O$ applied in parallel to the body described by $(\vec{f}, \vec{m}_O)$ at O. All external actions on rigid body are of this type. Analogous to the system of forces, the instantaneous motion of a particle system B is $\{\vec{v}_P \mid P \in B\}$. The instantaneous motion at O is mathematically denoted as $\Upsilon_O = \{\varrho_O, \tau_O\}$, where ϱ_O is the instantaneous rotation through O with amplitude and direction $\vec{\omega}$ and the instantaneous translation τ_O is with velocity $\vec{v}_O$ applied in series to the body described by $(\vec{\omega}, \vec{v}_O)$ at O. All instantaneous motions are of this type.

A **wrench** is a system of forces [75] (reduced at a point) with equivalent systems identified. For a given origin, O, it is given by a pair of vectors: ζ=$(\vec{f}, \vec{m}_O)$, the resultant force and moment at O. A wrench is an entity invariant of frame choice. The equivalence class, ζ= $[\Phi]$ is called a wrench.
A **twist** is an instantaneous motion (reduced at a point) with equivalent motions identified. For a given origin, O, it is given by a pair of vectors: ξ =$(\vec{\omega}, \vec{v}_O)$, the

*A field is a set $\mathbb{F}$ of numbers with the property that if $a, b \in \mathbb{F}$, then $a + b, a - b, ab$ and a/b are also in $\mathbb{F}$ (assuming, of course, that $b \neq 0$ in the expression a/b). The more accurate definition of field uses the concept of a *commutative ring* instead of a number.

body angular velocity and the velocity of the point coinciding with O. A twist is an entity invariant of frame choice. The equivalence class, $\xi = [\Upsilon]$, is called a twist [75].

Property 2. Wrenches form a vector space [75], $se(3)^*$ and twists form a vector space, $se(3)$. It can be inferred from the above property that the vector addition and scalar multiplication is applicable for wrenches and twists.

Definition 3. *A line l with a pitch h is a geometric element called a* ***screw****.* [75] A screw (geometric) is not a vector. The screws form the projective space underlying the space of twists and wrenches. The screw of a couple or translation has no axis, only a direction, which is called as infinite pitch screw with $h = \infty$.

Definition 4. *The span of $\boldsymbol{v}_1, \ldots, \boldsymbol{v}_n \in V$ is the set of their linear combinations: Span($\boldsymbol{v}_1, \ldots, \boldsymbol{v}_n$)=$\{\lambda_1 \boldsymbol{v}_1 + \cdots + \lambda_n \boldsymbol{v}_n \mid \lambda_1 \in \mathbb{R}\}$.*

Utilizing concepts of screw theory [76] and linear algebra gives useful interpretations. For example, all end-effector motions of a serial chain is equivalent to Span(twists) and all end-effector constraints of a parallel chain is equivalent to Span(wrenches).

Definition 5. *$dimV < \infty$ if V= Span($\boldsymbol{v}_1, \ldots, \boldsymbol{v}_n$). $dimV$=n if $\exists$ linearly independent $\{\boldsymbol{v}_1, \ldots, \boldsymbol{v}_n\}$ is a basis such that V= Span($\boldsymbol{v}_1, \ldots, \boldsymbol{v}_n$).*

For example, the Plücker bases for a frame $Oxyz$ is represented by the 3 unit rotations about the axes and the 3 unit translations directed as the axes $\{\rho_{Ox}, \rho_{Oy}, \rho_{Oz}, \tau_x, \tau_y, \tau_z\}$.

Definition 6. *The dual V^* of a vector space V ($dimV = n$), V^*= $\{\boldsymbol{f} : V \to \mathbb{R} \mid \boldsymbol{f} : linear\}$ ($dim\ V^* = n$).* An example of dual space is the wrenches, $se(3)^*$, are dual to the twists, se(3)

$$\zeta(\xi) = \zeta \circ \xi = \vec{f} \cdot \vec{v}_O + \vec{m}_O \cdot \vec{\omega} \tag{2.1}$$

The application of a wrench on a twist (also called their reciprocal product [76]) measures the power exerted by the system of forces for the instantaneous motion. When dual bases are used $\zeta \circ \xi = \zeta^{\mathsf{T}} \xi$ interpreting as column coordinate vectors. Hence, the notation $\zeta \cdot \xi$ is used. When a wrench exerts no power on a twist, they are orthogonal (also called reciprocal).

In general, a screw \$ can be represented as

$$\$ = \begin{bmatrix} s \\ \mathbf{r} \times s + hs \end{bmatrix} \tag{2.2}$$

where s is the direction vector of the screw, h is the pitch of the screw and $\mathbf{r}$ is the position vector of any point on the screw. The canonical representation of a screw (twist/ wrench) describes the axis closest to the origin $\mathbf{r}$ and pitch h in the following way:

$$\mathbf{r} = \frac{\omega \times \mathbf{v}}{\omega \cdot \omega}, h = \frac{\omega \cdot \mathbf{v}}{\omega \cdot \omega}, s = \frac{\omega}{\|\omega\|} \tag{2.3}$$

Similarly, the parameters are defined for a wrench with $(\vec{f}, \vec{m}_O)$. Depending on the pitch, the following classifications of screws are defined:

1. *Zero-pitch screws*: $h = 0$, $\$_0 = \begin{bmatrix} s \\ \mathbf{r} \times s \end{bmatrix}$
2. *Infinite-pitch screws*: $h = \infty$, $\$_\infty = \begin{bmatrix} \mathbf{0}_{3\times1} \\ s \end{bmatrix}$
3. *Finite-pitch screws*: $h \neq 0$, $h \neq \infty$ Expressed as linear combination of zero-pitch and infinite pitch screws.

A *zero-pitch twist* and an *infinite-pitch twist* are represented as ξ_0 and ξ_∞, respectively, while a *zero-pitch wrench* and an *infinite-pitch wrench* are represented as ζ_0 and ζ_∞.

Definition 7. *The projective space underlying a twist or wrench subspace is called a screw system. An n-system underlies an n-dimensional subspace* [75].

2.2.1.1 Reciprocity conditions

Definition 8. *Two screw systems are reciprocal when any wrench acting on a screw in one system exerts no power on any twist on a screw in the other system* [76].

In Fig. 2.8, a body is constrained about the instantaneous screw axis(ISA) ξ with pitch h. Its instantaneous angular velocity and translational velocity are ω

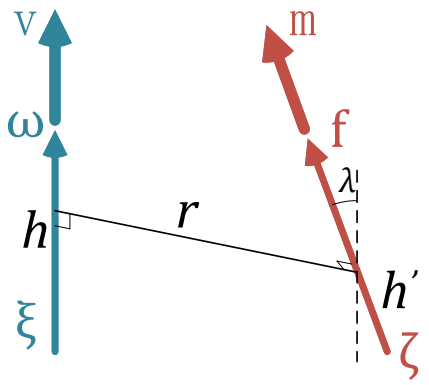

Figure 2.8: Reciprocal screws

and $\boldsymbol{v}$, respectively. The pitch h satisfies the requirement $\boldsymbol{v} = h\omega$. The screw ζ contains a wrench with pitch $h^{'}$ has its intensity $\boldsymbol{f}$ and the moment $\boldsymbol{m} = h^{'}\boldsymbol{f}$. The shortest distance between ξ and ζ is r and the angle between them is λ.

The work done by the wrench ζ on the twist ξ can be represented as:

$$\zeta \circ \xi = \boldsymbol{f} \cdot \vec{v} + \boldsymbol{m} \cdot \omega \tag{2.4}$$

where, $\circ$ is the *reciprocal product* between two screws. For Fig. 2.8, when no work is done, the following relationship is obtained:

$$\begin{aligned} \zeta \circ \xi = (\boldsymbol{f}\vec{v} + \boldsymbol{m}\omega)cos(\lambda) - \boldsymbol{f}r\omega sin(\lambda) = 0 \\ \Rightarrow \boldsymbol{f}\omega((h + h^{'})cos(\lambda) - rsin(\lambda)) = 0 \end{aligned} \tag{2.5}$$

If the locations and pitches of the screws ξ and ζ are such that,

$$\begin{aligned} (h + h^{'})cos(\lambda) - rsin(\lambda) = 0 \\ (h + h^{'}) = r\tan(\lambda) \end{aligned} \tag{2.6}$$

then, irrespective of the intensity of the applied wrench or the amplitude of the instantaneous twist, the contribution the wrench makes to the instantaneous

Screw 1	Screw 2	Reciprocity condition
$\$_{10}$	$\$_{20}$	Coplanar axes
$\$_{1\infty}$	$\$_{2\infty}$	Always reciprocal
$\$_{10}$	$\$_{2\infty}$	Perpendicular axes
$\$_{1\infty}$	$\$_{20}$	Perpendicular axes

Table 2.1: Reciprocity conditions

working rate is zero and the screws are reciprocal. Some of the reciprocity conditions are listed in the Table. 2.1 The geometric conditions can be expressed explicitly by taking instantaneous motions and system of forces.

Screw 1	Screw 2	Reciprocity condition
A rotation	A force	Coplanar (parallel or intersecting)
A translation	A couple	Always reciprocal
A twist	A couple	Perpendicular axes
A translation	A wrench	Perpendicular axes

Table 2.2: Reciprocity rules

2.2.2 The instantaneous motion space and its dual

The configuration space

A *serial kinematic chain* has $p+1$ rigid bodies (links) and p joints (pairs). A generalized joint is understood as any smooth submanifold of $SE(3)$, describing the feasible relative location of the two bodies in the pair*. The base link is fixed in space. To adapt the model to mechanisms with a mobile base, only joint one (between the base and link one) is allowed to be SE(3) itself, i.e., to permit full 6-dof mobility of body one [15].

*The notations $SE(3)$ and $se(3)$ refer to the 6-dimensional Lie group of rigid-body displacement in space and its Lie algebra. The discussion equally applies to the 3-dimensional group $SE(2)$ of the rigid displacements in the plane

The *joint space*, $\mathcal{Q}$, of the chain is the direct product of the joint manifolds, $\mathcal{Q} = \mathcal{Q}_1 \times \cdots \times \mathcal{Q}_p$. Each element of $\mathcal{Q}$, is a joint configuration $\boldsymbol{q} = (\boldsymbol{q}_1, \ldots, \boldsymbol{q}_p)$. The joint displacements are independent in a serial chain and so all such configurations are possible. Thus the joint space $\mathcal{Q}$ of a serial chain is also referred to as its joint configuration space, $\mathcal{C}$. For closed loop chains, the joint and configuration spaces are distinct. The link space is $\mathcal{B} = SE(3)^p$, the p-tuples of absolute displacements of the links with respect to the base. The elements of $\mathcal{B}$ allowed by the joints form the link configuration space, $\mathcal{D}$.

For a given joint configuration, the absolute displacement of body i is obtained by its kinematic map, $\boldsymbol{k}_i : \mathcal{Q} \to SE(3)$. The image $\boldsymbol{k}_i(\boldsymbol{q})$ depends only on the displacement in the first i joints, $(\boldsymbol{q}_1, \ldots, \boldsymbol{q}_i)$. The body maps are combined in a chain map $\boldsymbol{k} : \mathcal{Q} \to \mathcal{B}, (\boldsymbol{q}_1, \ldots, \boldsymbol{q}_p) \mapsto (\boldsymbol{k}_1(\boldsymbol{q}), \ldots, \boldsymbol{k}_p(\boldsymbol{q}))$, which specifies the absolute displacements of all bodies. While some of the individual maps $\boldsymbol{k}_i$ may be many-to-one or have singularities, the total kinematic map $\boldsymbol{k}$ is a smooth embedding into the link space, $\mathcal{B}$ and a diffeomorphism onto the link configuration space, $\mathcal{D}$.

The instantaneous motion space

The feasible instantaneous motions (or flexes) of the kinematic chain, at a given configuration, $\boldsymbol{q} \in \mathcal{Q}$, form a vector space,$\mathcal{M}_{\boldsymbol{q}}$, the (instantaneous) *motion space* of the chain. Its dimension, $n_{\mathbf{q}} = dim\mathcal{M}_{\mathbf{q}}$, is the *instantaneous mobility* of the mechanism. For a serial chain, the space $\mathcal{M}_{\boldsymbol{q}}$ is identified with the tangent joint space at $\boldsymbol{q}$, $\mathrm{T}_{\boldsymbol{q}}\mathcal{Q} = \mathrm{T}_{\boldsymbol{q}_1}\mathcal{Q}_1 \oplus \cdots \oplus \mathrm{T}_{\boldsymbol{q}_p}\mathcal{Q}_p$, which consists of the p-tuples of the relative twists in the joints.

As the joints are smooth submanifolds, we have $n_{\boldsymbol{q}} = \sum_{i=1}^{p} dim\mathrm{T}_{\boldsymbol{q}_i}\mathcal{Q}_i = \sum_{i=1}^{p} dim\mathcal{Q}_i = n$ for every $\boldsymbol{q}$. Similarly, we can define the space of feasible instantaneous link motions, $\mathcal{L}_{\boldsymbol{q}} \subset se(3)^p$, with elements the feasible p-tuples of link twist velocities (with respect to the base). The vector addition in $\mathcal{M}_{\boldsymbol{q}}$, and $\mathcal{L}_{\boldsymbol{q}}$, is realized by adding the joint, and link, twists of two flexes, respectively. The explicit dependence on $\boldsymbol{q}$ will be dropped since we will be concerned with a given (though arbitrary) configuration. The joint tangent spaces $\mathrm{T}_{\boldsymbol{q}_i}\mathcal{Q}_i$ will be denoted by T_i, and $\mathrm{T}_{\boldsymbol{q}}\mathcal{Q}$ by T. Thus $\mathcal{M} = \oplus_{i=1}^{p}\mathrm{T}_i = \mathrm{T}$. The twist systems that the joints allow in $\boldsymbol{q}$ will be denoted by $\mathcal{T}_i$. We will consider all screw quantities, including the systems $\mathcal{T}_i$, expressed in the same (though arbitrary) reference frame. (So

the T_i are twist systems in different spaces, while the $\mathcal{T}_i$ are in the same copy of $se(3)$.)

The dual to the motion space [15] If $\mathcal{V}$ is a real vector space, $\dim\mathcal{V} = n$, $\mathcal{V}^*$ is the *dual* vector space of linear 1-forms mapping each vector into a scalar. For finite-dimensional spaces, $\dim\mathcal{V}^* = \dim\mathcal{V}$. There is no canonical isomorphism between the two, and they cannot be identified. Rather, every basis of $\mathcal{V}$, $\boldsymbol{E} = \{v_1, \ldots, v_n\}$, has a unique *dual basis* $\boldsymbol{E}^* = \{v_1^*, \ldots, v_n^*\}$ of $\mathcal{V}^*$. More generally, any decomposition of $\mathcal{V}$ into a direct sum of complementary $\mathcal{V} = \mathcal{V}_1 \oplus \cdots \oplus \mathcal{V}_k$ induces a decomposition $\mathcal{V}^* = \mathcal{V}_1^* \oplus \cdots \oplus \mathcal{V}_k^*$, where $\mathcal{V}_i^* = (\sum_{j\neq i} \mathcal{V}_j)^\perp = \cap_{j\neq i}\mathcal{V}_j^\perp$ * We can write $\mathcal{M}^* = \mathrm{T}_1^* \oplus \cdots \oplus \mathrm{T}_p^*$, $se(3)^{p^*} = se(3)^* \oplus \cdots \oplus se(3)^*$.

For a single rigid body, the dual to the space of twists, $se(3)$, are the wrenches, $se(3)^*$.

$$\zeta(\xi) = \zeta \cdot \xi = \vec{\boldsymbol{f}} \cdot \vec{\boldsymbol{v}}_o + \vec{\boldsymbol{m}}_o \cdot \vec{\omega} \tag{2.7}$$

where $\zeta = (\vec{\boldsymbol{f}}, \vec{\boldsymbol{m}}_o)$ represent the wrench (resultant force and moment) at O and $\xi = (\vec{\omega}, \vec{\boldsymbol{v}}_o)$ represent the instantaneous motion or twist (instantaneous rotational and translational velocity) of the system described at O. Similarly, the tangent space of the unconstrained link space is $se(3)^p$ while the elements of $se(3)^{p^*}$ are the p-tuples of wrenches acting on the bodies. The vectors in $\mathcal{M}^*$, the *coflexes*, i.e., the linear functionals on the space of flexes, are viewed as generalized forces/torques acting on the chain. (In a dynamics context they are seen as generalized moments.)

Just as wrenches acting on a free body are interpreted as constraints on its possible twists, the coflexes [15] are constraints on the possible flexes. Feasible are only those flexes that are mapped to zero by all the constraint coflexes, i.e. these are the instantaneous motions on which the coflexes "do no work". When a body is bound by a device that can generate any constraint wrench, no twist is possible and the body cannot move. Similarly, when a mechanical device which can generate any coflex is applied to a kinematic chain, no flex is possible and the chain is immobilized. To choose a valid set of actuators for a parallel manipulator one needs to ensure that the structural and actuated constraints together can span $se(3)^*$. Analogously, a kinematic chain is well actuated when all coflexes can

*For any subspace $\mathcal{U} \subset \mathcal{V}$, the subspace of $\mathcal{V}^*$ given by $\mathcal{U}^\perp = \{\boldsymbol{a} \in \mathcal{V}^* \mid \boldsymbol{a} \cdot \boldsymbol{u} = 0 \forall \boldsymbol{u} \in \mathcal{U}\}$ is called the orthogonal annihilator of $\mathcal{U}$.

be generated (at least instantaneously at $\boldsymbol{q}$).

2.2.3 The tangent and cotangent maps

The transition between the joint and link vector spaces is done via (what are usually called in robotics) the Jacobian maps.

The map $\boldsymbol{j}_i : \mathcal{M} \to se(3), (\xi_1, \ldots, \xi_q) \mapsto \boldsymbol{\eta}_i$, $\boldsymbol{\eta}_i = \xi_1 + \cdots + \xi_i$ returns the instantaneous motion of the i-th link. Here the twists $\boldsymbol{\eta}_i, \xi_j$ are expressed in the same frame. The usual Jacobian is a matrix, in the standard bases, of j_{n+1}, when the joints are all with 1 DOF. The composite map, $\boldsymbol{j} = \boldsymbol{j}_1 \times \cdots \times \boldsymbol{j}_p, (\xi_1, \ldots, \xi_p) \mapsto (\eta_1, \ldots, \eta_p)$ identifies the joint and link flexes [15].

The induced dual map, $\boldsymbol{j}_i^* : se(3)^* \to \mathcal{M}^*, \zeta_i \mapsto z_i$, is defined by $\boldsymbol{j}_i^*(\zeta_i) \cdot \boldsymbol{x} = \zeta_i \cdot \boldsymbol{j}(\boldsymbol{x})$ for any flex $\boldsymbol{x}$, i.e., $\boldsymbol{j}_i^* \cdot (\zeta_1, \ldots, \zeta_p) = \zeta \cdot \boldsymbol{j}_i(\zeta_1, \ldots, \zeta_i)$. It sends a wrench applied to the i-th link into a linear functional z on $\mathcal{M}$, which however acts only on the first i joints. The dual of the chain Jacobian, $\boldsymbol{j}^*$, is similarly defined by $\boldsymbol{j}^*(\zeta_1, \ldots, \zeta_p) \cdot \boldsymbol{x} = (\zeta_1, \ldots, \zeta_p) \cdot \boldsymbol{j}(\boldsymbol{x}) = \zeta_1 \cdot \boldsymbol{j}(\boldsymbol{x}) + \cdots + \zeta_p \cdot \boldsymbol{j}(\boldsymbol{x})$ [*]. Thus $\boldsymbol{j}^* = (\boldsymbol{j}_1 \times \cdots \times \boldsymbol{j}_p)^* = \boldsymbol{j}_1^* + \cdots + \boldsymbol{j}_p^*$.

2.2.4 Convex cones

In applications such as cable-robots, grasping or pushing the possible resultant wrenches do not span a vector space but rather a convex cone [4] in the complete screw space. The unilateral positive force constraint can be represented as conic combinations which are linear combinations with non-negative coefficients and their union forms the conic hull of the generating vectors/generators. With cables, you can increase or decrease the intensity of the tension, but cannot reverse the sign. The intuitive geometric representations provide a designer of mechanical systems with valuable ability to visualize a set of possible resultant wrenches and estimate how it would change when the generators are modified. A convex cone in $\mathbb{R}^n$ consists of rays from the origin with their intersections with unit sphere. A ray can also be described by its intersection point with a hyperplane away from the origin as shown in Fig. 2.9. When a ray is parallel to the hyperplane, we

[*] "$\cdot$" is used to denote the application of any dual space element (a linear functional) on a vector, including the reciprocal product of a twist and a wrench

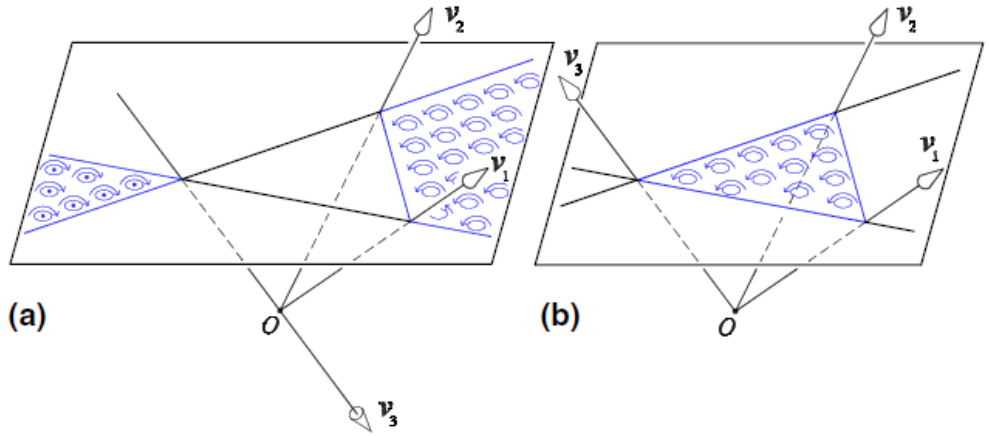

Figure 2.9: Conic hulls in a model of projective space [4]

identify it with a point at infinity. If the ray points away from the hyperplane, we use the intersection point of the opposite ray. The convex hull [4] of independent generators includes no more than one unit vector on a given line. The hull of a basis corresponds to a generalized simplex in the hyperplane. The simplex is called external when it has two connected components, Fig. 2.9(a). The internal $(k-1)$simplex is the usual convex hull of k points, Fig. 2.9(b). The concept of convex hull can be applied to cable driven robots, here suitable for cable driven suspended robots. The convex screw spaces is studied in detail in [4]. The basic definition of convex cone in a vector space is represented as:

$$Cone(\boldsymbol{v}_1, ..., \boldsymbol{v}_k) = \{a_1\boldsymbol{v}_1, ..., a_k\boldsymbol{v}_k \mid a_i \geqslant 0, \forall i\} \tag{2.8}$$

The generalized form is when you have a basis, then the intersection with hyperplane generates a simplex in the hyperplane. The oriented points are represented in the internal and external triangles and not the intersection points with the cone. If you consider 3 forces in a plane (for example, a planar cable robot) the linear span is the whole plane of three forces and a couple perpendicular to the plane. The conic span (if you cannot reverse the force directions) are given in

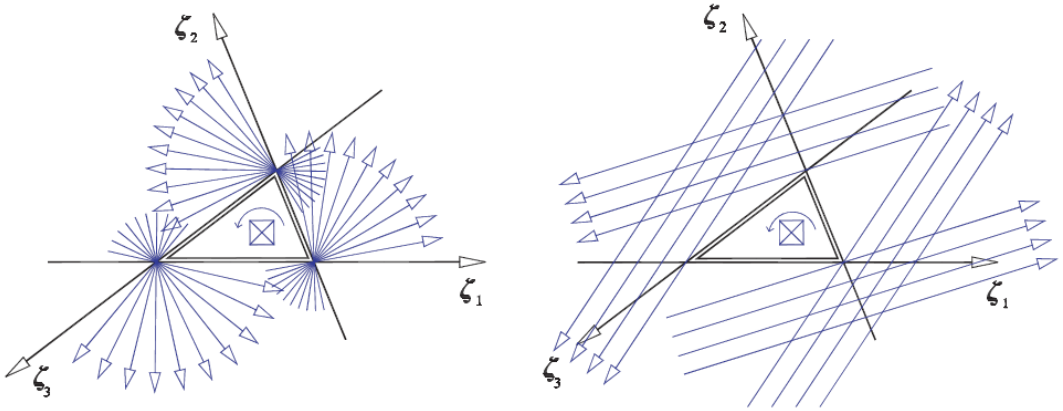

Figure 2.10: A convex cone [4]

Fig. 2.10. The cones are all lines shown in Fig. 2.10(b) and these lines do not intersect the triangle, whereas they go around the triangle in the same way as the generators. The resultant of 3 planar forces and couple is represented in the figure. Here the generators are cyclic. The triangle is denoted as the forbidden zone [4] as the resultant doesn't pass through that zone. If the generators are not cyclic, you will get an external triangle as shown in Fig. 2.11.

The three-system lines on plane representation of coplanar horizontal h-screws and vertical ∞-screws is shown in Fig. 2.10. This is the system of wrenches applied by planar grippers and cable robots.

If the wrenches are not of the same pitch, then each screw projects on a different line and every line corresponds to an unique screw. If you consider three of them, and view in a model of projective space, the representation will be as shown in Fig. 2.12. The characteristic triangle becomes a vertical prism and the screws go around the prism similar to the characteristic triangle. The forbidden area is a prism. These representations are designed for single body system, whereas the concept can be extended to mutibody chains as well. The great variety of conic hulls can be the theoretical foundation for study of many problems in robotics where sign reversal of twists/ wrenches is not allowed.

It is desirable to generate the entire space only with conic combinations. For this purpose, one needs at least one more vector than there are in a basis. The

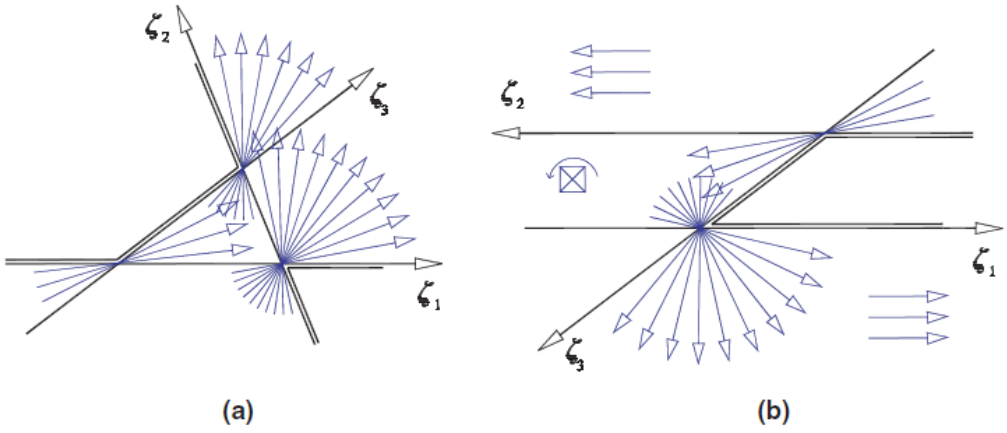

Figure 2.11: A convex cone with external triangle [4]

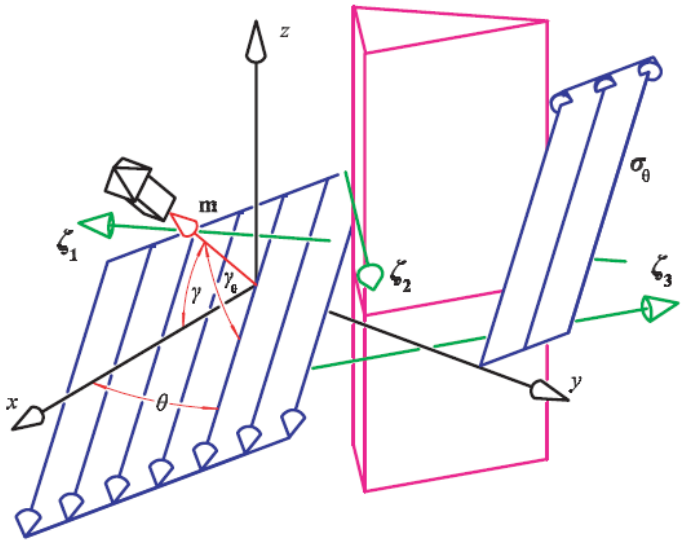

The screws with a given direction in a cone of type 3–IB$(h, \frac{\pi}{4})\{\triangle A_1A_2A_3, +\}$.

Figure 2.12: The prism extruded from the characteristic triangle of cone [4]

following proposition gives the conditions that a collection of vectors must satisfy to be a minimal set of conic generators for the whole space.

Proposition 9. Let $\mathcal{V}$ be a vector space, $\dim\mathcal{V} = n$ and $\boldsymbol{v}_1, \ldots, \boldsymbol{v}_{n+1} \in \mathcal{V}$.

The following are equivalent [15].

1. $\mathcal{V} = Cone(\boldsymbol{v}_1, ..., \boldsymbol{v}_{n+1})$
2. *For some i, (a) the set* $\{\boldsymbol{v}_j \mid j \neq i\}$ is *linearly independent (b)* $-\boldsymbol{v}_i = \sum_{j \neq i} \lambda_j \boldsymbol{v}_j, \lambda_j > 0$
3. *For all i, (a) the set* $\{\boldsymbol{v}_j \mid j \neq i\}$ is *linearly independent (b)* $-\boldsymbol{v}_i = \sum_{j \neq i} \lambda_j \boldsymbol{v}_j, \lambda_j > 0$
4. *For some nonempty proper subset,*A,*of* $\{1, \ldots, n+1\}$, *(a) the sets* $\{\boldsymbol{v}_j \mid j \in \mathrm{A}\}$, $\{\boldsymbol{v}_j \mid j \notin \mathrm{A}\}$ *are linearly independent (b)* $-\sum_{j \in \mathrm{A}} \lambda_j \boldsymbol{v}_j = \sum_{j \notin \mathrm{A}} \lambda_j \boldsymbol{v}_j, \lambda_j > 0$
5. *For every nonempty proper subset,*A,*of* $\{1, \ldots, n+1\}$, *(a) the sets* $\{\boldsymbol{v}_j \mid j \in \mathrm{A}\}$, $\{\boldsymbol{v}_j \mid j \notin \mathrm{A}\}$ *are linearly independent (b)* $-\sum_{j \in \mathrm{A}} \lambda_j \boldsymbol{v}_j = \sum_{j \notin \mathrm{A}} \lambda_j \boldsymbol{v}_j, \lambda_j > 0$

The proposition collects fairly standard facts. It can be based on the fact that $n+1$ vectors include the whole space in their conic hull if and only if they have a unique (up to scalar multiplication) linear combination with strictly positive coefficient which equals zero.

Definition 10. *In an n-dimensional space* $\mathcal{V}$*, we call a collection of* $n+1$ *vectors which contain the whole space in their conic hull, a conic frame of* $\mathcal{V}$*.* [15]

A difference between a conic frame and a basis is that any vector has infinitely many sets of conic coordinates in one given conic frame. (Because the zero vector can be expressed as a nontrivial conic combination.) In every n-dimensional space, $\mathcal{V}$, we can always find $n+1$ vectors providing a conic frame. However, if our choice of vectors in $\mathcal{V}$ is restricted to a subset $\mathcal{F}$, this is not always possible even if $\mathcal{F}$ is a spanning system (i.e., $\mathcal{V} = \mathrm{Span}\ (\ \mathcal{F})$) with infinitely many elements. This situation is relevant when we attempt to generate a conic frame of coflexes by applying only individual forces on individual links of a kinematic chain (rather than via arbitrary systems of forces).

2.2.4.1 Single-body lemmas in the space of coflexes

Several key facts about the wrenches acting on a single body is described in this section. These screw-theory lemmas will will allow us to implement a procedure

for the generation of a conic frame in the coflex space while using only unilateral forces on the links.

Lemma 11. *Any k linearly independent twists/wrenches, can be complemented to a basis by* $6-k$ *pure rotations/forces.* [15]

Example 12. A single revolute joint is descibed with 0-pitch twist ρ and its 5-dimensional constraint wrench system, $\mathcal{W}$=Span$(\rho)^{\perp}$. Any force, φ on a line not coplanar with the joint axis complements any basis of $\mathcal{W}$ to a basis of $se(3)^*$, Span$(\rho)^{\perp}\oplus$ Span$(\varphi) = se(3)^*$.

Example 13. A single spherical joint at the origin O with its 3-dimensional constraint system, $\mathcal{S}$, consisting of the forces with axes through O. Let φ_1, φ_2 and φ_3 be three linearly independent forces with non-concurrent axes. They are the generators of a (possibly degenerate) hyperboloid of one sheet. Then, if this hyperboloid does not contain O, we have $\mathcal{S}\oplus$ Span$(\varphi_1, \varphi_2$ and $\varphi_3) = se(3)^*$. This is true even if the hyperboloid degenerates to a double plane, which is the case when φ_1, φ_2 and φ_3 have their axes along the sides of the triangle, $\triangle\, A_1A_2A_3$ in a plane π not through O.

Lemma 14. *For any twist/wrench basis there exists a pure rotation/force with nonzero coordinates in the basis*

Remark 15. The proof the lemma [15] can be modified to prove a stronger statement. Given a finite number of wrench systems one can always find a force that does not belong to any of them.

Remark 16. Lemma 6 allows to complement any given basis of $se(3)^*$ to a conic frame with a *pureforce* after possibly changing the signs of some of the basis vectors. This fact is useful to construct the unilateral forces that immobilize a one-joint chain [15].

Given a single body attached to the base with a joint, we can immobilize it by applying any set of wrenches whose span, $\mathcal{V}$, complements the joint constraint system to span the wrench space, $\mathcal{V}\oplus\mathcal{T} = se(3)^*$.

Lemma 17. *Consider a one-joint kinematic chain, i.e., a constrained body with twist freedoms* $\mathcal{T}, dim\mathcal{T} = d$ *and let* $\{\boldsymbol{v}_1,\ldots,\boldsymbol{v}_m\}$, $m = 6-d$ *be a basis of the system of wrench constraints,*$\mathcal{T}^{\perp}$. *Let the wrenches* $\{\psi_{m+1},\ldots,\psi_6\}$ *complement* $\{\boldsymbol{v}_1,\ldots,\boldsymbol{v}_m\}$ *to a basis of* $se(3)^*$. *Then the coflexes* $\{z_1,\ldots,z_d\}$, *caused by the wrenches* $\{\psi_{m+1},\ldots,\psi_6\}$,$z_i = \boldsymbol{j}^*(\psi_{m+i})$, *form a basis of* $\mathcal{M}^*$.

The close relationship between cable robots and grasping, which are both based on unilateral constraints has been pointed out in literature [77, 78]. The antipodal grasp theorem has been applied to cable robots and antipodal cable theorem was studied. The Planar Antipodal Cable theorem [79] is stated as follows:
Theorem 18.: A planar cable robot with two pairs of cables with coincident attachment points P and Q is force closed if, and only if, the line from P to Q lies completely in the two open force triangles defined by the reversed forces of the two cable pairs. Spatial Antipodal Cable Theorem [79] is stated as follows :
Theorem 19.: Consider a spatial cable robot with two three-cable sets that coincide at two points, P and Q, and two additional cables. If the following conditions are both satisfied, the cable robot pose is force closed. 1) The line connecting points P and Q lies strictly inside the two reversed force tetrahedra spanned by the two three-cable sets. 2) The remaining two cable forces create moments of opposing direction along the line segment PQ. The above theorem states sufficient conditions but not that they are necessary for force closure.

2.3 Theoretical Problems

The positive cable tension constraint has created a set of challenging and interesting problems in the analysis of CDPRs. The determination of cable forces required in motion generation and control needs to be discussed. The workspace analysis and the necessary conditions to achieve force-closure is a precursor in designing cable robots. The determination of positive cable forces to achieve desired motion for a CDPR is the inverse dynamics problem. $M(\mathbf{q}, \ddot{\mathbf{q}}) + C(\mathbf{q}, \dot{\mathbf{q}}) + G(\mathbf{q}) + \Gamma_{ext} = -\mathbf{J}(\mathbf{q})^{\mathsf{T}}$. where $M \in \mathbb{R}^{nxn}$, $C \in \mathbb{R}^{nx1}$, $G \in \mathbb{R}^{nx1}$ and $\Gamma_{ext} \in \mathbb{R}^{nx1}$ represent the mass-inertia matrix, centrifugal and Coriolis force vector, gravity force vector and external wrench vector, respectively for a n DoF m cable CDPR. The transpose of the Jacobian matrix represents the mapping between the cable forces and the resultant wrench that the cables generate on the end-eefector of the system. The positive cable tension constraint is expressed as $\mathbf{f} \geqslant 0$. Due to the actuation redundancy, the inverse dynamics problem is treated as an optimization problem [80] that ensured the cable forces are positive and within the minimum and maximum allowable

bounds. 1-norm and 2-norm of the cable forces are simple objective functions and are solved using linear programming (LP) and quadratic programming (QP) solvers [81, 82]. Other approaches are also investigated and discussed in the literature [83, 84].

2.3.1 Vector Closure

A parallel-cable driven mechanism (n-DoF m-cable) has actuator units installed at the base and winds all/part of its cables by pulleys to generate actuating tension in the cables. One end of each cable is connected by point contact to a controlled object and the other end is tensioned by some external force, such as an actuator unit installed at the base or gravity. Tension in the wires is positive. When matrix $\mathbf{A}$ satisfies the following two conditions simultaneously, it is called Vector closure [85].

1. Atleast n vectors in row vectors $\mathbf{a_i}(i = 1, ..., m)$ are linearly independent
2. There exists a vector η=$[\eta_1, ..., \eta_m]^\mathsf{T}$ that will satisfy the following equation:

$$\mathbf{A}(\mathbf{q})\boldsymbol{\eta} = \sum_{i=1}^{m} \mathbf{a_i}\eta_\mathbf{i} = 0 \tag{2.9}$$

where all components of vector $\boldsymbol{\eta}$ are positive. Vector closure means that tension in the positive direction of m cables in number can generate any n-dimensional force-moment at the end-effector. When force is applied in the compressive direction of a cable, the cable becomes slack and cannot transmit any force. At least $n + 1$ sets of a cable and an actuator/ some external force are needed.

2.3.2 Kinematics and Redundancy Resolution

As one of important topics in robotics, kinematics is concerned with the motion of the robot's joints in relation to the motion of the robot's end-effector, including forward kinematics and inverse kinematics. For a CDPR, calculating the mobile platform (end-effector) by the given cable lengths represents forward kinematics; computing the cable lengths by the given the mobile platform position denotes

inverse kinematics. For a serial robot, forward kinematics is used to calculate the position and orientation of the end-effector when the joint angles are provided; inverse kinematics is used to compute the joint angles (the position and orientation of the end-effector are given. Generally, geometric or algebraic methods can be utilized to find analytical solutions (closed-form solutions), and use numerical approaches to find solutions. Redundancy resolution is another important topic in kinematics and has existed for years. Generally, approximate methods can be utilized to find numerical solutions, such as Jacobian pseudoinverse [86], Jacobian transpose, damped least squares [87], and quasi-Newton and conjugate gradient approaches [88]. Singularity analysis is another problem in robot kinematics. For a CDPR, cable tensions cannot hold in a singularity zone (force-closure singularity), so the robot should not work within the singularity area. Gosselin and Angeles [89] used closed-loop chains to analyze the singularity, and Zlatanov [90] developed a more generalized method to solve several singularity problems.

2.3.3 Workspace Analysis

The generation of operational region of the cable driven manipulator is workspace analysis. For serial and rigid link parallel manipulators, these conditions depend on the kinematics of the system. The system's ability to generate motion or external forces given the actuation bounds of the manipulator is defined as dynamic workspace. The workspace of manipulators are generated using two techniques, analytical [91] and numerical approaches. Analytical method determines the geometric boundary and solves the equations that defines the workspace. Numerical methods are point-wise evaluation [92, 93] techniques where the workspace condition is evaluated at each point in the discretised search space [41, 94].

The types of workspaces studied for CDPMs are *static workspace*, *wrench-feasible workspace* and *wrench-closure workspace* [95–106]. The static workspace of CDPMs refers to the set of poses in which the manipulator can achieve static equilbrium, to sustain its own weight under gravity force and no external wrenches.

$$SW = (q : G(q) = -\mathbf{J}(\mathbf{q})^{\mathsf{T}}\mathbf{t}, \exists \mathbf{t} \in [0, \mathbf{t}_{max}]) \tag{2.10}$$

The wrench-feasible workspace (WFW) of a cable-driven body refers to the set of

poses for which a specified set of external wrenches, velocities and accelerations can be satisfied within a given range of positive cable forces. The WFW can be defined as

$$WFW = (q : \mathbf{w} = -\mathbf{J}(\mathbf{q})^{\mathsf{T}}\mathbf{t}, \exists \mathbf{t} \in [\mathbf{t}_{min}, \mathbf{t}_{max}]) \tag{2.11}$$

where $\mathbf{w} = -[M(\mathbf{q}, \ddot{\mathbf{q}}) + C(\mathbf{q}, \dot{\mathbf{q}}) + G(\mathbf{q}) + \Gamma_{ext}]$. The wrench-closure workspace (WCW) is defined as the set of poses in which the manipulator can sustain any arbitrary external wrench. Mathematically, it is defined as

$$WCW = (q : \mathbf{w} = \mathbf{J}(\mathbf{q})^{\mathsf{T}}\mathbf{t}, \exists \mathbf{t} \geqslant 0) \tag{2.12}$$

2.3.4 Wrench-Closure Workspace and Conditions

The Wrench Closure Workspace (WCW) [101] is a well studied type of workspace analysis for CDPRs. It is defined as the set of poses in which the manipulator can sustain any arbitrary external wrench when no upper bounds are placed on the cable forces. WCW, tensionable workspace, and controllable workspace are equivalent. They depend on the kinematics of the manipulator rather than the dynamic equilibrium or cable properties. WCW can be used in trajectory generation between a start and end pose as CDPR is capable of producing motion to any adjacent poses if it satisfies the wrench closure condition [107] (Wrench closure condition (WCC)). By constructing a path that lies within the WCW, the trajectory can be performed by the CDPR while satisfying the positive force constraint. In the future chapters, we will see how the attachment locations of the cables of CDPRs/CDSKCs have a significant impact on the size and shape of WCW. By using optimal cable routing and cable attachment points, the WCW about a desired pose can be optimized. The WCW is a more useful workspace definition than the Wrench Feasible Workspace (WFW) since no requirement on wrench exertion is required. Geometrically, the WCW definition implies if the columns of $\mathbf{J}^{\mathsf{T}}$ positively span $\in \mathbb{R}^n$ for full rank $\mathbf{J}^{\mathsf{T}}$. There exists some positive cable force vector within the nullspace of $\mathbf{J}^{\mathsf{T}}$, where

$$\begin{aligned} rank(J^{\mathsf{T}}) &= n \\ \exists \mathbf{f} \in ker(J^{\mathsf{T}}) &: \mathbf{f} > 0 \end{aligned} \tag{2.13}$$

To positive spanning problem for WCW was solved by various approaches. For a planar parallel mechanism driven by four cables with three linearly independent columns w_1, w_2 and w_3. A geometric interpretation of (5.23) is that the column vector w_4 is inside and not on the boundary of the convex polyhedral cone [4] (which was discussed above) generated by the set $-w_1$, $-w_2$, $-w_3$. Such a WCC is referred to as a four-vector WCC. 4,5 and 6 cable cases were solved using this concept in [101]. The analytical study of the WCW for both planar and spatial manipulators were investigated in [108]. Numerical approaches were applied to generic CDPM structure and checked for linearly independent columns of $\mathbf{J}^{\mathsf{T}}$ forming a convex hull around the origin.

2.3.5 Performance Evaluation

The quality of the workspace is determined using various performance indices. For CDPRs, Tension factor (TF) is proposed to evaluate the quality of force closure at a specific configuration. It is defined as the minimum tension over the maximum tension of the cables [109]. The TF is a measure of the positive tension condition of the structure matrix. It reflects the relative tension distribution among the cables for a specific platform pose inside the force-closure workspace. If $\mathbf{N}$ is the homogeneous solution of the cable forces, then

$$TF = \frac{min(N)}{max(N)} \tag{2.14}$$

The range of TF varies from zero to one. When the TF approaches to zero, one of the cable tension is close to zero, i.e. the platform is located near to the workspace boundary. Hence if the TF approaches one, the platform is positioned far from the boundary. The isotropic behavior is when TF always attains the value of one. A larger TF if favorable as there is a balance of cable forces. The TF is a local measure because it characterizes the distribution at a given posture of the platform. So Global Tension Index (GTI) [109], was defined in order to evaluate the quality of the whole workspace. It is obtained by integrating the local TF over the workspace.

Ronald Kurtz and Vincent Hayward [110] replaced the ordinary concepts

of dexterity, singularity, isotropy, maximum force amplification and maximum dexterity gradient by measures based on the unilateral statics such as unilateral dexterity, unilateral singularity [110] etc. The condition number is a common measure of dexterity but it does not apply to unilateral actuation. The unilaterally actuated mechanisms have constraints that affects the statics and workspace. It is not surprising that conventional dexterity measures cannot be applied to cable robots. If a pose does not satisfy WCC, it is said to be in unilateral singularity. The dexterity χ_{dex} determines the upper bound on the propagation of errors in the linear system (joint space and operational space) such that

$$\frac{\parallel \delta f \parallel}{\parallel f \parallel} \leqslant \chi_{dex}(q) \frac{\parallel \delta w \parallel}{\parallel w \parallel} \tag{2.15}$$

where w is the external wrench applied to the mechanism, $\mathbf{f}$ is the vector of tendon forces and $\chi_{dex}(q)$ is the condition number of the Jacobian matrix calculated as

$$\chi_{dex}(q) = \frac{\sigma_1}{\sigma_n} \tag{2.16}$$

where $\sigma_1 \geqslant ... \geqslant \sigma_n \geqslant 0$ are the singular values of the matrix $\mathbf{J}$.

The local unilateral dexterity measure Unilateral dexterity (UD) is defined as:

$$UD = \begin{cases} \sqrt{n+2} \dfrac{1}{\chi_{dex}(q)} \dfrac{h_{min}}{\sqrt{{h_{min}}^2 + 1}}, & \text{if} h_{min} \geqslant 1 \\ 0, & \text{if} h_{min} < 0 \end{cases}$$

where $h_{min} = min_i(\widehat{h_i})$. Also, $\hat{h}$ is a unit vector in the nullspace of the Jacobian with all its elements positive. The UD is one when the linear system is isotropic, $\chi_{dex}(q) = 1$ and when the nullspace vector is uniform in all directions. This will be referred to as unilateral isotropy. In this case, the null space vector is comprised of elements of equal magnitude such that $h_{min} = \frac{1}{\sqrt{n+1}}$. The measure $\chi_{dex}(q)\frac{\sqrt{{h_{min}}^2+1}}{h_{min}}$ incorporates condition number for UARs. The maximum force amplification (MFA) determines the upper bound on the maximum force in operational space for a

given joint space wrench such that

$$\kappa_{MFA}(q) = \frac{1}{\sigma_n} \tag{2.17}$$

The unilateral maximum force amplification (Unilateral maximum force amplification (UF)) is the second dexterity measure applied to UARs which is given as:

$$UF = \begin{cases} \sqrt{n+2}\dfrac{1}{\sigma_n}\dfrac{h_{min}}{\sqrt{{h_{min}}^2+1}}, & \text{if} h_{min} \geqslant 1 \\ 0, & \text{if} h_{min} < 0 \end{cases}$$

The Unilateral Manipulability Quality Indices [110, 111] (UMQI): UD and UF are defined for $m = n + 1$ cables. This is because the unit vector $\hat{h}$ is not uniquely defined when the dimension of null space is greater than 1. The generalized Unilateral Manipulability Quality Indices (UMQI) is studied in [111]. The wrench set quality indices including Available Wrench Set (AWS) [112], capacity margin [113] have been defined to identify unilateral singularity (US). The twist feasibility analysis of CDPR was studied using Available Twist Set (ATS) quality index in [114, 115]. A novel approach to cable robot performance evaluation has been proposed and applied to solely redundant cable robots. The method is based on the computation of the maximum force which can be exerted by the active cables on the moving platform along a specific direction. A novel performance index called Wrench Exertion Capability (WEC) [116]. Predicting the maximum force or torque that can be exerted on the moving platform along a direction of interest is useful while designing a cable robot.

$$\mathbf{W} = \mathbf{w_c} + \mathbf{w_e} = \mathbf{Af} + \mathbf{w_e} \tag{2.18}$$

where $\mathbf{A}$ is the structure matrix, $\mathbf{f}$ is the vector of cable forces and $\mathbf{w_e}$ is the external wrench. $\mathbf{W}$ wrench matrix is introduced which is obtained by simply aggregating the structure matrix and the external wrench. Once the matrix definition of $\mathbf{W}$ is introduced, it is possible to develop the cable robot performance analysis.

Chapter 3

Modeling of Redundant Unilaterally Actuated Robots

The first section in this chapter serves as an introduction to cable-driven parallel robots(CDPRs). The modeling of specific example CDPRs are presented to motivate the need for extending the concepts for serial kinematic chains. The subsequent section presents the kinematic modeling of cable driven serial kinematic chains. The presented examples serve to illustrate the ability for the proposed formulation to model complex engineered and biomechanical systems.

3.1 Completely restrained CDPRs

In modeling of CDPRs, it is important to represent the system states through different kinematic spaces and mappings. For a n DoF system, the joint space $\mathbf{q} \in \mathbb{R}^n$ represents the generalized coordinates that describes the pose of the manipulator. The cable/tendon/wire space contains the cable kinematics and cable dynamics i.e. cable lengths and cable forces respectively. For a system actuated by m cables, $\boldsymbol{l} = [l_1, l_2, \ldots, l_m]^\mathsf{T}$ and $\boldsymbol{f} = [f_1, f_2, \ldots, f_m]^\mathsf{T}$ denote the vector of cable lengths and cable forces, respectively. Due to the unilateral force constraint, the condition $f_i \geqslant 0 \forall i$ must be satisfied. The body space represents the absolute position of center of mass and orientation of rigid bodies. The operational/ task space corresponds to the space of end effector poses. In existing

CDPR literature, the joint space has been used to refer to set of cable lengths. For the study of CDSKCs, joint space represents the pose of the joints to remain uniform with the studies in serial kinematic chains.

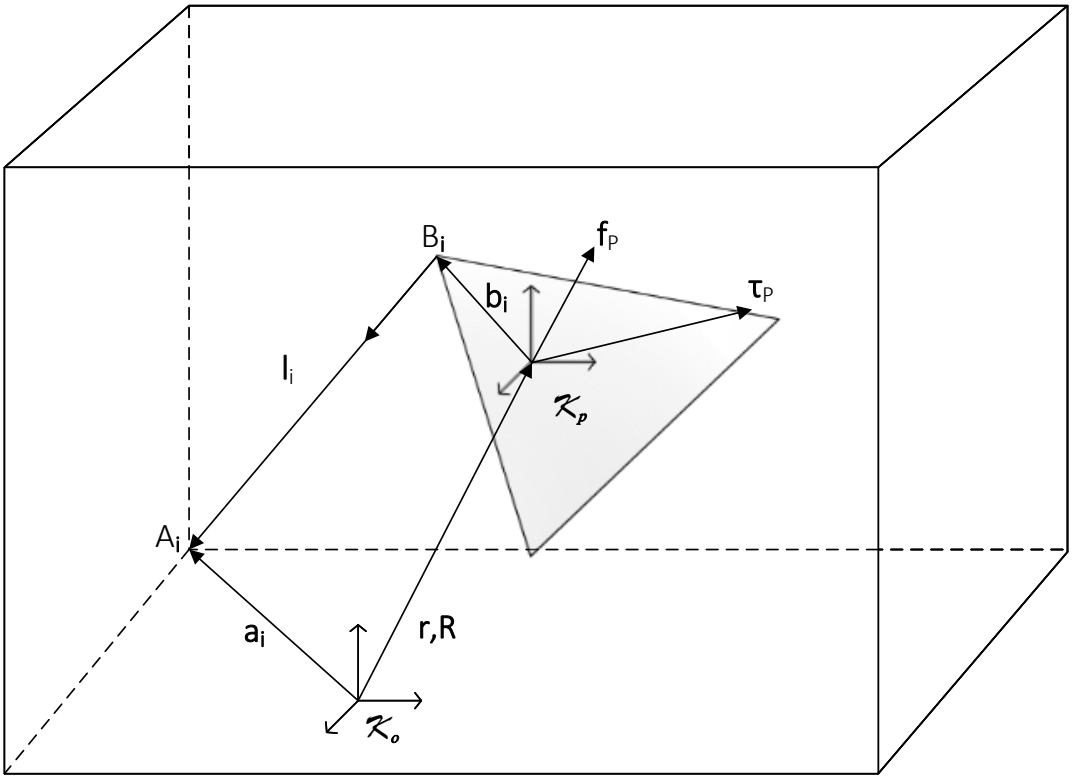

Figure 3.1: Definition of the geometry and kinematics of a general cable robot

In CDPRs,the kinematics and forces between the joint space and cable spaces are defined by the kinematic map $J \in \mathbb{R}^{mxn}$, the system Jacobian matrix. It relates the time derivative of cable lengths and the time derivative of the joint space vector, which reads

$$\dot{\mathbf{l}} = \mathbf{J}(\mathbf{q})\dot{\mathbf{q}} \tag{3.1}$$

The transpose of the Jacobian matrix represents the effect of the cable forces $\mathbf{f}$ onto the joint space force. The equations of motion in the general form is given as

$$[M(\mathbf{q}, \ddot{\mathbf{q}}) + C(\mathbf{q}, \dot{\mathbf{q}}) + G(\mathbf{q}) + \Gamma_{ext}] = -\mathbf{J}(\mathbf{q})^{\mathsf{T}}\mathbf{f} \tag{3.2}$$

where $M \in \mathbb{R}^{nxn}$, $C \in \mathbb{R}^{nx1}$, $G \in \mathbb{R}^{nx1}$ and $\Gamma_{ext} \in \mathbb{R}^{nx1}$ represent the mass-inertia matrix, centrifugal and Coriolis force vector, gravity force vector and external wrench vector, respectively for a n DoF m cable CDPR. The equations (3.1) and (3.2) represent the kinematic and dynamic models for the system. For redundantly restrained CDPRs, the Jacobian matrix $\mathbf{J}$ is non-square matrix.

3.1.1 Inverse Kinematics

The kinematic background for general CDPR is discussed here. The inverse kinematics(IK) problem deals with the determination of cable lengths $\mathbf{l}$ given the pose of the system $\mathbf{q}$. The Inverse kinematics (IK) for CDPRs is trivial and a unique solution exists which can be expressed analytically. The kinematic scheme of a CDPR with m cables, proximal docking points $\mathbf{a_i}$ and distal docking points $\mathbf{b_i}$ is shown in Fig. 3.1. $\mathbf{b_i}$ vector is from the center of mass of the end-effector to an attachment point on the cable in global coordinate system and $\mathbf{u_i}$ is the unit vector along the cable. The vector $\mathbf{l_i}$ represents the cable and it is oriented to start at the platform and point towards the robot frame. The pose of the platform is characterized by the position vector $\mathbf{r}$ and the rotation matrix $\mathbf{R}$ which transforms platform coordinates from the platform frame to world coordinates. The applied wrench $\mathbf{w_p} = [\mathbf{f_P^T}, \tau_\mathbf{P}^\mathsf{T}]^\mathsf{T}$ is composed from the applied force $\mathbf{f_P}$ and the applied torque $\tau_\mathbf{P}$. The kinematic closure equation for $i = 1, ..., m$ is given by:

$$\mathbf{l}_i = \mathbf{a}_i - \mathbf{r} - \mathbf{R}\mathbf{b_i} \tag{3.3}$$

3.1.2 Forward Kinematics

The forward kinematics (FK) problem is dual of IK analysis. It deals with the determination of the manipulator pose $\mathbf{q}$ given the cable lengths $\mathbf{l}$. It is a challenging problem where a closed form solution may not exist. For redundantly restrained CDPRs, one approach is to select a subset of n equations to solve for the manipulator pose $\mathbf{q}$ similar to rigid link parallel manipulators [117, 118]. From (3.3), we get k nonlinear equations ϑ_i for the forward kinematics

$$\vartheta(\mathbf{l}, \mathbf{r}, \mathbf{R}) = \|\mathbf{a}_i - \mathbf{r} - \mathbf{R}\mathbf{b_i}\|_2^2 - l_i^2 \tag{3.4}$$

for $i = 1, ..., k$ that form an over-constrained system for the case with $m > n$. In general, we cannot expect to solve the above equation analytically. A standard approach to this class of problems is the use of a least square method which minimizes the influence of cable length measurement errors.

3.1.3 Inverse Dynamics

The inverse dynamics(ID) [119] problem for CDPRs deals with calculation of a set of positive cable forces $\mathbf{f}$ to achieve desired motion in joint space described by $\mathbf{q_d}$,$\dot{\mathbf{q}}_\mathbf{d}$ and $\ddot{\mathbf{q}}_\mathbf{d}$. The resulting cable forces must satisfy the equations of motion as well as other constraints of the system. For redundantly restrained system, there exists greater number of actuators than number of DoFs. Therefore, there may exist infinite number of cable tension solutions to ID problem. To resolve the redundancy problem, the resolution of positive cable tensions can be formulated as an optimization problem which can be expressed in the form

$$\begin{aligned} \mathbf{f}^* &= minQ(\mathbf{f}) \\ s.tM(\mathbf{q_d}, \ddot{\mathbf{q}}_\mathbf{d}) + C(\mathbf{q_d}, \dot{\mathbf{q}}_\mathbf{d}) + G(\mathbf{q_d}) + \Gamma_{ext} &= -\mathbf{J}(\mathbf{q_d})^\mathsf{T}\mathbf{f} \\ 0 \leqslant \mathbf{f_{min}} &\leqslant \mathbf{f} \leqslant \mathbf{f_{max}} \end{aligned} \tag{3.5}$$

where $\mathbf{f}^*$ denotes the optimum cable forces solution subject to all constraints and the objective function $Q(\mathbf{f})$. The lower and upper bound on cable tensions are $\mathbf{f_{min}}$ and $\mathbf{f_{max}}$ respectively. A cable tension planner is necessary to implement the above optimization problem. The purpose of the cable tension planner is to solve for optimum positive cable forces. The objective function can minimize the sum of all cable tensions such that each cable tension falls within the bounds. An optimal set of cable tensions can be found using linear programming. The minimum-tension planner is useful for two reasons as it is computationally efficient and favorable for realtime implementation. Minimizing the cable total cable force would normally reduce the total energy consumption. If $Q(\mathbf{f})$ is a quadratic function like $\mathbf{f_1^2} + \mathbf{f_2^2} + \mathbf{f_3^2} + \mathbf{f_4^2} = \mathbf{f}^\mathsf{T}\mathbf{f}$ as in the case of planar CDPR, where the sum of cable forces squared is minimized, a continuous tension planner is used. The planner is based on quadratic programming which can solve for positive

cable tensions and provides continuous cable tension trajectories. This is due to the fact that the linear programming problem is susceptible to discontinuities in planned cable tension trajectories as the optimal solution is always at the corner of the convex hull of the feasible set. The cable force set $\mathbf{f}(\mathbf{t})$ required to produce described trajectory motion is determined by solving the Inverse dynamics (ID) problem at every instant of time.

The forward dynamics (FD) problem deals with solving the motion of the manipulator $\mathbf{q}(\mathbf{t})$ for a given cable force set $\mathbf{f}(\mathbf{t})$. Due to the non-linearity in the Equations of Motion (EOM), the equation is solved using numerical methods.

3.1.4 Static equilibrium condition

The cable tension is found to be critical in determining workspace. As seen in Fig. 3.1, in order to resist any external wrench applied on the moving platform, m cables must create unilateral tension forces $\mathbf{f}_i(i= 1,..,m)$ to achieve equilibrium of the n-Dof platform. The equilibrium conditions at the moving platform is given as:

$$\begin{bmatrix} \hat{\mathbf{l}}_1 & \hat{\mathbf{l}}_2 & \dots & \hat{\mathbf{l}}_m \\ \mathbf{b}_1 \times \hat{\mathbf{l}}_1 & \mathbf{b}_2 \times \hat{\mathbf{l}}_2 & \dots & \mathbf{b}_m \times \hat{\mathbf{l}}_m \end{bmatrix} \begin{bmatrix} f_1 \\ f_2 \\ \vdots \\ f_m \end{bmatrix} = - \begin{bmatrix} \mathbf{f}_P \\ \mathbf{m}_p \end{bmatrix} \tag{3.6}$$

Equation (3.6) is simplified as:

$$\mathbf{A}(\mathbf{r}, \mathbf{R})\mathbf{f} = \mathbf{W} \tag{3.7}$$

$\mathbf{A}$ is called the cable structure or wire matrix which allows us to investigate the existence and quality of the workspace, $\mathbf{f}$ is a column vector containing cable tensions and $\mathbf{W}$ is the sum of all external forces and moments including weight, inertial forces and moments. One can determine the tension factor(TF) by application of a singular value decomposition of the matrix $\mathbf{A}$ and determining the minimum and maximum value of the one-dimensional kernel. It is noteworthy that the structure matrix can be derived as the transpose of the Jacobian of the inverse kinematics, but generally it is easier to construct it based on the force

approach.

3.1.5 6 DoF Spatial Manipulator

As demonstrated in Section 3.1, the analysis of redundantly restrained CDPRs requires the model of the manipulator. We discuss the case of minimal fully actuated case with $m = n+1$ cable configuration for both CDPRs and CDSKCs. In this section, the generally studied model of 6 DOF spatial manipulator is presented. In subsequent sections, the model of 2, 3 and 4-DoF multi link manipulators are formulated, elucidating the increased complexity involved with the modeling of both the kinematic structure and the cable routing of multilink serial kinematic chains. The 6 DOF spatial manipulator is shown in Fig. 3.5. A typical completely restrained ($m = n + 1$ cables) CDPR consists of two fixed platforms and a moving platform with several cables. The geometry of each platform is considered circular, without loss of generality. The top and the bottom platforms are fixed, the moving platform is actuated by cables connected between two platforms. The frame of reference K_A and K_B is set at the center of the bottom and the center of mass of the moving platform B respectively. It is important to have the parameterized form of the cable attachment points.

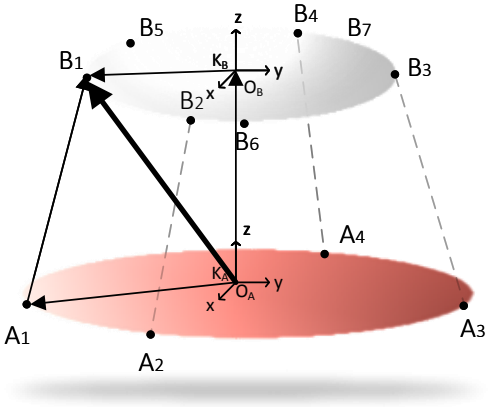

Figure 3.2: Geometry of the system

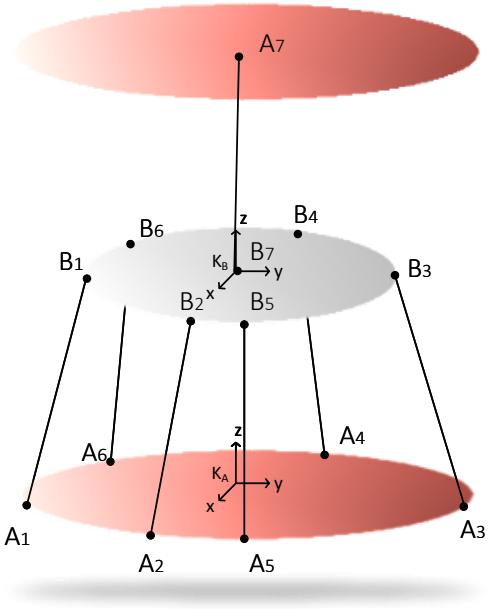

Figure 3.3: Type 1-6 CDPR Architecture

3.1.5.1 Kinematic geometry

$\mathbf{a_i}$ and $\mathbf{b_i}$ are expressed by radius R_a and angles θ in K_A, and radius R_b and angles ϕ in K_B.

$$\mathbf{a_i} = \begin{bmatrix} R_a c\theta_i \\ R_a s\theta_i \\ h_i \end{bmatrix}, \mathbf{b_i} = \begin{bmatrix} R_b c\phi_i \\ R_b s\phi_i \\ 0 \end{bmatrix} \; i = 1...m \tag{3.8}$$

where $c(.)$ and $s(.)$ notations are used for cosine and sine of the arguments respectively. The attachment points are fully expressed by $R_a, Rb, \theta_i, \phi_i$ and h_i. The end-effector pose of the manipulator can be described by $\mathbf{q}$=$[Px, Py, Pz, \alpha, \beta, \gamma]^\mathsf{T}$. From Section 3.1.1, the kinematic loop closure reads $A_iB_i = O_AO_B + O_BB_i - O_AA_i$ and in vector form as

$$\mathbf{l}_i = \mathbf{r} - \mathbf{a}_i + \mathbf{R}\mathbf{b_i} \tag{3.9}$$

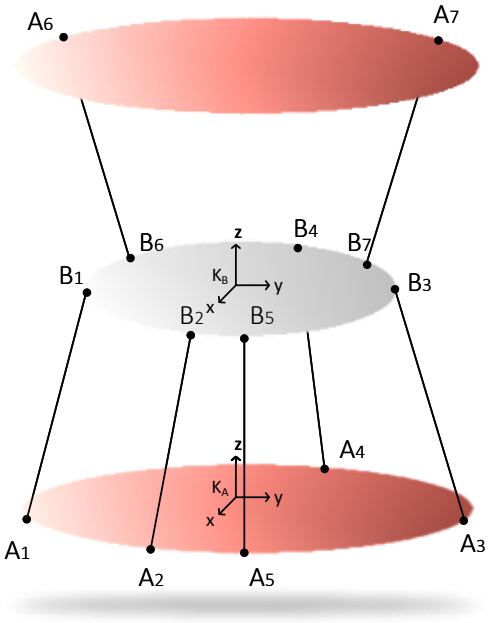

Figure 3.4: Type 2-5 CDPR Architecture

where $\mathbf{r}$ is the end-effector position vector ($\mathbf{r} = [P_x, P_y, P_z]^\mathsf{T}$) and the rotation matrix $\mathbf{R}$ is constructed using 3-2-1 intrinsic Euler angle representation such as

$$\mathbf{R} = \mathbf{R_x}(\alpha)\mathbf{R_y}(\beta)\mathbf{R_z}(\gamma) \tag{3.10}$$

$$= \begin{bmatrix} c\beta c\gamma & s\alpha s\beta c\gamma - c\alpha s\gamma & c\alpha s\beta c\gamma + s\alpha s\gamma \\ c\beta s\gamma & s\alpha s\beta s\gamma + c\alpha c\gamma & s\alpha s\beta s\gamma - s\alpha c\gamma \\ -s\beta & s\alpha c\beta & c\alpha c\beta \end{bmatrix} \tag{3.11}$$

$\boldsymbol{l} = [l_1, l_2, \ldots, l_m]^\mathsf{T}$ is the vector of actuated joint coordinates and $\boldsymbol{q}$=[$\boldsymbol{r}, \boldsymbol{\Theta}$] where $\boldsymbol{\Theta}$ represent the vector of three rotation angles. The Jacobian matrix can be determined by taking the time derivative of $\mathbf{l_i}$ for each cable ($i = 1...6$), which results in the relationship

$$\dot{\mathbf{l}}_i = \dot{\mathbf{r}} + \omega \times \mathbf{R}\mathbf{b}_i \tag{3.12}$$

The angular velocity of the end-effector with respect to K_A expressed in K_B is obtained as

$$\omega = \mathbf{S}\dot{\boldsymbol{\Theta}} \tag{3.13}$$

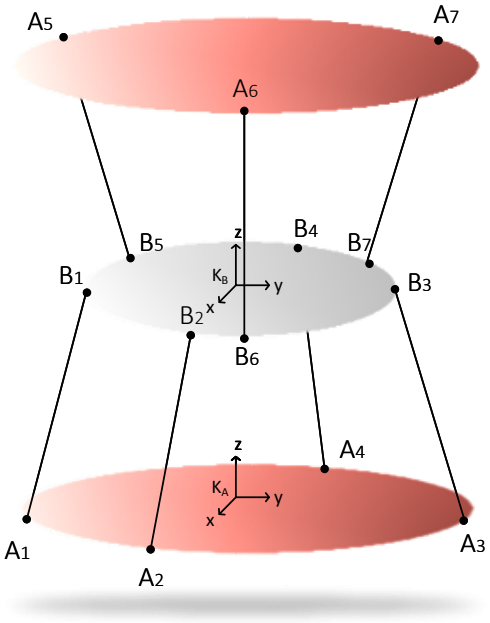

Figure 3.5: Type 3-4 CDPR Architecture

where

$$\omega = \begin{bmatrix} \omega_x \\ \omega_y \\ \omega_z \end{bmatrix}, \dot{\mathbf{\Theta}} = \begin{bmatrix} \dot{\alpha} \\ \dot{\beta} \\ \dot{\gamma} \end{bmatrix}, \mathbf{S} = \begin{bmatrix} 1 & 0 & -s\beta \\ 0 & c\alpha & s\alpha c\beta \\ 0 & -s\alpha c\beta & c\alpha c\beta \end{bmatrix} \tag{3.14}$$

It should be noted that $\mathbf{S}$ is dependent on the choice of generalized coordinates and may result in singularities as Euler angles have been used in this case for the purpose of elucidation. This could be avoided by twist or quaternion representations for generalized coordinates. The inverse Jacobian mapping $\mathbf{J}$ is derived as,

$$\dot{\mathbf{l}} = \mathbf{J}\dot{\mathbf{q}}, \mathbf{J} = \begin{bmatrix} \hat{\mathbf{l}}_1^\mathsf{T} & (\mathbf{b}_1 \times \hat{\mathbf{l}}_1)^\mathsf{T} \\ \hat{\mathbf{l}}_2^\mathsf{T} & (\mathbf{b}_2 \times \hat{\mathbf{l}}_2)^\mathsf{T} \\ \dots & \dots \\ \hat{\mathbf{l}}_m^\mathsf{T} & (\mathbf{b}_m \times \hat{\mathbf{l}}_m)^\mathsf{T} \end{bmatrix}_{m \times 6} \tag{3.15}$$

The wrench of the moving platform at static equilibrium is obtained as,

$$\mathbf{W} = -\mathbf{J}^\mathsf{T}\mathbf{f} \tag{3.16}$$

where $\mathbf{f}$ is the vector of cable forces and $\mathbf{W} = [F_x, F_y, F_z, M_x, M_y, M_z]^\mathsf{T}$ is the external wrench applied on the moving platform. The cable structure matrix or wire matrix can be simply expressed as $\mathbf{A} = -\mathbf{J}^\mathsf{T}$.

The dynamics of the manipulator can be modeled using Newton-Euler laws and expressing in the general form of Lagrangian equation of motion. The equations of motion for the spatial manipulator can be determined by taking sum of forces and the sum of moments about the center of mass G in K_P.

$$\begin{aligned} m\ddot{\mathbf{r}}_{OG} &= \sum \mathbf{F} \\ \mathbf{I_G}\dot{\omega} + \omega \times (\mathbf{I_G}\omega) &= \sum \mathbf{M} \end{aligned} \tag{3.17}$$

where m and $\mathbf{I_G}$ represent the mass and moment of inertia of the manipulator about the center of mass of the platform. The forces and moments acting on the system include the gravity force, the platform interaction force $\mathbf{F_G}$ and the platform interaction moment $\mathbf{M_G}$ at G, the cable force vectors for 7 cables. The cable force vector of cable i can be expressed as $\mathbf{f_i} = -\hat{\mathbf{l}}_i f_i$. The equations of motion can be expressed as

$$\begin{aligned} m\ddot{\mathbf{r}}_{OG} &= {}^{\mathbf{E}}\mathbf{R}_o m\mathbf{g} + \mathbf{F}_G - \sum_{i=1}^{7} \hat{\mathbf{l}}_i f_i \\ \mathbf{I_G}\dot{\omega} + \omega \times (\mathbf{I_G}\omega) &= \mathbf{M}_G - \sum_{i=1}^{7} \mathbf{b}_i \times \hat{\mathbf{l}}_i f_i \end{aligned} \tag{3.18}$$

Under no external forces on the manipulator, the external force vector $\mathbf{\Gamma_{ext}} = 0$. Eqn (3.18) follows the general form of Lagrangian equation of motion:

$$M(\mathbf{q}, \ddot{\mathbf{q}}) + C(\mathbf{q}, \dot{\mathbf{q}}) + G(\mathbf{q}) + \Gamma_{ext} = -\mathbf{J}^\mathsf{T}\mathbf{f} \tag{3.19}$$

Finally, using the definition of $\mathbf{f_i}$, J^T can be expressed as

$$\mathbf{J}^\mathsf{T} = \begin{bmatrix} \hat{\mathbf{l}}_1 & \hat{\mathbf{l}}_2 & \dots & \hat{\mathbf{l}}_m \\ \mathbf{b}_1 \times \hat{\mathbf{l}}_1 & \mathbf{b}_2 \times \hat{\mathbf{l}}_2 & \dots & \mathbf{b}_m \times \hat{\mathbf{l}}_m \end{bmatrix} \tag{3.20}$$

It can be observed that the (3.20) relates the cable forces to the manipulator motion and is the transpose of Jacobian matrix obtained from the kinematic

relationship (3.15).

3.1.5.2 Workspace Determination

An important property of the CDPR is the usable workspace. As aforementioned, there exist various definitions to express the workspace property. The wrench-closure workspace(WCW) is examined with the assumption that each external wrench can be balanced by tightening the cables, thus making WCW a geometric property of the robot. There are various approaches to calculate the workspace of the robot. The key approach used here is the analytical computation of boundary surfaces using Cramer's rule(which will also be extended to CDSKC's). The polynomial structure of the workspace hull will be presented for a given orientation of the platform. The workspace hull is constructed by the union of several boundary parts where the number of segments corresponds with the system redundancy. This is achieved through analytical derivation of null space vectors and evaluation of the regions that satisfy the WCC. A single boundary element can be obtained by analytically evaluating the determinant of the quadratic subsystem of the structure matrix. The simulation parameters are given in Appendix 1.

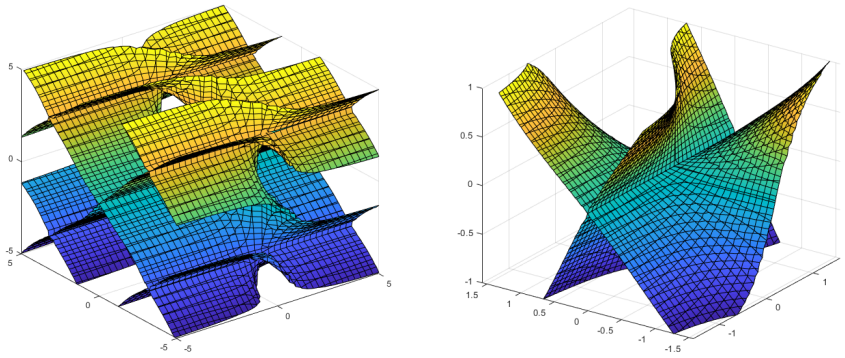

(a) Tensionable surface boundary **(b)** Boundary with limits

Figure 3.6: Tensionable workspace boundaries of 6-DOF Spatial CDPM 7 cables

For a CDPR shown in Fig. 3.5 with redundancy 1, Eqn. (3.7) can be rewritten

with $\mathbf{A_i}$ denoting the i^{th} column of $\mathbf{A}$.

$$\begin{aligned} \mathbf{A_{6\times 7}} &= \begin{bmatrix} \mathbf{A_1} & \mathbf{A_2} & \dots & \mathbf{A_7} \end{bmatrix} \\ \mathbf{A_1 f_1} + \mathbf{A_2 f_2} + \mathbf{A_3 f_3} + \cdots + \mathbf{A_7 f_7} &= \mathbf{W_{6\times 1}} \end{aligned} \tag{3.21}$$

The general approach for solving cable tensions using the pseudo inverse of $\mathbf{A}$. The equation reads

$$\begin{aligned} \mathbf{f} &= \mathbf{A}^{+}\mathbf{W} + N(\mathbf{A})\lambda \\ \|\mathbf{f}\| &:= \mathbf{A}^{+}[M\ddot{\mathbf{q}} + C\dot{\mathbf{q}} + G] \\ \mathbf{A} &= -\mathbf{J}^{\mathsf{T}} \end{aligned} \tag{3.22}$$

where $\|\mathbf{f}\|$ is the minimum norm solution of $\mathbf{Af} = \mathbf{W}$, $N(\mathbf{A})$ representing the null space or kernel of the cable structure matrix $\mathbf{A}$ and λ representing a 1-D vector in this system. In general it is an underdetermined R-dimensional vector, where R denotes the system redundancy. $\mathbf{A}^{+}(= \mathbf{A}^{\mathsf{T}}(\mathbf{A}\mathbf{A}^{\mathsf{T}})^{-1})$ is the pseudoinverse of $\mathbf{A}$ as the system is under-constrained. The necessary and sufficient condition for a pose to be inside the WCW is

$$\begin{aligned} rank(\mathbf{A}) &= 6 \\ \exists \mathbf{f} \in N(\mathbf{A}) &: \mathbf{f} > 0 \end{aligned} \tag{3.23}$$

The null space of $\mathbf{A}$ consists of all the homogeneous solutions of the equation $\mathbf{Af} = 0$. It can be stated that

$$\mathbf{A_1}N_1 + \mathbf{A_2}N_2 + \mathbf{A_3}N_3 + \cdots + \mathbf{A_6}N_6 = -\mathbf{A_7}N_7 \tag{3.24}$$

$$\begin{bmatrix} \mathbf{A_1} & \mathbf{A_2} & \dots & \mathbf{A_6} \end{bmatrix}_{6\times 6} \begin{bmatrix} N_1 \\ N_2 \\ \dots \\ N_6 \end{bmatrix}_{6\times 1} = -\begin{bmatrix} \mathbf{A_7}N_7 \end{bmatrix}_{6\times 1} \tag{3.25}$$

Using Cramer's rule, knowing that the matrix $\mathbf{A}$ is full rank, we obtain the

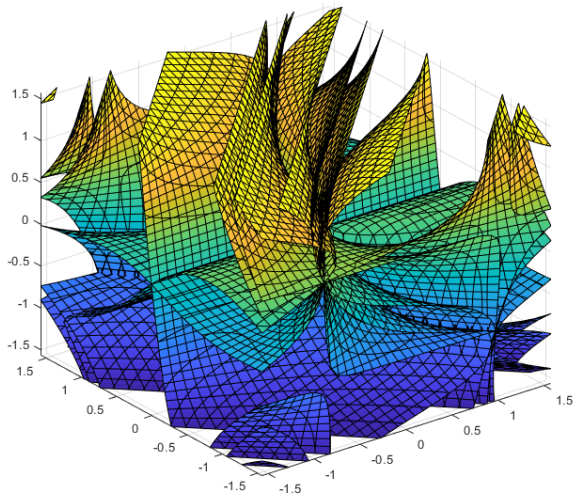

Figure 3.7: Orientation Workspace Boundaries

solutions by solving six sets of linear system in Eqn. (3.32).

$$
\begin{aligned}
N_1 &= \frac{\left|-\mathbf{A_7}N_7 \quad \mathbf{A_2} \quad \mathbf{A_3} \quad \mathbf{A_4} \quad \mathbf{A_5} \quad \mathbf{A_6}\right|}{\left|\mathbf{A_1} \quad \mathbf{A_2} \quad \mathbf{A_3} \quad \mathbf{A_4} \quad \mathbf{A_5} \quad \mathbf{A_6}\right|} \\
N_2 &= \frac{\left|\mathbf{A_1} \quad -\mathbf{A_7}N_7 \quad \mathbf{A_3} \quad \mathbf{A_4} \quad \mathbf{A_5} \quad \mathbf{A_6}\right|}{\left|\mathbf{A_1} \quad \mathbf{A_2} \quad \mathbf{A_3} \quad \mathbf{A_4} \quad \mathbf{A_5} \quad \mathbf{A_6}\right|} \\
N_3 &= \frac{\left|\mathbf{A_1} \quad \mathbf{A_2} \quad -\mathbf{A_7}N_7 \quad \mathbf{A_4} \quad \mathbf{A_5} \quad \mathbf{A_6}\right|}{\left|\mathbf{A_1} \quad \mathbf{A_2} \quad \mathbf{A_3} \quad \mathbf{A_4} \quad \mathbf{A_5} \quad \mathbf{A_6}\right|} \\
N_4 &= \frac{\left|\mathbf{A_1} \quad \mathbf{A_2} \quad \mathbf{A_3} \quad -\mathbf{A_7}N_7 \quad \mathbf{A_5} \quad \mathbf{A_6}\right|}{\left|\mathbf{A_1} \quad \mathbf{A_2} \quad \mathbf{A_3} \quad \mathbf{A_4} \quad \mathbf{A_5} \quad \mathbf{A_6}\right|} \\
N_5 &= \frac{\left|\mathbf{A_1} \quad \mathbf{A_2} \quad \mathbf{A_3} \quad \mathbf{A_4} \quad -\mathbf{A_7}N_7 \quad \mathbf{A_6}\right|}{\left|\mathbf{A_1} \quad \mathbf{A_2} \quad \mathbf{A_3} \quad \mathbf{A_4} \quad \mathbf{A_5} \quad \mathbf{A_6}\right|} \\
N_6 &= \frac{\left|\mathbf{A_1} \quad \mathbf{A_2} \quad \mathbf{A_3} \quad \mathbf{A_4} \quad \mathbf{A_5} \quad -\mathbf{A_7}N_7\right|}{\left|\mathbf{A_1} \quad \mathbf{A_2} \quad \mathbf{A_3} \quad \mathbf{A_4} \quad \mathbf{A_5} \quad \mathbf{A_6}\right|}
\end{aligned}
\tag{3.26}
$$

The null space is constructed by 1-dimensional basis. Therefore, N_7 is formulated as $N_7 = -\left|\mathbf{A_1} \quad \mathbf{A_2} \quad \mathbf{A_3} \quad \mathbf{A_4} \quad \mathbf{A_5} \quad \mathbf{A_6}\right|$. Under the consideration of spatial system

with single redundancy the polynomials can be stated as,

$$\begin{aligned} N_1 &: det(\mathbf{A_7}, \mathbf{A_2}, \mathbf{A_3}, \mathbf{A_4}, \mathbf{A_5}, \mathbf{A_6}) = 0, \\ N_2 &: det(\mathbf{A_1}, \mathbf{A_7}, \mathbf{A_3}, \mathbf{A_4}, \mathbf{A_5}, \mathbf{A_6}) = 0, \\ &\vdots \\ N_6 &: det(\mathbf{A_1}, \mathbf{A_2}, \mathbf{A_3}, \mathbf{A_4}, \mathbf{A_5}, \mathbf{A_7}) = 0, \\ N_7 &: det(\mathbf{A_1}, \mathbf{A_2}, \mathbf{A_3}, \mathbf{A_4}, \mathbf{A_5}, \mathbf{A_6}) = 0. \end{aligned} \tag{3.27}$$

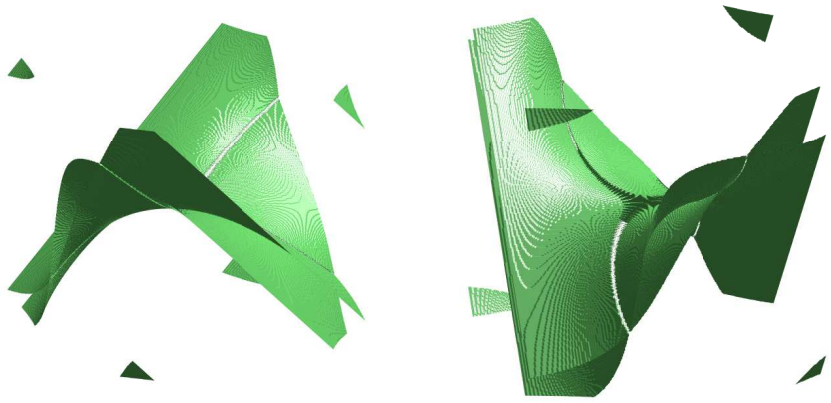

(a) Tensionable workspace atlas **(b)** Tensionable workspace atlas

Figure 3.8: Tensionable orientation WCW

The subscript of $N_{(.)}$ denotes the column which was dropped. The above equations are multivariate polynomials and represent the boundary of seven surface patches. The spatial system results in polynomial surfaces of degree three respectively. The WCW condition can be modified to the spatial CDPR which implies N_i $(i = 1, ..., 7)$ should be either be all positive or all negative, the critical case being Eqn. (3.27). The closed form solution for N_i after substituting the geometry parameters is given by

$$N_i = N_i(\boldsymbol{r}, \boldsymbol{\Theta}, \mathbf{a}, \mathbf{b}) \tag{3.28}$$

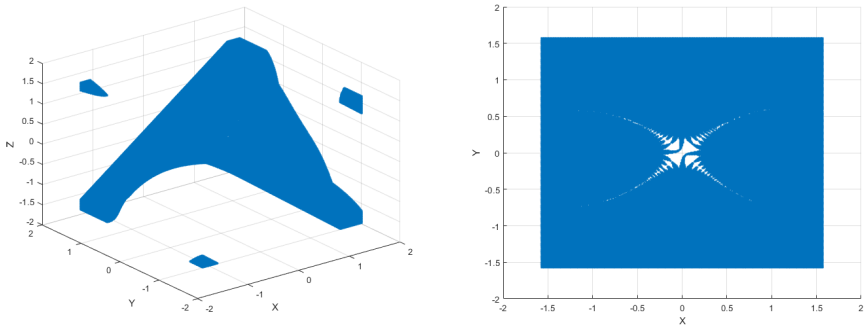

(a) Orientation Workspace **(b)** Projection onto Plane

Figure 3.9: Tensionable orientation workspace of 6-DOF Spatial CDPM

Three pose variables are set to constant values in order to plot the WCW in three dimensional space. In order to obtain the polynomial form of N_i, the transcedental terms can be eliminated by Weierstrass substitution (tangent half-angle substitution).

$$T = \tan\frac{\beta}{2}, \sin\beta = \frac{2T}{1+T^2}, \cos\beta = \frac{1-T^2}{1+T^2} \tag{3.29}$$

where β is a pose variable. The WCW will consist of 2 regions, one generated from $N_i \geqslant 0$ and other generated from $N_i \leqslant 0$, each spans $\mathbb{R}^3$ as follows, For a constant orientation WCW,

$$\begin{aligned} {I^+}_j &= \{(P_x, P_y, P_z) \mid N_j(P_x, P_y, P_z) > 0\} \\ {I^-}_j &= \{(P_x, P_y, P_z) \mid N_j(P_x, P_y, P_z) < 0\} \\ I_{WCW} &= ({I^+}_1 \cap {I^+}_2 \cdots \cap {I^+}_7) \cup ({I^-}_1 \cap {I^-}_2 \cdots \cap {I^-}_7) \end{aligned} \tag{3.30}$$

The same formulation is extended to investigate the WCW of spatial CDPR with $n+2$ cables. The null space is spanned by two column vectors $\aleph_1$ and $\aleph_2$. It is desired to find the two column vectors forming a set of basis for the null space of matrix $\mathbf{A}_{6\times 8}$.

$$\begin{aligned} \mathbf{A_1}N_1 + \mathbf{A_2}N_2 + \mathbf{A_3}N_3 + \cdots + \mathbf{A_6}N_6 + \mathbf{A_7}N_7 + \mathbf{A_8}N_8 = 0 \\ \mathbf{A_1}N_1 + \mathbf{A_2}N_2 + \mathbf{A_3}N_3 + \cdots + \mathbf{A_6}N_6 = -\mathbf{A_7}N_7 - \mathbf{A_8}N_8 \end{aligned} \tag{3.31}$$

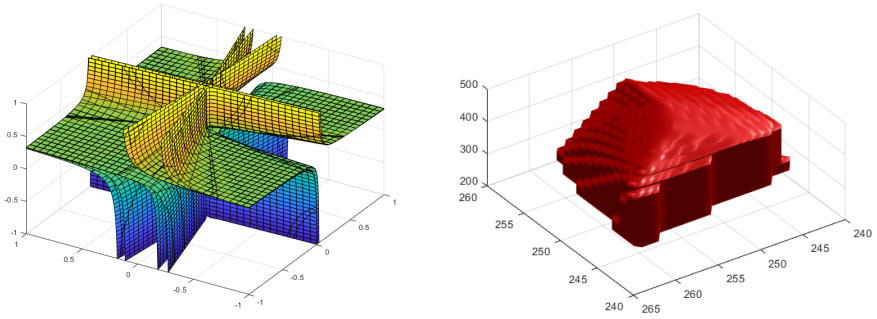

(a) Tensionable surface boundary **(b)** Tensionable position workspace atlas

Figure 3.10: Tensionable translational workspace of 6-DOF Spatial CDPM

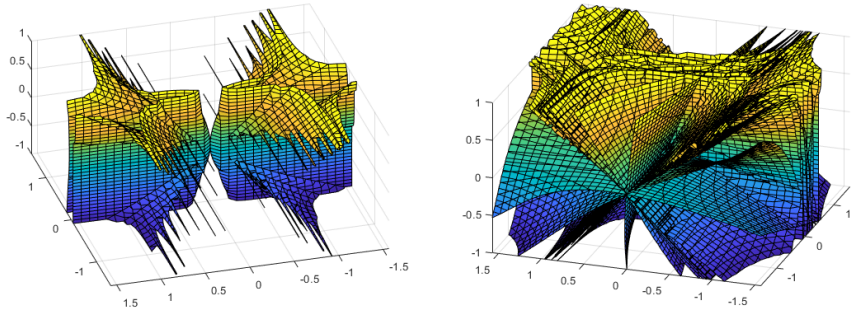

(a) Tensionable surface boundaries **(b)** Tensionable workspace atlas

Figure 3.11: Tensionable workspace boundaries of 6-DOF Spatial CDPM 8 cables

$$\begin{bmatrix} \mathbf{A_1} & \mathbf{A_2} & \dots & \mathbf{A_6} \end{bmatrix}_{6\times 6} \begin{bmatrix} N_1 \\ N_2 \\ \dots \\ N_6 \end{bmatrix}_{6\times 1} = \begin{bmatrix} -\mathbf{A_7} N_7 - \mathbf{A_8} N_8 \end{bmatrix}_{6\times 1} \tag{3.32}$$

By applying Cramer's rule, we obtain

$$
\begin{aligned}
N_1 &= \frac{\left|-\mathbf{A_7}N_7 - \mathbf{A_8}N_8 \quad \mathbf{A_2} \quad \mathbf{A_3} \quad \mathbf{A_4} \quad \mathbf{A_5} \quad \mathbf{A_6}\right|}{\left|\mathbf{A_1} \quad \mathbf{A_2} \quad \mathbf{A_3} \quad \mathbf{A_4} \quad \mathbf{A_5} \quad \mathbf{A_6}\right|} \\
N_2 &= \frac{\left|\mathbf{A_1} \quad -\mathbf{A_7}N_7 - \mathbf{A_8}N_8 \quad \mathbf{A_3} \quad \mathbf{A_4} \quad \mathbf{A_5} \quad \mathbf{A_6}\right|}{\left|\mathbf{A_1} \quad \mathbf{A_2} \quad \mathbf{A_3} \quad \mathbf{A_4} \quad \mathbf{A_5} \quad \mathbf{A_6}\right|} \\
N_3 &= \frac{\left|\mathbf{A_1} \quad \mathbf{A_2} \quad -\mathbf{A_7}N_7 - \mathbf{A_8}N_8 \quad \mathbf{A_4} \quad \mathbf{A_5} \quad \mathbf{A_6}\right|}{\left|\mathbf{A_1} \quad \mathbf{A_2} \quad \mathbf{A_3} \quad \mathbf{A_4} \quad \mathbf{A_5} \quad \mathbf{A_6}\right|} \\
N_4 &= \frac{\left|\mathbf{A_1} \quad \mathbf{A_2} \quad \mathbf{A_3} \quad -\mathbf{A_7}N_7 - \mathbf{A_8}N_8 \quad \mathbf{A_5} \quad \mathbf{A_6}\right|}{\left|\mathbf{A_1} \quad \mathbf{A_2} \quad \mathbf{A_3} \quad \mathbf{A_4} \quad \mathbf{A_5} \quad \mathbf{A_6}\right|} \\
N_5 &= \frac{\left|\mathbf{A_1} \quad \mathbf{A_2} \quad \mathbf{A_3} \quad \mathbf{A_4} \quad -\mathbf{A_7}N_7 - \mathbf{A_8}N_8 \quad \mathbf{A_6}\right|}{\left|\mathbf{A_1} \quad \mathbf{A_2} \quad \mathbf{A_3} \quad \mathbf{A_4} \quad \mathbf{A_5} \quad \mathbf{A_6}\right|} \\
N_6 &= \frac{\left|\mathbf{A_1} \quad \mathbf{A_2} \quad \mathbf{A_3} \quad \mathbf{A_4} \quad \mathbf{A_5} \quad -\mathbf{A_7}N_7 - \mathbf{A_8}N_8\right|}{\left|\mathbf{A_1} \quad \mathbf{A_2} \quad \mathbf{A_3} \quad \mathbf{A_4} \quad \mathbf{A_5} \quad \mathbf{A_6}\right|}
\end{aligned}
\tag{3.33}
$$

We obtain the first basis $\aleph_1$ by choosing $N_7 = -\left|\mathbf{A_1} \quad \mathbf{A_2} \quad \mathbf{A_3} \quad \mathbf{A_4} \quad \mathbf{A_5} \quad \mathbf{A_6}\right|$ and $N_8 = 0$. Similarly, the second basis $\aleph_2$ as $N_7 = 0$ and $N_8 = -\left|\mathbf{A_1} \quad \mathbf{A_2} \quad \mathbf{A_3} \quad \mathbf{A_4} \quad \mathbf{A_5} \quad \mathbf{A_6}\right|$. Hence the nullspace of $\mathbf{A}$ is formulated as:

$$
N(\mathbf{A}) = \left(\begin{bmatrix} \left|\mathbf{A_7} \quad \mathbf{A_2} \quad \dots \quad \mathbf{A_6}\right| \\ \left|\mathbf{A_1} \quad \mathbf{A_7} \quad \dots \quad \mathbf{A_6}\right| \\ \vdots \\ \left|\mathbf{A_1} \quad \mathbf{A_2} \quad \dots \quad \mathbf{A_7}\right| \\ -\left|\mathbf{A_1} \quad \mathbf{A_2} \quad \dots \quad \mathbf{A_6}\right| \\ 0 \end{bmatrix}, \begin{bmatrix} \left|\mathbf{A_8} \quad \mathbf{A_2} \quad \dots \quad \mathbf{A_6}\right| \\ \left|\mathbf{A_1} \quad \mathbf{A_8} \quad \dots \quad \mathbf{A_6}\right| \\ \vdots \\ \left|\mathbf{A_1} \quad \mathbf{A_2} \quad \dots \quad \mathbf{A_8}\right| \\ 0 \\ -\left|\mathbf{A_1} \quad \mathbf{A_2} \quad \dots \quad \mathbf{A_6}\right| \end{bmatrix} \right)
\tag{3.34}
$$

It can be seen from Eqn. (3.34) that there are two cases to be considered that determine the sign of $N_{ij}(i = 1, 2); j = (1, ..., 6)$ either positive or negative which

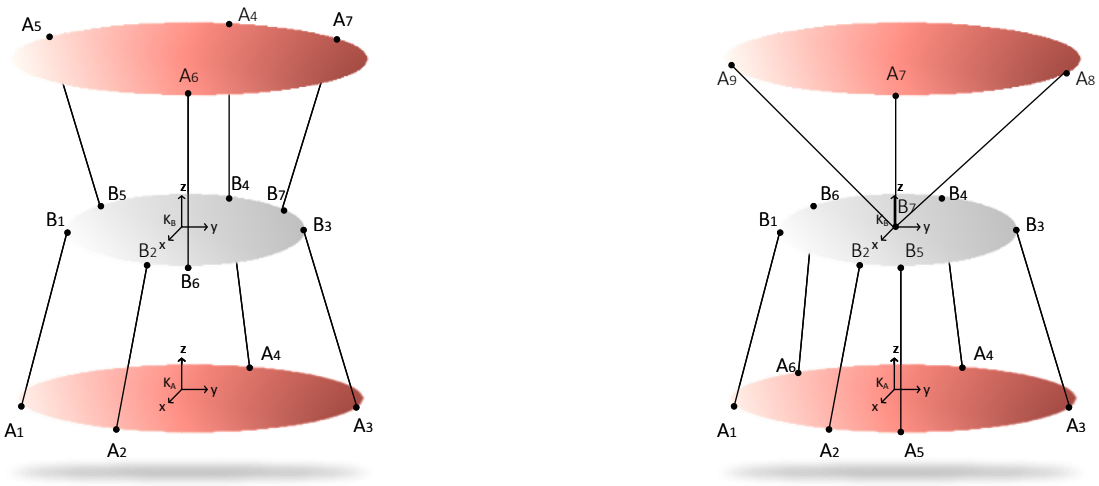

(a) **(b)**

Figure 3.12: Spatial CDPR with (a) n+2 cables (b) n+3 cable architecture

will constitute the WCW.

$$\begin{aligned} Case1\{q \mid N_{17} = N_{28} = -\left|\mathbf{A_1} \quad \mathbf{A_2} \quad \dots \quad \mathbf{A_6}\right| > 0\} \\ Case2\{q \mid N_{17} = N_{28} = -\left|\mathbf{A_1} \quad \mathbf{A_2} \quad \dots \quad \mathbf{A_6}\right| < 0\} \end{aligned} \tag{3.35}$$

The necessary and sufficient condition to satisfy the WCW applied to Case 1 implies

$$\forall i = 1 \dots 6 \exists \lambda_1 > 0, \lambda_2 > 0 s.t. N_{1i}\lambda_1 + N_{1i}\lambda_2 > 0 \tag{3.36}$$

The condition is to evaluate the existence of λ_1 and λ_2 which is equivalent to finding a feasible region in 2D-space. There are total 8 configurations considering the different signs of N_{1i} and N_{2i}. The inequality formulation is given as

$$\begin{aligned} N_{11}\lambda_1 + N_{21}\lambda_2 > 0 \\ N_{12}\lambda_1 + N_{22}\lambda_2 > 0 \\ N_{13}\lambda_1 + N_{23}\lambda_2 > 0 \\ N_{14}\lambda_1 + N_{24}\lambda_2 > 0 \\ N_{15}\lambda_1 + N_{25}\lambda_2 > 0 \\ N_{16}\lambda_1 + N_{26}\lambda_2 > 0 \end{aligned} \tag{3.37}$$

The feasible region is defined as the intersection of the all the areas expressed by Eqn. (3.37). In the case of a nine-cable robot [120], the base of the nullspace is composed by three nine-component vectors, a linear combination of which may provide the desired homogeneous solutions. $N(\mathbf{A}) \in \mathbb{R}^{9\times3}$, the matrix whose columns $\aleph_1$, $\aleph_2$ and $\aleph_3$ generate the nullspace. The inequality formulation is given where N_{ij} are the components of the null space vector which can analytically derived using Cramer's rule as discussed in the previous section. Here the Eqn. (3.38) shows that either it has no solution or in the 3-D space generated by λ_1, λ_2 and λ_3 it determines a polyhedral angle with vertex in the origin. If the polyhedral angle exists, there is an infinite number of sets $(\lambda_1, \lambda_2, \lambda_3)$ containing inside the polyhedral angle satisfying the equation. The analytical formulation discussed above can be extended to nine-wire configuration as well.

$$\begin{aligned}
N_{11}\lambda_1 + N_{12}\lambda_2 + N_{13}\lambda_3 > 0 \\
N_{21}\lambda_1 + N_{22}\lambda_2 + N_{23}\lambda_3 > 0 \\
N_{31}\lambda_1 + N_{32}\lambda_2 + N_{33}\lambda_3 > 0 \\
N_{41}\lambda_1 + N_{42}\lambda_2 + N_{43}\lambda_3 > 0 \\
N_{51}\lambda_1 + N_{52}\lambda_2 + N_{53}\lambda_3 > 0 \\
N_{61}\lambda_1 + N_{62}\lambda_2 + N_{63}\lambda_3 > 0 \\
N_{71}\lambda_1 + N_{72}\lambda_2 + N_{73}\lambda_3 > 0 \\
N_{81}\lambda_1 + N_{82}\lambda_2 + N_{83}\lambda_3 > 0 \\
N_{91}\lambda_1 + N_{92}\lambda_2 + N_{93}\lambda_3 > 0
\end{aligned} \tag{3.38}$$

The wrench feasible workspace of 6 DoF spatial manipulator driven by 8 cables crossed configuration is used for wide range of applications is shown in Fig. 3.13. The WFW was calculated using the principles explained in the previous section. The WFW is the set of poses of its mobile platform for which the cables can balance any wrench in a specified set of wrenches, such that the tension in each cable remains within a prescribed range. It takes into account both the requirement of non-negative cable tension and the maximum admissible cable tension.

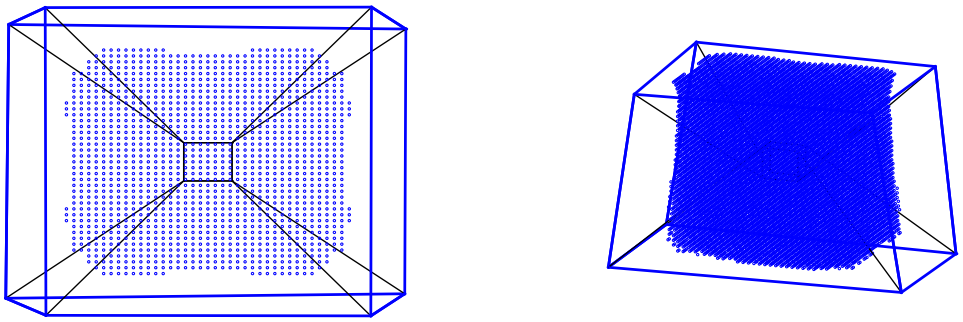

(a) CDPR with n+2 workspace **(b)** Wrench Feasible Workspace

Figure 3.13: 6-DOF Spatial CDPR

3.2 One- joint kinematic chain

The modeling of the kinematic and dynamics for CDPRs were introduced in the previous section. The direct kinematics and inverse dynamics problems for CDPMs are quite challenging compared to that of traditional rigid link manipulators. It was observed that the Jacobian matrix is required for each system depending on the manipulator structure. For a single body manipulator, owing to the simplicity of the manipulator design and single way of cable routing the derivation of Jacobian is relatively straightforward. However for CDKSCs, the kinematic chain and the cable routing presents challenges in individually formulating the system model. This motivates the need for investigating the model for cable driven serial kinematic chains.

3.2.1 Modeling of single revolute joint

A single revolute joint with a vertical axis is shown in Fig. 3.14. The dimension of the joint constraint system is 5. Let $\mathcal{W}$ be its 5-dimensional constraint wrench system, $\mathcal{W}$ =Span($\rho^{\perp}$). These 5 independent wrenches can be complemented to a basis of $se(3)^*$ by a force ψ with axis non-coplanar with the revolute axis.

$$\mathcal{W} \oplus Span(\psi) = se(3)^* \tag{3.39}$$

(a) **(b)**

Figure 3.14: A single revolute joint with two unilateral force constraints

Consider another force φ on a different axis also not reciprocal to the joint rotation. This force φ can be decomposed into two non-zero components one in Span(ψ) and one in $\mathcal{W}$. Hence, it is possible to apply two unilateral force constraints along ψ and φ which will

1. immobilize the joint and
2. transmit a nonzero wrench through the joint to the base.

It is only sufficient to chose the sign of ψ and φ such that they try to turn the joint in opposite ways. This is illustrated in the Fig. 3.14(a). If ψ and φ are on the same line, they can still be used to fix the joint (as long as they have opposite directions) however they could not then apply a force through the joint. However, this ability, to transmit a force onto the predecessor link, is the key to the solution when there are more joints. As long as the axes of ψ and φ are in two different vertical planes, a basis of $\mathcal{W}$ can be chosen in such a way that all coordinates of φ will be nonzero and the transmitted force through the joint will not belong to any of the coordinate subspaces of $\mathcal{W}$. This property will be used to create novel routing schemes which will be explained in the next chapter.

3.2.2 Kinematic Analysis

The rigid link rotates by two pulling cables that are oppositely attached on the link. The external force is applied normal to the link direction. Applying static

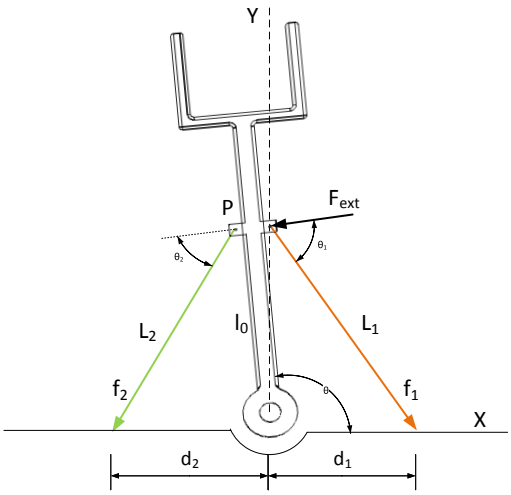

Figure 3.15: R-joint constrained by planar cables

equilibrium condition $\mathbf{Af} = \mathbf{W}$,

$$-\begin{bmatrix} l_0 cos\theta_1 & -l_0 cos\theta_2 \end{bmatrix} \begin{bmatrix} f_1 \\ f_2 \end{bmatrix} = \mathbf{W} \tag{3.40}$$

where $\mathbf{f} = \begin{bmatrix} f_1 & f_2 \end{bmatrix}^{\mathsf{T}}$ is the vector of tensions and the cable space Jacobian is defined by

$$\begin{bmatrix} \dot{L}_1 \\ \dot{L}_2 \end{bmatrix} = \begin{bmatrix} l_0 cos\theta_1 \\ -l_0 cos\theta_2 \end{bmatrix} \dot{\theta} \tag{3.41}$$

which is equivalent to $\dot{\mathbf{l}} = \mathbf{J}\dot{\mathbf{q}}$.

The revolute joint shown in Fig. 3.16 is fixed by cable lines not coplanar but perpendicular to the joint axis. There exist two forces $\mathbf{f}_1$ and $\mathbf{f}_1$, along the lines shown, which constrain the moving link. The reason is that the moments with respect to the rotation axis of any such forces have opposite signs. Therefore, the five-plane of bi-lateral constraint wrenches, together with the two unilateral force wrenches, each in a different half-space, span the whole wrench space and allow any wrench to be generated as a sum of a reciprocal wrench (in the five-hyperplane) and a positive linear combination of the two cable forces. As a result, the two forces can block/control the joint and can transmit a resultant wrench to the base link. The resultant is a wrench with axis perpendicularly intersecting the

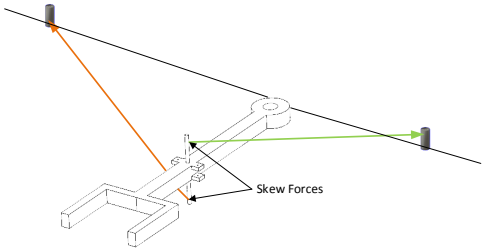

Figure 3.16: R-joint constrained by non-coplanar cables

common normal of the two cable lines as well as the joint axis. This is because in the span of two skew forces there are no pure forces apart from the (multiples of) the generators themselves.

3.2.3 Modeling of Spherical Joint Manipulator

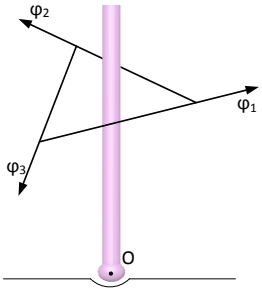

Figure 3.17: Spherical joint at Origin O

Consider a spherical joint S with the 3-dimensional constraint system. S consists of three forces with axes through O. Let the span of three other non-concurrent and linearly independent forces φ_1, φ_2, φ_3 complement S to $se(3)^*$.

$$S \oplus Span(\varphi_1, \varphi_2, \varphi_3) = se(3)^* \tag{3.42}$$

There are multiple ways to consider φ_1, φ_2, φ_3. One way is to consider them

coplanar (on a plane π not containing O) along the sides of triangle shown in Fig. 3.17. Another force φ_4 is considered which doesn't contain the origin and outside plane π. Then φ_4 can be decomposed into two non-zero components: a force through O and another in π, $\varphi_4 = \varphi_4^O + \varphi_4^\pi$. This implies, after a possible change of sign, the four forces φ_i can be used as unilateral constraints which fix the joint and transmit a non-zero force through 0. To choose the directions, it is necessary that the perspective projection of $-\varphi_4$ from O onto π, $-\varphi_4$ is in Cone(φ_1, φ_2, φ_3). If φ_4 is away from $\triangle A_1A_2A_3$, the directions of φ_1, φ_2, φ_3 and $-\varphi_4$ must be such that they "try to turn" $\triangle A_1A_2A_3$ in π the same way. The geometric descriptions of various convex cones including three forces in the plane is described in [4], previous chapter. If φ_4 is chosen in π , it cannot transmit a non-zero force through O , If If φ_4 misses each point A_i, a basis of $\mathcal{M}$ can be chosen so that the transmitted force is not in any coordinate plane.

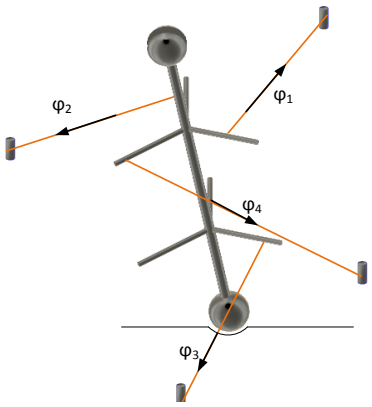

Figure 3.18: Spherical joint constrained by four cables

The spherical joint constrained by four cables, three of them lying in the same plane are shown in Fig. 3.18. The forbidden area is the triangle plane formed by the forces φ_1, φ_2, φ_4. When two of the forces lie in the same plane, the forbidden area becomes a prism containing the forces as indicated in the Fig. 3.19. In the illustration, the forces φ_{1s} and φ_{2s} are in the same plane.

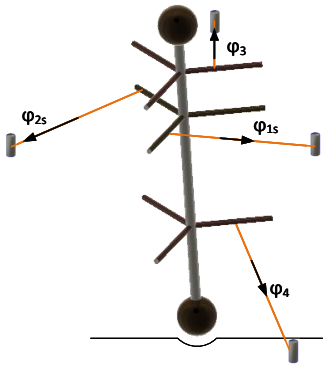

Figure 3.19: Spherical joint constrained by four cables with two forces in the same plane

3.2.4 Kinematic Analysis

The primitive form of spatial CDSKC is single link CDPR such as 3-dof ball joint manipulator as shown in Fig. 3.20. These manipulators can be seen as parallel manipulators with cables. These CDPRs with multiple rigid links form CDSKCs as shown in Fig. 4.16b. So it is important to study and understand the kinematics and statics of single link CDPRs. The manipulator possesses three rotational degrees of freedom where the end-effector is constrained to the base frame at O through a ball joint. The 3-dof system is actuated by 4 cables and is a completely restrained system. The cable attachments for cable i at the base and the end-effector are denoted by A_i and B_i (i= 1,..,4), respectively. The end-effector pose can be described by $\mathbf{q} = [\alpha, \beta, \gamma]^\mathsf{T}$, where α, β and γ represent the xyz- Euler angles of the spherical joint, respectively. The rotational matrix ${}^{\mathbf{O}}\mathbf{R}_E$ transforms a vector expressed in frame F_E to F_O, where

$$ {}^{O}R_E(\mathbf{q}) = \begin{bmatrix} c\beta c\gamma & -c\beta s\gamma & s\beta \\ c\alpha s\gamma + s\alpha s\beta c\gamma & c\alpha c\gamma - s\alpha s\beta s\gamma & -s\alpha c\beta \\ s\alpha s\gamma - c\alpha s\beta c\gamma & s\alpha c\gamma + c\alpha s\beta s\gamma & c\alpha c\beta \end{bmatrix} \tag{3.43} $$

The cable vector $\mathbf{l}_i$ for cable i with respect to F_E is described as

$$ {}^{E}\mathbf{l}_i = -{}^{\mathbf{E}}\mathbf{R}_O {}^{\mathbf{O}}\mathbf{r}_{OA_i} + {}^{\mathbf{E}}\mathbf{r}_{OB_i} \tag{3.44} $$

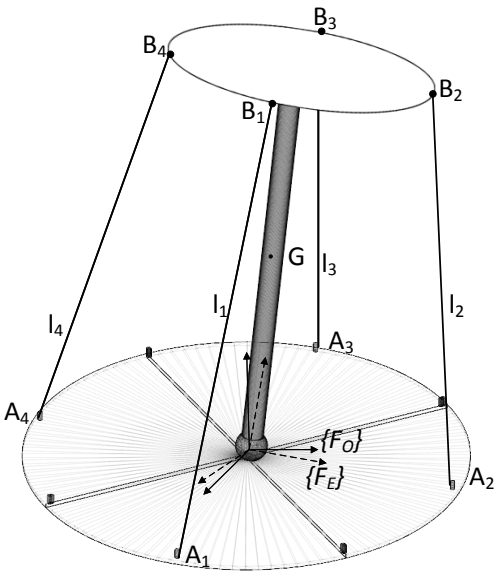

Figure 3.20: Spherical joint with unilateral force constraints

From Eqn. (3.43) and Eqn. (3.44), the cable length l_i can be expressed with respect to $\mathbf{q}$ as $l_i = \|\mathbf{l}_i\|$. The inverse kinematics is solved by solving for cable lengths.

The Jacobian matrix is determined by taking time derivative of l_i for each cable. The time derivative of the length of the cable is given as $\hat{l}_i = \hat{\mathbf{l}}_i \cdot \dot{\mathbf{l}}_i$. Since $\mathbf{r}_{OA_i}$ is fixed to the inertial frame, the derivative is null. The time derivative of vector $\mathbf{r}_{OB_i}$ in F_E is expressed as $\dot{\mathbf{r}}_{OB_i} = \omega_E \times \mathbf{r}_{OB_i}$, where ω_E is the absolute angular velocity of the end-effector. The kinematic relationship is given as

$$\dot{l}_i = (\mathbf{r}_{OB_i} \times \hat{l}_i) \cdot \omega_E \tag{3.45}$$

The angular velocity of the end-effector can be expressed in the form

$$\omega = \mathbf{S}\dot{\boldsymbol{q}} \tag{3.46}$$

where

$$\omega = \begin{bmatrix} \omega_x \\ \omega_y \\ \omega_z \end{bmatrix}, \dot{\mathbf{q}} = \begin{bmatrix} \dot{\alpha} \\ \dot{\beta} \\ \dot{\gamma} \end{bmatrix}, \mathbf{S} = \begin{bmatrix} c\beta c\gamma & s\gamma & 0 \\ -c\beta s\gamma & c\gamma & 0 \\ s\beta & 0 & 1 \end{bmatrix} \tag{3.47}$$

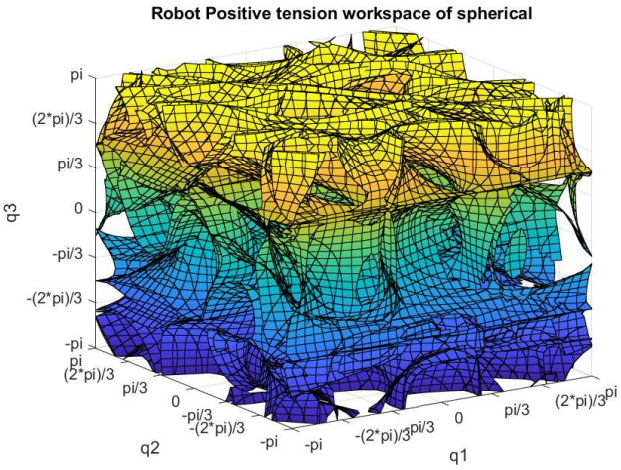

Figure 3.21: Workspace Boundaries using analytical null space formulation

It should be noted that **S** is dependent on the choice of generalized coordinates and may result in singularities as Euler angles have been used in this case for the purpose of elucidation. This could be avoided by twist or quaternion representations for generalized coordinates. The invese Jacobian mapping **J** is derived as,

$$\dot{\mathbf{l}} = \mathbf{J}\dot{\mathbf{q}}, \mathbf{J} = \begin{bmatrix} (\mathbf{r}_{OB_1} \times \hat{\mathbf{l}}_1)^\mathsf{T} \\ (\mathbf{r}_{OB_2} \times \hat{\mathbf{l}}_2)^\mathsf{T} \\ (\mathbf{r}_{OB_3} \times \hat{\mathbf{l}}_3)^\mathsf{T} \\ (\mathbf{r}_{OB_4} \times \hat{\mathbf{l}}_4)^\mathsf{T} \end{bmatrix} \tag{3.48}$$

3.2.4.1 Statics Analysis of Spherical Joint Manipulator

Assuming the cable tensions, $\mathbf{t}_i (i = 1, 2, 3, 4)$ provide the total required torques τ, the force equilbrium equation can be defined using the Jacobian matrix $\boldsymbol{J}$ as

$$\sum_{i=1}^{4} \widehat{l}_i . t_i = \boldsymbol{f} \tag{3.49}$$

$$\sum_{i=1}^{4} J_i . t_i = \boldsymbol{\tau} \tag{3.50}$$

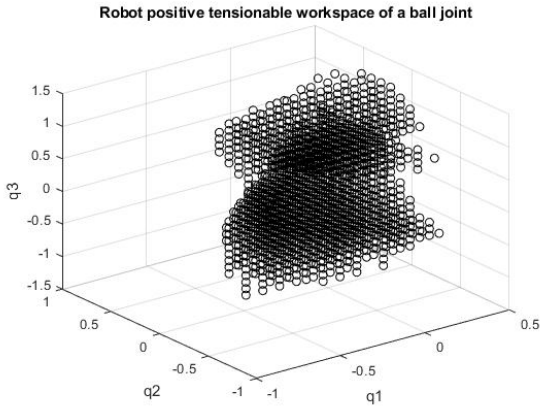

Figure 3.22: Wrench closure workspace of 3-DOF ball joint with no cable collision constraints

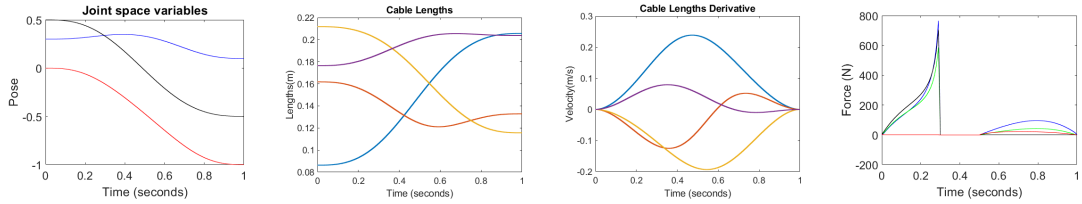

(a) **(b)** **(c)** **(d)**

Figure 3.23: Results of inverse kinematics and inverse dynamic analysis for a test trajectory. Infeasible solution of cable forces for the trajectory

$$J_i = \mathbf{r}_i \times \widehat{\mathbf{l}}_i \tag{3.51}$$

where the cable vector is denoted as $\boldsymbol{l}_i$ and the vector from joint center to cable ending point as $\boldsymbol{r}_i$. The jacobian matrix $\mathbf{J} : \mathbf{R^4} \mapsto \mathbf{R^3}$ maps cable tensions to the spherical joint torque(here considering wrist joint torque as an example). We can obtain the tension solution:

$$\mathbf{T} = \mathbf{J}^{+}\boldsymbol{\tau} + \lambda N(\mathbf{J}) \tag{3.52}$$

where $(\mathbf{J}^{+})$ is the pseudo-inverse matrix of $\mathbf{J}$. The cable tensions have redundant solutions to optimize. Linear and quadratic programming approaches are employed to calculate cable tensions. Quadratic programming is used because of its capacity to avoid discontinuities in the solution and smoothen the tension trajectory.

Mathemetically, it is expressed as:

$$\begin{aligned} minf(t) &= \frac{1}{2}\mathbf{T}^{\mathsf{T}}\mathbf{T} \\ s.t.\mathbf{T}_{min} \leqslant \mathbf{J}^{+}\boldsymbol{\tau} + \lambda N(\mathbf{J}) &\leqslant \mathbf{T}_{max} \end{aligned} \tag{3.53}$$

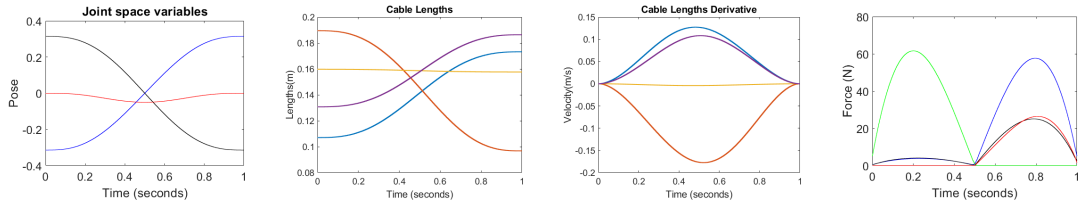

(a) **(b)** **(c)** **(d)**

Figure 3.24: Results of inverse kinematics and inverse dynamic analysis for a test trajectory. Feasible solution of cable forces for the specified trajectory

3.2.4.2 Dynamic Modeling

The dynamics of the manipulator can be modeled using Newton-Euler laws and expressing in the general form of Lagrangian equation of motion. The equations of motion for the ball joint manipulator can be determined by taking the sum of moments about the inertial point of rotation O.

$$\mathbf{I_O}\dot{\omega} + \omega \times (\mathbf{I_O}\omega) = \sum \mathbf{M} \tag{3.54}$$

where $\mathbf{I_O}$ represent the moment of inertia of the manipulator about O. The forces and moments acting on the system include the gravity force, the joint interaction force $\mathbf{F_O}$ and the joint interaction moment $\mathbf{M_O}$ at O, the cable force vectors for 4 cables. The cable force vector of cable i can be expressed as $\mathbf{f_i} = -\hat{\mathbf{l}}_i f_i$. The equations of motion can be expressed as

$$\mathbf{I_O}\dot{\omega} + \omega \times (\mathbf{I_O}\omega) = \mathbf{r}_{OG} \times ({}^{\mathbf{E}}\mathbf{R}_o m\mathbf{g}) + \mathbf{M}_O + \sum_{i=1}^{4} \mathbf{r}_{OB_i} \times \hat{\mathbf{l}}_i f_i \tag{3.55}$$

Under no external forces on the manipulator, the external force vector $\mathbf{\Gamma_{ext}} = 0$. Eqn (3.55) follows the general form of Lagrangian equation of motion:

$$M(\mathbf{q}, \ddot{\mathbf{q}}) + C(\mathbf{q}, \dot{\mathbf{q}}) + G(\mathbf{q}) + \Gamma_{ext} = -\mathbf{J}^{\mathsf{T}}\mathbf{f} \tag{3.56}$$

Finally, using the definition of $\mathbf{f_i}$, J^{T} can be expressed as

$$\mathbf{J}^{\mathsf{T}} = \begin{bmatrix} \mathbf{r}_{OB_1} \times \hat{\mathbf{l}}_1 & \mathbf{r}_{OB_2} \times \hat{\mathbf{l}}_2 & \mathbf{r}_{OB_3} \times \hat{\mathbf{l}}_3 & \mathbf{r}_{OB_4} \times \hat{\mathbf{l}}_4 \end{bmatrix} \tag{3.57}$$

It can be observed that the (3.57) relates the cable forces to the manipulator motion and is the transpose of Jacobian matrix obtained from the kinematic relationship (3.48).

3.2.4.3 Workspace Analysis

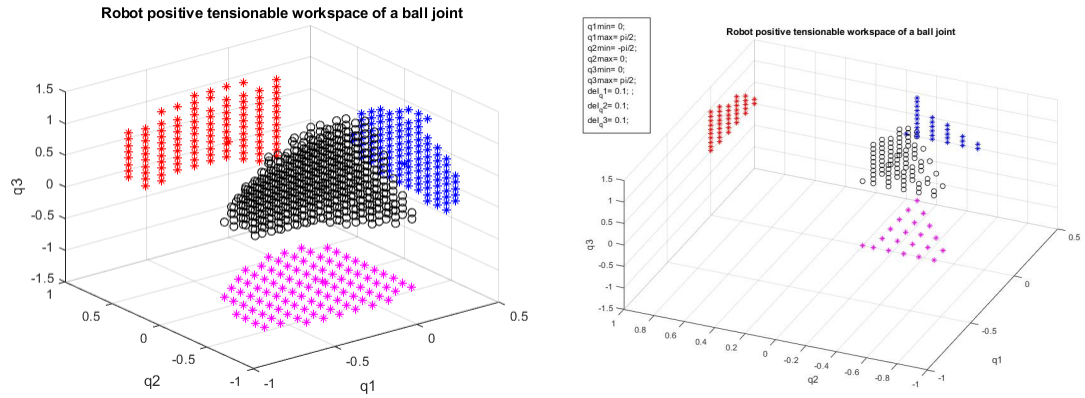

(a) Feasible Workspace of a ball joint **(b)** WFW of a ball joint with joint limits

Figure 3.25: WFW of 3-DOF ball joint manipulator driven by 4 cables

The feasible workspace of the ball joint manipulator was developed by analyzing the normal human wrist range of motion, $q1 \in [-pi/6, pi/6], q2 \in [-pi/4, pi/4], q3 \in [-pi/6, pi/2]$. Fig. 3.22 shows the feasible workspace with no cable collisions. In order to optimize the tension condition and maximize the force-closure workspace, the cables are used in crossed configuration similar to the spatial 6 DoF CDPR architecture. When the two pairs of cables are skew, no collision occurs. The boundaries of cable collision are defined by the case with

zero-distance between cables. The search workspace is discretized and the discrete points are checked for with the combination of all constraints. In order to avoid collision between cables, the cable routing and attachment points are positioned accordingly. The collision constraint can be expressed by the distance formula of skew lines. The feasible workspace is obtained by considering the following constraints:

$$\begin{aligned} (\mathbf{l}_i \times \mathbf{l}_j)^{\mathsf{T}}.(\mathbf{r}_{OAj} - \mathbf{r}_{OAi}) \leqslant 0 \quad i = 1,2 \quad j = 3,4 \\ rank(J^{\mathsf{T}}) = 3 \\ \exists \mathbf{f} \in ker(J^{\mathsf{T}}) : \mathbf{f} > 0 \end{aligned} \tag{3.58}$$

A feasible workspace as shown in Fig. 3.25, is obtained by satisfying all the three constraints shown in (3.58). Fig. 3.25b shows the workspace with joint limits $q1 \in [0, pi/2], q2 \in [-pi/2, 0], q3 \in [0, pi/2]$.

3.2.4.4 Stiffness Modeling

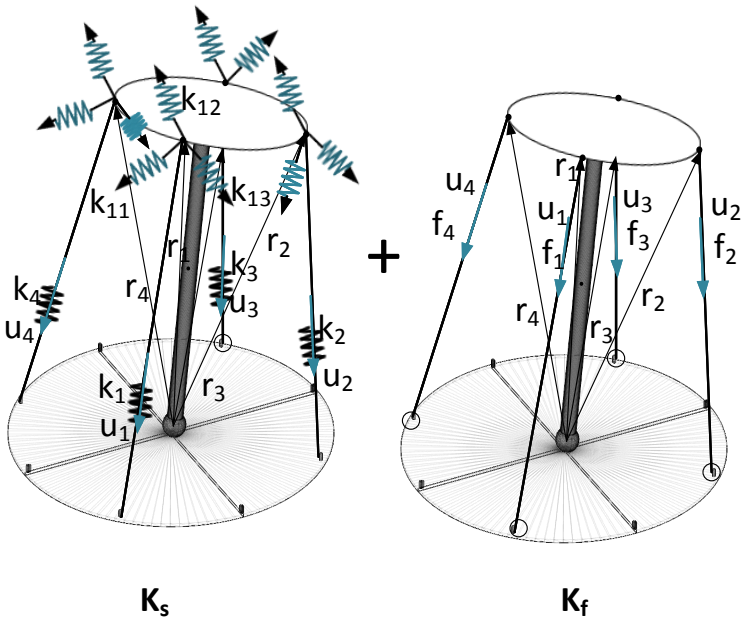

Figure 3.26: Stiffness model of spherical joint with unilateral force constraints

The stiffness modeling of cable-based manipulator depends both on the cable stiffness and antagonistic forces and was studied in [121]. The stiffness model

is shown in Fig. 3.26. Some assumptions are made for simplifying the stiffness model which is, the stiffness of mechanical structure is considered to be infinitely large and the stiffness of cables is set as a constant for a meter length cable. The spherical joint has 3-DOF rotational stiffness as $diag(k_{rs1}, k_{rs2}, k_{rs3})$ and is stiff in translational directions. Based on the modeling from [121], using an equivalent stiffness model for CDPR results in the following mathematical equation.

$$\mathbf{K}_{cdpr} = \mathbf{K}_s + \mathbf{K}_f \tag{3.59}$$

where

$$\mathbf{K}_s = \sum_{i=1}^{4}(k_i - \frac{f_i}{l_i}) \begin{bmatrix} u_i u_i^\mathsf{T} & u_i u_i^\mathsf{T} \hat{r}_i^\mathsf{T} \\ \hat{r}_i u_i u_i^\mathsf{T} & \hat{r}_i u_i u_i^\mathsf{T} \hat{r}_i^\mathsf{T} \end{bmatrix} + \sum_{i=1}^{4} \frac{f_i}{l_i} \begin{bmatrix} I & \hat{r}_i^\mathsf{T} \\ \hat{r}_i & \hat{r}_i \hat{r}_i^\mathsf{T} \end{bmatrix} \tag{3.60}$$

$$\mathbf{K}_f = \sum_{i=1}^{4} f_i \begin{bmatrix} 0 & 0 \\ 0 & \hat{u}_i \hat{r}_i \end{bmatrix} \tag{3.61}$$

where u_i, $i = 1, \ldots, 4$ are unit vectors of cables. r_i are vectors of spherical joint center point to cable attachment point of the end-effector points. k_i denote cable stiffness, I is 3×3 unit matrix and l_i is the magnitude of cable length vector. The stiffness model of cable driven spherical joint manipulator is presented here using equivalent stiffness model. It is essential to analyze the stiffness of cable driven robot which can be utilized for exoskeletal devices. A similar model is defined in the following chapter that will be useful for static stiffness evaluation of unilaterally actuated serial kinematic chains.

3.3 Conclusion

The kinematics and dynamics modeling of the single link CDPRs were introduced in this chapter. The actuation redundancy and unilateral positive force constraint conditions were presented geometrically using theory of convex cones. The different types of kinematic and dynamic principles were presented for single body cable driven systems. The workspace analysis was presented and simulation results were shown for both planar and spatial single-link cable driven robots. To demonstrate the modeling approach in CDPRs, the model for 6 DoF spatial, 1 DoF single link

planar and 3 DoF single link spatial manipulators were formulated. The Jacobian matrix was derived symbolically as analytical expressions for each individual system depending on the manipulator type. For single link CDPRs, the single type of cable routing and simplicity in manipulator structure makes the modeling easy. However, for cable driven serial kinematic chains, the cable routing presents challenges in formulating the kinematic model which will be discussed in the next chapter. The modeling of single link manipulators will be extended to consider cable routing through multiple links.

Chapter 4

Modeling of Cable Driven Serial Kinematic Chains

In this chapter, we study the kinematic and dynamics analysis of a serial chain subject to unilateral constraint forces. Firstly, the problem is best posed in terms of convex cones in the space of the coflexes of the kinematic chain, i.e., the dual space of the chain's instantaneous motions/ flexes. Any serial kinematic chain subject to a weak non-degeneracy condition, can be immobilized with $n+1$ forces. We can imagine the coflexes as generated by a system of external wrenches each acting on a different link of the chain. There are different such systems of wrenches generating the same coflex. In the second part of the chapter, we also define different cable routing types that will be useful while designing cable driven robots. The presented kinematic chains serve to illustrate the ability of the proposed highly coupled minimally actuated cable robots to model complex mechanical systems.

4.1 Serial chain subject to unilateral constraint forces

The goal is to find $n+1$ attachments whose coflexes form a conic frame. Each cable attachment, with or without routing, to a link of the serial chain generates a coflex. Not every coflex is given by an admissible application of a cable as it is

hard to see how a single cable can apply couple on one link. In every n-dimensional space, $\mathcal{V}$, we can always find $n+1$ vectors providing a conic frame. If our choice of vectors in $\mathcal{V}$ is restricted to a subset $\mathcal{F}$, this is not always possible. From the previous chapter, it was evident that it is possible:

1. To complement any basis of the constraint wrench system of the single joint to a basis of $se(3)^*$ using only pure forces

2. To use this basis and one additional pure force to obtain a conic frame immobilizing the joint.

For example, a single revolute joint can be fixed using two unilateral constraint forces that are not reciprocal to the hinge rotation (i.e. are skew with the joint axis) and have opposite-sign moments. An important subtlety is that these cable forces must be independent if we would like to be able to transmit a wrench through the joint. (Transmitting such a resultant reaction wrench is particularly crucial when trying to control a chain with cables without routing, as in [15]). Similarly, it is possible to find four independent unilateral forces that will fix a spherical joint and transmit a force through its center. When constructing these one-body convex cones, it can be useful to know the geometrical properties of the conic spans of wrenches [4]. Some of the important definitions and remarks are reestablished from [15].

Definition 20. *We call a coflex* ***wrench-generated*** *when it can be caused by applying a single wrench on one body of the chain. We say that a coflex is* ***force-generated*** *(momentgenerated) when it is wrench-generated by a zero-pitch (infinite-pitch) wrench.*

Definition 21. *We call a serial chain with p joints* ***non-degenerate*** *if* $\mathcal{T}_k \not\subset \mathcal{T}_{k+1} \forall 1 \leqslant k < p$*, i.e., no joint is (instantaneously) contained in its immediate successor.*

Definition 22. *A non-degenerate serial chain admits a conic frame of force-generated coflexes.*

Theorem 23. *Consider a non-degenerate serial chain with p joints with mobilities* d_i, $1 \leqslant d_1 \leqslant 6, 1 \leqslant di \leqslant 5$, $i = 2, \ldots, p$, *at a configuration with motion space* $\mathcal{M}$, $dim\mathcal{M} = \sum_{i=1}^{p} d_i = n$. *Let* ψ *be any wrench applied to the end effector but not*

reciprocal to the last joint, $\psi \notin \mathcal{T}_p^{\perp}$. Then there exist n pure forces.
$(\varphi_1, \ldots, \varphi_n) = (\varphi_1^1, \ldots, \varphi_{d_1}^1, \varphi_1^2, \ldots, \varphi_{d_2}^2, \varphi_1^p, \ldots, \varphi_{d_p}^p)$,
such that

1. *Each φ_j^i is applied to link i*
2. *Cone $(z_1, \ldots, z_{n+1}) = \mathcal{M}^*$, where $z_j, j = 1, \ldots, n$, is the image of $\varphi_j = \varphi_k^i$ into $\mathcal{M}^*$ by the dual Jacobian map of the corresponding link i, $z_j = \boldsymbol{j}_{\boldsymbol{i}}^*(\varphi_k^i)$ and z_{n+1} is the image of ψ, $z_{n+1} = \boldsymbol{j}_p^*(\psi)$.*

The proof of the above theorem is established in [15].

Remark 24. As the first joint can be with six DoF, that a free-floating serial chain with n DoF can be fixed with $n + 7$ cables. Note that if a joint other than the first is with 6 DoF the chain will be degenerate according to our definition. In fact, in this case, the chain splits in two and each part will require at least one unilateral constraint in excess of its DoF. When planar mechanisms with "planar wrenches" are considered, i.e. the applied wrenches are assumed to be forces in a common plane, and the serial planar chain's base is mobile in the plane, $n + 4$ unilateral constraints are needed.

4.1.1 Constructing Conic Frames: A Recursive Procedure

A recursive procedure [15, 122] to construct the force generators of the coflex conic frame for a serial kinematic chain is described here. This procedure will be utilized to create novel cable based actuation schemes, which will be discussed in following sections.

1. First, a force, ψ applied to the end-effector and not reciprocal to the last joint is found.
2. Then, only the end-effector, link p, is considered mobile while the other bodies are assumed fixed. A minimum number of unilateral forces (equal to the mobility d_p of the last joint) are found such that they that will fix the last joint when acting together with the wrench ψ. In this process, care is taken so that the single wrench, ξ, which these $d_p + 1$ wrenches transmit through joint p is nonzero and is not reciprocal to the preceding joint $p - 1$.

3. The previous step is repeated for $p := p - 1$ and $\psi := \xi$ until all forces are generated.

Thus all joints are immobilized in turn, starting from the most distant from the base. For joint p, one force in excess of the joint DoF d_p is needed. However, for each preceding joint i, only d_i additional forces are needed. This is so because the excess wrench is supplied through joint $j + 1$ from the forces acting on the successor bodies.

4.1.2 RR kinematic chain

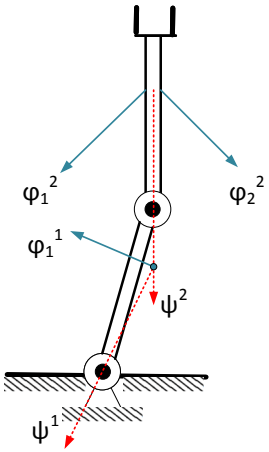

Figure 4.1: Coflex conic frame of two link planar kinematic chain. The superscript of a force notation denotes to which body the force is applied.

The recursive algorithm is applied to multi-link kinematic chains. The algorithm is performed by appling a force to the end-effector not reciprocal to the last joint firstly. The generation of conic frame on RR chain is shown in Fig. 4.1 and Fig. 4.2. The forces 1 and 2 constrain the end joint as described in the algorithm. To constrain the first joint, this resultant force transmitted through the end joint, must be complemented with another force with an opposite moment with respect to the first joint axis. Thus the two link chain is constrained completely. The blue arrows denote the unilateral constraint forces (cables) and the red arrows represent

the resultant force transmitted through the joint. The algorithm is repeated until all forces are generated. The non-zero wrench transmitting through the base joint is shown for visualization. In the following chains, it will be ignored as the chain is fully constrained once we choose the n+1 unilateral forces.

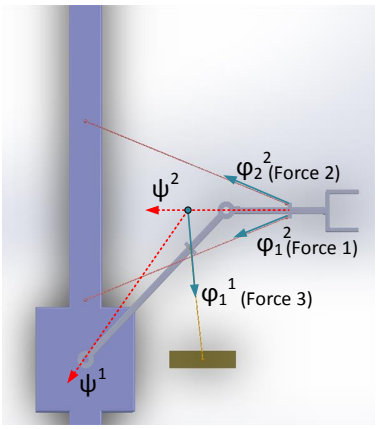

Figure 4.2: RR Chain constrained by planar cables. The superscript of a force notation denotes to which body the force is applied.

4.1.3 3R and 4R kinematic chain

The conic frame construction is illustrated for 3R and 4R chain in Fig. 4.3 and Fig. 4.4. To construct a conic frame (for Fig. 4.4), for a 4R chain we begin by fixing joint 4. For this purpose, we select two forces φ_1^4 and φ_2^4. Their axes can be arbitrary lines satisfying two conditions: (a) neither axis passes through the center of joint 4; (b) the intersection point, P_4 of the two axes (possibly at infinity) is *not on the line joining* the centers of joints 4 and 3. The directions of φ_1^4 and φ_2^4, must be such, that (c) joint 4 is in the "pie slice" determined by these directions (or the pie slice of the opposite directions). Assuming joints 1 to 3 fixed, two cables are able to pull link 4 along φ_1^4 and φ_2^4 would fix joint 4.

Moreover, a force, $\psi^3 \neq 0$, would be transmitted from link 4 to link 3. Its axis is on the line connecting P4 and joint 4 and its direction is such that it points into the same half-plane with both φ_1^4 and φ_2^4.

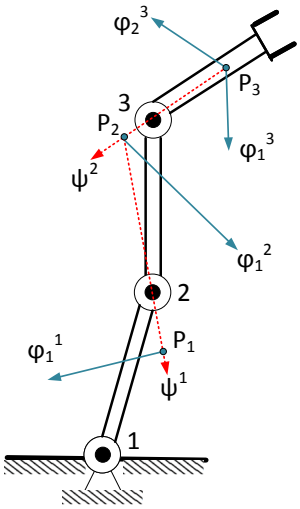

Figure 4.3: Coflex conic frame of three link planar kinematic chain. The superscript of a force notation denotes to which body the force is applied.

Next, we fix joint 3 in the same manner using ψ^3 as one of the forces. We proceed till we fix joint 1. (At this last step condition (b) is mute.) The n + 1 = 5 external forces, $\varphi_1^1, \varphi_1^2, \varphi_1^3, \varphi_1^4$ and φ_2^4, generate a conic frame of coflexes fixing the whole chain. Note that the procedure works in the same way at any configuration. In particular, nothing changes if the chain is at a singularity, e.g., with all four joint centers aligned.

4.1.4 RPP kinematic chain

The algorithm can be applied when there are prismatic joints. Consider a RPP chain as shown in Fig. 4.5. The two sliders are not parallel in order to satisfy non-degeneracy condition. To fix joint 3, two forces φ_1^3 and φ_2^3 are chosen (not reciprocal to the last joint) such that: (a) neither has an axis perpendicular to the direction of joint 3; (b) their axes have a finite intersection point P_3 and (c) their directions project with opposite signs on the direction of joint 3. These forces fix the slider 3 and transmit a force, ψ^2, perpendicular to its direction. ψ^2 is not reciprocal to joint 2, it is not perpendicular to the slider 2 as the sliders are not

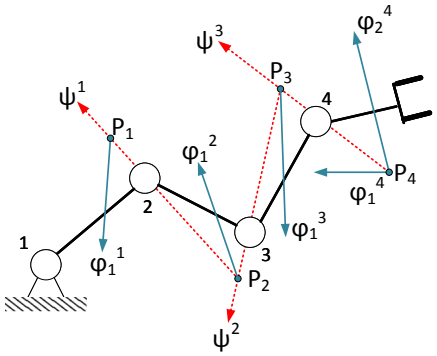

Figure 4.4: Coflex conic frame of 4R chain. The superscript of a force notation denotes to which body the force is applied.

parallel. Next, we fix joint 2 in a similar manner using ψ^2 as one of the forces. We need to consider the condition (b) that the intersection point P_2 is not on the line through the center of joint 1 perpendicular to joint 2. Thus, psi^1 will not pass through the 1 joint center, and can be used to fix joint 1 with one last force, φ_1^1. The four forces, $\varphi_1^1, \varphi_1^2, \varphi_1^3$ and φ_2^3, generate the conic frame.

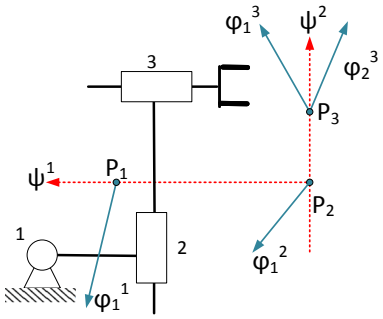

Figure 4.5: Coflex conic frame of RPP chain.

4.1.5 Alternative conic frames and chain reductions

When a force-generated conic frame of coflexes exists, there are infinitely many solutions possible:

1. By choosing a different wrench basis.

2. By changing the number of unilateral constraints applied to different links.

Such alternative conic frames can be generated by applying the same algorithm but to a modified chain. The chain is changed by grouping two or more adjacent joints and treating them as one compound joint. One such example is shown in Fig. 4.6. Consider Fig. 4.7. Force 1 and Force 2 constrain the end joint as

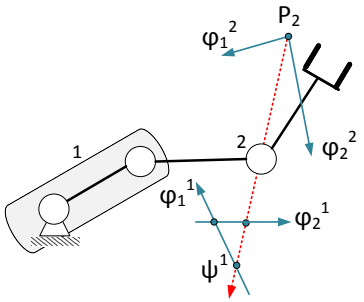

Figure 4.6: Coflex conic frame of (RR)R chain. The first two joints are grouped and considered as a single 2-DoF joint

explained previously. Their resultant is transmitted through the end joint. This transmitted resultant along with Force 3 is used to fix the second joint. The transmitted resultant and Force 1 are used to fix the first joint. But its important to note that the unilateral force constraints are applied on the second link, since it is prohibited to put any cables on the first link. Thus the RRR chain can be controlled by $n+1$ unilateral forces using alternative conic frame reductions. It is an alternative solution than the one where we are allowed apply cables to all the three links.

4.2 Kinematic Analysis of CDSKC

The kinematic model of cable driven serial kinematic chain with different types of routing [30, 123, 124] are shown in Fig. 4.8. The cable actuation of the serial chain

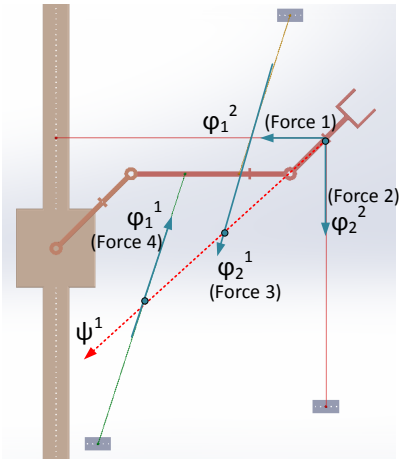

Figure 4.7: The generation of the conic frame of (RR)R chain.

is examined under the assumption that the cables can be routed from the fixed frame to the links or routed through the links forming multiple cable segments leading to highly coupled actuation. Frame $\{F_O\}$ denotes the inertial coordinate with origin O and frame $\{F_k\}$ represents the coordinate frame of link k.

Cables are connected to the links with attachment points at B_i and C_i (i= 1,..,m) and to the base with attachment points at A_i, respectively. The position vectors $\mathbf{r}_A, \mathbf{r}_B$ and $\mathbf{r}_C$ are constant positions in inertial frame, $\{F_O\}$ and non-inertial frames, $\{F_1\}$ and $\{F_2\}$, respectively. ${}^{\mathbf{0}}\mathbf{r}, {}^{\mathbf{1}}\mathbf{r}$ and ${}^{\mathbf{2}}\mathbf{r}$ represent the vector $\mathbf{r}$ in $\{F_O\}$ and $\{F_1\}$ and $\{F_2\}$, respectively. Hence, the attachment point for cable i can be expressed with vectors ${}^{\mathbf{0}}\mathbf{r}_{\mathbf{A_i}}$, ${}^{\mathbf{1}}\mathbf{r}_{\mathbf{B_i}}$ and ${}^{\mathbf{2}}\mathbf{r}_{\mathbf{C_i}}$. The cable lengths present in the manipulator is represented as $\mathbf{l} = [l_1, l_2, \ldots, l_m]^{\mathsf{T}}$, where l_i is the length of cable i. For the cable connecting from base to link 1, the cable vector is kinematically defined as:

$$\mathbf{l}_i = \mathbf{r}_{Oo_1} + \mathbf{r}_{B_i} - \mathbf{r}_{A_i} \tag{4.1}$$

For the cable connecting from base to link 2, the cable vector is:

$$\mathbf{l}_i = \mathbf{r}_{Oo_2} + \mathbf{r}_{C_i} - \mathbf{r}_{A_i} \tag{4.2}$$

For the cable connecting from link 1 to link 2, the cable vector is:

$$\mathbf{l}_i = \mathbf{r}_{Oo_2} + \mathbf{r}_{C_i} - \mathbf{r}_{B_i} \tag{4.3}$$

Allowing cables to be routed through multiple links, each cable consists of multiple cable segments. The kinematics of a cable with multiple routing points can be described by segment vectors. For the cable connecting from base through link 1 to link 2, the cable vector is:

$$\begin{aligned} \mathbf{l}_{i1} &= \mathbf{r}_{Oo_1} + \mathbf{r}_{B_i} - \mathbf{r}_{A_i} \\ \mathbf{l}_{i2} &= \mathbf{r}_{Oo_2} + \mathbf{r}_{C_i} - \mathbf{r}_{B_i} \end{aligned} \tag{4.4}$$

where $\mathbf{l}_{i1}$ and $\mathbf{l}_{i2}$ are cable segment vectors.

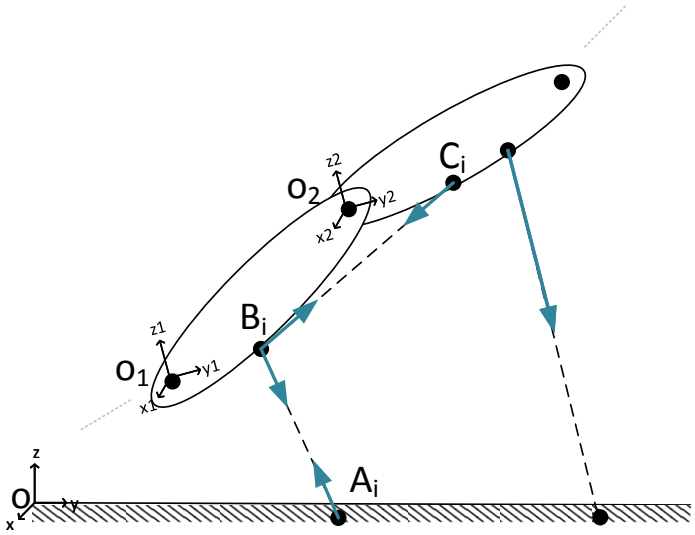

Figure 4.8: Kinematic model of two link cable driven multibody

The length of the cable i with routed segment j can be expressed as:

$$\mathbf{l}_i = \sum_{j=1}^{jmax} |\mathbf{l}_{ij}| \tag{4.5}$$

In order to find the cable structure matrix, the differential relationship is used:

$$\dot{\mathbf{l}} = \mathbf{J}\dot{\mathbf{q}} \tag{4.6}$$

where $\mathbf{q}$ is the joint configuration of the manipulator. From (4.6), the differential relationship of the length of cable i can be expressed as $\dot{l}_i = \hat{\mathbf{l}}_i \cdot \mathbf{l}_i$. Applying the differential relationship for cable connecting from base to link 1:

$$\begin{aligned}
\dot{l}_i &= \hat{\mathbf{l}}_i.(\dot{\mathbf{r}}_{Oo_1} + \dot{\mathbf{r}}_{B_i} - \dot{\mathbf{r}}_{A_i}) \\
&= {}^1\hat{\mathbf{l}}_i.({}^1\dot{\mathbf{r}}_{Oo_1} + {}^1\dot{\mathbf{r}}_{B_i}) \\
&= {}^1\hat{\mathbf{l}}_i.({}^1\dot{\mathbf{r}}_{Oo_1} + {}^1\omega_1 \times {}^1\mathbf{r}_{B_i}) \\
&= {}^1\hat{\mathbf{l}}_i.{}^1\dot{\mathbf{r}}_{Oo_1} + ({}^1\mathbf{r}_{B_i} \times {}^1\hat{\mathbf{l}}_i).{}^1\omega_1 = \begin{bmatrix} ({}^1\hat{\mathbf{l}}_i)^\mathsf{T} & ({}^1\mathbf{r}_{B_i} \times {}^1\hat{\mathbf{l}}_i)^\mathsf{T} & 0 & 0 \end{bmatrix} \begin{bmatrix} {}^1\dot{\mathbf{r}}_{Oo_1} \\ {}^1\omega_1 \\ {}^2\dot{\mathbf{r}}_{Oo_2} \\ {}^2\omega_2 \end{bmatrix}
\end{aligned} \tag{4.7}$$

Similarly, the kinematic relationship for other cable routings are given. For cable connecting from base to link 2:

$$\dot{l}_i = \begin{bmatrix} 0 & 0 & ({}^2\hat{\mathbf{l}}_i)^\mathsf{T} & ({}^2\mathbf{r}_{C_i} \times {}^2\hat{\mathbf{l}}_i)^\mathsf{T} \end{bmatrix} \begin{bmatrix} {}^1\dot{\mathbf{r}}_{Oo_1} \\ {}^1\omega_1 \\ {}^2\dot{\mathbf{r}}_{Oo_2} \\ {}^2\omega_2 \end{bmatrix} \tag{4.8}$$

For cable connecting from link 1 to link 2:

$$\dot{l}_i = \begin{bmatrix} -({}^1\hat{\mathbf{l}}_i)^\mathsf{T} & -({}^1\mathbf{r}_{B_i} \times {}^1\hat{\mathbf{l}}_i)^\mathsf{T} & ({}^2\hat{\mathbf{l}}_i)^\mathsf{T} & ({}^2\mathbf{r}_{C_i} \times {}^2\hat{\mathbf{l}}_i)^\mathsf{T} \end{bmatrix} \begin{bmatrix} {}^1\dot{\mathbf{r}}_{Oo_1} \\ {}^1\omega_1 \\ {}^2\dot{\mathbf{r}}_{Oo_2} \\ {}^2\omega_2 \end{bmatrix} \tag{4.9}$$

For cable connecting from base through link 1 to link 2:

$$\dot{l}_i = \begin{bmatrix} ({}^1\hat{\mathbf{l}}_{i1} - {}^1\hat{\mathbf{l}}_{i2}) & ({}^1\mathbf{r}_{B_i} \times ({}^1\hat{\mathbf{l}}_{i1} - {}^1\hat{\mathbf{l}}_{i2}))^\mathsf{T} & ({}^2\hat{\mathbf{l}}_{i2})^\mathsf{T} & ({}^2\mathbf{r}_{C_i} \times {}^2\hat{\mathbf{l}}_{i2})^\mathsf{T} \end{bmatrix} \begin{bmatrix} {}^1\dot{\mathbf{r}}_{Oo_1} \\ {}^1\omega_1 \\ {}^2\dot{\mathbf{r}}_{Oo_2} \\ {}^2\omega_2 \end{bmatrix} \tag{4.10}$$

The $\mathbf{J}$ matrix can be derived in two parts. Firstly, we calculate the Jacobian matrix which maps the cable space and body space velocities $\mathbf{J_v}$. The cable-body Jacobian matrix $\mathbf{J_v}$ for the routed chain is expressed as

$$\dot{\mathbf{l}} = \mathbf{J_v}\dot{\mathbf{x}} \tag{4.11}$$

where $\dot{\mathbf{x}}$ (body space velocity) is the twist vector that contains angular velocities of link 1 and link 2. The twist vector of serial kinematic chain can be related to generalized coordinate velocities using kinematic maps thereby giving

$$\dot{\mathbf{x}} = \mathbf{J_w}\dot{\mathbf{q}} \tag{4.12}$$

$$\mathbf{J} = \mathbf{J_v}\mathbf{J_w} \tag{4.13}$$

where $\mathbf{J_w}$ maps the joint space velocities into the absolute velocities of body space and the Jacobian matrix $\mathbf{J} \in \mathbb{R}^{m \times n}$ for m cable and n DoF chain.

This kinematic dependence can be applied to the serial chain with fully routed cable bundles where the cables are both externally and internally routed, which will be discussed in the following chapter.

4.2.1 Static equilbrium condition

The static equilibrium equation of the CDPR was discussed in the previous chapter which is given as:

$$\begin{bmatrix} \hat{\mathbf{l}}_1 & \hat{\mathbf{l}}_2 & \dots & \hat{\mathbf{l}}_m \\ \mathbf{b}_1 \times \hat{\mathbf{l}}_1 & \mathbf{b}_2 \times \hat{\mathbf{l}}_2 & \dots & \mathbf{b}_m \times \hat{\mathbf{l}}_m \end{bmatrix} \begin{bmatrix} f_1 \\ f_2 \\ \vdots \\ f_m \end{bmatrix} = - \begin{bmatrix} \mathbf{f}_P \\ \mathbf{m}_p \end{bmatrix} \tag{4.14}$$

One can write the equilibrium equations of the systems in the form of

$$\mathbf{A}(\mathbf{r}, \mathbf{R})\mathbf{f} = \mathbf{W} \tag{4.15}$$

Due to the existence of interlink constraints, the tensionability of CDSKC is a problem of higher complexity [125]. Similar to cable driven rigid body system, the equilibrium equations of a serial multibody chain with M links, $\bar{m}$ cables and $\bar{k}$ constraints in Cartesian space is of the form:

$$(\mathbf{A_s})_{(nM)\times(\bar{m}+\bar{k})}(\mathbf{f_s})_{(\bar{m}+\bar{k})\times 1} = \mathbf{W_s}_{(nM)\times 1} \tag{4.16}$$

where $\mathbf{f_s}$ and $\mathbf{A_s}$, unlike the rigid body case contain constrain wrenches too. For example, in a two-link multibody chain shown in Fig. 4.8, we have,

$$(\mathbf{A_s})_{2n\times(m_1+m_2+\bar{k})} = \begin{bmatrix} (\mathbf{A_1})_{n\times m_1} & \mathbf{C}_{n\times\bar{k}} & \mathbf{0}_{n\times m_2} \\ \mathbf{0}_{n\times m_1} & -\mathbf{C}_{n\times\bar{k}} & (\mathbf{A_2})_{n\times m_2} \end{bmatrix} \tag{4.17}$$

$$(\mathbf{f_s})_{(m_1+m_2+\bar{k})\times 1} = \begin{bmatrix} t_{1,1} & \dots & t_{m_1,1} & \varphi_1 & \dots & \varphi_{\bar{k}} & t_{1,2} & \dots & t_{m_2,1} \end{bmatrix}^\mathsf{T} \tag{4.18}$$

$$\mathbf{W_s} = \begin{bmatrix} \mathbf{w}_1 \\ \mathbf{w}_2 \end{bmatrix} \tag{4.19}$$

where m_i is the number of cables attached to the i^{th} link, $\bar{k}$ is the number of constraint forces or moments between the two links, $(\mathbf{A}_i)_{n\times m_i}$ contains the unit force wrench of the cables (similar to the Eqn. 4.17) attached to the link i, $\mathbf{C}$

contains the unit force constraint wrenches, $t_{i,j}$ is the tension of the i_{th} cable of link j, φ_i is the magnitude of the i^{th} constraint wrench, and $\mathbf{w}_1$ and $\mathbf{w}_2$ contain all other external wrenches with negative sign together with inertia terms applied to links 1 and 2, respectively. For two link system, $\mathbf{C}_1 = -\mathbf{C}_2$ due to the Newton's third law of motion. Similarly for three-link CDSKC, $\mathbf{A_s}$ is defined as:

$$(\mathbf{A_s}) = \begin{bmatrix} \mathbf{A_1} & \mathbf{C}_{12} & \mathbf{0} & \mathbf{0} & \mathbf{0} \\ \mathbf{0} & -\mathbf{C}_{12} & \mathbf{A_2} & \mathbf{C}_{23} & \mathbf{0} \\ \mathbf{0} & \mathbf{0} & \mathbf{0} & -\mathbf{C}_{23} & \mathbf{A_3} \end{bmatrix}_{3n\times(m_1+m_2+m_3+\bar{k})} \tag{4.20}$$

where $\mathbf{C}_{12}$ denotes the constraints between links i and j. $\mathbf{A}$ contains cable wrenches similar to previous case. The size of $\mathbf{A}_s$ increases for kinematic chain with multiple links. The large size is due to the Newtonian formulation of the dynamics, which leads to the presence of internal forces and moments. If we use Newton's method, internal reaction forces/ moments between the bodies must be explicitly considered and then eliminated. Using Lagrange's approach and notion of generalized forces eliminates the internal unknown forces/ moments from the equations. The equations of motion are given as:

$$\frac{d}{dt}(\frac{\partial L}{\partial \dot{q}_i}) - \frac{\partial L}{\partial q_i} = Q_i, i = 1, \ldots, n \tag{4.21}$$

where L is the Lagrangian, n is the DOF of the chain, and q_i, Q_i are the generalized coordinates and generalized forces, respectively. For CDSKCs, the contribution of cables is modeled as point forces applied to the links, i.e., the inertia and stiffness of the cables are neglected. $Q_i = Q_i^c + Q_i^r$, where Q_i^c are the cable forces and all other generalized external forces/ moments are Q_i^r. The cable forces are presented in generalized coordinates as:

$$Q_i^c = \sum_{j=1}^{m} (f_j l_j \cdot \frac{\partial r_j}{\partial q_i}) \tag{4.22}$$

where r_j is the length of the j^{th} cable from base to the chain and f_j denotes the

j^{th} cable force. The Eqn. 4.22 can be expressed in matrix form as:

$$\begin{bmatrix} \frac{d}{dt}(\frac{\partial L}{\partial \dot{q}_1}) - \frac{\partial L}{\partial q_1} - Q_1^r \\ \vdots \\ \frac{d}{dt}(\frac{\partial L}{\partial \dot{q}_n}) - \frac{\partial L}{\partial q_n} - Q_n^r \end{bmatrix} = \begin{bmatrix} l_1 \cdot \frac{\partial r_1}{\partial q_1} & \dots & l_m \cdot \frac{\partial r_m}{\partial q_m} \\ \vdots & \ddots & \vdots \\ l_1 \cdot \frac{\partial r_1}{\partial q_{DOF}} & \dots & l_m \cdot \frac{\partial r_m}{\partial q_{DOF}} \end{bmatrix} \begin{bmatrix} f_1 \\ \vdots \\ f_m \end{bmatrix} \tag{4.23}$$

Consequently, the general equilibrium equations of the system in 4.23 can be written in the following form:

$$\mathbf{A}_L \mathbf{f} = \mathbf{W}_L \tag{4.24}$$

where $\mathbf{W}_L$ is the left side term in Eqn. 4.24 that includes all external forces and inertia terms. The right side term is a linear combination of the columns of $\mathbf{A}_L$ multiplied by the cable tensions. This is general form of the equilibrium equations for cable driven serial kinematic chains.

4.3 Workspace Analysis

The workspace definition and types were earlier discussed in Chapter. 2. The WCW is defined as the set of poses in which the manipulator can sustain any arbitrary external wrench. Mathematically, it is defined as

$$WCW = (q : \mathbf{w} = \mathbf{J}(\mathbf{q})^{\mathbf{T}}\mathbf{t}, \exists \mathbf{t} \geqslant 0) \tag{4.25}$$

where $\mathbf{w} = -[M(\mathbf{q}, \ddot{\mathbf{q}}) + C(\mathbf{q}, \dot{\mathbf{q}}) + G(\mathbf{q}) + \Gamma_{ext}]$.

$$\begin{aligned} rank(J^T) &= n \\ \exists \mathbf{f} \in ker(J^T) &: \mathbf{f} > 0 \end{aligned} \tag{4.26}$$

The workspace can be calculated analytically and numerically. Analytical approach determines the geometric boundary and by solving the equations defining the workspace. Numerical methods are point-wise evaluation techniques. It is required to find the regions in the workspace in which the CDSKC is tensionable. One can see that, tensionable workspace and WCW are equivalent. For simplicity and

reducing the number of parameters, the cables are assumed to be attached to the central line of the rigid body, i.e, the line connecting the joint and the center of mass. The more general case is discussed in the next section where the connection position of each cable is indicated with routing points at a distance. x_i and y_i are the coordinates of the i^{th} winch and d_i is the distance of the point of connection of the i^{th} cable to the body from the joint. The possible cable routing distribution for the cables routed from a fixed frame/ base are $\{1, 2\}$ and $\{0, 3\}$. The topology shown is known as direct-connecting cable routing scheme where the actuating cables directly connects one of the links to the base. The mechanism shown in Fig. 4.9 has 2 DOFs and three cables. $\mathbf{A}_L$ is 2-by-3. The symbolic expressions of

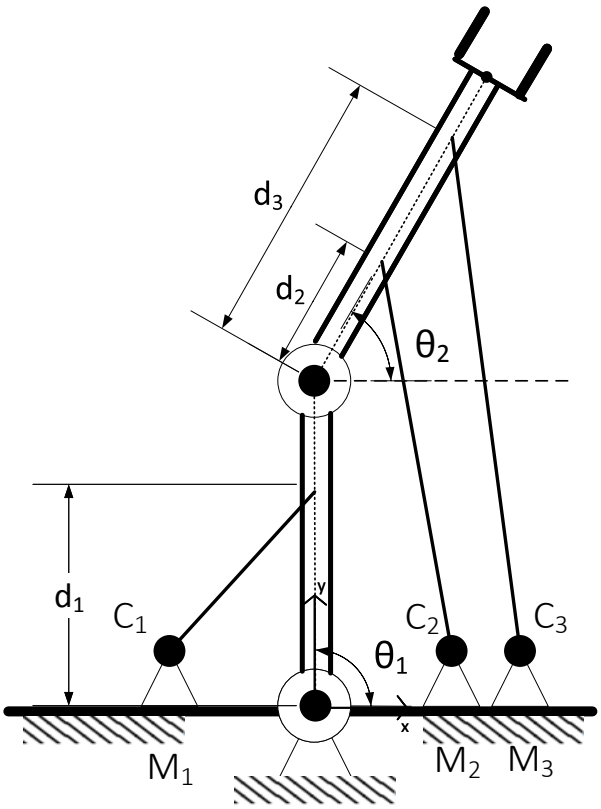

Figure 4.9: Schematic of a 2DOF CDSKC driven by three cables having direct connecting scheme

the cable structure matrix for 2 link CDSKC with the direct connecting scheme is

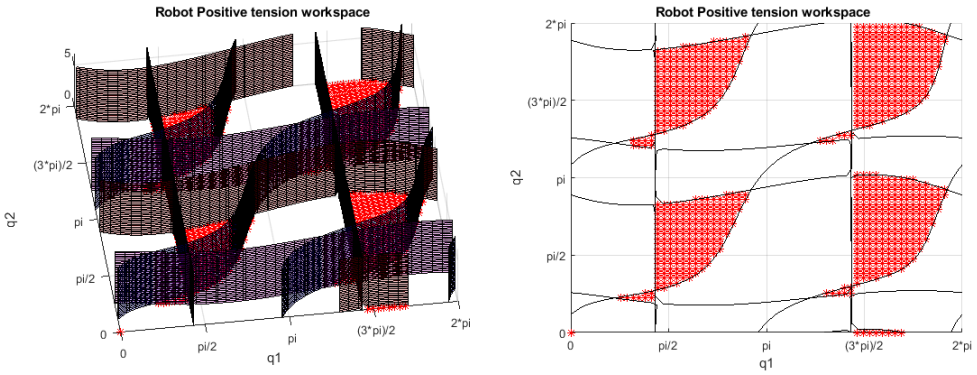

(a) Tensionable surface boundaries **(b)** Regions of tensionable space

Figure 4.10: Tensionable workspace of 2-DOF 2-link CDSKC

given:

$$\begin{bmatrix} Q_1 \\ Q_2 \end{bmatrix} = \mathbf{A}_L \begin{bmatrix} t_1 \\ t_2 \\ t_3 \end{bmatrix} \tag{4.27}$$

$$\mathbf{A}_L = \begin{bmatrix} a_{11} & a_{12} & a_{13} \\ 0 & a_{22} & a_{23} \end{bmatrix} \tag{4.28}$$

where

$$\begin{aligned} a_{11} &= d_1 c(\theta_1)(y_1 - d_1 s(\theta_1)) - d_1 s(\theta_1)(x_1 - d_1 c(\theta_1)) \\ a_{21} &= 0 \\ a_{12} &= l_1 c(\theta_1)(d_2 s(\theta_2) - y_2 + l_1 s(\theta_1)) - l_1 s(\theta_1)(d_2 c(\theta_2) - x_2 + l_1 c(\theta_1)) \\ a_{22} &= d_2 c(\theta_2)(d_2 s(\theta_2) - y_2 + l_1 s(\theta_1)) - d_2 s(\theta_2)(d_2 c(\theta_2) - x_2 + l_1 c(\theta_1)) \\ a_{13} &= l_1 c(\theta_1)(d_3 s(\theta_2) - y_3 + l_1 s(\theta_1)) - l_1 s(\theta_1)(d_3 c(\theta_2) - x_3 + l_1 c(\theta_1)) \\ a_{23} &= d_3 c(\theta_2)(d_3 s(\theta_2) - y_3 + l_1 s(\theta_1)) - d_3 s(\theta_2)(d_3 c(\theta_2) - x_3 + l_1 c(\theta_1)) \end{aligned} \tag{4.29}$$

where $c(.)$ and $s(.)$ notations are used for cosine and sine of the arguments respectively. Q_1 and Q_2 are generalized joint torques of the kinematic chain, t_j are the j^{th} cable tensions respectively.

4.3.1 Workspace of Planar CDSKC

For two-link 2 DOF CDSKC, having $n+1$ cables routed to its links as shown in Fig. 4.9, boundaries of the workspace are calculated analytically using Cramer's rule. $\mathbf{A}_L$ is of order (2×3). $\mathbf{A}_L$ can be expressed using i^{th} column, A_i as follows:

$$\mathbf{A}_L \mathbf{f} = \mathbf{W}_L \tag{4.30}$$

$$\mathbf{f} = \mathbf{A}^{+}\mathbf{W}_L + N(\mathbf{A})\lambda \tag{4.31}$$

$N(\mathbf{A})$ denotes the null space of the structure matrix and λ is an arbitrary vector.

$$\mathbf{A}_{2\times 3} = \begin{bmatrix} \mathbf{A_1} & \mathbf{A_2} & \mathbf{A_3} \end{bmatrix} \tag{4.32}$$

$$\mathbf{A}_1 t_1 + \mathbf{A}_2 t_2 + \mathbf{A}_3 t_3 = \mathbf{W}_{L_{2\times 1}} \tag{4.33}$$

With the linear system obtained From Eq. 4.33, the constraint that the set of poses have to satisfy to be part of WCW is given by,

$$\forall\, \mathbf{W}_L > 0 : \mathbf{A}_L \mathbf{f} = \mathbf{W}_L \tag{4.34}$$

From Eq. 4.31

$$\mathbf{A}_1 N_1 + \mathbf{A}_2 N_2 + \cdots + \mathbf{A}_m N_m = 0 \tag{4.35}$$

$$\mathbf{A}_1 N_1 + \mathbf{A}_2 N_2 + \mathbf{A}_3 N_3 = 0 \tag{4.36}$$

$$\begin{bmatrix} \mathbf{A}_1 & \mathbf{A}_2 \end{bmatrix}_{2\times 2} \begin{bmatrix} N_1 \\ N_2 \end{bmatrix}_{2\times 1} = - \begin{bmatrix} \mathbf{A}_3 N_3 \end{bmatrix}_{2\times 1} \tag{4.37}$$

The solution of Eq. 4.37 can be computed using Cramer's rule.

$$N_1 = \frac{\begin{vmatrix} -\mathbf{A}_3 N_3 & \mathbf{A}_2 \end{vmatrix}}{\begin{vmatrix} \mathbf{A}_1 & \mathbf{A}_2 \end{vmatrix}} \tag{4.38}$$

$$N_2 = \frac{\begin{vmatrix} -\mathbf{A}_1 & \mathbf{A}_3 N_3 \end{vmatrix}}{\begin{vmatrix} \mathbf{A}_1 & \mathbf{A}_2 \end{vmatrix}} \tag{4.39}$$

$$\eta = \begin{bmatrix} N_1 \\ N_2 \\ N_3 \end{bmatrix} = \begin{bmatrix} \begin{vmatrix} \mathbf{A}_3 & \mathbf{A}_2 \end{vmatrix} \\ \begin{vmatrix} \mathbf{A}_1 & \mathbf{A}_3 \end{vmatrix} \\ -\begin{vmatrix} \mathbf{A}_1 & \mathbf{A}_2 \end{vmatrix} \end{bmatrix} \tag{4.40}$$

To find WCW, Eq. (4.40) can be used to find regions where N_1, N_2 and N_3 are of same sign. If N_i^- denotes negative values of N_i negative and N_i^+ denotes positive values of N_i, then WCW can be expressed as the union of the regions which are formed from the intersection of N_i^i and N_i^+. The equation can be formed as below:

$$WCW = (N_1^- \cap N_2^- \cap N_3^-) \cup (N_1^+ \cap N_2^+ \cap N_3^+) \tag{4.41}$$

The null space can also be derived in an efficient way as explained in [126]. The structure matrix is represented as $\mathbf{A}_L = [\mathbf{a}_1, \mathbf{a}_2, \ldots, \mathbf{a}_{n+1}]$. $\mathbf{a}_i$ is the i^{th} column vector of the cable structure matrix. Let $\mathbf{A}_{sj}$ be a submatrix formed by the first n columns of $\mathbf{A}_L$ such as $\mathbf{A}_{sj} = [\mathbf{a}_1, \mathbf{a}_2, \ldots, \mathbf{a}_n]$. The one-dimensional null space is given as

$$\boldsymbol{n}_L = \begin{bmatrix} -\mathbf{adj}(\mathbf{A}_{sj})\mathbf{a}_{n+1}/|\mathbf{A}_{sj}| \\ 1 \end{bmatrix} \tag{4.42}$$

where $\mathbf{adj}(\mathbf{A}_{sj})$ is the adjoint matrix of $\mathbf{A}_{sj}$. A scaled version of $\mathbf{n}_L$, named $\mathbf{n}_A$, in order to avoid singularity is given as

$$\boldsymbol{n}_A = \begin{bmatrix} -\mathbf{adj}(\mathbf{A}_{sj})\mathbf{a}_{n+1} \\ |\mathbf{A}_{sj}| \end{bmatrix} \tag{4.43}$$

The tensionability condition states that all components of the spanning vector of the kernel should be of same sign. A sign change occurs if and only if one of the components becomes zero. The boundaries are obtained by solving the roots of each component of (5.24).

Fig. 4.10 shows the tensionable workspace atlas of 2-link CDSKC. The mechanism has 2-dof and three cables. The kernel is spanned by the vector $\mathbf{n}_{3\times1}$ which is found symbolically in terms of joint variables. The roots of each component of

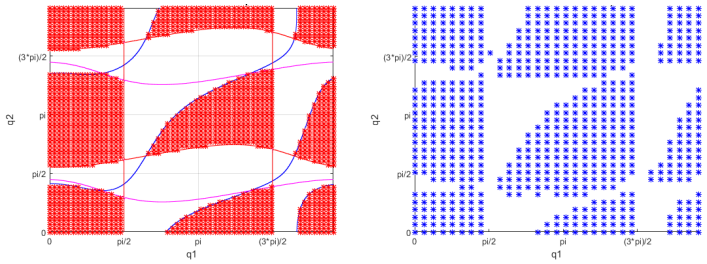

(a) Without Spring **(b)** With Spring

Figure 4.11: Reshaping and improvement of WFW of two-link CDSKC by adding springs

M_1	M_2	M_3	d_1	d_2	d_3	l_1	l_2
$[1.2, 5.6]'$	$[3.0, -0.6]'$	$[5.0, 3.9]'$	0.62	0.35	0.7	1	1

Table 4.1: Parameter values for 2-link CDSKC with $n+1$ actuated cables (all in meters)

the kernel provides three equations that are nonlinear and have multiple solutions. For instance, the three equations result in four curves in the $\theta_1 - \theta_2$ plane. One of the equation is expressed as

$$\theta_2 = \tan^{-1}\left(\frac{y_3 - l_1 \sin\theta_1}{x_3 - l_1 \cos\theta_1}\right) \pm k\pi \tag{4.44}$$

Eqn. 4.44 is a set of curves separated by a multiple of π. Similarly, the other three curves are plotted. The curves are shown in Fig. 4.10b. The cable attachment points and the location of cable winch were chosen for the evaluation of workspace. The parameters of motor locations (M_1, M_2, M_3), cable attachment distances (d_1, d_2, d_3) and link lengths (l_1, l_2) are specified in the Table. 4.1.

The curves are partitioned into several regions with positive and negative components. The points plotted in red are the tensionable areas. As long as the robot configuration falls inside any of these regions, $\mathbf{A}_L$ is full rank, which satisfies the first condition of tensionability. The signs of the component of $\mathbf{n}_A$ vector are verified. One can distinguish nine separate regions in which the components of null space vector have the same sign and the system is tensionable. Since the angular coordinates are periodic, some of these regions are connected. The nine

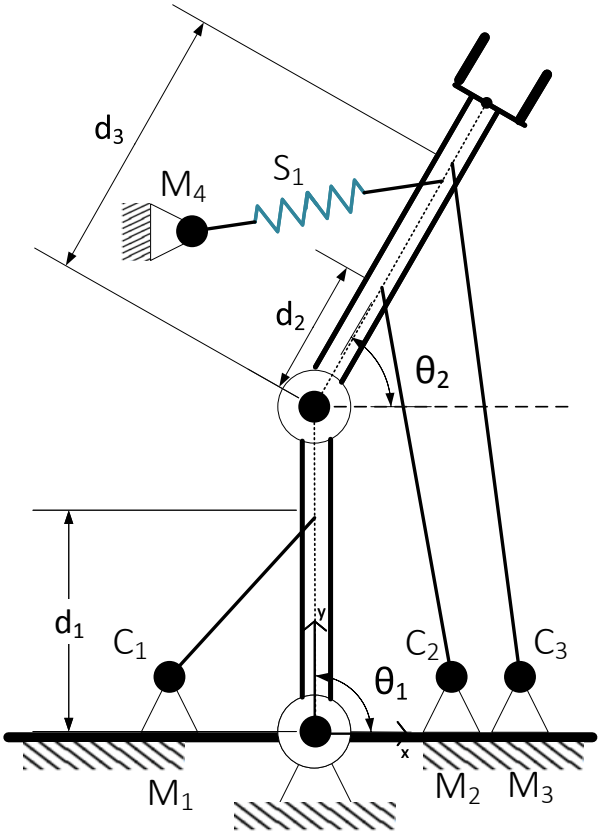

Figure 4.12: Schematic of a 2DOF CDSKC driven by cables and springs

abovementioned regions will form four continuous regions. One cannot move the mechanism from one tensionable configuration to any other one along a tensionable path if the regions are disconnected. If any two configurations are tensionable, one cannot expect that any configuration in between the two will be tensionable as well. The tensionable areas can be controlled by altering the placement of cables and modifying the cable routing points. One can manipulate the sign string of null space component by reversing the direction of cables, thereby improving the tensionable workspace. In order to improve the performance of the CDSKC, springs are added to the cable driven system. Addition of springs and its impact on cable driven parallel manipulator and serial manipulator were studied in [123, 127, 128]. There has been not enough literature about the impact of springs on internally routed and bundled CDSKCs which will be discussed in the next chapter. Addition

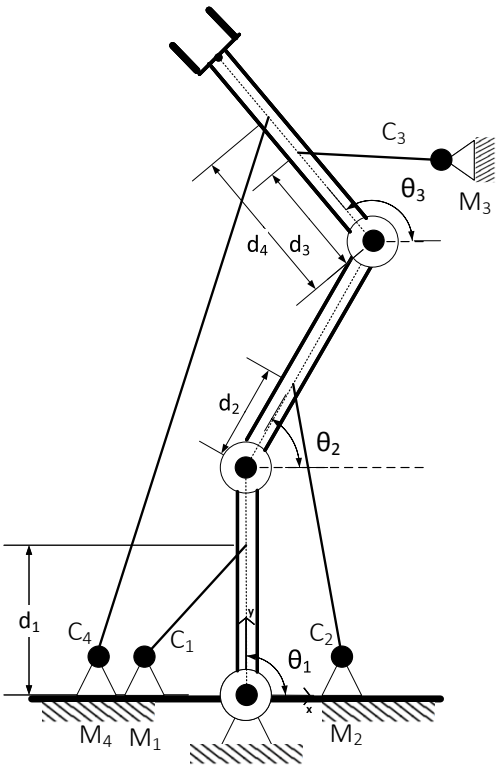

Figure 4.13: Schematic of a 3DOF CDSKC driven by four cables having direct connecting scheme

of springs may keep cables in tension with optimized placement parameters and reshape or potentially increase the workspace of a CDPR or a CDSKC.

Different cable routings result in different workspaces of the manipulator. The WFW can be modified/reshaped and optimized by adding springs. Without additional actuators, the impact of adding springs to the two link CDSKC was studied. The WFW is obtained from kinematics and equilibrium conditions along with tension bounds in the cables. We consider linear axial springs for simulation. The potential energy of the spring is written in generalized coordinates for the

M_1	M_2	M_3	M_4	d_1	d_2	d_3	d_4	l_1	l_2	l_3
$[1.2, 5.6]'$	$[3.2, -0.8]'$	$[5.1, 4.3]'$	$[-6.9, -4.8]'$	0.6	0.3	0.4	0.7	1	1	1

Table 4.2: Parameter values for 3-link CDSKC with 4 actuated cables (all in meters)

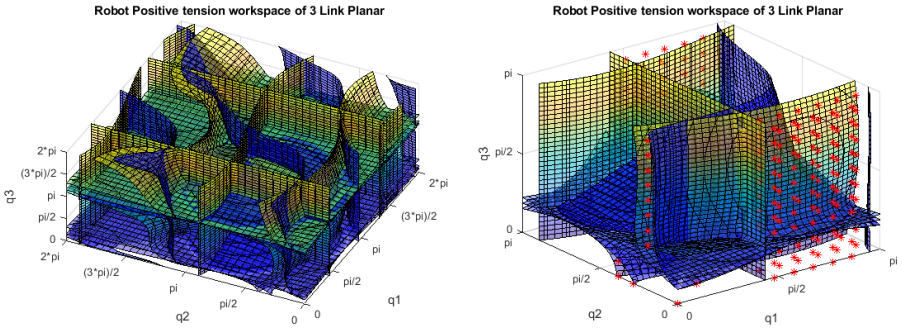

(a) Tensionable surface boundaries **(b)** Tensionable workspace atlas

Figure 4.14: Tensionable workspace of 3-DOF 3-link CDSKC

incorporation of spring forces in Lagrangian formulation.

$$\begin{bmatrix} \frac{d}{dt}(\frac{\partial L_s}{\partial \dot{q}_1}) - \frac{\partial L_s}{\partial q_1} - Q_1^r \\ \vdots \\ \frac{d}{dt}(\frac{\partial L_s}{\partial \dot{q}_n}) - \frac{\partial L_s}{\partial q_n} - Q_n^r \end{bmatrix} = \begin{bmatrix} l_1 \cdot \frac{\partial r_1}{\partial q_1} & \dots & l_m \cdot \frac{\partial r_m}{\partial q_m} \\ \vdots & \ddots & \vdots \\ l_1 \cdot \frac{\partial r_1}{\partial q_{DOF}} & \dots & l_m \cdot \frac{\partial r_m}{\partial q_{DOF}} \end{bmatrix} \begin{bmatrix} f_1 \\ \vdots \\ f_m \end{bmatrix} \tag{4.45}$$

where $L_s = L - V_s$ and V_s is the potential energy contribution from a spring. Using linear axial spring models, the potential energy is given as:

$$V_s = \frac{1}{2}k(l_i - l_{0i})^2 \tag{4.46}$$

Consequently, the equations of the system in 4.45 can be written in the following form:

$$\begin{aligned} \mathbf{A}_L\mathbf{f} &= \mathbf{W}_{L_S} \\ s.t.(f_{min} \leqslant f_i \leqslant f_{max}) \forall i 1 \leqslant i \leqslant m \end{aligned} \tag{4.47}$$

When multiple passive stiffness elements are added, the composition of forces and moments is changed. The generated force from spring cables with a stiffness constant K is given by

$$\mathbf{F_s} = \mathbf{K}\mathbf{u_s} \tag{4.48}$$

$$\mathbf{u_s} = (l - l_o)\mathbf{u} \tag{4.49}$$

where $\mathbf{F_s}$ is the force vector of spring, $\mathbf{u_s}$ is the elongation vector of the spring

and **u** is the unit vector along the axis of spring cable.

l and l_o are the current and initial lengths of the spring cable. The elongation vector of the spring cable is expressed in terms of generalized coordinates and the spring wrenches are incorporated with the gravity torques in equations of motion for the serial manipulator. Fig. 4.11 shows the result of adding springs in between the links to a two-link CDSKC which not only reshapes/improves the workspace but also prevents cable interference. The stiffness of the spring was selected to be 0.5 N/mm and the initial length of 30 mm. The workspace was evaluated using both null-space and hyperplane shifting method [112]. While introduction of springs do not reduce the number of cables, their placement does effect the cable tension values required and force-closure. They assist in supplying additional torques at various joints. This alters the external wrench to lie anywhere within the convex hull, which previously could have been lying outside/near the boundary of the bounded hull due to cable tension constraints.

The symbolic expressions of the cable structure matrix for 3 link CDSKC with the direct connecting scheme is obtained from:

$$\begin{bmatrix} Q_1 \\ Q_2 \\ Q_3 \end{bmatrix} = \mathbf{A}_L \begin{bmatrix} t_1 \\ t_2 \\ t_3 \\ t_4 \end{bmatrix} \tag{4.50}$$

$$\mathbf{A}_L = \begin{bmatrix} a_{11} & a_{12} & a_{13} & a_{14} \\ 0 & a_{22} & a_{23} & a_{24} \\ 0 & 0 & a_{33} & a_{34} \end{bmatrix} \tag{4.51}$$

where the symbolic expressions of $\mathbf{A}_L$ are given in Appendix A.

Similarly, the boundaries and the workspace atlas for joint coordinates varying from 0 to pi are plotted for 3-link planar CDSKC as shown in Fig. 4.14. The parameters used for simulation is shown in Table. 4.2. The wrench closure validity of the three link manipulator can be verified using the necessary conditions proposed in [129] for three link multi link cable driven robots. For the routing configuration given in Fig. 4.13, the indices m_2^*, m_2^* and m_1^* (The number of cables that have the potential to actuate link 3, link 2 and link 1 respectively) are equal

to 2 and the necessary conditions for three link MCDMs as discussed in [129] are $m_3^* \geqslant 2$, $m_2^* \geqslant 2$ and $m_1^* \geqslant 2$, respectively. In general, for a CDPR, the necessary condition for n DOF CDPR is $m \geqslant n+1$. For the workspace analysis of the two

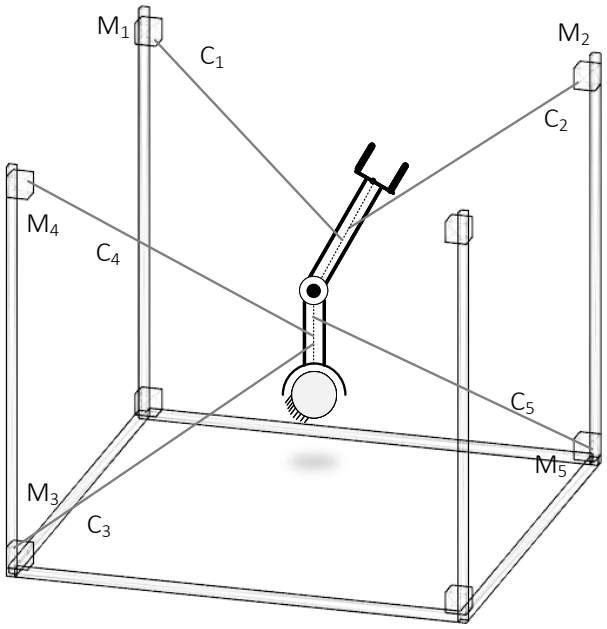

Figure 4.15: Schematic of a SR chain driven by cables routed from a fixed frame

link spatial CDSKC with cables routed from a fixed frame (Direct-connecting scheme) as shown in Fig. 4.16b, the cables are routed from the fixed frame and the kinematics are decoupled as the cables are not routed through the links. If the second link is assumed to be massless, the system will be simplified to a single link 3-dof ball joint manipulator as shown in Fig. 4.16a. We have seen that for a single link 3-dof manipulator, $m \geqslant 4$ cables are required to completely or redundantly restrain the system. In the next Chapter, we will briefly discuss the benefits of fully routed cable bundle scheme and study the two-link 4-dof redundantly restrained manipulator actuated by $m = 5$ cables. Minimal fully routed cable actuation is achieved through internal routing and re-routing which will be further elaborated in the next section. One can obtain the cable structure matrix $\mathbf{A}_L$ for the two link spatial CDSKC with direct-connecting scheme as a function of the generalized coordinates. The analytical expressions of the boundaries of the WCW

can be obtained using the below formulation. The generalized coordinates of the manipulator can be described by $\mathbf{q}=[\alpha, \beta, \gamma, \delta]^{\mathsf{T}}$

$$\mathbf{R}_\alpha = \begin{bmatrix} c\alpha & -s\alpha & 0 \\ s\alpha & c\alpha & 0 \\ 0 & 0 & 1 \end{bmatrix} \mathbf{R}_\beta = \begin{bmatrix} c\beta & 0 & s\beta \\ 0 & 1 & 0 \\ -s\beta & 0 & c\beta \end{bmatrix} \mathbf{R}_\gamma = \begin{bmatrix} 1 & 0 & 0 \\ 0 & c\gamma & -s\gamma \\ 0 & s\gamma & c\gamma \end{bmatrix} \tag{4.52}$$

$$\mathbf{R}_\delta = \begin{bmatrix} c\delta & -s\delta & 0 \\ s\delta & c\delta & 0 \\ 0 & 0 & 1 \end{bmatrix} \tag{4.53}$$

The cable attachment points greatly affects the Jacobian matrix, it plays a key role in the volume of the tensionable workspace. Firstly, these attachment points must be paramterized. We consider polar coordinates to express it in spatial system. A point on the first link initially is defined as:

$$\mathbf{r_{01_j}} = \begin{bmatrix} d_{a1_j} \\ p_{a_j} c\sigma_j \\ p_{a_j} s\sigma_j \end{bmatrix}, \mathbf{r_{02_k}} = \begin{bmatrix} d_{a2_k} \\ p_{a_k} c\sigma_k \\ p_{a_k} s\sigma_k \end{bmatrix} j = 1, 2, 3; k = 4, 5 \tag{4.54}$$

where $c(.)$ and $s(.)$ notations are used for cosine and sine of the arguments respectively. d_{a1} is the distance of the point from yz plane, p_a and σ are the polar coordinates of the point at that part of the arm. $j = 1, 2, 3$ implies, that the point belongs to link 1. The coordinates of the point with respect to the fixed frame is given as:

$$\mathbf{r_{f1_j}} = \mathbf{R}_\alpha \mathbf{R}_\beta \mathbf{R}_\gamma \mathbf{r_{01_j}} \tag{4.55}$$

where $j = 1, 2, 3$. This is the generic form of expressing point on link 1 using generalized coordinates. This point can be an anchor point of the cable. For the second link, then point is initally described using $\mathbf{r_{02_k}}$ where $k = 4, 5$ and d_{a2} is the distance of the center of the part of the arm containing the point from the

revolute joint. The final coordinate is obtained as:

$$\mathbf{r_{f2_k}} = \mathbf{R}_\alpha \mathbf{R}_\beta \mathbf{R}_\gamma (\mathbf{R}_\delta \mathbf{r_{02_k}} + \begin{bmatrix} l_{a1} \\ 0 \\ 0 \end{bmatrix}) \tag{4.56}$$

where l_{a1} is the length of the first link. The symbolic expressions of the cable structure matrix for 2 link Spatial CDSKC shown in Fig. A.5 with the direct connecting scheme is given:

$$\begin{bmatrix} Q_1 \\ Q_2 \\ Q_3 \\ Q_4 \end{bmatrix} = \mathbf{A}_L \begin{bmatrix} t_1 \\ t_2 \\ t_3 \\ t_4 \\ t_5 \end{bmatrix} \tag{4.57}$$

$$\mathbf{A}_L = \begin{bmatrix} a_{11} & a_{12} & a_{13} & a_{14} & a_{15} \\ a_{21} & a_{22} & a_{23} & a_{24} & a_{25} \\ a_{31} & a_{32} & a_{33} & a_{34} & a_{35} \\ a_{41} & a_{42} & a_{43} & a_{44} & a_{45} \end{bmatrix} \tag{4.58}$$

The structure matrix is obtained using the above formulation and the symbolic form is given in the Appendix 1. This concludes the parameterization of the attachment points. Using $\mathbf{A}_L$, the boundaries of tensionable workspace can be obtained. By assuming one or two of the generalized coordinate to be fixed, the workspace can be represented in 3D or 2D respectively. The WCW is identical for the single link 3-dof ball joint manipulator and two-link 4-dof manipulator, differing only in the dimension of the Jacobian matrix. For the purpose of visualization, the WCW of 3-dof system which was analyzed in the previous section is only shown. The WCW along with it's projections on different planes are shown in Fig. 3.25. The manipulator will not be able to travel from poses in one region to another in the disconnected regions of the workspace.

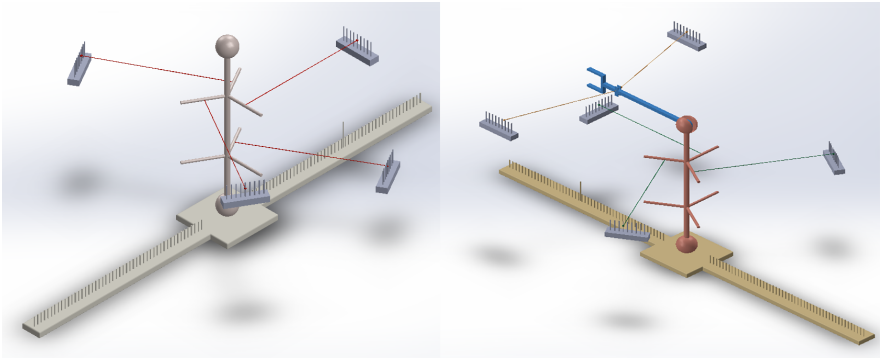

(a) Single link spatial CDSKC **(b)** Two link spatial CDSKC

Figure 4.16: CAD Model of spatial CDSKC with cables routed from the fixed frame

4.4 Conclusions

In this Chapter, a methodology for finding $n+1$ attachments whose coflexes form a conic frame was described and illustrated with several examples of planar and spatial kinematic chains. The method requires only that each joint of the chain allows motion that are not permitted by the immediate successor joint. In particular, planar 2-, 3-, 4-R and RPP and spatial S and SR chains were investigated using this technique. The alternative conic frames and chain reduction rules were utilized effectively to immobilize the chain by grouping two or more adjacent joints and treating them as one compound joint. The kinematic and static analysis of such chains with direct-connecting cable routing scheme was investigated. It was observed that the static conditions for CDSKC's is a problem of higher complexity due to the existence of interlink constraints unlike the single body CDPR. Using Lagrange's approach and notion of generalized forces, the cable structure matrix (the cable space Jacobian) was derived analytically. One can see that the complexity of expressions that are useful for obtaining the boundaries of the WCW is high for spatial CDKSC's as given in the Appendix. Also, for the representation of the WCW, it is impossible to depict it in all of the system's DOF at once. Having the boundaries of WCW is not only beneficial for investigating the tensionability of the system in different topologies, but also can be used to improve the WCW. Using the analytical expressions, one can modify, reshape or shift them by changing the parameters such as the location of the cable winches. The null

space approach is utilized as we investigated the tensionablity of systems with one redundant cable. The null space approach is computationally less intensive for systems with redundancy 1.

We have demonstrated the reshaping and improvement of wrench feasible workspace of CDSKC's with direct-connecting cable routing scheme by adding passive springs with optimized parameters at different locations. The addition of springs can assist in reducing/augmenting the joint torque thereby reducing the tension in the cables. Due to cable routing, the kinematics is coupled and it also alters tension in the other cables because the tension in those cables are function of external wrenches. We will investigate the workspace, stiffness and motion generation analysis for CDSKC's with cables routing through links instead of direct-connecting cable routing scheme. The cable routing and kinematic structure presents challenges in individually formulating the model. This motivates the need for a generalized approach for CDKSC's with fully routed cables.

Chapter 5

Fully Routed Multi Link Unilateral Manipulators

In this chapter, we study the kinematics of a serial chain subject to unilateral constraint forces with different routing topologies. The effects of cable routing and number of cables on tensionable workspace is investigated. Utilizing workspace analysis as a meaningful computational tool to evaluate the different operational regions of the proposed cable robot topologies. A comprehensive lineup of cable routing topologies are listed and novel cable routing schemes are proposed using internal routing and re-routing forming cable bundles.

Firstly, the problem is best posed in terms of convex cones in the space of the coflexes of the kinematic chain, i.e., the dual space of the chain's instantaneous motions/ flexes. Any serial kinematic chain subject to a weak non-degeneracy condition, can be immobilized with $n+1$ forces. A feasible cable actuation of an arbitrary serial chain using fully-routed cable bundling scheme is established and analyzed with different kinematic chains. The recursive algorithm using convex cones is utilized to generate a cable actuation with full routing, i.e, one where each cable attached to a link k is routed through all links $1, \ldots, k$ that are closer to the base. Routing and re-routing is allowed to actuate any serial chain overcoming the constraint that exist when cables are applied directly (direct-connecting cable routing scheme). The presented kinematic chains with fully-routed cable bundles serve to illustrate the ability of the proposed highly coupled minimally actuated

cable robots to model complex biomechanical systems.

To achieve a minimum number of actuating cables while possessing a large workspace region, a novel internal cable routing scheme is proposed. It is shown that by incorporating internal routing with multi-segment cables, any serial chain with n degrees of freedom can be controlled with $n+1$ cables. In this work, through studying the kinematics and dynamics, we demonstrate how internally-routed cable actuation of multilink manipulators have an increased workspace and reduced cable forces to execute trajectories.

5.1 Routing Topology for CDSKCs

In the previous Chapter, we established the fact that each cable attachment, with or without routing, to a link of the serial chain generates a coflex. The goal is to find $n+1$ attachments whose coflexes form a conic frame. Each coflex are generated by a set of external wrenches, each acting on different link of the chain. A cable attached to only one body results in a single force on one link and zero wrenches on other links, a routed cable applies wrenches on several links. As these wrenches are the components of same coflex, the intensities of these wrenches are in proportion for every given configuration.

Theorem 25. *Any serial chain admits a conic frame of coflexes generated by a fully-routed cable bundle.*

The proof of the above theorem is established in [33]. Simply put, any serial chain with mobility $n{=}\sum_{i=1}^{p} dim\mathcal{T}_i$ can be immobilized with $n+1$ unilateral force constraints. Cable routing and bundling allows to create a displaced resultant force which can always be made non-reciprocal to the joint and applied to the proximal body.

Definition 26. ***Cable routing type*** *refers to the path that a cable routes through the links of a cable driven serial kinematic chain.*

Definition 27. ***Cable segment*** *refers to the single section of cable between two attachment/ anchor points where cable are tied.*

Definition 28. ***Cable attachment/ anchor point*** *refers to the point where a cable is connected or passes through a link.*

Definition 29. ***Proximal link*** *refers to greater closeness to the base in a serial chain.*

Definition 30. ***Distal link*** *refers to greater closeness to the end-effector in a serial chain.*

Fig. 5.1 shows different cable routing schemes of a planar CDSKC. The blue parts are rigid connections between the cable and the actual link, and the black dots are cable attachments in contrast with white dots which are pass-through elements. This holds for internal and external routing, the latter being sections of cables connecting a link with a proximal neighbour.

Definition 31. ***External routing*** *refers to routing of cable with an end fixed in link $k > 0$ through each proximal link, passing through points fixed in links $k-1$, $k-2$, ..., 0.*

Definition 32. ***Internal routing*** *refers to re-routing of cable between two points in the same link.*

The first topology is known as *direct-connecting* cable routing scheme as shown in Fig. 5.1(b), where the actuating cables directly connects one of the links to the base. The second topology of cable routing is the *pass-through* cable routing scheme as shown in Fig. 5.1(c), where a cable with an end fixed on distal link is routed through each proximal link, passing through points fixed in proximal connections. The benefits of this arrangement are minimal number of actuating cables and reduced cable interference.

Definition 33. ***Direct-connecting scheme*** *refers to the routing scheme where the actuating cables directly connects one of the links to the base.*

Definition 34. ***Internal routing scheme*** *refers to scheme where cables are routed internally in addition to being externally routed.*

Definition 35. ***Pass-through scheme*** *refers to cable routing scheme where a cable is routed through each proximal link, passing through fixed points. The routed cables are also termed as co-shared cables.*

Fig. 5.1(d) is called the *internal routing* scheme, where a cable can be re-routed within the link internally, in addition to being externally routed. This type of routing can be considered as the most generalized form of the *multi-segment pass-through routing scheme* where a cable segment can be attached within the same link. The configuration can be non-crossing or cross-over. The non-crossing

internal routing configuration allows the cable to re-route within the same link without having crossing cables. The cross-over configuration allows cable to cross through the manipulator to create a new cable configuration, thereby achieving highly coupled actuation.

A configuration is said to be *fully-routed* (as shown in Fig. 5.1(a)) if the CDSKC consists of cables routed from a link to its proximal and cables that are re-routed internally between two points in the same link. In the following proximal connections, the internally routed cables can pass precisely through the same routing points. This guarantees that the robot has a policy of minimal actuation. The routed cables can be kept parallel throughout the complete joint cycle.

A 2-DOF serial chain with two hinges with coinciding axes with direct-connecting cable routing scheme would require four constraint forces to immobilize the chain. Infact, two are needed to prevent each joint from moving. Any reaction wrench transmitted from link 2 to link 1 would be reciprocal to joint 1 and cannot be used to control it. With the internal routing scheme, we attach two cables to the second body so that neither line of action is coplanar with the common joint axis and when in tension have opposite moments with respect to the hinge. The two cables are routed to body 1, then re-routed/ bundled at another point of body 1, and directed together along a line not coplanar with the axis. Thus pulling on the two cables allows to control hinge 2 and produces a moment on hinge 1. Only one more cable, attached to body one is necessary to control hinge 1 and the whole chain. Totally, 3 cables are required to immobilize the chain in contrast to the 4-cable direct connecting cable routing scheme.

Definition 36. ***Bundling*** *refers to routing scheme where all cables originating at a link $k > 1$, after being routed to the proximal link, are re-routed to a common point within the same link $k - 1$, where they are combined together and hence pass through exactly the same routing points in the further proximal links.* Once the cables form a bundle, it is treated as a single cable and is combined with other cables in the proximal links.

Definition 37. ***Biarticular*** *refers to those muscles that cross two joints rather than one (monoarticular).*

In this Chapter, a novel internal cable routing scheme for CDSKCs is proposed

to have policy of minimal actuation and improved workspace. This internally routed scheme is obtained by employing both externally routed and internally routed cables between adjacent links. The proposed manipulator has cables being connected through multiple links resulting in kinematic coupling during actuation. The cable routing scheme is similar to the structure of a human arm, where muscles are able to generate a wide range of motion due to their dense arrangement close to the links. The kinematics, inverse-dynamics and wrench-closure workspace (WCW) of planar and spatial CDKSCs with internal routing scheme are analyzed. It is shown that the WCW of two-link and three-link CDSKCs with internally routed cables are significantly increased with reduced maximal cable tensions.

We first review the kinematic modeling of a two link cable driven robot with different routing topologies in the next Section. In the upcoming sections, the workspace, the trajectory generation and inverse dynamics of such systems are discussed. In order to design a better human-robot interaction paradigm, the stiffness variations during a postural task is examined. The stiffness variations during human arm movement are simulated and results are demonstrated. We will also review the conditions needed to obtain an isotropic stiffness performance. We model the upper arm musculoskeletal system as two links where the first link acts as the upper arm and the second link consists of forearm and hand. The shoulder and elbow joints are represented as the two rotational joints. The tendons/cables are actuated by muscle type actuators and are attached to the links of the robot arm.

5.2 Methods

5.2.1 Architecture

We consider a two link robot driven by cables in various routing topologies. The cables are routed both externally and internally. To prevent coupling between adjacent moment arms, multi point internal routing is deployed where we use multiple points instead of single routing point per link [130]. This paper also discusses the case of antagonistic mono- and biarticular muscle arrangement. Fully-routed single bundle tendon actuation scheme is used where a tendon can be

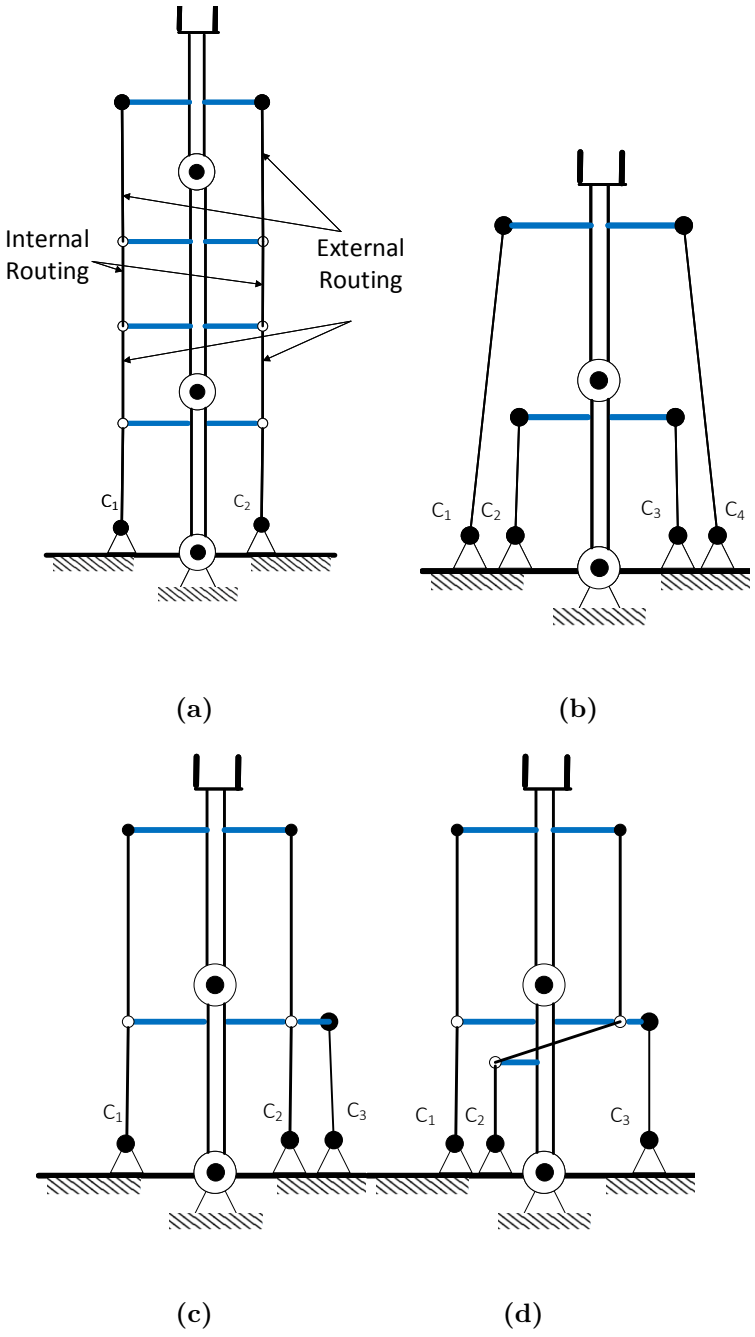

Figure 5.1: (a) Routing types (b) Direct-connecting (c) Pass-through (d) Internal(crossover) Cable routing schemes

Table 5.1: Cable-driven robot architecture

Type	Architecture
1	3 cables externally routed
2	3 cables single-point internal routing
3	3 cables multi-point internal routing
4	3 cables single-point internal routing and bundle
5	3 cables multi-point internal routing and bundle
6	4 cables
7	5 cables
8	6 cables biarticular

re-routed internally between two points apart from being routed from a link to its proximal and are joined in bundles [15, 33]. Grouping of independent cables from the base is called as a bundle. The bundled cables pass through exactly the same routing points in following proximal links. This ensures that the robot have a minimal actuation strategy. The bundled cables can be maintained parallel across the joint full-cycle. We assume the cables to be bundled to the maximum. Robot configurations with cross routing [131] and cross bundling is also studied where the tendons/cables cross over the links and are directly routed to the base. In this paper, we will study about 8 different architectures that are listed in Table 5.1. The definitions of different routing terminologies are described to provide the user with a clear background.

5.2.2 Kinematic Modeling

The kinematic parameters of the two-link cable driven robot actuated with $n+1$ cables are shown in Fig. 5.2. The cables are routed through the proximal link passing through points fixed in links. The symbolic expressions for the length of the cable segments can be written in the following form:

$$[l_{11}\, l_{21}\, l_{31}\, l_{12}\, l_{22}]^{\mathrm{T}} = \tag{5.1}$$

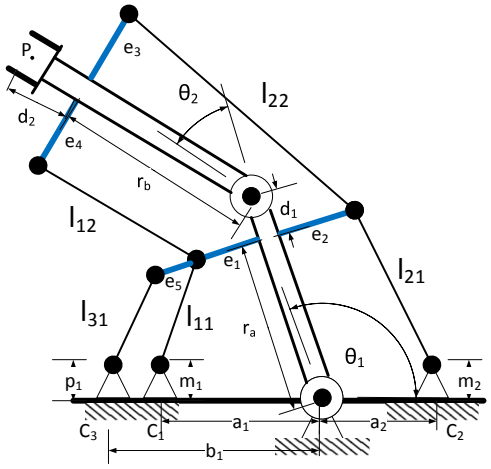

Figure 5.2: $n+1$ cables with external routing

$$\begin{bmatrix} \sqrt{(a_1 + r_a c_{\theta_1} - e_1 s_{\theta_1})^2 + (-m_1 + r_a s_{\theta_1} + e_1 c_{\theta_1}))^2} \\ \sqrt{(-a_2 + r_a c_{\theta_1} + e_2 s_{\theta_1})^2 + (-m_2 + r_a s_{\theta_1} - e_2 c_{\theta_1}))^2} \\ \sqrt{(b_1 + r_a c_{\theta_1} - (e_1 + e_5) s_{\theta_1})^2 + (-p_1 + r_a s_{\theta_1} + (e_1 + e_5) c_{\theta_1})^2} \\ \sqrt{(d_1 c_{\theta_1} + e_1 s_{\theta_1} + r_b c_{\theta_{12}} - e_4 s_{\theta_{12}})^2 + (d_1 s_{\theta_1} - e_1 c_{\theta_1} + r_b s_{\theta_{12}} + e_4 c_{\theta_{12}})^2} \\ \sqrt{(d_1 c_{\theta_1} - e_2 s_{\theta_1} + r_b c_{\theta_{12}} + e_3 s_{\theta_{12}})^2 + (d_1 s_{\theta_1} + e_2 c_{\theta_1} + r_b s_{\theta_{12}} - e_3 c_{\theta_{12}})^2} \end{bmatrix}$$

where $s_{\theta_1} = \sin\theta_1$, $c_{\theta_1} = \cos\theta_1$, $s_{\theta_2} = \sin\theta_2$, $c_{\theta_2} = \cos\theta_2$, $s_{\theta_{12}} = \sin(\theta_1 + \theta_2)$, $c_{\theta_{12}} = \cos(\theta_1 + \theta_2)$. Each cable can be comprised of multiple segments. The total length of the tendon can be determined by summing the length of each of its segments.

$$\begin{bmatrix} l_1 \\ l_2 \\ l_3 \end{bmatrix} = \begin{bmatrix} l_{11} + l_{12} \\ l_{21} + l_{22} \\ l_{31} \end{bmatrix} \tag{5.2}$$

Fig. 5.3 shows the schematic of CDKSC in an external routing configuration with pass-through scheme. This is a special case of Fig. 5.2 where the offset attachment distance e_5 is set to zero. The cables 1 and 3 are co-shared in link 1. At the anchor points, the cables are modeled as a source of pure force on the links to generate the joint torques. As discussed in Chapter 4, Section 4.2.1, the

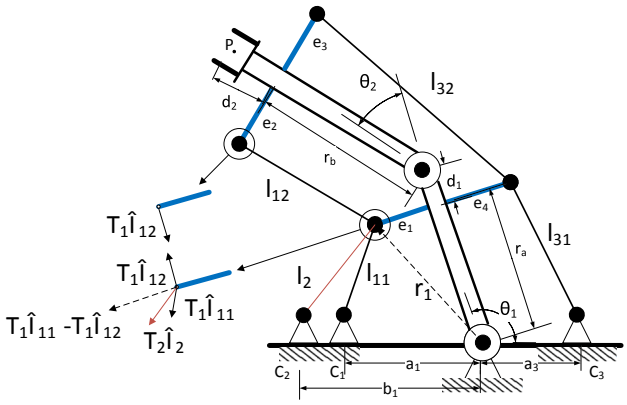

Figure 5.3: An illustration of the CDSKC with pass-through scheme with cable 2 and the first segment of cable 1 routed to a common point

dynamic model of the two DOF CDSKC can be formulated using Lagrange's method. The equations of motion are given as:

$$\frac{d}{dt}(\frac{\partial L}{\partial \dot{q}_i}) - \frac{\partial L}{\partial q_i} = Q_i, i = 1, \ldots, n \tag{5.3}$$

where L is the Lagrangian, n is the DOF of the chain, and q_i, Q_i are the generalized coordinates and generalized forces, respectively. The joint torques are presented in generalized coordinates as:

$$Q_i^c = \sum_{j=1}^{m} (T_j \hat{l}_j \cdot \frac{\partial \vec{r}_j}{\partial q_i}) \tag{5.4}$$

where $\vec{r}_j$ is the length of the j^{th} cable from base to the chain and T_j denotes the j^{th} cable force. To understand the effect of cable routing, let us look at the scenario of the torque generated respective joints due to cable 1 in Fig. 5.3. Considering cable 1 attached on link 2, one can model the contributed torque at joint 2 due to cable tension force T_1 as, $T_1 \hat{l}_{12} \frac{\partial \vec{r}_2}{\partial \theta_2}$. Here, $\hat{l}_{12}$ denotes the second segment of cable 1, which is the vector from attachment point on link 2 till link 1. The joint torque contribution due to cable 1 on joint 1 is given as, $T_1 \hat{l}_{12} \frac{\partial \vec{r}_2}{\partial \theta_1} + T_1(\hat{l}_{11} - \hat{l}_{12}) \frac{\partial \vec{r}_1}{\partial \theta_1}$. Here, the first term signifies the torque contribution by cable 1 on link 1 and the second

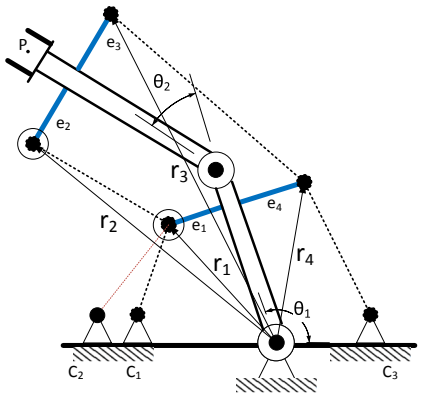

Figure 5.4: An illustration of the CDSKC with pass-through scheme showing cable attachment points and vectors r_i

term gives the torque contributed due to the routing (co-sharing) of cable 1 that is passing through link 1. Thus the torque contributed at joint 1 due to all cables, considering cables 1 and 3 to be co-shared and cable 2 attached individually to links 1 and 2, is given as,

$$Q_1^c = \begin{bmatrix} \hat{l}_{12}\frac{\partial \vec{r}_2}{\partial \theta_1} + (\hat{l}_{11} - \hat{l}_{12})\frac{\partial \vec{r}_1}{\partial \theta_1} & \hat{l}_2\frac{\partial \vec{r}_1}{\partial \theta_1} & \hat{l}_{32}\frac{\partial \vec{r}_3}{\partial \theta_1} + (\hat{l}_{31} - \hat{l}_{32})\frac{\partial \vec{r}_4}{\partial \theta_1} \end{bmatrix} \begin{bmatrix} T_1 \\ T_2 \\ T_3 \end{bmatrix} \tag{5.5}$$

Similarly, the torque contribution at joint 2, due to all cables are modeled and the expression results in,

$$\begin{bmatrix} Q_1^c \\ Q_2^c \end{bmatrix} = \begin{bmatrix} \hat{l}_{12}\frac{\partial \vec{r}_2}{\partial \theta_1} + (\hat{l}_{11} - \hat{l}_{12})\frac{\partial \vec{r}_1}{\partial \theta_1} & \hat{l}_2\frac{\partial \vec{r}_1}{\partial \theta_1} & \hat{l}_{32}\frac{\partial \vec{r}_3}{\partial \theta_1} + (\hat{l}_{31} - \hat{l}_{32})\frac{\partial \vec{r}_4}{\partial \theta_1} \\ \hat{l}_{12}\frac{\partial \vec{r}_2}{\partial \theta_2} & \hat{l}_2\frac{\partial \vec{r}_1}{\partial \theta_2} & \hat{l}_{32}\frac{\partial \vec{r}_3}{\partial \theta_2} \end{bmatrix} \begin{bmatrix} T_1 \\ T_2 \\ T_3 \end{bmatrix} \tag{5.6}$$

In contrast, the case when there is no routing of cable 2 and cable 3 along the links, which is equivalent to the direct-connecting scheme, then the formulation

can be written as,

$$\begin{bmatrix} Q_1^c \\ Q_2^c \end{bmatrix} = \begin{bmatrix} \hat{l}_1 \frac{\partial \vec{r}_1}{\partial \theta_1} & \hat{l}_2 \frac{\partial \vec{r}_2}{\partial \theta_1} & \hat{l}_3 \frac{\partial \vec{r}_3}{\partial \theta_1} \\ \hat{l}_1 \frac{\partial \vec{r}_1}{\partial \theta_2} & \hat{l}_2 \frac{\partial \vec{r}_2}{\partial \theta_2} & \hat{l}_3 \frac{\partial \vec{r}_3}{\partial \theta_2} \end{bmatrix} \begin{bmatrix} T_1 \\ T_2 \\ T_3 \end{bmatrix} \tag{5.7}$$

Modeling and evaluation of different actuation schemes are challenging due to various forms of tendon or cable routing. The kinematics are coupled since a single cable affects the motion of multiple links. In Fig. 5.5, the first cable is externally routed from the fixed end and is internally routed in the first link and then to the base. The internally routed cable is visualized as if the cables are rounding through the pulley rather than directly being attached on the link.

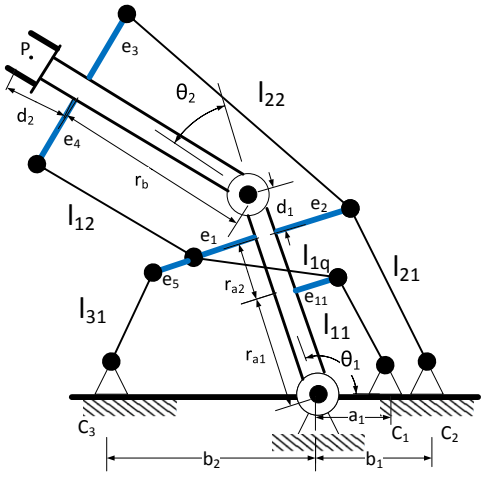

Figure 5.5: With single-point internal routing

$$\begin{bmatrix} l_1 \\ l_2 \\ l_3 \end{bmatrix} = \begin{bmatrix} l_{11} + l_{1q} + l_{12} \\ l_{21} + l_{22} \\ l_{31} \end{bmatrix} \tag{5.8}$$

$$\begin{aligned} l_{11} &= ((r_{a1}c_{\theta_1} + e_{11}s_{\theta_1} - a_1)^2 + (r_{a1}s_{\theta_1} - e_{11}c_{\theta_1} - m_1)^2)^{1/2} \\ l_{1q} &= ((r_{a2}c_{\theta_1} + e_{11}s_{\theta_1} + e_1 s_{\theta_1} - a_1)^2 + (r_{a2}s_{\theta_1} - e_{11}c_{\theta_1} - e_1 c_{\theta_1} - m_1)^2)^{1/2} \end{aligned} \tag{5.9}$$

where $r_a = r_{a1} + r_{a2}$. In the single point internal routing scheme, the first cable is split into three segments. There is a cross-over cable segment in the first link whose length is denoted by l_{1q}. Here q denotes the internally routed segment index. The rest of the configuration remains similar to the case described in Fig. 5.2.

We use two instead of one routing point per cable and link in Fig. 5.6. Likewise, if we can employ this actuation scheme over multiple links, it can aid in preventing coupling between adjacent moment arms. The coupling due to force along the cable remains. The symbolic expression of the cable length vector for the system shown in Fig. 5.6 is given in (5.10).

$$\begin{aligned} l_{11} &= (((r_{a1} - t_1)c_{\theta_1} - e_{12}s_{\theta_1} + a_1)^2 + ((r_{a1} - t_1)s_{\theta_1} + s_{12}c_{\theta_1} - m_1)^2)^{1/2} \\ l_{1r} &= ((t_1 c_{\theta_1} + e_{11}s_{\theta_1} + e_1 2s_{\theta_1} + a_1)^2 + (t_1 s_{\theta_1} - e_{11}c_{\theta_1} - e_{12}c_{\theta_1} - m_1)^2)^{1/2} \end{aligned} \tag{5.10}$$

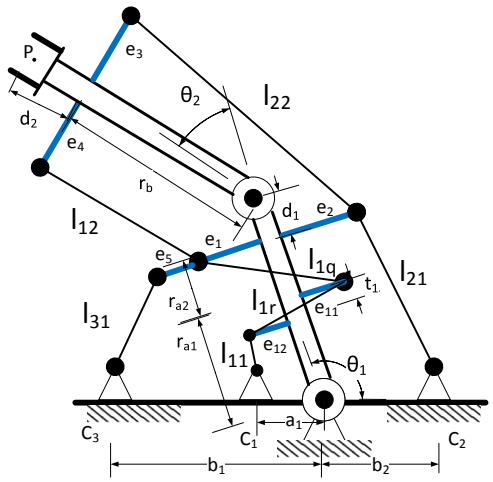

Figure 5.6: With multi-point internal routing

$$\begin{bmatrix} l_1 \\ l_2 \\ l_3 \end{bmatrix} = \begin{bmatrix} l_{11} + l_{1r} + l_{1q} + l_{12} \\ l_{21} + l_{22} \\ l_{31} \end{bmatrix} \tag{5.11}$$

Fully routed cable driven network consists of both external and internal routing.

Fig. 5.7 and Fig. 5.8 has a topology different from the above actuation schemes. Here, the cables form a bundle and are routed to the base. Cables C_1 and C_2 are bundled to the base in Fig. 5.7. C_1 and C_3 are bundled at the base in Fig. 5.8, C_1 is both externally and internally routed. The bundling here signifies that many cables are optimally joined to move with distinct speeds along the same lines possibly and can be regarded as one common cable from the statics perspective. The bundled cables are not purely coincidental.

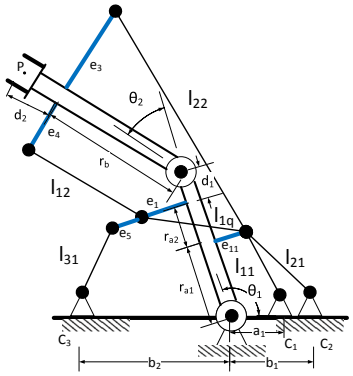

Figure 5.7: With single-point internal routing and bundling

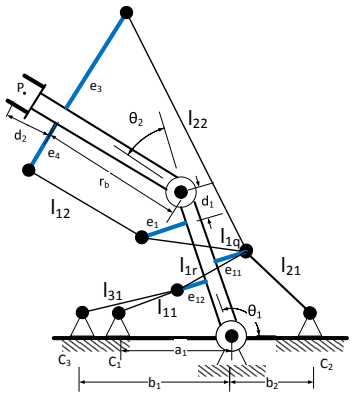

Figure 5.8: With multi-point internal routing and bundling

The tendon(cable) driven systems appear similar to the musculoskeletal structure in terms of using unilateral forces. The shoulder and elbow joints can be modeled with six muscles (two biarticular and four simple joint muscles) under

zero gravity. This model is shown in Fig. 5.9. The muscle is regarded as massless rigid wire with changeable length. The length vectors of the musculoskeletal system is given in Eqn. 5.2.2. There are three spaces (cable, joint and task) and two kinematic maps which constitutes the Jacobian. Muscle Jacobian relates cable and joint spaces. The taskspace-joint Jacobian matrix is defined for the kinematic serial chain.

$\boldsymbol{q} = [\theta_1, \theta_2]^T$ constitutes the joint angles. The cable length vector $\mathbf{l}$ for the six cable arrangement is given by:

$$[l_1\ l_2\ l_3\ l_4\ l_5\ l_6]^{\mathrm{T}} = \tag{5.12}$$

$$\begin{bmatrix} \sqrt{(a_1 + r_a c_{\theta_1} - e_1 s_{\theta_1})^2 + (m_1 - r_a s_{\theta_1} - e_1 c_{\theta_1}))^2} \\ \sqrt{(a_2 - r_b c_{\theta_1} - e_2 s_{\theta_1})^2 + (m_2 - r_b s_{\theta_1} + e_2 c_{\theta_1}))^2} \\ \sqrt{(a_3 + (L_1 - r_a) c_{\theta_2} - e_3 s_{\theta_2})^2 + (m_3 - (L_1 - r_a) s_{\theta_2} - e_3 c_{\theta_2})^2} \\ \sqrt{(a_4 - (L_1 - r_b) c_{\theta_2} - e_4 s_{\theta_2})^2 + (m_4 - (L_1 - r_b) s_{\theta_2} + e_4 c_{\theta_2})^2} \\ \sqrt{(b_1 - L_1 c_{\theta_1} + b_3 c_{\theta_{12}} - p_3 s_{\theta_{12}})^2 + (p_1 - L_1 s_{\theta_1} - b_3 s_{\theta_{12}} - p_3 c_{\theta_{12}})^2} \\ \sqrt{(b_2 - L_1 c_{\theta_1} + b_4 c_{\theta_{12}} + p_4 s_{\theta_{12}})^2 + (p_2 - L_1 s_{\theta_1} + b_4 s_{\theta_{12}} - p_4 c_{\theta_{12}})^2} \end{bmatrix}$$

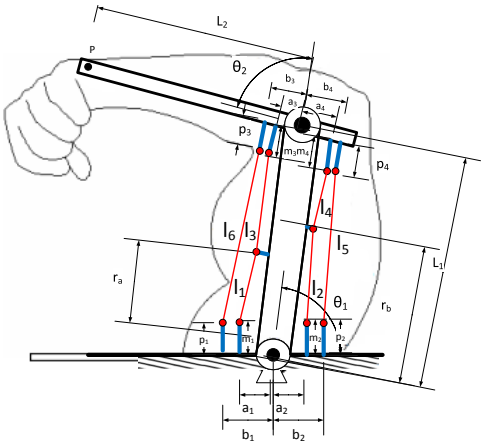

Figure 5.9: Human arm with mono- and bi-articular muscles

Table 5.2: Specifications of cable driven robot (in mm)

i	1	2	3	4
a_i	50	50	50	50
b_i	70	70	70	70
e_i	10	10	10	10
p_i	0	0	0	0
m_i	0	0	0	0
r_{a_i}	100	100	-	-
r_b	100	-	-	-
t_1	50	-	-	-
d_i	20	50	-	-
L_i	234	315	-	-
com_i	117	157.5	-	-

5.2.3 Workspace evaluation of different cable driven robots

The end-effector can reach the workspace when the tension in the cables are kept positive and all other motion and force constraints are satisfied.

The workspace of the musculoskeletal two-link cable driven robot for different routing configurations was evaluated with the parameters shown in Table 5.2. The inertia parameters I_{xx} and I_{zz} are 0.00780 and $0.00397\,\mathrm{kg}\cdot\mathrm{m}^2$ for the two link system. The results of WCW evaluation for cable routings without bundling is presented in Fig. 5.10. The minimal fully-routed and bundled cable actuation's WCW is given in Fig. 5.11.

5.2.4 Hardware Design

A reconfigurable and modular robot(shown in Fig. 1.3) was designed tailoring the needs and requirements of testing different routing topologies. The key hardware components are the muscle actuators, NEMA 17 stepper motors with drive pulleys (a winding device) that allows the easy control of the robot motion, the cable material is 0.48 mm 80lbs braided fishing line selected according to the task requirements. The body of the robot is made of 3D-printed thermoplastic Polylactic acid(PLA) and a variable spacer is employed to facilitate multiple routing configurations.

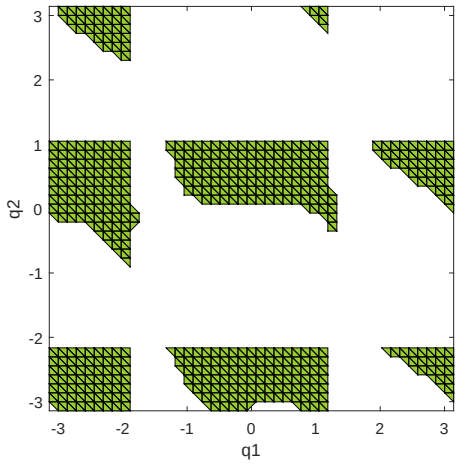

(a) Externally routed with 3 cables

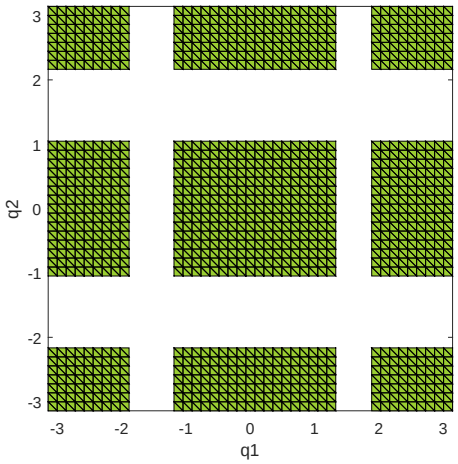

(b) Internally routed 3 cables single-point without bundle

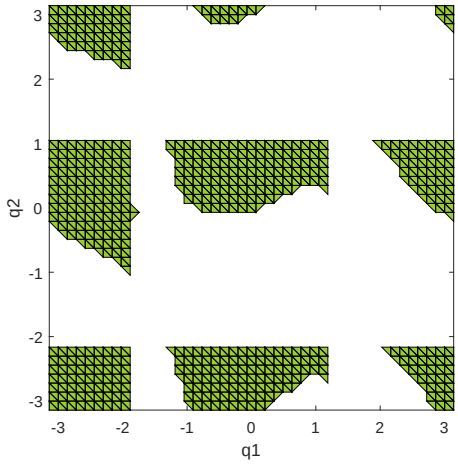

(c) Internally routed 3 cables multipoint without bundle

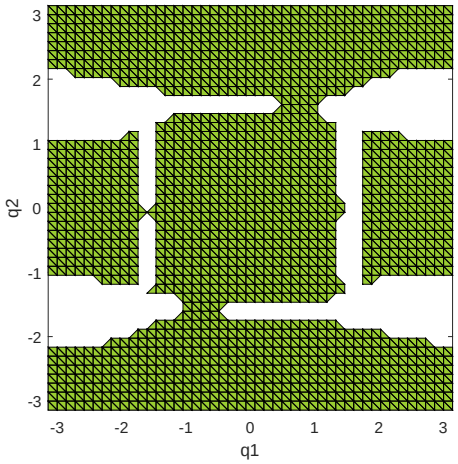

(d) With 4 cables

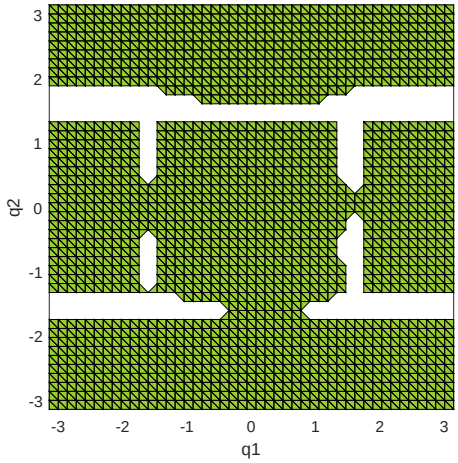

(e) With 5 cables

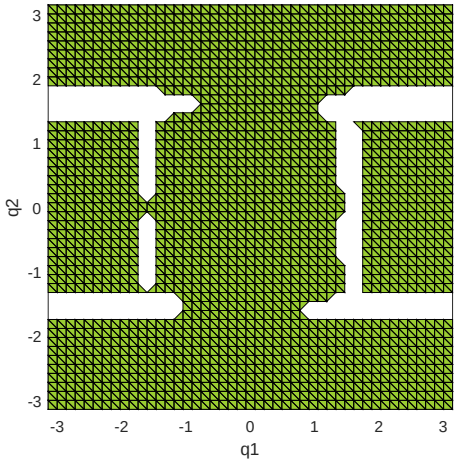

(f) Biarticular 6 cables

Figure 5.10: Results of wrench closure evaluation of cable driven robot with different routing topologies

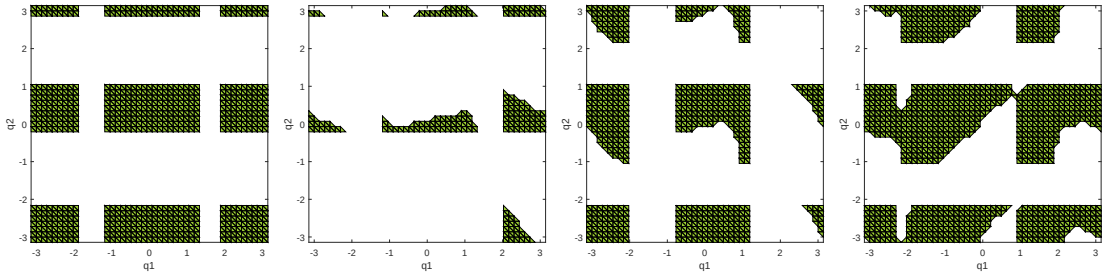

(a) Internally routed 3 cables single-point with bundle **(b)** Internally routed 3 cables multipoint with bundle **(c)** Internally routed 3 cables multipoint cross-bundle **(d)** Cross routed 3 cables single-point

Figure 5.11: Results of wrench closure evaluation of minimally routed and bundled cable driven robots

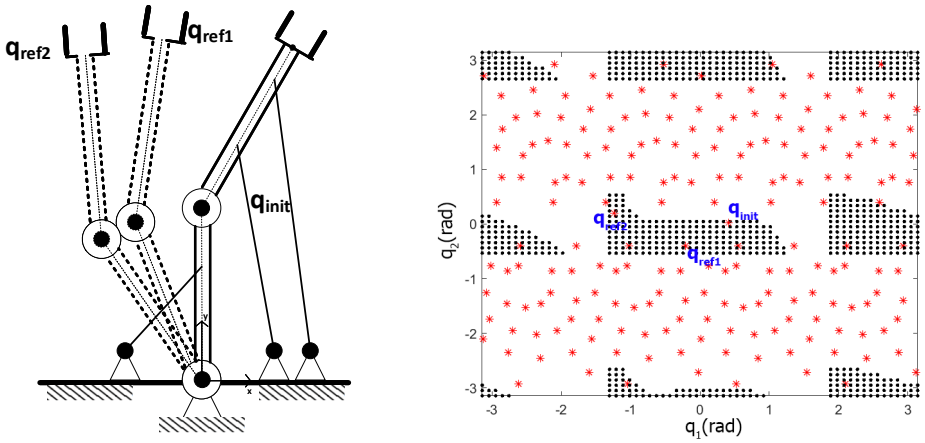

Figure 5.12: Example of a 2DOF CDSKC driven by three cables performing Point to Point motion problem in body and joint space

The cable pulling force is applied to the mounting point on the robot's body rather than generating torques directly between two rigid bodies. The slider based routing holes are 1.3mm in diameter and the distance between the holes are 2mm. The base slider can be shifted thereby changing the distance of the routing point and modifying parameter values in the cable space Jacobian. This allows the user to reconfigure the robot into a new configuration and checking the wrench-feasible workspace. The number of routing holes are 12 at the base and 30 at the mounting parts. The length of fabricated links are 234mm and 315mm including the end effector. There are a total of 30 routing points. The two links are cylindrical and

hollow that simplifies the internal routing, bundling and cross routing actuation schemes. The CAD model of the proposed experimental setup is shown in Fig. 5.17a). The wrench feasible motion generation for different topologies is explained in the following section.

5.2.5 Motion Generation Problem

The motion generation problem is defined for two coordinate spaces: the joint space and the operational space(task space). The joint space refers to the generalized coordinates of the mechanism and the task space refers to the coordinates attached to the mechanism's end effectors. The end-effector pose may correspond to potentially infinite distinct joint space poses in the case of CDKSC's. The point to point motion in joint space considers the problem of constructing a trajectory to connect a disjoint sequence of κ joint space poses. In contrast, the task space point to point motion considers the problem of constructing a joint space trajectory which connects a disjoint sequence of κ task space poses. Fig.

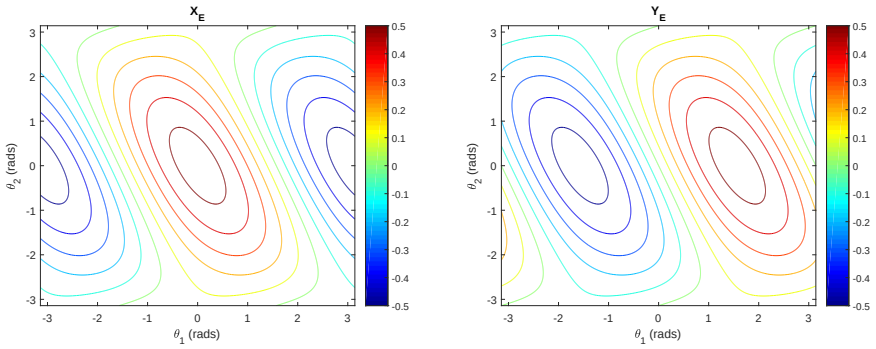

(a) **(b)**

Figure 5.13: Joint space with operational space contours (X and Y coordinate) of 2R robot - Each contour represents a set of joint space configurations that map to the end effector pose

5.12(a)-(b) shows an example problem in body space and joint space respectively. The WCW is overlayed in the joint space in order to visualize the WCC. Fig. 5.12(b) is equivalent to a sequence of standard trajectory problems that connect two points in the configuration space to one another. It is observed that the CDKSC is free to move along any path within the allowable configuration space

with the constraints from dynamics, unilateral actuation and pose dependent cable structure matrix. In order to ensure trajectory feasibility, the unilateral cable force constraint is an imperative condition for the proposed system. It is possible for the robot to generate motion in one direction and change as the robot configuration changes. Also, it can be incapable of generating the desired motion. The joint space motion generation is identical to connecting two points in the joint space considering the unilateral actuation constraint and pose dependent cable space matrix. The wrench closure evaluation is made in order to ensure that the feasible trajectory can be achieved.

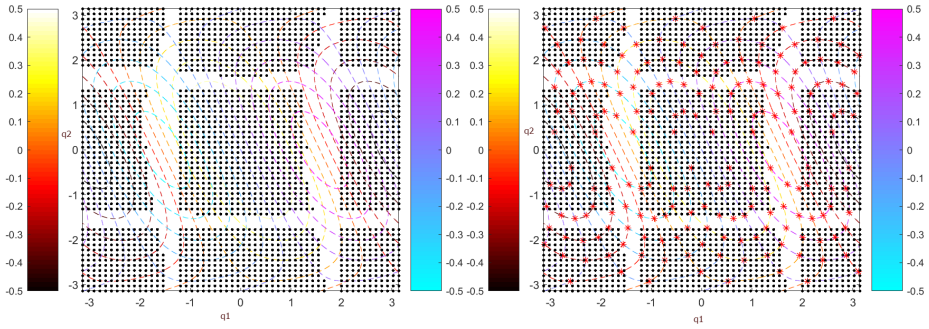

(a) **(b)**

Figure 5.14: WCW with task space contours of two link planar CDSKC with internal routing topology

For task space motion generation, the task space contours along with the joint space is necessary along with the wrench closure evaluation. Fig. 5.13(a)-(b) shows the X and Y coordinate of the end effector plotted as task space contours in the joint space. Each contour represents a set of joint space configuration that maps to the end-effector pose through the forward kinematics map. Since the operational space pose is two dimensional, the intersection of contours are plotted in a single representation in Fig. 5.14(a)-(b). It can be seen that the task space point to point motion planning corresponds to the problem of connecting an initial point in the joint space to a sequence of joint space contours. Any point on the same intermediate contour can be reached in the task space. The structural redundancy of CDKSC can be utilized to keep the robot within favorable regions. Fig. 5.14(a)-(b) shows the WCW of the two link CDSKC with internal routing topology with

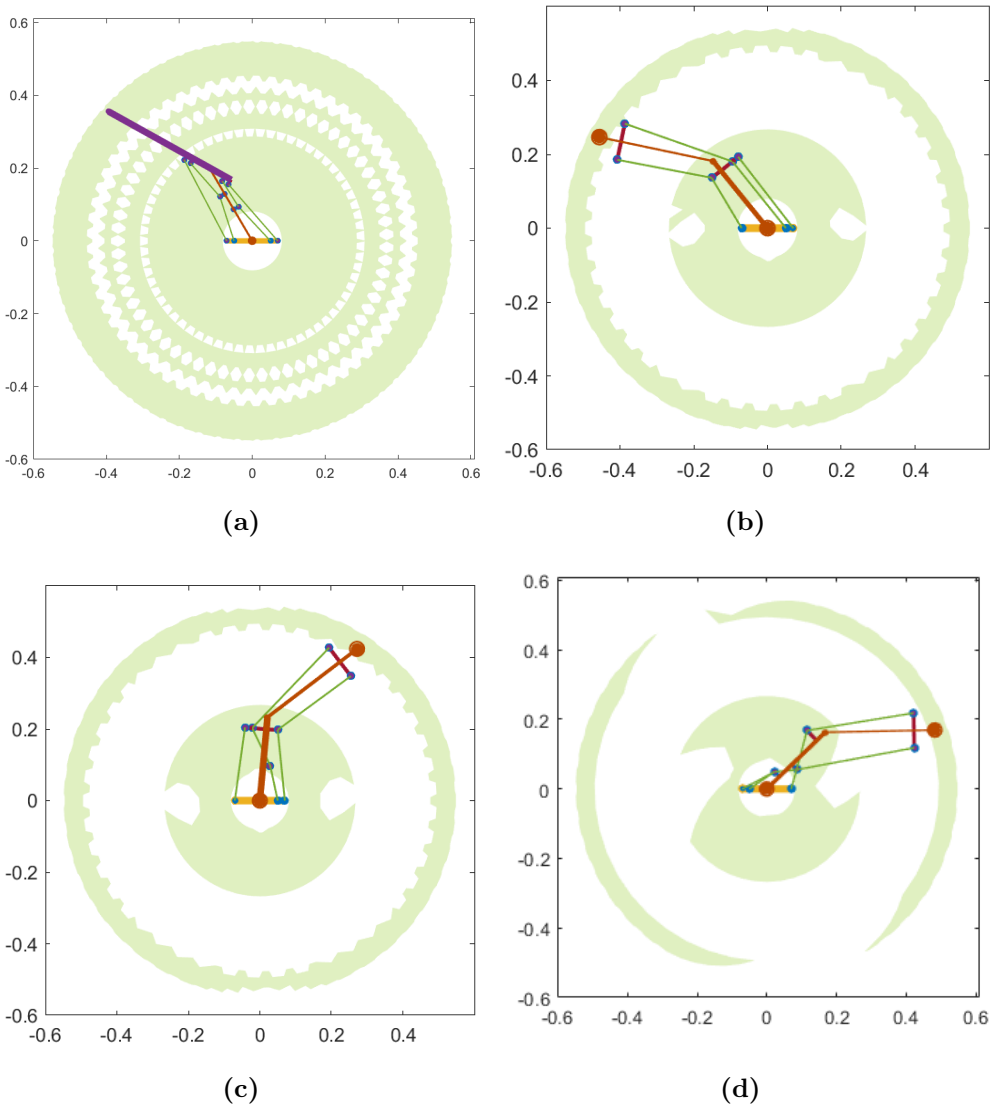

Figure 5.15: End-effector reachable area of two link planar CDSKC with a) 6 cable b) 3 cable externally routed (pass-through scheme) c) 3 cable with single point internal routing d) 3 cable with multi point internal routing and bundling topology

task space contours. We can observe a square property with the internal routing topology unlike the other routing topologies. So we choose this robot for study of motion generation capabilities. The workspace possesses multiple regions that are disconnected. For all poses within the same connected components, the point to point motion planning can be performed. Simply put, There exists a solution for the point to point task space motion planning problem for all paths and trajectories contained with the same connected set. The problem cannot be solved for joint space motion generation where the path goes from one of the connected components to another. The use of WCC as a condition for planning motions online can be observed in Fig. 5.14(a)-(b). In contrast, complete knowledge of contours is required in addition to WCC for task space motion planning. This requires the designer to store the necessary workspace information in prior for online task space planning.

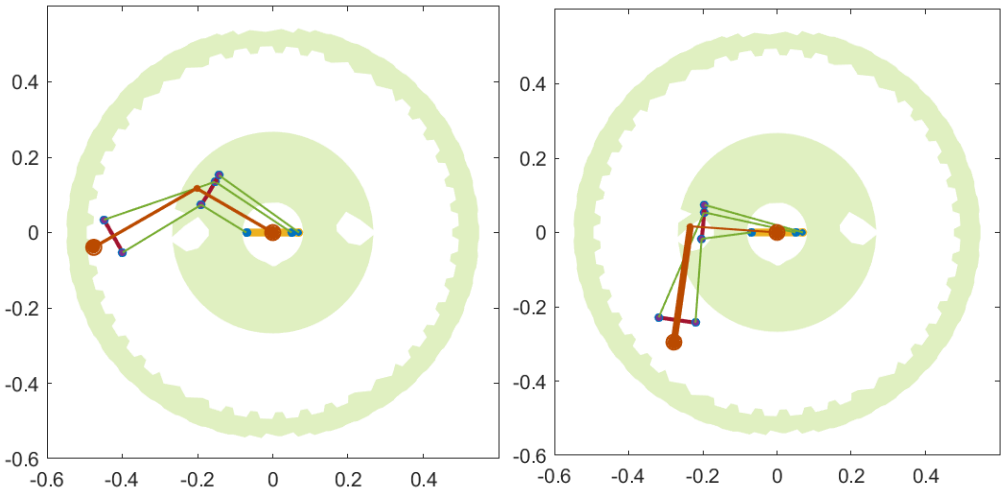

Figure 5.16: Restricted poses for the robot due to collisions between cables and frame

The end-effector reachable area is one of the workspace metric that will be used to quantify a given robot configuration. For a 2R robot, the robot has a physical workspace which is limited between two circles of radii $L_1 + L_2$ and $L_1 - L_2$. By applying the forward kinematics map to the allowable joint angles that satisfies the WCC, the end-effector reachable area can be found. The end-effector reachable area for two link CDKSC with 6 cables in biarticular muscle configuration (simulating

the human arm) and with 3 cables externally routed, single-point internally routed and multi-point internally routed and bundled topology is shown in Fig. 5.15(a)-(d) respectively.

The operation space of two link CDSKC with 6 cables arranged in biarticular configuration is the maximum among different cable routing configurations. This is due to two reasons as the cables are directly connected to the base without co-sharing or routed through links via attachment points. One can observe the 3-cable configuration has minimal workspace compared to the 6-cable configuration. There is a loss of workspace in Fig. 5.15(b) and the reachable workspace is primarily along the boundaries and across the origin. This is due to the fact that the routed cables results in actuation of link 1 even when minimal actuation of link 2 is required leading to instability in the joint 1. The point where the cable is routed through link 1 serves as the actuation point for link 2. It is unable to generate enough moment arm for link 2 to get actuated as the point is closer to link 1. By increasing the offset distance of the attachment points, the workspace can be improved. This, in effect, facilitates the existence of sufficient moment arm for link 2 from the connection point on link 1. The configuration with the least workspace is shown in Fig. 5.15(d). This is due to the fact the configuration is highly coupled with multiple points of routing and bundling. The loss of workspace is observed along the side on which cable is routed and bundled.

The robot is constrained from attaining poses which causes cable to collide with the rigid bodies as shown in Fig. 5.16. These constraints are translated into joint angle limits and the 'constraint-map' region in the joint-space is generated. A sample of restricted poses in task space are shown in Fig. 5.16. The simulated result of cable robot with single point internal routing configuration performing a feasible joint space trajectory is shown in Fig. 5.17b). Three sample trajectories were generated using quintic splines and was simulated using RViz for all configurations. The first trajectory was from $q_{start} = [-1, 0]$, $q_{mid} = [-0.05, 0.01]$ and $q_{mid} = [0.0, 0.0]$. This joint space trajectory is feasible for all configurations. Similarly, the other two trajectories were generated for which robots with certain routing topology didn't satisfy the wrench closure condition. The results of inverse kinematic analysis for two cases: 4 cable and 3 cable with internal routing are shown in Fig. 5.18 and 5.19 for the given trajectory.

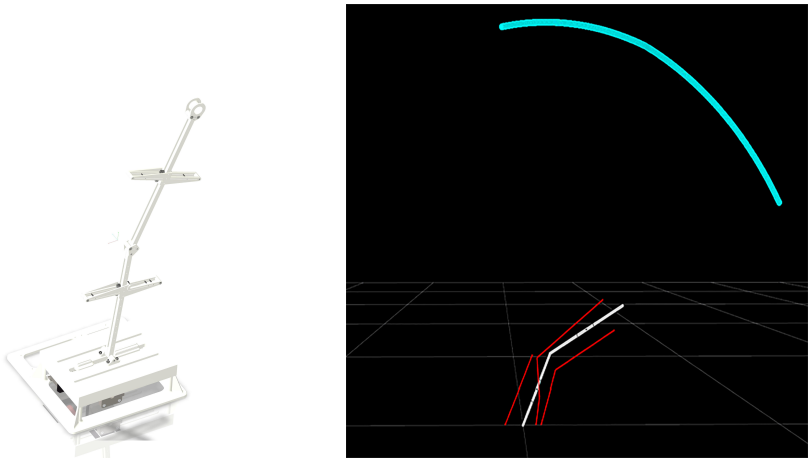

(a) **(b)**

Figure 5.17: a) CAD model of the modular robotic system enabling different routing topologies b) Joint space trajectory simulation of robot with single point internal routing without bundling

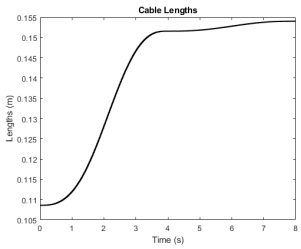

(a) Cable 1 length $l_1(t)$

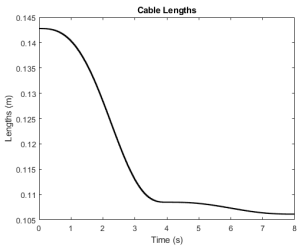

(b) Cable 2 length $l_2(t)$

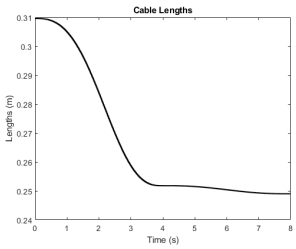

(c) Cable 3 length $l_3(t)$

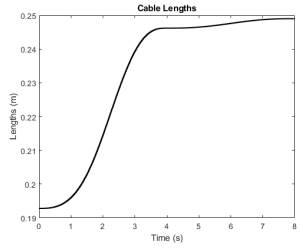

(d) Cable 4 length $l_4(t)$

Figure 5.18: The cable lengths from the inverse kinematic analysis on 2 link planar CDSKC for a given trajectory. The length $l_i(t)$ for cables 1 to 4 are shown for 4 cable configuration 5.10(d)

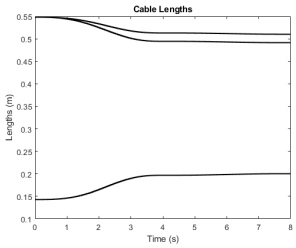

(a) Cable lengths $l_i(t)$

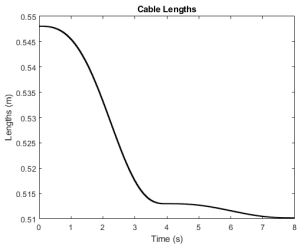

(b) Cable 1 length $l_1(t)$

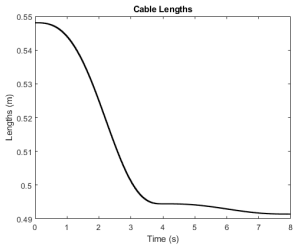

(c) Cable 2 length $l_2(t)$

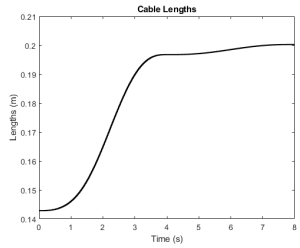

(d) Cable 3 length $l_3(t)$

Figure 5.19: The cable lengths from the inverse kinematic analysis on 2 link planar CDSKC for a given trajectory. The length $l_i(t)$ for cables 1 to 3 are shown for single point internal routing configuration 5.10(b)

5.2.6 Stiffness Evaluation

For small change in joint torque there will be changes in joint angles.

$$d\mathbf{W} = \mathbf{K}dq \tag{5.13}$$

where $\mathbf{K}$ denotes the relation between joint torques and angles, which is called as stiffness matrix. From the relation between $\mathbf{W}$ and $\mathbf{A}$, we obtain,

$$\begin{aligned} d\mathbf{W} &= (d\mathbf{A})f + \mathbf{A}(df) \\ s.t., \mathbf{K}dq &= (d\mathbf{A})f + \mathbf{A}(df) \end{aligned} \tag{5.14}$$

where df denotes the small changes in cable tensions which can be related to changes in cable lengths through cable stiffness k_c,

$$df = k_c dl \tag{5.15}$$

where dl, is the change in cable lengths. The rate of change of cable length can be related to joint rates as

$$dl = -\mathbf{A}^{\mathsf{T}}(dq) \tag{5.16}$$

Utilizing Eqn. 5.14 and 5.16, we obtain

$$\mathbf{K}dq = (d\mathbf{A})f - \mathbf{A}k_c\mathbf{A}^{\mathsf{T}}dq \tag{5.17}$$

where, k_c is the cable stiffness matrix which is represented as $diag[k_1, \ldots, k_m] \in \mathbb{R}^{m\times m}$ is the diagonal matrix of cable stiffness, m is the number of cables. $d\mathbf{A}$ can be written as,

$$d\mathbf{A} = \sum_{i=1}^{n} \frac{\partial \mathbf{A}}{\partial q_i} dq_i \tag{5.18}$$

Hence,

$$\mathbf{K} = \left[\frac{d\mathbf{A}}{dq_1}f \frac{d\mathbf{A}}{dq_2}f \ldots \frac{d\mathbf{A}}{dq_n}f\right] - \mathbf{A}k_c\mathbf{A}^{\mathsf{T}} \tag{5.19}$$

where,

$$\begin{aligned} \mathbf{K} &= \mathbf{K}_d + \mathbf{K}_e \\ s.t, \mathbf{K}_d &= \left[\frac{d\mathbf{A}}{dq_1}f \frac{d\mathbf{A}}{dq_2}f \ldots \frac{d\mathbf{A}}{dq_n}f\right] \\ \mathbf{K}_e &= -\mathbf{A}k_c\mathbf{A}^{\mathsf{T}} \end{aligned} \tag{5.20}$$

The overall stiffness matrix $\mathbf{K}$ of CDSKC is a function of stiffness of each cable, cable tension distribution and the pose dependent structure matrix (i.e the attachment points on the link and on the motors). $\mathbf{K}_e$ is a matrix of the end-point stiffness. For a two link CDSKC, $\mathbf{K}_e \in \mathbb{R}^{2\times 2}$. A stiffness ellipse can be defined for matrix $\mathbf{K}$ using the principle axis theorem. The stiffness behavior of the robot can be analyzed using indices based on eigenvalues of $\mathbf{K}$. These are the stiffness magnitude and condition number. The isotropic stiffness behavior represents the condition number equal to one. The major axis of the ellipse is directed along the eigenvector with smaller eigenvalue and the minor axis is direct along the eigen vector with larger eigen value. For a 3D representation, stiffness ellipsoids can be visualized. Stiffness modulation can be achieved in the articulated cable robot by changing the system configuration, cable tension and the joint stiffness which are useful for variable stiffness applications.

The stiffness evaluation of two link robot with 4 cables in direct connecting

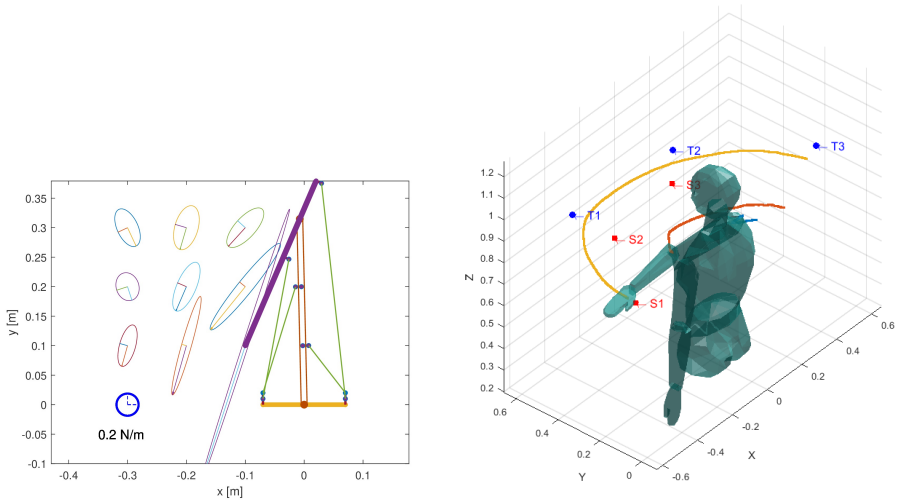

(a) (b)

Figure 5.20: a) Static stiffness evaluation of two link robot with 4 cables b)Simulated human arm trajectory with the hand path following S1→T1 → T2 → T3

cable routing scheme is shown in Fig. 5.20. The calibration circle is shown at the bottom of the plot. Each stiffness ellipse represents the direction and magnitude of resisting forces to unit-displacement perturbations in all directions. The major axis represents the maximum force which indicates the highest stiffness. Conversely, the minor axis indicates the least stiffness. The stiffness ellipses were evaluated at nine different end point positions as indicated in Table 5.3. The stiffness performance is dependent on cable stiffness value, cable routing points on links and the base

Table 5.3: Arm end point positions

Arm-position	Value[m]
P_1	[-0.3,0.3]
P_2	[-0.3,0.2]
P_3	[-0.3,0.1]
P_4	[-0.2,0.3]
P_5	[-0.2,0.2]
P_6	[-0.2,0.1]
P_7	[-0.1,0.3]
P_8	[-0.1,0.2]
P_9	[-0.1,0.1]

and tension. The evaluation was performed by holding the end-point posture of the robot.

At end-point position P9, the stiffness ellipse is anisotropic and it is stretched compared to other ellipses. At end-point position P9, the stiffness ellipse reaches isotropy and the condition number approaches 1. The magnitude and condition number is lower compared to the ellipses at different postures as indicated in the table. The static evaluation for different routing topologies were investigated and presented. The magnitude of cable driven robots with larger number of cables is high and the stiffness ellipse is larger. The condition number of the cables with internally routed and bundled chains is lower than the human arm mimicking cable robot.

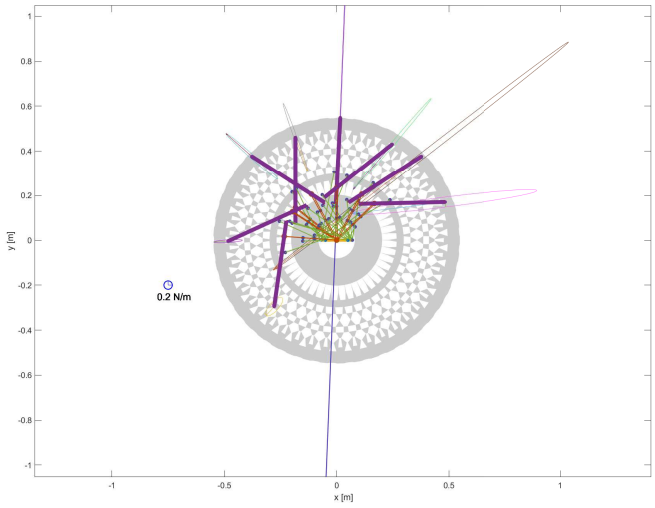

Figure 5.21: Externally routed with 4 cables

5.2.7 Experimental protocol

The planning modality for trajectory is based on an experiment with a test subject. Human arm trajectory with the subject was performed and recorded using MoCap Optitrack system equipped with 8 cameras. The length of the upper arm and forearm are 315mm and 234mm respectively. The subject was seated and placed

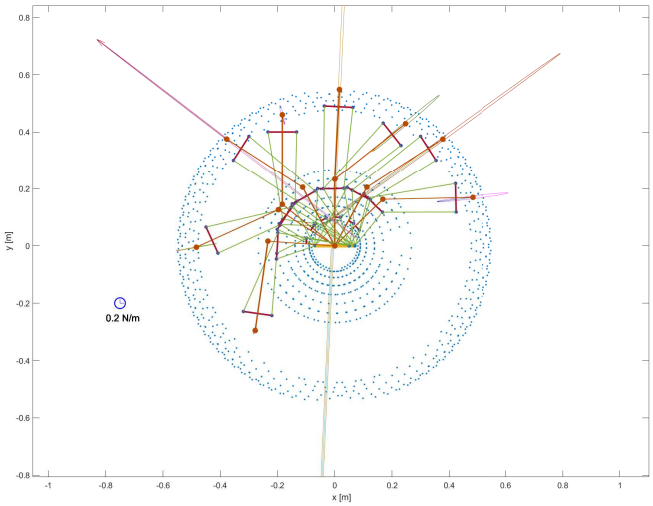

Figure 5.22: Internally routed 3 cables single-point without bundle

the right arm on the horizontal surface. The subject was right-handed and free of musculoskeletal abnormalities. This setup facilitated flexion/extension of the shoulder and elbow joints in the horizontal plane. The subject is to perform the postural task by moving the ping ball to the target cube (T_1, T_2 and T_3) from different start points (S_1, S_2 and S_3). The selected arm postures and the hand positions where the subject will perform the arm reaching movements are shown in Fig. 5.20(b).

The experiment of arm reaching movements were made by one subject for three test trials per task. The motion capture reflective markers for optical tracking was utilized and 3 trackers were attached to the shoulder, elbow and wrist joint centers. Prior measurements were made with the subject in order to accomplish accurate tracking. $S_1 \rightarrow T_1 \rightarrow T_2 \rightarrow T_3$ was selected among different trajectories performed. The kinematic profile of the measured trajectory was mathematically formulated by using polynomial curve fitting. The end point positions for evaluating the stiffness ellipsoids for the experimental trajectory were selected and optimized based on task space point to point motion planning. The segment of trajectory is specified by assigning initial and final conditions on duration, position, velocity and acceleration. This boundary condition problem is solved by considering a

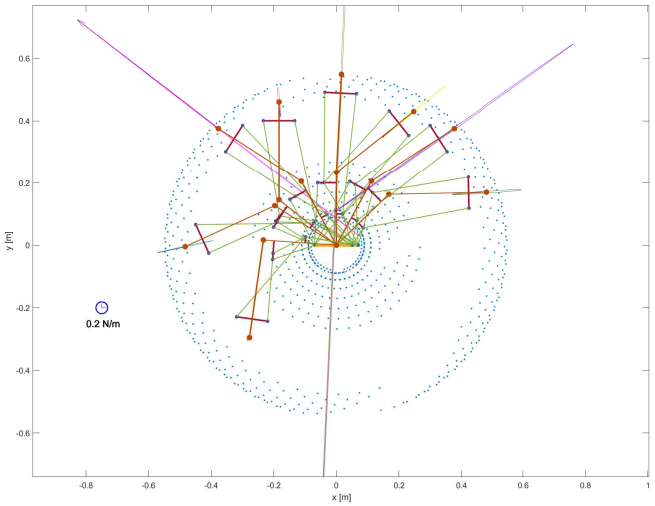

Figure 5.23: Internally routed 3 cables single-point with bundle

quintic polynomial. It was observed that there is significant shift in stiffness behavior with the change in tendon routing, number and architecture. In the tasks where the end effector of the robot must be compliant in one direction and stiff in another, it is desirable to use the internally routed singlepoint bundle topology where the routing is asymmetric. The nearly isotropic endpoint stiffness can be achieved with asymmetrically routed tendon driven robots by changing the cable attachment points. The size of the stiffness ellipse increases for the internally routed cable driven kinematic chains for increasing the length of the attachment point.

We observe that there is significant shift in wrench closure workspace with the change in tendon/cable routing, number and architecture. The biarticular muscle topology with six cables in Fig. 5.10f) has the highest workspace thereby making it the best candidate for exoskeletal and musculoskeletal robots. The four cable and five cable configuration in Fig. 5.10d) and e) also has continuous wrench closure workspace. The WCW of minimally actuated configuration$(n+1)$actuators are shown in Fig. 5.10(a-d). The single point internal routing configuration proved to be the best candidate among the minimal fully routed configuration. The workspace of multi-point internal routing and bundling is a subset of the single-

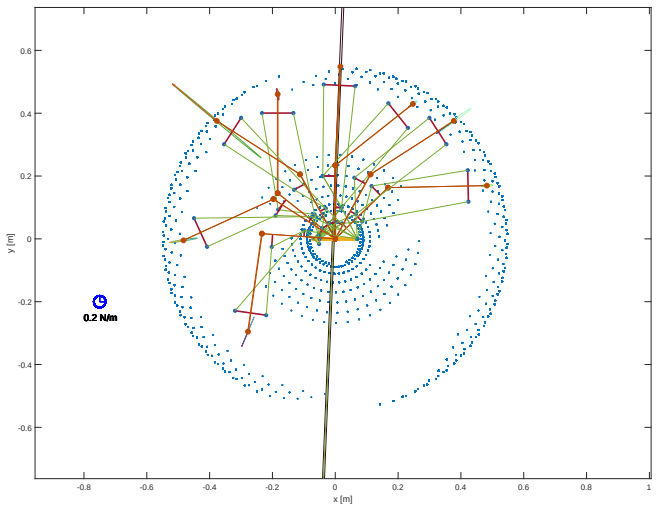

Figure 5.24: Internally routed 3 cables multi-point with bundle

point internal routing configuration as shown in the Fig. 5.10 b). The multi-point internal routing with bundling configuration has the least WCW among all the minimal fully routed configurations. The cross routing and cross bundling are two special cases where the cables are directly routed to the base rather than internally routing to the point and then to the base. The cross-bundle configuration is still a subset of single-point internal routing configuration. By routing the cable to the left or right of the robot, WCW can be shifted/flipped. Keeping in mind, the minimal actuator configuration, single-point internal routing configuration proved to be effective. The inverse dynamics of the cable driven robots were evaluated using linear programming solver and the desired cable forces were evaluated for the specified trajectory. The cable forces for a specified set of routing configurations are shown in Fig. 5.29. It is observed that the 4 cable case has minimal cable force distribution compared to the minimal actuator configuration. In the minimal actuator configuration, the cable tensions in the multi-point bundling case is quite high. The single point internal routing and bundling cases proved to be the best candidate for the minimal fully routed actuation. This simulation was performed for 3 sets of trajectories and conclude that the single point- internal routing configuration is a suitable choice $n + 1$ routing topology. The stiffness

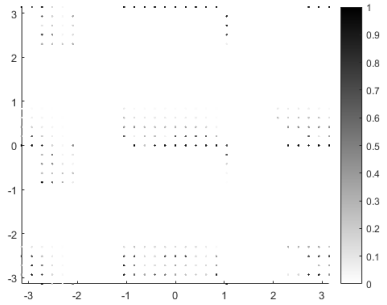

(a) Externally routed with 3 cables

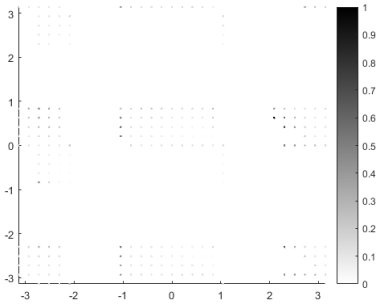

(b) Externally routed with 3 cables

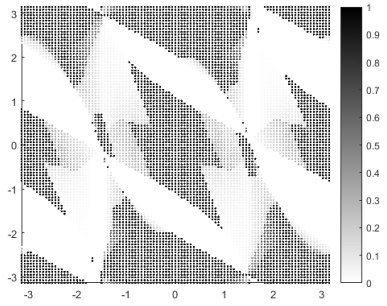

(c) With 4 cables

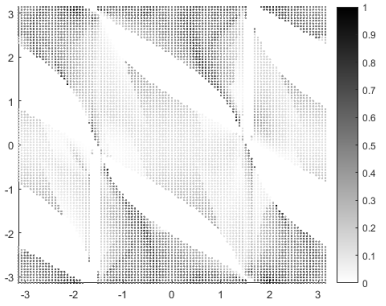

(d) With 4 cables

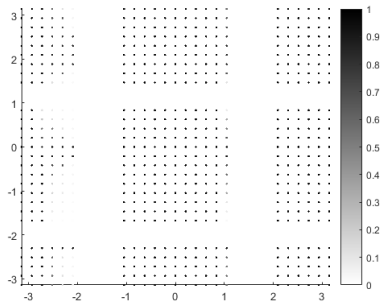

(e) Internally routed 3 cables single-point without bundle

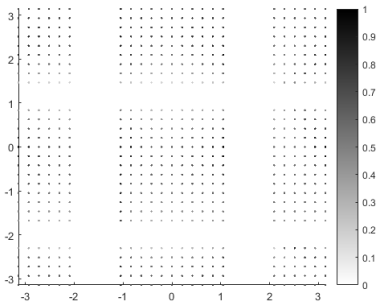

(f) Internally routed 3 cables single-point without bundle

Figure 5.25: Results of workspace metric: tension factor evaluation of cable driven robot with different routing topologies

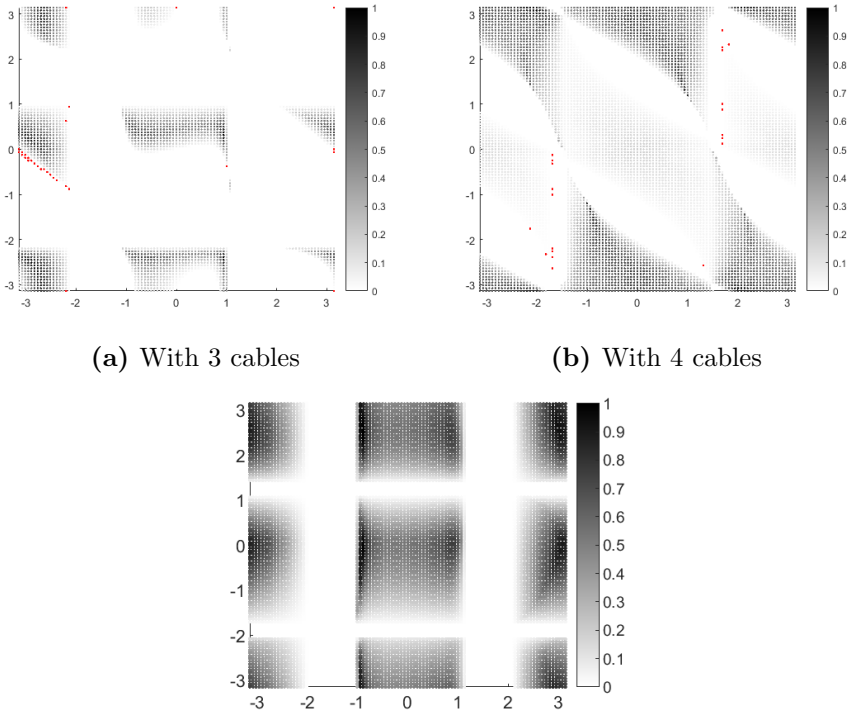

(a) With 3 cables

(b) With 4 cables

(c) Internal routing with 3 cables

Figure 5.26: Results of workspace metric: unilateral dexterity evaluation of cable driven robot with different routing topologies

ellipses were evaluated for the cases for which cable forces were computed. The same trajectory was used to calculate the stiffness ellipse of the mechanism. The trajectory is overlayed on the reachable workspace of the mechanism. The ellipse reaching the big line denotes that the mechanism is in its boundary, hence, tends to have infinite stiffness in one direction. The ellipse in third quadrant is out of workspace, therefore, is represented as a small ellipse. The four cable case seems to offer good stiffness in both directions ,then the single point internal routing case in 3 cable scenario followed by the single and multi point bundling cases. For the same postures, the bundling case has low stiffness values. Within the reachable workspace, more isotropic stiffness is favored.

The relative tension distribution among the driving cables for different routing topologies are measured using Tension factor index. This is an appropriate measure to evaluate the quality of force closure for CDSKCs. The optimal TF value is

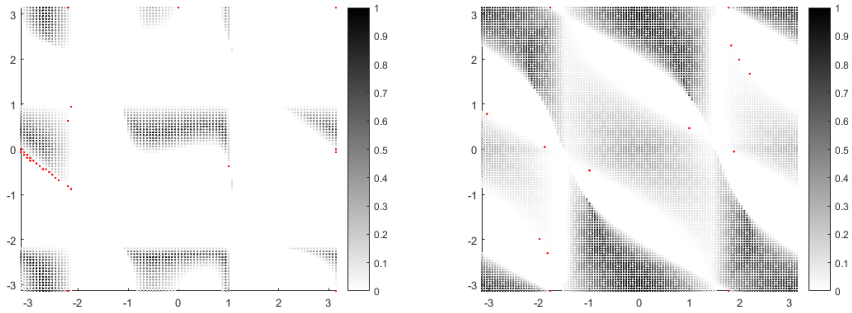

(a) With 3 cables

(b) With 4 cables

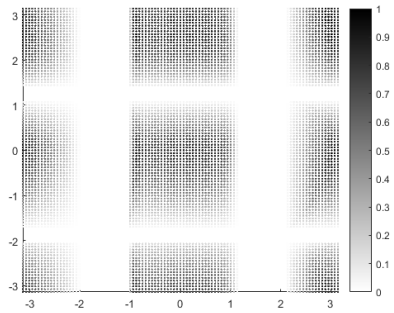

(c) Internal routing With 3 cables

Figure 5.27: Results of workspace metric: unilateral maximum force amplification evaluation of cable driven robot with different routing topologies

obtained through a linear optimization approach although the problem is essentially a non-linear optimization problem. The tension factor is the ratio of minimum tension over the maximum tension of the cables. It is a measure of the positive tension condition of the structure matrix. When the TF approaches to zero, the mechanism is located near to the workspace boundary and if TF approaches one, the mechanism is positioned far from the workspace boundary. Larger value of TF implies a balanced tension distribution among cables. A modified TF metric is also used that includes the singular value and effect of removing cables. The evaluation of TF and modified TF metric for two link planar CDKSC with different routing topologies are presented in Fig. 5.25. It can be observed that there is a uniform distribution of TF for two link planar CDSKC with 4 cables in direct connecting cable routing scheme. The internally routed scheme has better balance of TF in contrast to the pass-through routing scheme(externally routed) for two link

CDKSC with 3 cables.

In traditional CDPR analysis, workspace metrics denote physically meaningful metrics that are evaluated throughout the mechanism's workspace. It can be dexterity based or wrench based metrics. The dexterity analysis subjected to unilateral actuation constraints was mathematically elaborated in Chapter 1. Now, we will see how it is useful in the analysis of CDSKC motion generation capability. The unilateral dexterity and unilateral maximum force amplification are utilized as metrics for CDSKCs. Knowledge of these metrics provide insight into motion generation due to the quantification of cable force and joint wrench relationship. Maximizing UD and UF results in increased robustness of motion in presence of external disturbances, due to the lower cable forces required for opposing those disturbances. Fig. 5.26 depicts the UD measure over all poses of the WCW for 2 link CDSKC driven by 3 and 4 cables respectively. It can be observed that the UD of the CDSKC ranges from zero at poses outside or near the boundary of WCW to a maximum value away from the boundary. In general, this metric has a larger value at points away from the workspace boundaries. This suggests that the mechanism should be operated at such points to maximize its robustness. The WCW is singular when $q_1 = \pm\frac{\pi}{2}$, as the links are near to the physical location of the base attachment points. The UF (Unilateral maximum force amplification) metric measures the relationship between joint and cable space. Larger UF indicates minimal cable forces that will be needed to produce arbitrary joint space wrench. For the 2 link CDSKC, UF possesses a minimum value of 0 at workspace boundaries and maximum value away from the boundary. It has a similar pattern compared to UD metric. The mechanism needs to be operated in the regions where UF metric is maximum in order to minimize the cable forces required to oppose the undesired disturbance wrenches and in maximizing the capability to produce motion.

5.3 Cable Tension Planner

The kinetostatic equilbrium in matrix representation is expressed as:

$$\mathbf{J^T t} = \mathbf{W} \tag{5.21}$$

J^T is called the cable structure matrix, $\mathbf{t}$ is a column vector containing cable tensions and $\mathbf{W}$ is the sum of all external forces and moments including weight, inertial forces and moments. For CDKSCs, due to the fact that cables can pull but not push, the tensions must be kept positive. Mathematically the problem can be expressed as given in (5.21) where $\mathbf{A}$=$\mathbf{J^T}$. (5.21) is under-determined since the number of cables is greater than the number of DOFs. The goal of the cable tension planner is to find positive cable tensions $\mathbf{T}$ such that (5.21) is satisfied for given external torques at a certain pose. The solution of (5.21) is given by

$$\mathbf{T} = \bar{\mathbf{T}} + \lambda \mathbf{N} \tag{5.22}$$

where $\bar{\mathbf{T}}$ is the minimum norm solution of (5.21) which is given by

$$\bar{\mathbf{T}} = \mathbf{A^T}(\mathbf{A}\mathbf{A^T})^{-1}\mathbf{W} \tag{5.23}$$

$\mathbf{N}$ is a null space matrix of $\mathbf{A}$ and λ is a vector of arbitrary values (1-dimensional for redundancy one, 2-dimensional for $n+2$ cables), assuming $\mathbf{A}$ is full rank. The minimum tensions are chosen such that the cables are taut and the maximum tensions are limited both by safety and the maximum tension the motors are capable of delivering. Consider the above constraint on (5.22), this gives

$$\begin{bmatrix} \mathbf{N} \\ -\mathbf{N} \end{bmatrix} \lambda \geqslant \begin{bmatrix} \mathbf{T_{min}} - \bar{\mathbf{T}} \\ \mathbf{T_{max}} + \bar{\mathbf{T}} \end{bmatrix} \tag{5.24}$$

Using the equations (5.22) and (5.24), an optimal set of cable tensions can be found using linear or quadratic programming approaches. The linear programming problem formulation is as follows

$$\begin{aligned} & min \sum_i (\bar{\mathbf{T}} + \lambda \mathbf{N})_i \\ s.t. & \begin{bmatrix} \mathbf{N} \\ -\mathbf{N} \end{bmatrix} \lambda \geqslant \begin{bmatrix} \mathbf{T_{min}} - \bar{\mathbf{T}} \\ \mathbf{T_{max}} + \bar{\mathbf{T}} \end{bmatrix} \end{aligned} \tag{5.25}$$

The objective function minimizes the sum of all cable tensions such that each cable tension falls within the lower and upper bounds of cable tension. The

minimum-tension planner is computationally efficient and reduces the total energy consumption as the total cable tension is minimized. Due to the nature of linear programming problem, discontinuities are produced in the planned cable tension trajectories. The solution of a LP problem is always at the corner of the convex hull of feasible set and when the solution changes corner during motion, discontinuity occurs thereby making the low-level tension controller to have deteriorated tracking performance. The quadratic programming approach can provide continuous cable tension trajectories. The objective function is defined as

$$f(\mathbf{T}) = \frac{1}{2}(\mathbf{T} - \mathbf{T}_o)^\mathsf{T}(\mathbf{T} - \mathbf{T}_o), \tag{5.26}$$

where $\mathbf{T}_o$ is a constant vector of tensions ($(n+1) \times 1$ for redundancy one and $(n+2) \times 1$ for redundancy two). The objective is to minimize the deviation between $\mathbf{T}$ and $\mathbf{T}_o$. The objective function can be rewritten as

$$f(\mathbf{T}) = \frac{1}{2}\lambda^\mathsf{T}\mathbf{N}^\mathsf{T}\mathbf{N}\lambda + (\mathbf{T} - \mathbf{T}_o)^\mathsf{T}\mathbf{N}\lambda, \tag{5.27}$$

Thus, the continuous-tension cable planner is formulated using quadratic programming problem as,

$$\begin{aligned} min f(\mathbf{T}) &= \frac{1}{2}\lambda^\mathsf{T}\mathbf{N}^\mathsf{T}\mathbf{N}\lambda + (\mathbf{T} - \mathbf{T}_o)^\mathsf{T}\mathbf{N}\lambda \\ s.t. &\begin{bmatrix} \mathbf{N} \\ -\mathbf{N} \end{bmatrix} \lambda \geqslant \begin{bmatrix} \mathbf{T_{min}} - \bar{\mathbf{T}} \\ \mathbf{T_{max}} + \bar{\mathbf{T}} \end{bmatrix} \end{aligned} \tag{5.28}$$

The quadratic programming problem can be solved in bounded time and can be used for real time control.

5.3.1 Inverse Dynamics

The cable configuration of 2-link CDSKC with different set of routings are given in Table. 5.4 and Table. 5.5 respectively. All the cables are assumed to be ideal cables with minimum tension of 10N and maximum tension of 250N. The quadratic programming algorithm is utilized to compute the cable tensions. The evolution of pose variables of a joint space trajectory is shown in Fig. 5.29(a). Three different

	Link 0	Link 1	Link 2
Cable 1	$[-0.5, 0.025]'$	$[-0.3, 0.2]'$	$[-0.15, 0.31]'$
Cable 2	$[0.12, 0.025]'$	$[0.3, 0.2]'$	
Cable 3	$[1.5, 0.025]'$	$[0.3, 0.2]'$	$[0.15, 0.31]'$

Table 5.4: Cable configuration for 2-link MCDR with $n + 1$ actuated cables and pass-through routing scheme

	Link 0	Link 1	Link 1	Link 2
Cable 1	$[-0.5, 0.025]'$	$[-0.3, 0.2]'$		$[-0.15, 0.31]'$
Cable 2	$[1.5, 0.025]'$	$[0.3, 0.2]'$		
Cable 3	$[-0.45, 0.025]'$	$[-0.3, 0.1]'$	$[0.3, 0.5]'$	$[0.15, 0.31]'$

Table 5.5: Cable configuration for 2-link MCDR with internally routed $n + 1$ cables

cable routings were considered for comparison. Fig. 5.29(b-d) shows the tensions of the cables in the CDSKC while executing trajectory. The results are given in Table 5.7 for two link CDKSC. The maximum cable tensions is reduced in the internally routed scheme without loss to workspace performance through the use of internally routed configurations.

The above explained approach is applicable to the serial chain with cable bundles as shown in Figure 5.28. Fig. 5.28(a) and 5.28(b) shows the two-link planar CDSKC with $n + 2$ and $n + 1$ cables with direct-connecting and internal routing schemes respectively. Fig. 5.28(c) shows the pass-through scheme where the cables are both externally routed. Fig. 5.28(d) shows the internally routed scheme with minimal number of actuating cables. This is the minimal routed fully acutated configuration also called as fully routed configuration.

The symbolic expressions of the cable structure matrix are given in the ap-

	2N cables	N+1	N+1(internally routed scheme)
Maximal Cable Tension	92N	210N	32N

Table 5.6: The maximal cable tensions of two link CDSKCs with different cable routings

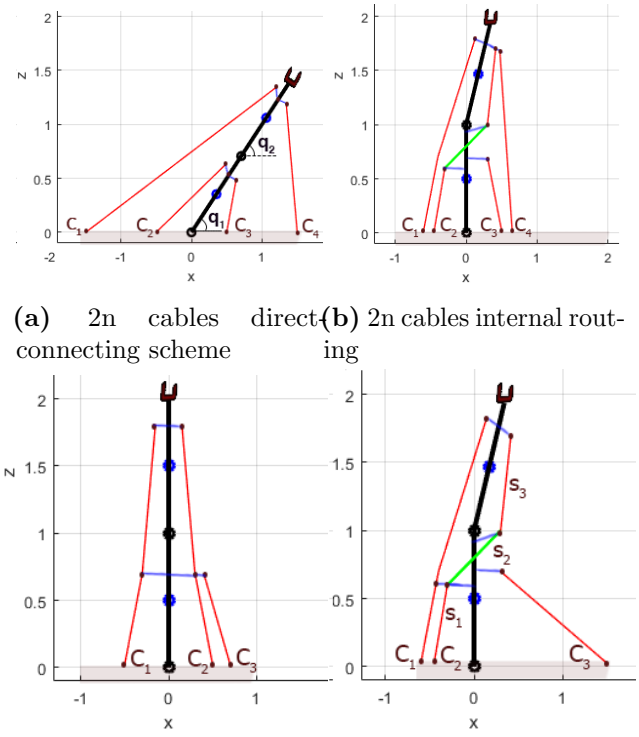

(a) 2n cables direct connecting scheme

(b) 2n cables internal routing

(c) n+1 cables pass-through scheme

(d) n+1 cables internal routing scheme

Figure 5.28: Two link cable driven robot with different routings

pendix. The WCW analysis for fully routed two-link, three-link planar and spatial CDSKC was performed. The designer has the flexibility to choose a particular routing configuration for a specific application. It can be seen that the cable attachments and routing scheme influences the performance of the cable-driven system. Table. 5.8 and Table. 5.9 shows the cable attachment points for three-link CDSKC used for simulation. The results of cable tensions for the three link planar CDSKC is shown in Fig. 5.31. The n+1 configuration shown in Fig. 5.30(b) was unable to achieve force-closure in the entire range of motion of the given trajectory

	2N cables	N+1	N+1(fully routed scheme)
Maximal Cable Tension	75N	∅	50N

Table 5.7: The maximal cable tensions of three link CDSKCs with different cable routings

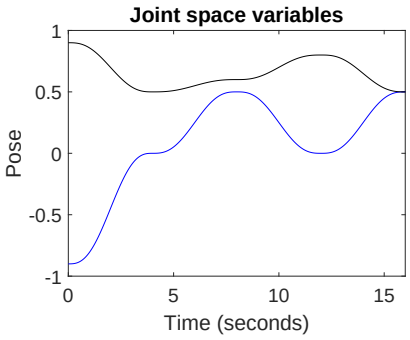

(a) Pose Variables

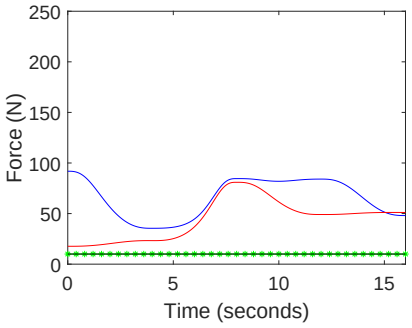

(b) With 2n cables

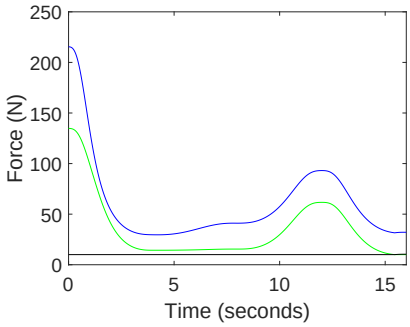

(c) With n+1 cables

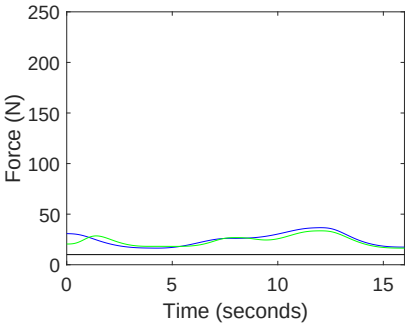

(d) Internally routed with n+1 cables

Figure 5.29: Tensions of cables for a given trajectory for two link planar robot with different cable routings

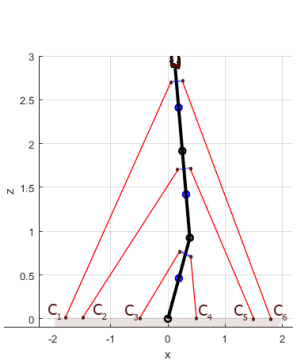

(a) Three Link Planar CDSKC with 2n actuated cables

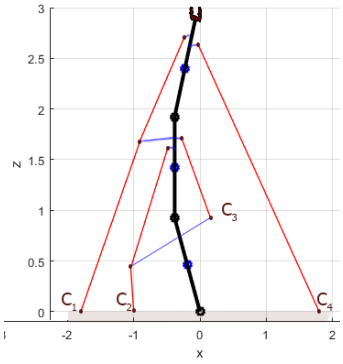

(b) n+1 cables with routing

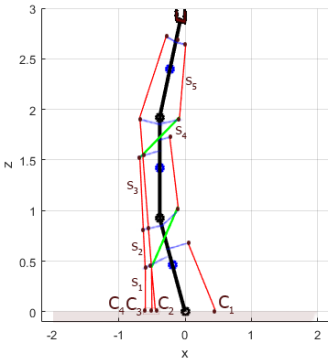

(c) Internal routing and bundling

Figure 5.30: Three link unilateral manipulator with routing and cable bundling

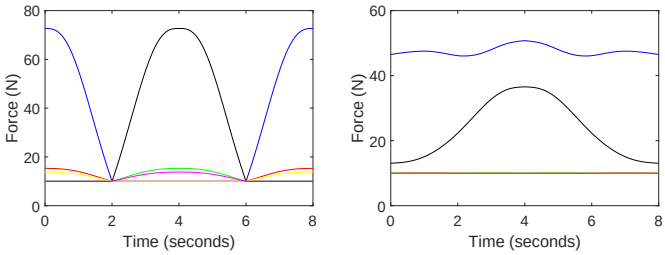

(a) 2n Cables **(b)** n+1 fully routed

Figure 5.31: Tensions of cables for a given trajectory for three link planar robot with different cable routings

which is represented as empty set in Table. 5.7. The fully routed configuration require less cable tension than the traditional 2N design.

Fig. 5.33 shows the workspace of three-link CDSKC as illustrated in Fig. 5.30(b). The workspace has disconnected regions but can be reshaped using spring elements and by changing the routing configuration. Fig. 5.34 shows the WCW for fully-routed three-link CDSKC. The WCW may not be possible to directly plot in Cartesian form for cable driven serial kinematic chain with greater than 3 DOF.

	Link 0	Link 1	Link 2	Link 3
Cable 1		$[0.5, 0.3]'$	$[0.1, 0.3]'$	
Cable 2	$[-1, 0.0]'$	$[-0.8, 0.3]'$	$[-0.1, 0.2]'$	
Cable 3	$[1.8, 0.0]'$		$[-0.5, 0.3]'$	$[-0.1, 0.3]'$
Cable 4	$[1.8, 0.0]'$			$[0.1, 0.3]'$

Table 5.8: Cable configuration for 3-link CDSKC with $n + 1$ actuated cables

Link 0	Link 1	Link 2	Link 3
C1 $[0.45, 0.02]'$	$[0.3, 0.12]'$		
C2 $[-0.5, 0.02]'$	$[-0.3, 0.1]'$	$[-0.3, 0.5]'$	$[-0.15, 0.3]'$
C3 $[-0.45, 0.02]'$	$[-0.3, 0.1]'$ $[0.3, 0.5]'$	$[0.15, 0.3]'$	
C4 $[-0.6, 0.02]'$	$[-0.4, 0.1]'$	$[-0.3, 0.1]'$ $[0.30.5]'$	$[0.15, 0.3]'$

Table 5.9: Cable configuration for 3-link CDSKC with internally routed $n + 1$ cables

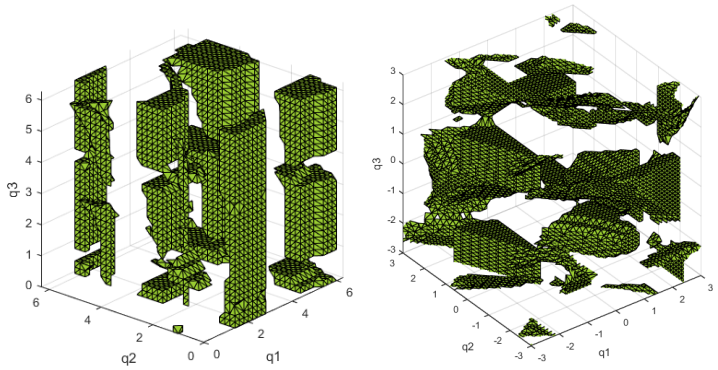

(a) Direct connecting scheme **(b)** Pass through scheme

Figure 5.32: The workspace hull of three-link CDSKC for the routing configurations shown in Fig. 5.30(a) and (b)

Fig. 5.36 shows the arrangement of five cables that actuate the two link 4-DOF spatial manipulator. The system has cables internally routed and bundled to the ground. The internal routing scheme is where a cable can be re-routed within the link internally, in addition to being externally routed. This type of routing can be considered as the most generalized form of the multi-segment pass-through routing scheme where a cable segment can be attached within the same link. In the following proximal connections, the internally routed cables can pass precisely through the same routing points. This guarantees that the robot has a policy of minimal actuation. The routed cables can be kept parallel throughout the complete joint cycle.

We also perform the kinematic and workspace analysis for three-link unilateral manipulator with different routing configurations. There is an exponential growth in number of combinations as the number of links increases. In the previous Chapter, the kinematics of two link 4-DOF SR chain with direct connecting cable routing scheme was discussed and the symbolic expressions of the structure matrix was derived analytically (Appendix 1). The fully routed cables makes the system highly coupled and the cable structure matrix complex, as the there are multiple segments in the cable vector.

For the 4DOF Spherical-Revolute chain with 5 cables in Fig. 5.35, three coordinates frames F_0, F_1 and F_2 can be used to describe the positions for the

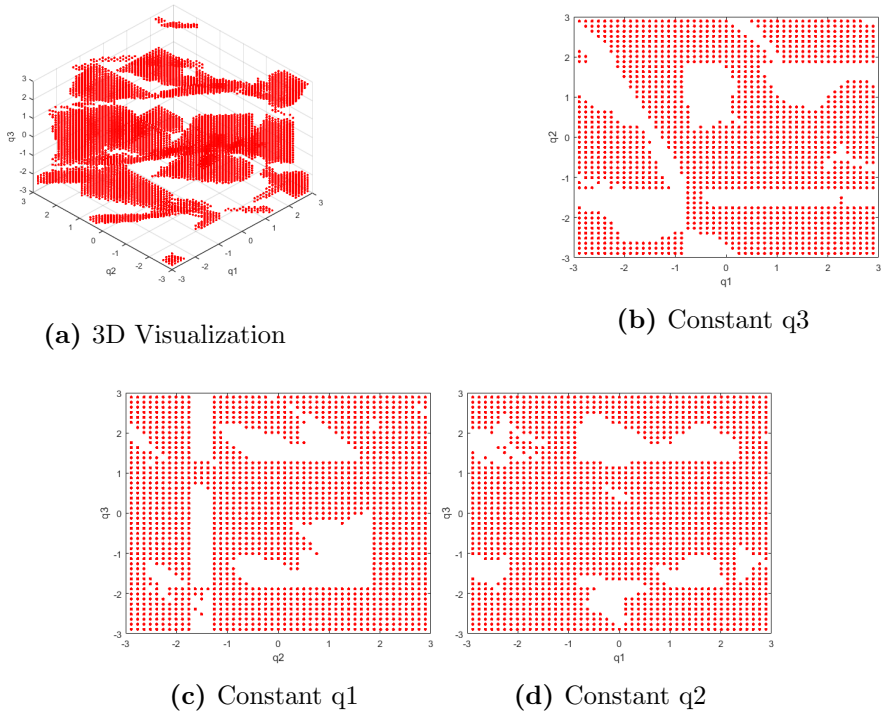

(a) 3D Visualization

(b) Constant q3

(c) Constant q1

(d) Constant q2

Figure 5.33: WCW for three link planar with a particular routing configuration as illustrated in Fig. 5.30(b)

system. F_0 is inertial coordinate frame attached to ground and the other two are rigidly attached onto link 1 and 2 respectively. Cables 1 to 3 are directly connected from the base to link 1. The attachment locations at the base and link 1 are denoted by A_i and B_i, respectively, for (i= 1,..,3). Cables 4 and 5 are connected from base at A_i to link 2 at C_i passing through link 1 at location Br_i. They are internally routed (red color) and can be joined as cable bundles via B_i for (i= 4,5). **J** matrix can be derived in two parts. Firstly, we calculate the Jacobian matrix which maps the cable space and body space velocities $\mathbf{J_v}$. The cable-body Jacobian matrix $\mathbf{J_v}$ for the fully routed chain is expressed as

$$\begin{bmatrix} \dot{l}_1 \\ \dot{l}_2 \\ \dot{l}_3 \\ \dot{l}_4 \\ \dot{l}_5 \end{bmatrix} = \begin{bmatrix} \hat{\mathbf{l}}_1^{\mathsf{T}} & (\mathbf{r}_{B1} \times \hat{\mathbf{l}}_1)^{\mathsf{T}} & \mathbf{0}^{\mathsf{T}} & \mathbf{0}^{\mathsf{T}} \\ \hat{\mathbf{l}}_2^{\mathsf{T}} & (\mathbf{r}_{B2} \times \hat{\mathbf{l}}_2)^{\mathsf{T}} & \mathbf{0}^{\mathsf{T}} & \mathbf{0}^{\mathsf{T}} \\ \hat{\mathbf{l}}_3^{\mathsf{T}} & (\mathbf{r}_{B3} \times \hat{\mathbf{l}}_3)^{\mathsf{T}} & \mathbf{0}^{\mathsf{T}} & \mathbf{0}^{\mathsf{T}} \\ (\hat{\mathbf{l}}_{41} - \hat{\mathbf{l}}_{42})^{\mathsf{T}} & ((\mathbf{r}_{B4} \times \hat{\mathbf{l}}_{41}) + (\mathbf{r}_{Br4} - \mathbf{r}_{B4}) \times \hat{\mathbf{l}}_{42})^{\mathsf{T}} & \hat{\mathbf{l}}_{43}^{\mathsf{T}} & ((\mathbf{r}_{C4} - \mathbf{r}_{Br4}) \times \hat{\mathbf{l}}_{43})^{\mathsf{T}} \\ (\hat{\mathbf{l}}_{51} - \hat{\mathbf{l}}_{52})^{\mathsf{T}} & ((\mathbf{r}_{B5} \times \hat{\mathbf{l}}_{51}) + (\mathbf{r}_{Br5} - \mathbf{r}_{B5}) \times \hat{\mathbf{l}}_{52})^{\mathsf{T}} & \hat{\mathbf{l}}_{53}^{\mathsf{T}} & ((\mathbf{r}_{C5} - \mathbf{r}_{Br5}) \times \hat{\mathbf{l}}_{53})^{\mathsf{T}} \end{bmatrix} \begin{bmatrix} {}^1\dot{\mathbf{r}}_{O_{O1}} \\ {}^1\omega_1 \\ {}^2\dot{\mathbf{r}}_{OG_2} \\ {}^2\omega_2 \end{bmatrix}$$

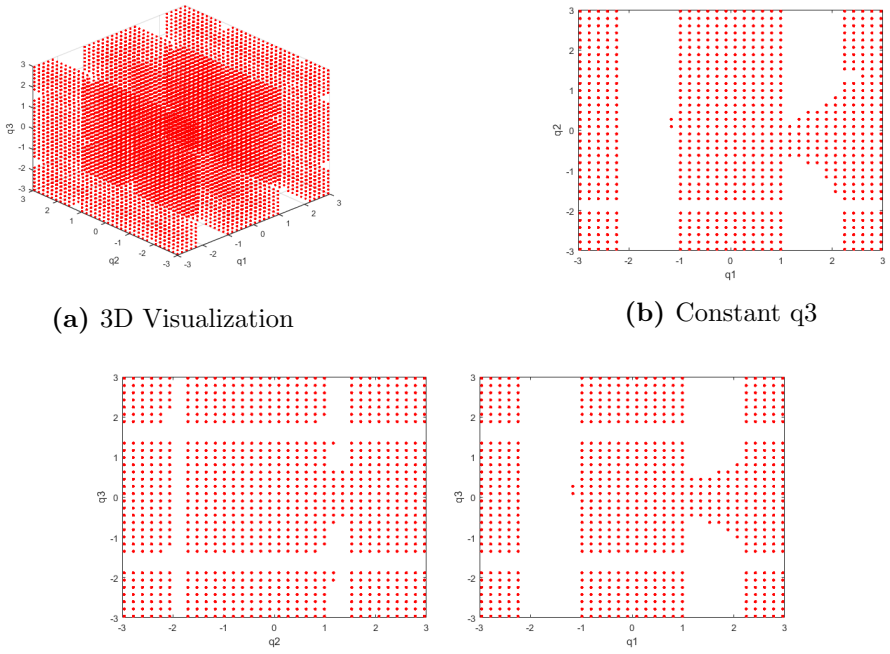

(a) 3D Visualization **(b)** Constant q3

(c) Constant q1 **(d)** Constant q2

Figure 5.34: WCW for three link planar with internal routing and cable bundling as illustrated in Fig. 5.30(c)

The column vector associated with $\dot{\mathbf{r}}_{O_{O1}}$ gets eliminated as the coordinate frames F_0 and F_1 are attached to the ground.

$$\dot{\mathbf{l}} = \mathbf{J_v}\dot{\mathbf{x}} \tag{5.29}$$

where $\dot{\mathbf{x}}$ (body space velocity) is the twist vector that contains angular velocities of link1 and link2. The twist vector of serial kinematic chain can be related to generalized coordinate velocities using kinematic maps thereby giving

$$\dot{\mathbf{x}} = \mathbf{J_w}\dot{\mathbf{q}} \tag{5.30}$$

$$\mathbf{J} = \mathbf{J_v}\mathbf{J_w} \tag{5.31}$$

For the SR chain visualization, we plot the subset of workspace by setting some variables as constant and with higher step-size. The simulation parameters are shown in Table. 5.10. By fixing the revolute joint, the WCW of the two-link

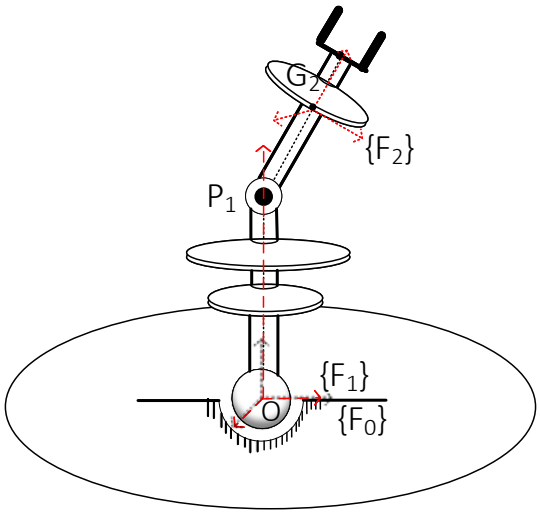

Figure 5.35: Schematic of a SR chain showing the coordinate frames and joint locations

	Link 0	Link 1	Link 2
C1	$[-0.1, 0.02, -0.1]'$	$[-0.025, 0.22, 0]'$	
C2	$[0, 0.02, 0.1]'$	$[0, 0.25, 0.0002]'$	
C3	$[0.1, 0.02, -0.1]'$	$[0.025, 0.22, 0.0002]'$	
C4	$[0, 0.02, -0.26]'$	$[-0.025, 0.26, 1.8E^{-04}]'$	$[7.6E^{-08}, 0.07, 0.025]'$
C5	$[0, 0.02, -0.28]'$	$[-0.025, 0.27, 1.8E^{-04}]'$	$[7.6E^{-08}, 0.07, -0.025]'$

Table 5.10: Cable configuration for 2-link spatial CDSKC with routed $n+1$ cables

4-DOF manipulator is identical to single link 3-DOF spherical joint manipulator differing only in dimension of the Jacobian matrix. The workspace of two- link spatial CDSKC with $q_4 = -pi$ is shown in Fig. 5.38.

For the workspace analysis of the two link spatial CDSKC with routing as shown in Fig. 5.39, the cables that are routed from the second link are responsible for the actuation of link 2 and its actuation will also affect the motion of link 1 due to the revolute joint and cable routing through the link. If the second link is assumed to be massless, the system will be simplified to a single link 3-dof ball joint manipulator as shown in Fig. 4.16a. We have seen that for a single link 3-dof manipulator, $m \geqslant 4$ cables are required to completely or redundantly restrain the system. The workspace of such system is shown in Fig. 3.25. Fig. 5.39 shows the

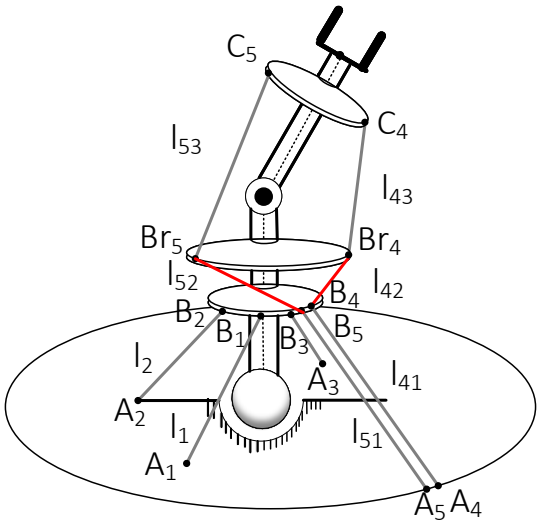

Figure 5.36: Two Link Spatial CDSKC with n+1 actuated cables fully routed to the base. 4-DOF spherical-revolute chain actuated with 5 cables. The cables in red color denoted internally routed cables.

cable arrangement configuration where a two-link 4-dof redundantly restrained manipulator is actuated by $m = 5$ cables. Minimal fully routed cable actuation is achieved through internal routing and re-routing which will be further elaborated in the next section.

From the Jacobian matrix derived in (3.51), it is apparent that the WCW in (5.22) is identical for the single link 3-dof ball joint manipulator and two-link 4-dof manipulator, differing only in the dimension of the Jacobian matrix. For the purpose of visualization, the WCW of 3-dof system which was analyzed in the previous section is only shown. The WCW along with it's projections on different planes are shown in Fig. 3.25. The manipulator will not be able to travel from poses in one region to another in the disconnected regions of the workspace.

5.4 Conclusions

The chapter discusses the design of CDSKCs with different cable routing schemes. Due to cable routing, the kinematics is coupled and it also alters tension in the other cables because the tension in those cables are function of external wrenches.

Using the theory of convex cones, a feasible cable actuation of an arbitrary serial chain using fully-routed cable bundling scheme was established. The recursive algorithm was utilized to actuate the serial kinematic chains. The kinematics of planar and spatial CDSKCs with internal routing and cable bundling schemes were investigated. Different cable routings lead to different workspaces. Our aim was to utilize fully-routed single bundle actuation scheme, where both external and internal routing exists. The cable is re-routed internally between two points in the same link to join cables in bundles and workspace of such maximally bundled serial chains were studied. The cables are parallel rather than strictly coincident after being bundled. The internal routing scheme is the most generalized form of multi-segment routing where the cable can be routed/ re-routed within the link. This leads to highly coupled actuation effects and poses challenges in modeling of such cable driven systems.

Simulations of wrench closure analysis for different manipulator were performed and the results were presented. The main purpose of this study was to demonstrate the effect of cable routing and number of actuators on tensionable workspace. We show that the fully routed cable bundling technique with fewer than 2N cables, that are asymmetric can have feasible workspace and reveals many design opportunities for cable driven exoskeletal systems. Through fully routed scheme, we have demonstrated that the number of actuators and maximum cable tension can be reduced. The inverse-dynamics of such chains were studied and the feasibility of different routing schemes were validated. It was shown that by incorporating the fully routed scheme with multi-segment cables, with the minimal actuator configuration, the multilink manipulators can have increased workspace and reduced cable forces to execute trajectories.

The motion generation capabilities and static stiffness evaluation of different CDSKCs were studied. The motion generation problem was formulated in joint space and task space, and the conditions required for constructing motions online was discussed. It was seen that, the wrench-closure condition can be used for point to point motion in joint space problem in order to ensure a feasible trajectory, and complete knowledge of task space contours are required in addition to the WCC. The end-effector reachable area was evaluated for different two link planar CDSKCs and stiffness ellipses were plotted for different CDSKCs. It was observed that the

single point internal routing topology can be utilized for application where it can be stiff in one direction and compliant in other direction. The ellipses dropped in magnitude when the robot was out of wrench-closure workspace and was very high near the workspace boundary. Workspace metrics such as tension factor, unilateral dexterity and unilateral maximum force amplification was evaluated throughout the mechanism's workspace which provided insight into motion generation due to the quantification of cable force and joint wrench relationship. These metrics were also useful in improving the robustness of the unilaterally actuated robot.

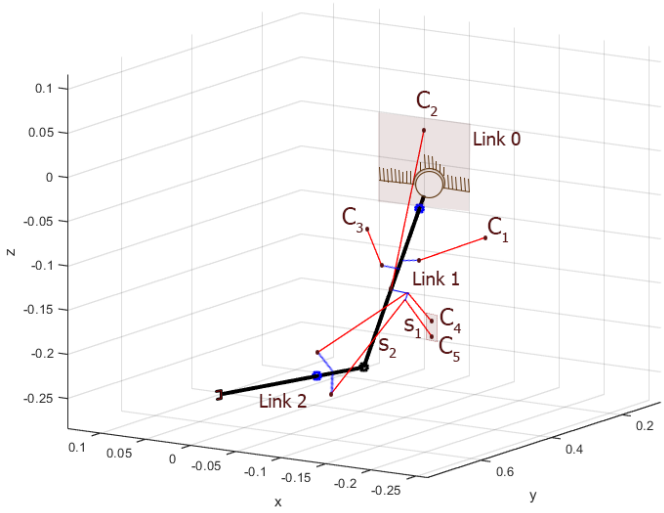

(a) Re-routing and cable bundling. The externally routed cables are in red color.

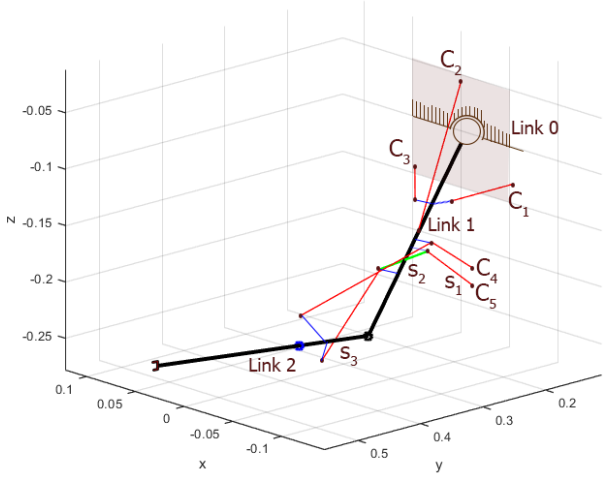

(b) Internal Routing. The s_2 cable segment(green) of cable 5 is internally routed from link2→ link1 → link1 → base

Figure 5.37: Two link Spatial CDSKC with minimal fully-routed cable $(n+1)$ actuation

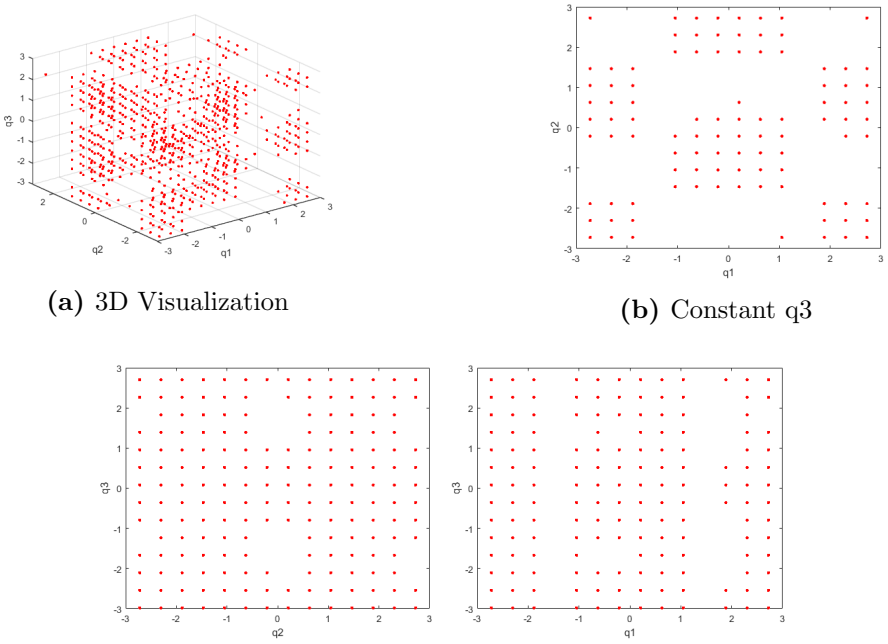

(a) 3D Visualization

(b) Constant q3

(c) Constant q1

(d) Constant q2

Figure 5.38: Subset of WCW for two link spatial CDSKC with cable routing through links as illustrated in Fig. 5.37(b)

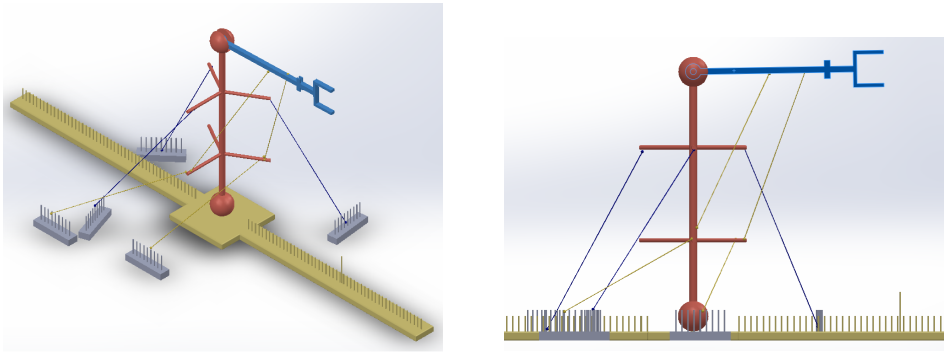

(a) Multiple cable segments

(b) Cable routed to the base

Figure 5.39: Two link spatial CDSKC with cable routing through links

Chapter 6

Modeling of a bio-inspired mechanism using bundled tendon actuation

In this Chapter, we utilize the tools established for the kinematics and dynamics of CDSKCs and model a large moving range shoulder joint driven by cables. Although most of the existing robotic shoulder possess some primary features of a human shoulder joint, their mechanism designs and actuation schemes are quite different from that of a human shoulder. The large moving range shoulder joint is composed of two ball joints stacked in a series-parallel configuration. Due to the stacked configuration, the range of motion is larger than that of an usual ball joint. Compliant mechanism design based on interlocked tetrahedron has a striking resemblance to that of a human shoulder. The shoulder serves as a highly effective six DOF joint and can be designed to accomplish high-precision, dynamic tasks such as writing, painting and throwing. Thus, this topology could be exploited to achieve large range of motion and applications in humanoid robots.

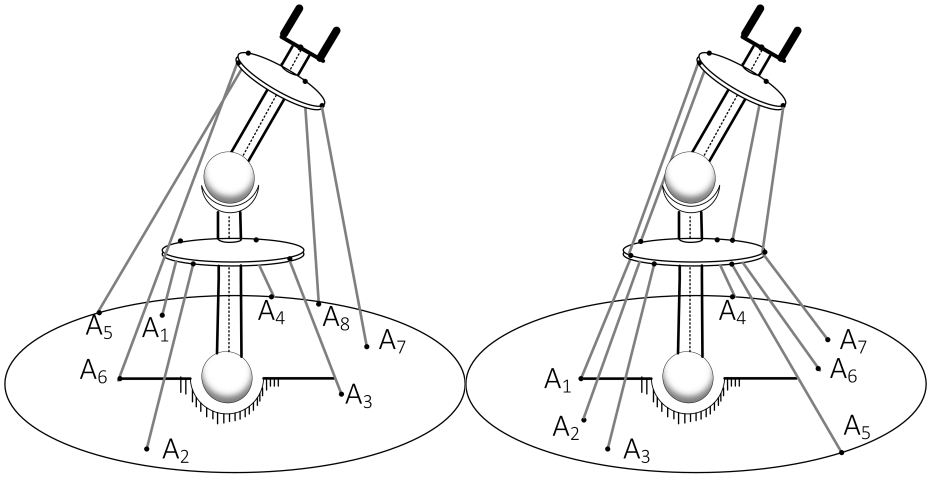

(a) Direct connecting scheme **(b)** Pass through scheme

Figure 6.1: Two link spatial CDSKC (Spherical-Spherical)

6.1 Modeling of cable driven double joint mechanism with direct connecting scheme

The double joint CDSKC possesses 6 DOF with different routing schemes: 8 cables with direct connecting scheme, 7 cables with pass through and internally routed scheme. The mechanism pose is defined using Euler angle convention such that $\mathbf{q}$=$[\alpha_1, \beta_1, \gamma_1, \alpha_2, \beta_2, \gamma_2]^\mathsf{T}$.

One can obtain the cable structure matrix $\mathbf{A}_L$ for the two link spatial CDSKC with direct-connecting scheme as a function of the generalized coordinates. The analytical expressions of the boundaries of the WCW can be obtained using the below formulation.

$$\mathbf{R}_{\alpha_1} = \begin{bmatrix} c\alpha_1 & -s\alpha_1 & 0 \\ s\alpha_1 & c\alpha_1 & 0 \\ 0 & 0 & 1 \end{bmatrix} \mathbf{R}_{\beta_1} = \begin{bmatrix} c\beta_1 & 0 & s\beta_1 \\ 0 & 1 & 0 \\ -s\beta_1 & 0 & c\beta_1 \end{bmatrix} \mathbf{R}_{\gamma_1} = \begin{bmatrix} 1 & 0 & 0 \\ 0 & c\gamma_1 & -s\gamma_1 \\ 0 & s\gamma_1 & c\gamma_1 \end{bmatrix} \tag{6.1}$$

Similarly the matrices $\mathbf{R}_{\alpha_2}, \mathbf{R}_{\beta_2}, \mathbf{R}_{\gamma_2}$ can be defined respectively. Firstly, the cable attachment points must be parameterized. We consider polar coordinates to

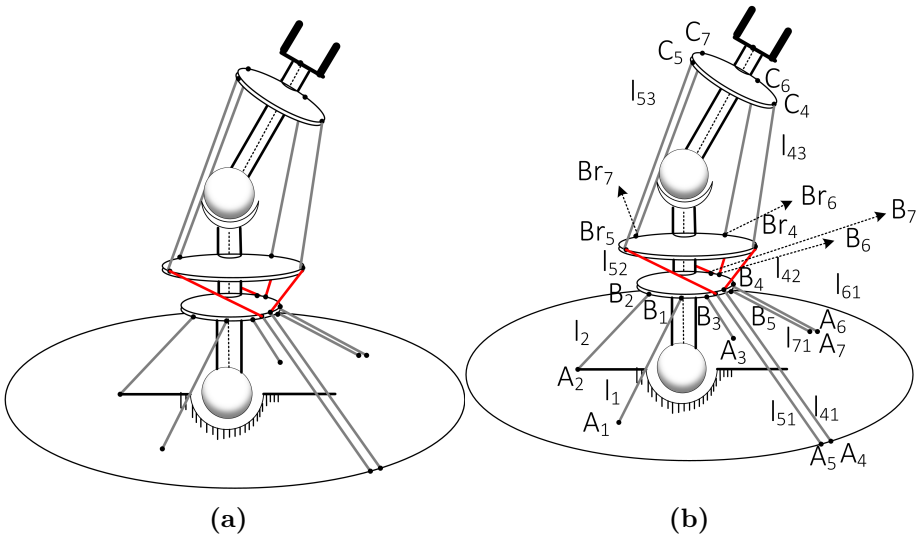

Figure 6.2: Two link spatial CDSKC (Spherical-Spherical) with internal routing scheme

express it in spatial system. A point on the first link initially is defined as:

$$\mathbf{r_{01_j}} = \begin{bmatrix} d_{a1_j} \\ p_{a_j} c\sigma_j \\ p_{a_j} s\sigma_j \end{bmatrix}, \mathbf{r_{02_k}} = \begin{bmatrix} d_{a2_k} \\ p_{a_k} c\sigma_k \\ p_{a_k} s\sigma_k \end{bmatrix} \; j = 1, 2, 3; k = 4, 5 \tag{6.2}$$

where $c(.)$ and $s(.)$ notations are used for cosine and sine of the arguments respectively. d_{a1} is the distance of the point from yz plane, p_a and σ are the polar coordinates of the point at that part of the arm. $j = 1, 2, 3$ implies, that the point belongs to link 1. The coordinates of the point with respect to the fixed frame is given as:

$$\mathbf{r_{f1_j}} = \mathbf{R}_{\alpha_1} \mathbf{R}_{\beta_1} \mathbf{R}_{\gamma_1} \mathbf{r_{01_j}} \tag{6.3}$$

where $j = 1, 2, 3$. This is the generic form of expressing point on link 1 using generalized coordinates. This point can be an anchor point of the cable. For the second link, then point is initally described using $\mathbf{r_{02_k}}$ where $k = 4, 5$ and d_{a2} is the distance of the center of the part of the arm containing the point from the

revolute joint. The final coordinate is obtained as:

$$\mathbf{r_{f2_k}} = \mathbf{R}_{\alpha_1}\mathbf{R}_{\beta_1}\mathbf{R}_{\gamma_1}(\mathbf{R}_{\alpha_2}\mathbf{R}_{\beta_2}\mathbf{R}_{\gamma_2}\mathbf{r_{02_k}} + \begin{bmatrix} l_{a1} \\ 0 \\ 0 \end{bmatrix}) \tag{6.4}$$

where l_{a1} is the length of the first link. Using 6.3 and 6.4, the Lagrangian structure matrix is obtained using the above formulation and the symbolic form is obtained. This concludes the parameterization of the attachment points. Using $\mathbf{A}_L$, the boundaries of tensionable workspace can be obtained. By assuming one or two of the generalized coordinate to be fixed, the workspace can be represented in 3D or 2D respectively.

6.2 Modeling of cable driven double joint mechanism with internal routing scheme

For the two link manipulator, three coordinate frames, F_0, F_1 and F_2 are used to describe positions for the system. It is defined similar to the schematic shown for SR chain in Fig. 5.35 and is shown in Fig. 6.5. The rotational matrices ${}^0R_1(\mathbf{q})$ and ${}^0R_2(\mathbf{q})$ are defined as:

$${}^0R_1(\mathbf{q}) = \begin{bmatrix} c\beta_1 c\gamma_1 & -c\beta_1 s\gamma_1 & s\beta_1 \\ c\alpha_1 s\gamma_1 + s\alpha_1 s\beta_1 c\gamma_1 & c\alpha_1 c\gamma_1 - s\alpha_1 s\beta_1 s\gamma_1 & -s\alpha_1 c\beta_1 \\ s\alpha_1 s\gamma_1 - c\alpha_1 s\beta_1 c\gamma_1 & s\alpha_1 c\gamma_1 + c\alpha_1 s\beta_1 s\gamma_1 & c\alpha_1 c\beta_1 \end{bmatrix} \tag{6.5}$$

$${}^1R_2(\mathbf{q}) = \begin{bmatrix} c\beta_2 c\gamma_2 & -c\beta_2 s\gamma_2 & s\beta_2 \\ c\alpha_2 s\gamma_2 + s\alpha_2 s\beta_2 c\gamma_2 & c\alpha_2 c\gamma_2 - s\alpha_2 s\beta_2 s\gamma_2 & -s\alpha_2 c\beta_2 \\ s\alpha_2 s\gamma_2 - c\alpha_2 s\beta_2 c\gamma_2 & s\alpha_2 c\gamma_2 + c\alpha_2 s\beta_2 s\gamma_2 & c\alpha_2 c\beta_2 \end{bmatrix} \tag{6.6}$$

Figure 6.2 shows the arrangement of 7 cables that actuate the system. The system shows that the cables are routed from the distal end to proximal end and then internally routed to the same link and to the base. Cables 1 to 3 are directly connected from the base to link 1. The attachment points at the base and link 1 are denoted by A_i and B_i, respectively for $i = 1, \ldots, 3$. Cables 4 to 7 are connected

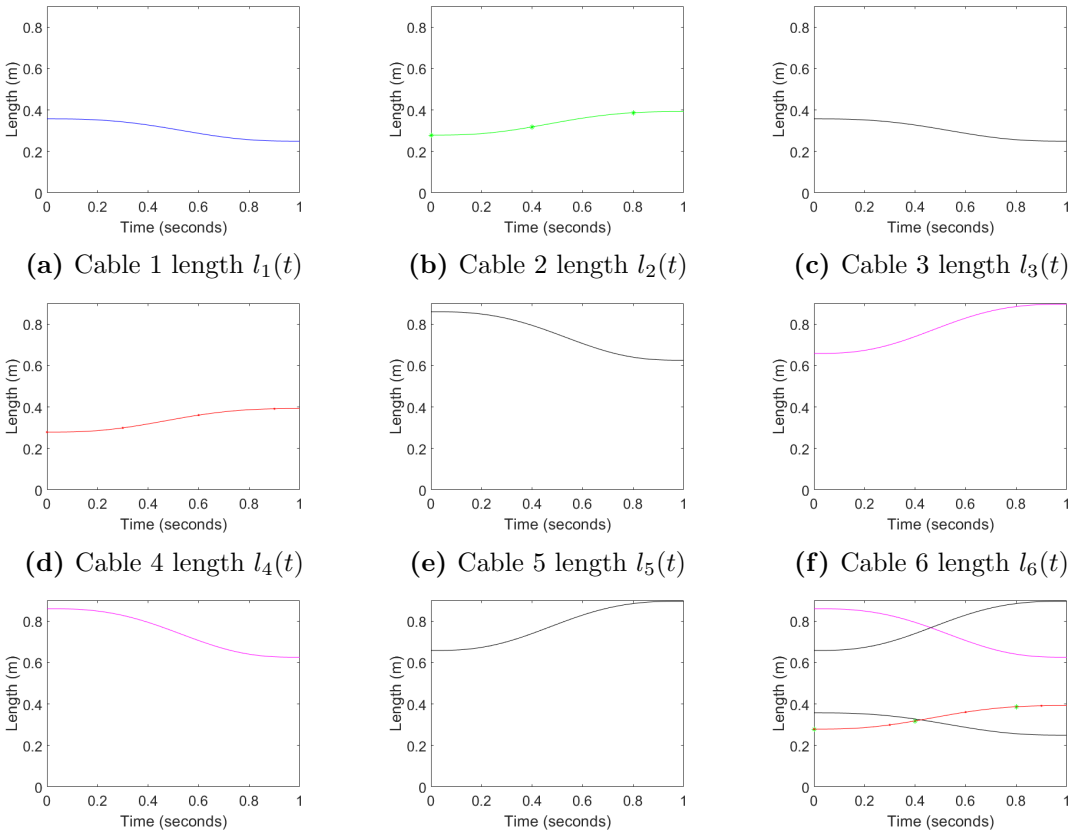

(a) Cable 1 length $l_1(t)$ **(b)** Cable 2 length $l_2(t)$ **(c)** Cable 3 length $l_3(t)$

(d) Cable 4 length $l_4(t)$ **(e)** Cable 5 length $l_5(t)$ **(f)** Cable 6 length $l_6(t)$

(g) Cable 7 length $l_7(t)$ **(h)** Cable 8 length $l_8(t)$ **(i)** All cables

Figure 6.3: The cable lengths from the inverse kinematic analysis on 2 link spatial CDSKC for a given trajectory. The length $l_i(t)$ for cables 1 to 8 are shown for direct-connecting routing configuration 6.1(a)

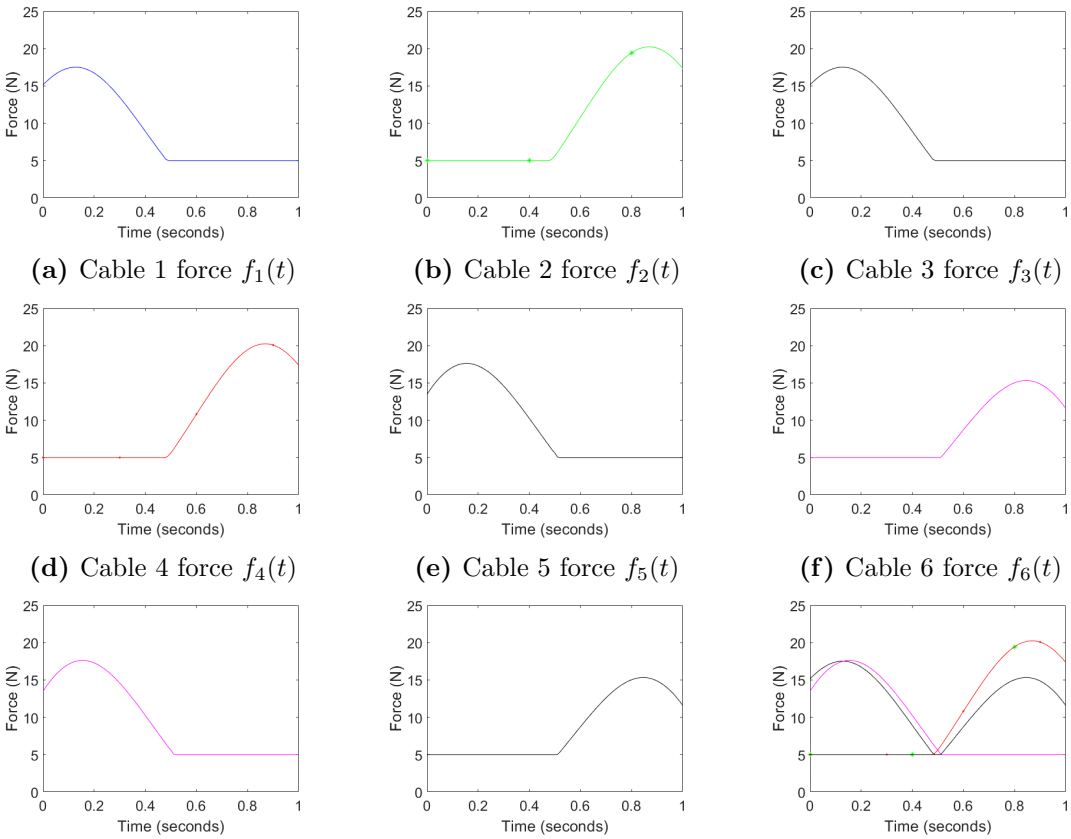

(a) Cable 1 force $f_1(t)$ **(b)** Cable 2 force $f_2(t)$ **(c)** Cable 3 force $f_3(t)$

(d) Cable 4 force $f_4(t)$ **(e)** Cable 5 force $f_5(t)$ **(f)** Cable 6 force $f_6(t)$

(g) Cable 7 force $f_7(t)$ **(h)** Cable 8 force $f_8(t)$ **(i)** All cables

Figure 6.4: The cable forces from the inverse dynamic analysis on 2 link spatial CDSKC for a given trajectory. The force $f_i(t)$ for cables 1 to 8 are shown for direct-connecting routing configuration 6.1(a)

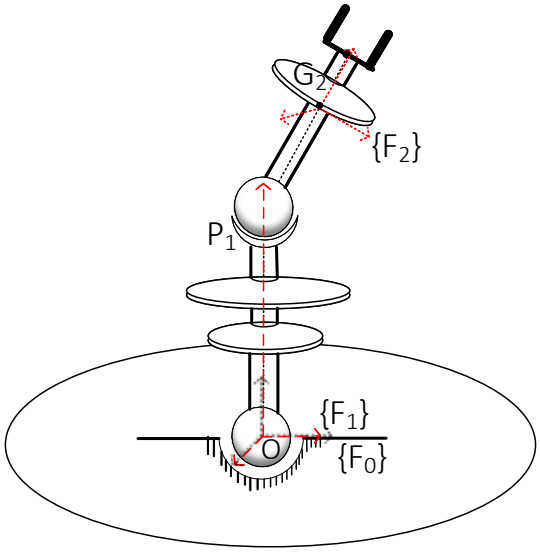

Figure 6.5: Schematic of a SS chain showing the coordinate frames and joint locations

from the base A_i to link 2 at C_i while passing through link 1 at locations B_i and Br_i for $i = 4, \ldots, 7$. The routing approach is based on the recursive algorithm of conic frames discussed in Chapter 3.

The cable length can be obtained by adding the lengths of each segment. This allows the inverse kinematics of the manipulator to be determined. The time derivative of the length of cable i must consider the change in length of all the segments. If the cable has two segments, then the time derivative is expressed as $\dot{l}_i = \hat{\mathbf{l}}_{i1} \cdot \dot{\mathbf{l}}_{i1} + \hat{\mathbf{l}}_{i2} \cdot \dot{\mathbf{l}}_{i2}$. The cable vector $\mathbf{l}_i$ for $i = 1, \ldots, 3$ with respect to F_1 can be expressed as

$$^1\mathbf{l}_i = -^1R_0\, ^0\mathbf{r}_{OA_i} + ^1\mathbf{r}_{OB_i} \forall i = 1, \ldots, 3. \tag{6.7}$$

Similarly for the multi-segment cables, the cable vectors are defined as discussed in Section 4.2 and the derivatives are obtained to obtain the Jacobian matrix. The cable-body Jacobian matrix $\mathbf{J_v}$ for the fully routed chain is expressed as

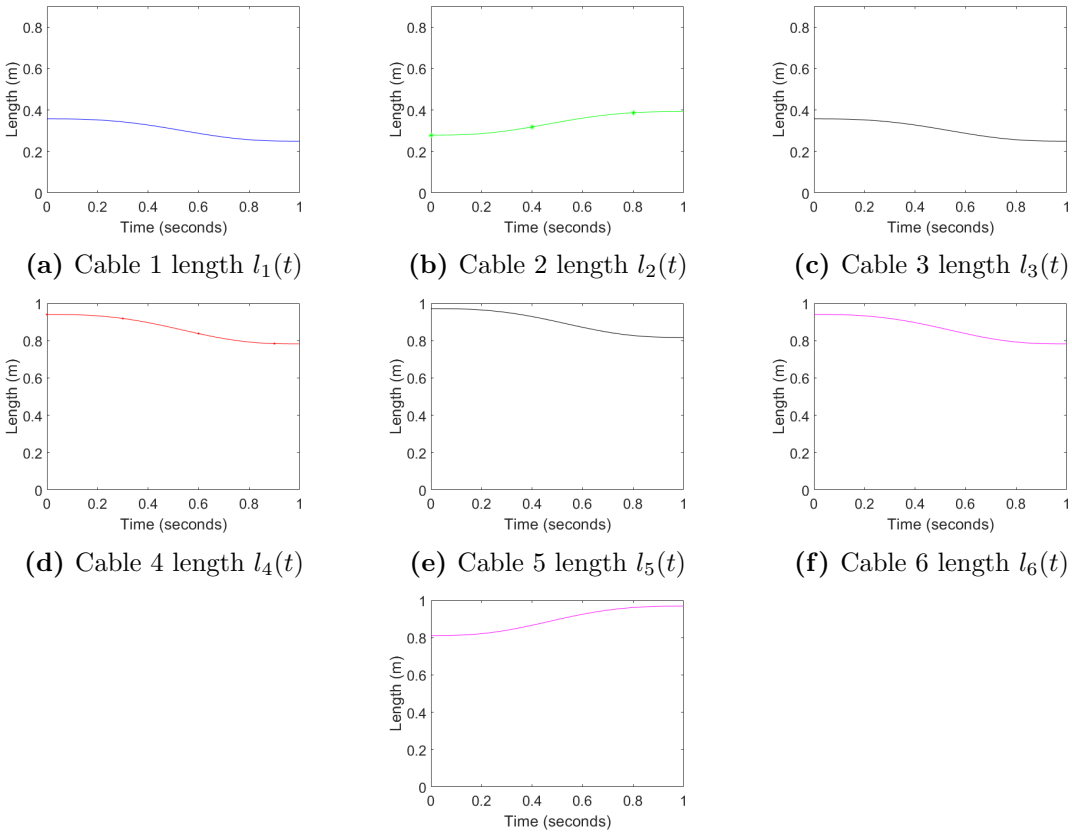

(a) Cable 1 length $l_1(t)$ **(b)** Cable 2 length $l_2(t)$ **(c)** Cable 3 length $l_3(t)$

(d) Cable 4 length $l_4(t)$ **(e)** Cable 5 length $l_5(t)$ **(f)** Cable 6 length $l_6(t)$

(g) Cable 7 length $l_7(t)$

Figure 6.6: The cable lengths from the inverse kinematic analysis on 2 link spatial CDSKC for a given trajectory. The length $l_i(t)$ for cables 1 to 7 are shown for internal routing configuration 6.2

$$\begin{bmatrix} \dot{l}_1 \\ \dot{l}_2 \\ \dot{l}_3 \\ \dot{l}_4 \\ \dot{l}_5 \\ \dot{l}_6 \\ \dot{l}_7 \end{bmatrix} = \begin{bmatrix} \hat{\mathbf{l}}_1^{\mathsf{T}} & (\mathbf{r}_{B1} \times \hat{\mathbf{l}}_1)^{\mathsf{T}} & \mathbf{0}^{\mathsf{T}} & \mathbf{0}^{\mathsf{T}} \\ \hat{\mathbf{l}}_2^{\mathsf{T}} & (\mathbf{r}_{B2} \times \hat{\mathbf{l}}_2)^{\mathsf{T}} & \mathbf{0}^{\mathsf{T}} & \mathbf{0}^{\mathsf{T}} \\ \hat{\mathbf{l}}_3^{\mathsf{T}} & (\mathbf{r}_{B3} \times \hat{\mathbf{l}}_3)^{\mathsf{T}} & \mathbf{0}^{\mathsf{T}} & \mathbf{0}^{\mathsf{T}} \\ (\hat{\mathbf{l}}_{41} - \hat{\mathbf{l}}_{42})^{\mathsf{T}} & ((\mathbf{r}_{B4} \times \hat{\mathbf{l}}_{41}) + (\mathbf{r}_{Br4} - \mathbf{r}_{B4}) \times \hat{\mathbf{l}}_{42})^{\mathsf{T}} & \hat{\mathbf{l}}_{43}^{\mathsf{T}} & ((\mathbf{r}_{C4} - \mathbf{r}_{Br4}) \times \hat{\mathbf{l}}_{43})^{\mathsf{T}} \\ (\hat{\mathbf{l}}_{51} - \hat{\mathbf{l}}_{52})^{\mathsf{T}} & ((\mathbf{r}_{B5} \times \hat{\mathbf{l}}_{51}) + (\mathbf{r}_{Br5} - \mathbf{r}_{B5}) \times \hat{\mathbf{l}}_{52})^{\mathsf{T}} & \hat{\mathbf{l}}_{53}^{\mathsf{T}} & ((\mathbf{r}_{C5} - \mathbf{r}_{Br5}) \times \hat{\mathbf{l}}_{53})^{\mathsf{T}} \\ (\hat{\mathbf{l}}_{61} - \hat{\mathbf{l}}_{62})^{\mathsf{T}} & ((\mathbf{r}_{B6} \times \hat{\mathbf{l}}_{61}) + (\mathbf{r}_{Br6} - \mathbf{r}_{B6}) \times \hat{\mathbf{l}}_{62})^{\mathsf{T}} & \hat{\mathbf{l}}_{63}^{\mathsf{T}} & ((\mathbf{r}_{C6} - \mathbf{r}_{Br6}) \times \hat{\mathbf{l}}_{63})^{\mathsf{T}} \\ (\hat{\mathbf{l}}_{71} - \hat{\mathbf{l}}_{72})^{\mathsf{T}} & ((\mathbf{r}_{B7} \times \hat{\mathbf{l}}_{71}) + (\mathbf{r}_{Br7} - \mathbf{r}_{B7}) \times \hat{\mathbf{l}}_{72})^{\mathsf{T}} & \hat{\mathbf{l}}_{73}^{\mathsf{T}} & ((\mathbf{r}_{C7} - \mathbf{r}_{Br7}) \times \hat{\mathbf{l}}_{73})^{\mathsf{T}} \end{bmatrix} \begin{bmatrix} {}^1\dot{\mathbf{r}}_{O_{O1}} \\ {}^1\omega_1 \\ {}^2\dot{\mathbf{r}}_{OG_2} \\ {}^2\omega_2 \end{bmatrix}$$

The absolute velocities of each link can be related to generalized coordinate velocities. In order to find the Jacobian matrix, the matrix $\mathbf{J}_W$, the kinematic map between the body twist vector $\dot{\mathbf{x}}$ and joint space velocity vector $\dot{\mathbf{q}}$ needs to be obtained. The cable structure matrix can also be obtained using the Lagrangian formulation as performed for the SR chain which relates generalized joint torques and cable tensions. The parameters of the 2 link spatial(spherical-spherical) CDSKC used for simulation are given in Appendix 1. The cable lengths and the resultant force profiles obtained by performing inverse kinematic and inverse dynamic analysis for the two link spatial CDSKC with direct-connecting cable routing scheme is shown in Fig. 6.3 and Fig. 6.4. The inverse kinematic analysis for the two link spatial CDSKC with internal routing scheme is shown in Fig. 6.6.

6.3 Conclusions

This chapter utilizes the fundamental tools in the kinematic analysis of CDSKCs established in the thesis and developed the model for a bio-inspired shoulder mechanism with large moving range. The double joint mechanism in a direct connecting scheme utilizes 8 cables, 4 cables each to actuate the spherical joint. Using the novel routing scheme, the cables were internally routed within the first link and minimal number of actuating cables $n+1$ were used. The kinematic model for different routing schemes were discussed and the results of inverse kinematic analysis were presented.

Chapter 7

General conclusions

7.1 Summary

The modeling of CDPRs actuated with $n+1$ cables were presented to motivate the need for extending the concepts for serial kinematic chains. The kinematic and dynamics analysis of a serial chain subject to unilateral constraint forces was presented. The problem was defined in terms of convex cones in the space of the coflexes of the kinematic chain, i.e., the dual space of the chain's instantaneous motions/ flexes. Any serial kinematic chain subject to a weak non-degeneracy condition, can be immobilized with $n+1$ forces. Different cable routing types were classified and modeled. Subsequently, the kinematics of a serial chain subject to unilateral constraint forces with different routing topologies were formulated. In particular, the effects of cable routing and number of cables on tensionable workspace was investigated. Utilizing workspace analysis as a meaningful computational tool, the evaluation of different operational regions of the proposed cable robot topologies was performed and a comprehensive lineup of cable routing topologies were listed.

Using the theory of convex cones, a feasible cable actuation of an arbitrary serial chain using fully-routed cable bundling scheme was established and analyzed with different kinematic chains. The recursive algorithm using convex cones was utilized to generate a cable actuation with full routing. Routing and re-routing was allowed to actuate any serial chain overcoming the constraint that exist when cables are applied directly like in direct-connecting cable routing scheme. To

achieve a minimum number of actuating cables while possessing a large workspace region, a novel internal cable routing scheme was proposed. It was shown that by incorporating internal routing with multi-segment cables, any serial chain with n degrees of freedom can be controlled with $n + 1$ cables.

In this work, through studying the kinematics and dynamics, it was demonstrated that internally-routed cable actuation of multilink manipulators have an increased workspace and reduced cable forces to execute trajectories. The workspace and inverse dynamic analysis of such chains were studied and the feasibility of different routing schemes were validated. The motion generation capabilities and static stiffness evaluation of different CDSKCs were analyzed. The conditions required for constructing motions online was discussed. Unilateral manipulability quality indices such as unilateral dexterity and unilateral maximum force amplification was evaluated throughout the mechanism's workspace to quantify the cable force and joint wrench relationship. Tension factor and condition number was evaluated for workspace performance optimization. The quality of entire workspace was evaluated by integrating the workspace metrics over the wrench closure workspace.

The presented kinematic chains with fully-routed cable bundles serve to illustrate the ability of the proposed highly coupled minimally actuated cable robots to model complex biomechanical systems.

The tools established for the kinematics and dynamics of CDSKCs were utilized to model a large moving range shoulder joint driven by cables. The large moving range shoulder joint is composed of two ball joints stacked in a series-parallel configuration. Due to the stacked configuration, the range of motion is larger than that of an usual ball joint. The shoulder serves as a highly effective six DOF joint and can be designed to accomplish high-precision, dynamic tasks such as writing, painting and throwing. Thus, this topology could be exploited to achieve large range of motion and applications in humanoid robots.

7.2 Future Research

The contributions in this thesis have created opportunities to study complex CDSKCs for the study of bio tensegrity systems and musculoskeletal robots. Future works would be to extend the analysis of CDSKCs such as wrench-closure workspace or the task space motion generation problems, to study biomechanical systems. Different routing topologies were proposed and in conclusion, the internal cable routing scheme was opted for a CDSKC as it can reduce the number of cables to the minimum without significantly reducing the workspace and the motion speed capability. The physical properties such as stiffness, sagging and wrapping, friction between the cables and links needs to be included the cable models. A higher fidelity cable model would ensure the applicability of the mathematical analysis to real world cable robots. Vibration modeling and collision effects should be considered for all CDSKCs thereby providing greater insight into the robot performance. On the control side, a robust joint space controller needs to be implemented and other multivariable control methods needs to be investigated. Incorporating the unilateral quality metrics into the joint space path planning algorithms would provide greater insight into improving the performance of the CDSKC. The workspace and stiffness analysis of internally-routed CDSKCs with the addition of active variable stiffness modules and passive elements needs to be investigated.

Appendix A

Analytical determination of Wrench Closure Workspace of Planar and Spatial Multi Link Unilateral Manipulators

A.1 6 DOF Spatial CDPR

The simulation parameters used for studying the 6 DOF Spatial CDPR is given in the tables A.1 and A.2. R_a and R_b are 0.110m and 0.09m respectively.

A.2 3 DOF Ball joint Manipulator

The simulation parameters used for studying the 3 DOF Spatial CDPR is given in Table A.3 and A.4. R_1 and R_2 are 115 and 95 mm respectively. d_1 and d_2 are 90 and 180 mm. The angle α is 18 degrees. The cable anchor points at the base

Table A.1: Simulation parameters of platform A

Anchor Point	θ_i[deg]	h_i[m]	
A_1	-120	0	
A_2	-60	0	
A_3	120	0	
A_4	60	0	
A_5	125	0.3	
A_6	18	0.3	
A_7	-110	0.3	

Table A.2: Simulation parameters of platform B

Anchor Point	θ_i[deg]	h_i[m]	
B_1	-120	0	
B_2	-60	0	
B_3	120	0	
B_4	60	0	
B_5	125	0	
B_6	18	0	
B_7	-110	0	

A_i and at the platform B_i are given in the table.

Table A.3: Simulation parameters of base A

Anchor Point	Coordinates
A_1	$[R_1\mathrm{s}(\alpha),R_1\mathrm{c}(\alpha),d_1]^\mathsf{T}$
A_2	$[-R_1,0,d_1]^\mathsf{T}$
A_3	$[-R_1\mathrm{s}(\alpha),-R_1\mathrm{c}(\alpha),d_1]^\mathsf{T}$
A_4	$[R_1,0,d_1]^\mathsf{T}$

Table A.4: Simulation parameters of platform B

Anchor Point	Coordinates
B_1	$[R_2,0,-d_2]^\mathsf{T}$
B_2	$[0,-R_2,-d_2]^\mathsf{T}$
B_3	$[-R_2,0,-d_2]^\mathsf{T}$
B_4	$[0,R_2,-d_2]^\mathsf{T}$

A.3 3 link Planar CDSKC

A.3.1 Direct connecting scheme with 4 cables

The symbolic expressions of the cable structure matrix for 3 link Planar CDSKC shown in Fig. A.1 with the direct connecting scheme is given:

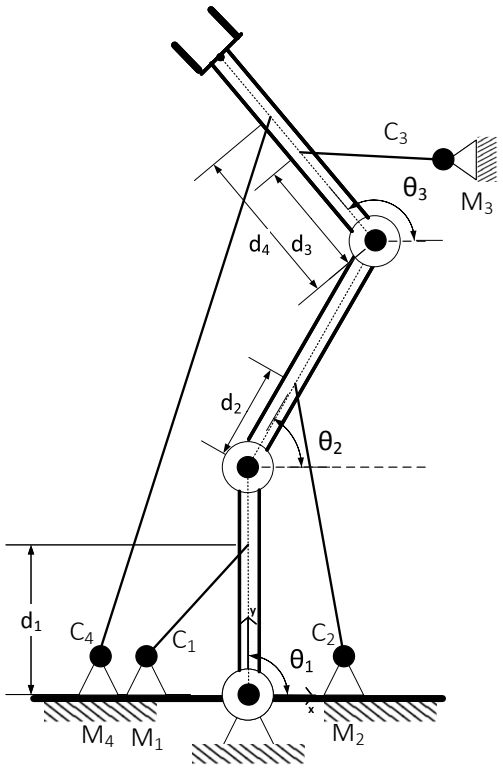

Figure A.1: Schematic of a 3DOF CDSKC driven by four cables having direct connecting scheme

$$\begin{bmatrix} Q_1 \\ Q_2 \\ Q_3 \end{bmatrix} = \mathbf{A}_L \begin{bmatrix} t_1 \\ t_2 \\ t_3 \\ t_4 \end{bmatrix} \tag{A.1}$$

$$\mathbf{A}_L = \begin{bmatrix} a_{11} & a_{12} & a_{13} & a_{14} \\ 0 & a_{22} & a_{23} & a_{24} \\ 0 & 0 & a_{33} & a_{34} \end{bmatrix} \tag{A.2}$$

$$\begin{aligned}
a_{11} &= d_1c(\theta_1)(y_1 - d_1s(\theta_1)) - d_1s(\theta_1)(x_1 - d_1c(\theta_1)) \\
a_{21} &= 0 \\
a_{31} &= 0 \\
a_{12} &= l_1c(\theta_1)(d_2s(\theta_2) - y_2 + l_1s(\theta_1)) - l_1s(\theta_1)(d_2c(\theta_2) - x_2 + l_1c(\theta_1)) \\
a_{22} &= d_2c(\theta_2)(d_2s(\theta_2) - y_2 + l_1s(\theta_1)) - d_2s(\theta_2)(d_2c(\theta_2) - x_2 + l_1c(\theta_1)) \\
a_{32} &= 0 \\
a_{13} &= l_1c(\theta_1)(d_3s(\theta_3) - y_3 + l_1s(\theta_1) + l_2s(\theta_2)) - l_1s(\theta_1)(d_3c(\theta_3) - x_3 + l_1c(\theta_1) + l_2c(\theta_2)) \\
a_{23} &= l_2c(\theta_2)(d_3s(\theta_3) - y_3 + l_1s(\theta_1) + l_2s(\theta_2)) - l_2s(\theta_2)(d_3c(\theta_3) - x_3 + l_1c(\theta_1) + l_2c(\theta_2)) \\
a_{33} &= d_3c(\theta_3)(d_3s(\theta_3) - y_3 + l_1s(\theta_1) + l_2s(\theta_2)) - d_3s(\theta_3)(d_3c(\theta_3) - x_3 + l_1c(\theta_1) + l_2c(\theta_2)) \\
a_{14} &= l_1c(\theta_1)(d_4s(\theta_3) - y_4 + l_1s(\theta_1) + l_2s(\theta_2)) - l_1s(\theta_1)(d_4c(\theta_3) - x_4 + l_1c(\theta_1) + l_2c(\theta_2)) \\
a_{24} &= l_2c(\theta_2)(d_4s(\theta_3) - y_4 + l_1s(\theta_1) + l_2s(\theta_2)) - l_2s(\theta_2)(d_4c(\theta_3) - x_4 + l_1c(\theta_1) + l_2c(\theta_2)) \\
a_{34} &= d_4c(\theta_3)(d_4s(\theta_3) - y_4 + l_1s(\theta_1) + l_2s(\theta_2)) - d_4s(\theta_3)(d_4c(\theta_3) - x_4 + l_1c(\theta_1) + l_2c(\theta_2))
\end{aligned} \tag{A.3}$$

A.3.2 Direct connecting scheme with 6 cables

The symbolic expressions for cable lengths can be obtained firstly by finding the coordinates of points $P_1, \ldots, P_6$. The base frame is attached to the revolute joint on the ground. The coordinates are expressed with respect to the base frame. So,

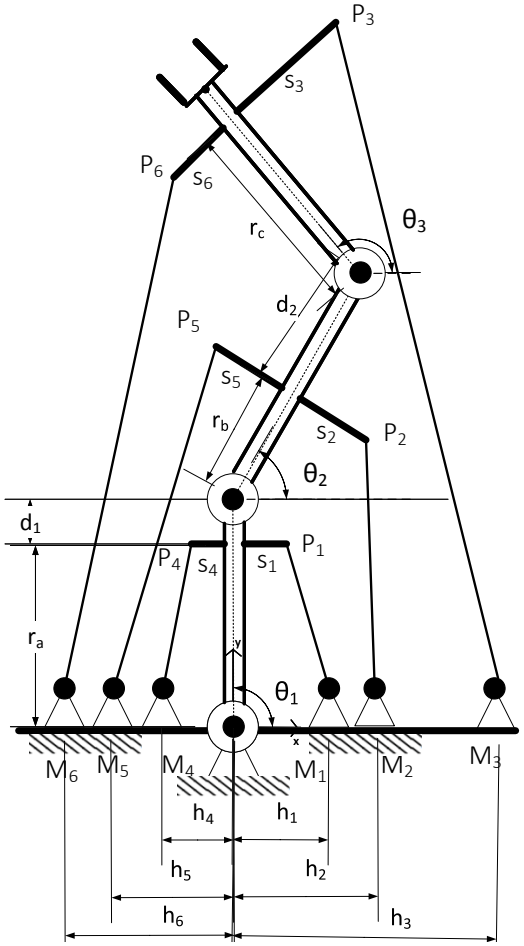

Figure A.2: Schematic of a 3DOF CDSKC driven by six cables having direct connecting scheme

the parameterization of the cable attachment points are given as,

$$P_1 = \begin{bmatrix} c\theta_1 & -s\theta_1 & 0 \\ s\theta_1 & c\theta_1 & 0 \\ 0 & 0 & 1 \end{bmatrix} \begin{bmatrix} r_a \\ -s_1 \\ 1 \end{bmatrix} \tag{A.4}$$

$$P_2 = \begin{bmatrix} c\theta_{12} & -s\theta_{12} & (r_a + d_1)c\theta_1 \\ s\theta_{12} & c\theta_{12} & (r_a + d_1)s\theta_1 \\ 0 & 0 & 1 \end{bmatrix} \begin{bmatrix} r_b \\ -s_2 \\ 1 \end{bmatrix} \tag{A.5}$$

$$P_3 = \begin{bmatrix} c\theta_{123} & -s\theta_{123} & (r_a + d_1)c\theta_1 + (r_b + d_2)c\theta_{12} \\ s\theta_{12} & c\theta_{12} & (r_a + d_1)s\theta_1 + (r_b + d_2)s\theta_{12} \\ 0 & 0 & 1 \end{bmatrix} \begin{bmatrix} r_c \\ -s_3 \\ 1 \end{bmatrix} \tag{A.6}$$

$$P_4 = \begin{bmatrix} c\theta_1 & -s\theta_1 & 0 \\ s\theta_1 & c\theta_1 & 0 \\ 0 & 0 & 1 \end{bmatrix} \begin{bmatrix} r_a \\ s_4 \\ 1 \end{bmatrix} \tag{A.7}$$

$$P_5 = \begin{bmatrix} c\theta_{12} & -s\theta_{12} & (r_a + d_1)c\theta_1 \\ s\theta_{12} & c\theta_{12} & (r_a + d_1)s\theta_1 \\ 0 & 0 & 1 \end{bmatrix} \begin{bmatrix} r_b \\ s_5 \\ 1 \end{bmatrix} \tag{A.8}$$

$$P_6 = \begin{bmatrix} c\theta_{123} & -s\theta_{123} & (r_a + d_1)c\theta_1 + (r_b + d_2)c\theta_{12} \\ s\theta_{12} & c\theta_{12} & (r_a + d_1)s\theta_1 + (r_b + d_2)s\theta_{12} \\ 0 & 0 & 1 \end{bmatrix} \begin{bmatrix} r_c \\ s_6 \\ 1 \end{bmatrix} \tag{A.9}$$

where $c(.)$ and $s(.)$ is cosine and sine of the argument respectively. $\theta_{12} = \theta 1 + \theta 2$ and $\theta_{123} = \theta 1 + \theta 2 + \theta 3$ respectively. r_a, r_b and r_c are the distances from the joint center to the mounting point on the link. $s_1, \ldots, s_6$ are the distance from the link to cable anchor point. $M_1, \ldots, M_6$ are the location of cable winches/ motors. $h_1, \ldots, h_6$ are the distances of the cable winches from the base joint.

A.3.3 Pass through scheme with 4 cables

The parameterization of the cable attachment points are,

$$P_1 = \begin{bmatrix} c\theta_1 & -s\theta_1 & 0 \\ s\theta_1 & c\theta_1 & 0 \\ 0 & 0 & 1 \end{bmatrix} \begin{bmatrix} r_a \\ -s_1 \\ 1 \end{bmatrix} \tag{A.10}$$

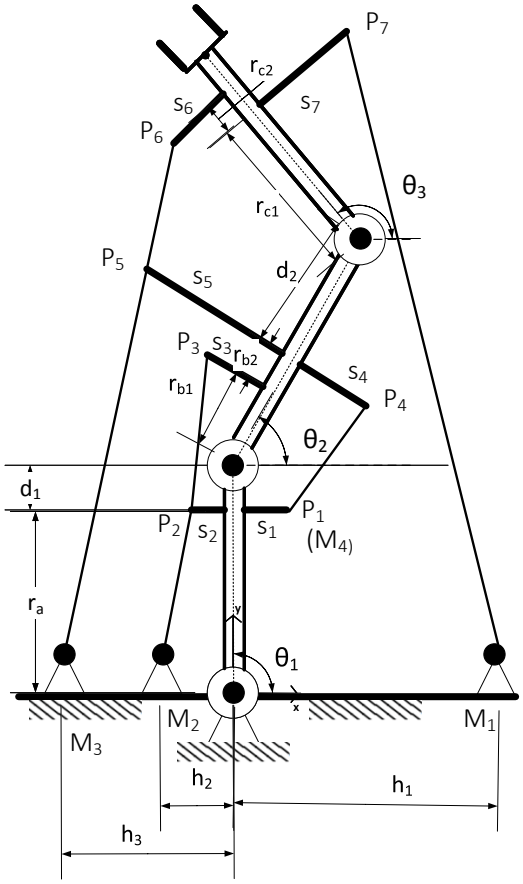

Figure A.3: Schematic of a 3DOF CDSKC driven by $n+1$ cables having pass through connecting scheme

$$P_2 = \begin{bmatrix} c\theta_1 & -s\theta_1 & 0 \\ s\theta_1 & c\theta_1 & 0 \\ 0 & 0 & 1 \end{bmatrix} \begin{bmatrix} r_a \\ s_2 \\ 1 \end{bmatrix} \tag{A.11}$$

$$P_3 = \begin{bmatrix} c\theta_{12} & -s\theta_{12} & (r_a + d_1)c\theta_1 \\ s\theta_{12} & c\theta_{12} & (r_a + d_1)s\theta_1 \\ 0 & 0 & 1 \end{bmatrix} \begin{bmatrix} r_{b_1} \\ s_3 \\ 1 \end{bmatrix} \tag{A.12}$$

$$P_4 = \begin{bmatrix} c\theta_{12} & -s\theta_{12} & (r_a + d_1)c\theta_1 \\ s\theta_{12} & c\theta_{12} & (r_a + d_1)s\theta_1 \\ 0 & 0 & 1 \end{bmatrix} \begin{bmatrix} r_{b_1} + r_{b_2} \\ -s_4 \\ 1 \end{bmatrix} \tag{A.13}$$

$$P_5 = \begin{bmatrix} c\theta_{12} & -s\theta_{12} & (r_a + d_1)c\theta_1 \\ s\theta_{12} & c\theta_{12} & (r_a + d_1)s\theta_1 \\ 0 & 0 & 1 \end{bmatrix} \begin{bmatrix} r_{b_1} + r_{b_2} \\ s_5 \\ 1 \end{bmatrix} \tag{A.14}$$

$$P_6 = \begin{bmatrix} c\theta_{123} & -s\theta_{123} & (r_a + d_1)c\theta_1 + (r_b + d_2)c\theta_{12} \\ s\theta_{12} & c\theta_{12} & (r_a + d_1)s\theta_1 + (r_b + d_2)s\theta_{12} \\ 0 & 0 & 1 \end{bmatrix} \begin{bmatrix} r_{c_1} + r_{c_2} \\ s_6 \\ 1 \end{bmatrix} \tag{A.15}$$

$$P_7 = \begin{bmatrix} c\theta_{123} & -s\theta_{123} & (r_a + d_1)c\theta_1 + (r_b + d_2)c\theta_{12} \\ s\theta_{12} & c\theta_{12} & (r_a + d_1)s\theta_1 + (r_b + d_2)s\theta_{12} \\ 0 & 0 & 1 \end{bmatrix} \begin{bmatrix} r_{c_1} \\ -s_7 \\ 1 \end{bmatrix} \tag{A.16}$$

$r_b = r_{b_1} + r_{b_2}$. r_{c_2} can be zero making P_6 and P_7 lie on a straight line. Using these coordinates, the cable lengths can be found by computing the length of each segment and adding it vectorially.

A.3.4 Internally routed scheme with 4 cables

In this scheme, the cables can be both externally and internally routed. The internally routed in crossing configuration is depicted in green color(dotted line). This highly coupled routing scheme is beneficial over the direct connecting or pass through routing scheme. The parameterization of the cable attachment points are,

$$P_1 = \begin{bmatrix} c\theta_1 & -s\theta_1 & 0 \\ s\theta_1 & c\theta_1 & 0 \\ 0 & 0 & 1 \end{bmatrix} \begin{bmatrix} r_{a_1} \\ -s_1 \\ 1 \end{bmatrix} \tag{A.17}$$

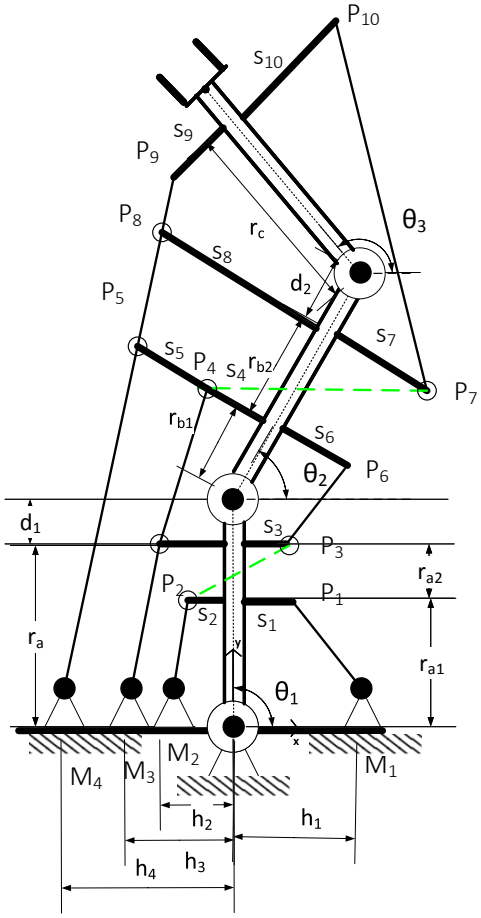

Figure A.4: Schematic of a 3DOF CDSKC driven by $n+1$ cables having internally routed connecting scheme

$$P_2 = \begin{bmatrix} c\theta_1 & -s\theta_1 & 0 \\ s\theta_1 & c\theta_1 & 0 \\ 0 & 0 & 1 \end{bmatrix} \begin{bmatrix} r_{a_1} \\ s_2 \\ 1 \end{bmatrix} \tag{A.18}$$

$$P_3 = \begin{bmatrix} c\theta_1 & -s\theta_1 & 0 \\ s\theta_1 & c\theta_1 & 0 \\ 0 & 0 & 1 \end{bmatrix} \begin{bmatrix} r_a \\ -s_3 \\ 1 \end{bmatrix} \tag{A.19}$$

$$P_4 = \begin{bmatrix} c\theta_{12} & -s\theta_{12} & (r_a + d_1)c\theta_1 \\ s\theta_{12} & c\theta_{12} & (r_a + d_1)s\theta_1 \\ 0 & 0 & 1 \end{bmatrix} \begin{bmatrix} r_{b_1} \\ s_4 \\ 1 \end{bmatrix} \tag{A.20}$$

$$P_5 = \begin{bmatrix} c\theta_{12} & -s\theta_{12} & (r_a + d_1)c\theta_1 \\ s\theta_{12} & c\theta_{12} & (r_a + d_1)s\theta_1 \\ 0 & 0 & 1 \end{bmatrix} \begin{bmatrix} r_{b_1} \\ s_4 + s_5 \\ 1 \end{bmatrix} \tag{A.21}$$

$$P_6 = \begin{bmatrix} c\theta_{12} & -s\theta_{12} & (r_a + d_1)c\theta_1 \\ s\theta_{12} & c\theta_{12} & (r_a + d_1)s\theta_1 \\ 0 & 0 & 1 \end{bmatrix} \begin{bmatrix} r_{b_1} \\ -s_6 \\ 1 \end{bmatrix} \tag{A.22}$$

$$P_7 = \begin{bmatrix} c\theta_{12} & -s\theta_{12} & (r_a + d_1)c\theta_1 \\ s\theta_{12} & c\theta_{12} & (r_a + d_1)s\theta_1 \\ 0 & 0 & 1 \end{bmatrix} \begin{bmatrix} r_{b_1} + r_{b_2} \\ -s_7 \\ 1 \end{bmatrix} \tag{A.23}$$

$$P_8 = \begin{bmatrix} c\theta_{12} & -s\theta_{12} & (r_a + d_1)c\theta_1 \\ s\theta_{12} & c\theta_{12} & (r_a + d_1)s\theta_1 \\ 0 & 0 & 1 \end{bmatrix} \begin{bmatrix} r_{b_1} + r_{b_2} \\ s_8 \\ 1 \end{bmatrix} \tag{A.24}$$

$$P_9 = \begin{bmatrix} c\theta_{123} & -s\theta_{123} & (r_a + d_1)c\theta_1 + (r_b + d_2)c\theta_{12} \\ s\theta_{12} & c\theta_{12} & (r_a + d_1)s\theta_1 + (r_b + d_2)s\theta_{12} \\ 0 & 0 & 1 \end{bmatrix} \begin{bmatrix} r_c \\ s_9 \\ 1 \end{bmatrix} \tag{A.25}$$

$$P_{10} = \begin{bmatrix} c\theta_{123} & -s\theta_{123} & (r_a + d_1)c\theta_1 + (r_b + d_2)c\theta_{12} \\ s\theta_{12} & c\theta_{12} & (r_a + d_1)s\theta_1 + (r_b + d_2)s\theta_{12} \\ 0 & 0 & 1 \end{bmatrix} \begin{bmatrix} r_c \\ -s_{10} \\ 1 \end{bmatrix} \tag{A.26}$$

With the given coordinates of cable winch locations, the cable lengths can be computed thereby solving the inverse kinematics problem.

A.4 2 link Spatial CDSKC

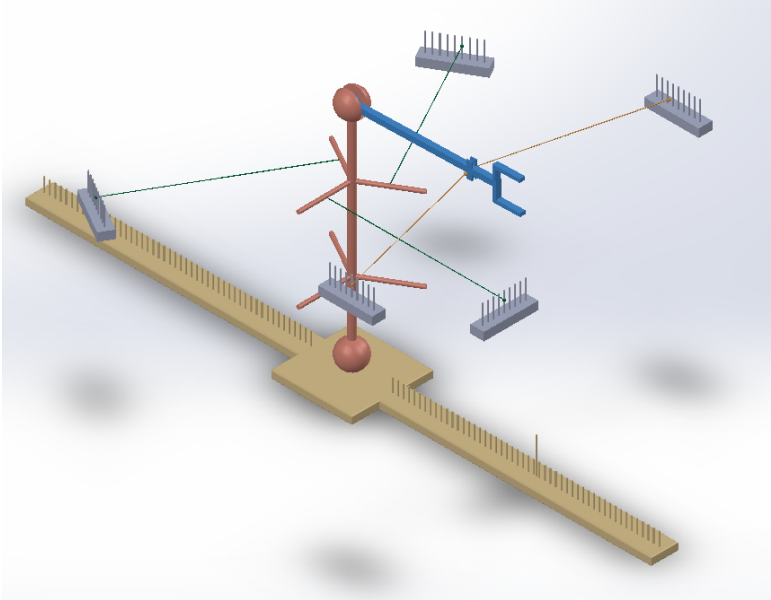

Figure A.5: Model of a 4DOF CDSKC driven by five cables having direct connecting scheme

The symbolic expressions of the cable structure matrix for 2 link Spatial CDSKC shown in Fig. A.5 with the direct connecting scheme is given:

$$\begin{bmatrix} Q_1 \\ Q_2 \\ Q_3 \\ Q_4 \end{bmatrix} = \mathbf{A}_L \begin{bmatrix} t_1 \\ t_2 \\ t_3 \\ t_4 \\ t_5 \end{bmatrix} \tag{A.27}$$

$$\mathbf{A}_L = \begin{bmatrix} a_{11} & a_{12} & a_{13} & a_{14} & a_{15} \\ a_{21} & a_{22} & a_{23} & a_{24} & a_{25} \\ a_{31} & a_{32} & a_{33} & a_{34} & a_{35} \\ a_{41} & a_{42} & a_{43} & a_{44} & a_{45} \end{bmatrix} \tag{A.28}$$

$$\begin{aligned} Nr_{a_{11}} = ((s(\sigma 1)(x1\,s(\theta) - y1\,c(\theta))s(\phi) + c(\sigma 1)(x1\,c(\theta) + s(\theta)y1))pa1\,c(\psi) + \\ s(\psi)c(\sigma 1)pa1\,(x1\,s(\theta) - y1\,c(\theta))s(\phi) - pa1\,s(\sigma 1)(x1\,c(\theta) + s(\theta)y1)s(\psi) \\ + da11\,c(\phi)(x1\,s(\theta) - y1\,c(\theta))) \end{aligned} \tag{A.29}$$

$$\begin{aligned} Dr_{a_{11}} = (|((s(\phi)s(\psi)c(\sigma 1)pa1 + s(\phi)s(\sigma 1)pa1\,c(\psi) + \\ da11\,c(\phi))c(\theta) + pa1\,(s(\psi)s(\sigma 1) - c(\sigma 1)c(\psi))s(\theta) - x1)|^2 + \\ |((s(\phi)s(\psi)c(\sigma 1)pa1 + s(\phi)s(\sigma 1)pa1\,c(\psi) + da11\,c(\phi))s(\theta) - \\ pa1\,(s(\psi)s(\sigma 1) - c(\sigma 1)c(\psi))c(\theta) - y1)|^2 + |(da11\,s(\phi) - c(\phi)(c(\sigma 1)s(\psi) + \\ c(\psi)s(\sigma 1))pa1 + z1)|^2)^{\frac{1}{2}} \end{aligned} \tag{A.30}$$

$$\begin{aligned} Nr_{a_{12}} = (pa2(s(\sigma 2)(x2\,s(\alpha) - y2\,c(\alpha))s(\beta) + c(\sigma 2)(x2\,c(\alpha) + \\ s(\alpha)y2))c(\gamma) + pa2(c(\sigma 2)(x2\,s(\alpha) - y2\,c(\alpha))s(\beta) - s(\sigma 2)(x2\,c(\alpha) + \\ s(\alpha)y2))s(\gamma) + c(\beta)da12(x2\,s(\alpha) - y2\,c(\alpha))) \end{aligned} \tag{A.31}$$

$$\begin{aligned} Dr_{a_{12}} = (|(pa2(c(\alpha)s(\beta)s(\gamma) - c(\gamma)s(\alpha))c(\sigma 2) + \\ pa2\,s(\sigma 2)(s(\alpha)s(\gamma) + c(\alpha)c(\gamma)s(\beta)) + da12\,c(\alpha)c(\beta) - x2)|^2 + \\ |((da12\,c(\beta) + pa2\,c(\gamma)s(\beta)s(\sigma 2) + pa2\,s(\beta)c(\sigma 2)s(\gamma))s(\alpha) + \\ pa2(c(\gamma)c(\sigma 2) - s(\gamma)s(\sigma 2))c(\alpha) - y2)|^2 + \\ |(da12\,s(\beta) - c(\beta)(c(\gamma)s(\sigma 2) + s(\gamma)c(\sigma 2))pa2 + z2)|^2)^{\frac{1}{2}} \end{aligned} \tag{A.32}$$

$$\begin{aligned} Nr_{a_{13}} = (pa3(s(\sigma 3)(x3\,s(\alpha) - y3\,c(\alpha))s(\beta) + \\ c(\sigma 3)(x3\,c(\alpha) + s(\alpha)y3))c(\gamma) + pa3(c(\sigma 3)(x3\,s(\alpha) - \\ y3\,c(\alpha))s(\beta) - s(\sigma 3)(x3\,c(\alpha) + s(\alpha)y3))s(\gamma) + \\ c(\beta)da13(x3\,s(\alpha) - y3\,c(\alpha))) \end{aligned} \tag{A.33}$$

$$\begin{aligned} Dr_{a_{13}} = (|(pa3(c(\alpha)s(\beta)s(\gamma) - c(\gamma)s(\alpha))c(\sigma 3) + \\ pa3\,s(\sigma 3)(s(\alpha)s(\gamma) + c(\alpha)c(\gamma)s(\beta)) + da13\,c(\alpha)c(\beta) - \\ x3)|^2 + |((c(\gamma)s(\sigma 3)pa3\,s(\beta) + s(\gamma)pa3\,s(\beta)c(\sigma 3) + \\ da13\,c(\beta))s(\alpha) + pa3(c(\gamma)c(\sigma 3) - s(\gamma)s(\sigma 3))c(\alpha) - y3)|^2 + \\ |(da13\,s(\beta) - c(\beta)(c(\gamma)s(\sigma 3) + s(\gamma)c(\sigma 3))pa3 + z3)|^2)^{\frac{1}{2}} \end{aligned} \tag{A.34}$$

$$\begin{aligned} Nr_{a_{14}} = ((s(\beta)da24\,(x4\,s(\alpha) - y4\,c(\alpha))s(\gamma) - pa4\,c(\sigma 4)(x4\,s(\alpha) - y4\,c(\alpha))c(\beta) + \\ c(\gamma)da24\,(x4\,c(\alpha) + s(\alpha)y4))s(\delta) + (c(\delta)c(\sigma 4)pa4\,(x4\,s(\alpha) - y4\,c(\alpha))s(\beta) - \\ s(\sigma 4)pa1\,(x4\,c(\alpha) + s(\alpha)y4))s(\gamma) + (da24\,c(\delta) + la1)(x4\,s(\alpha) - y4\,c(\alpha))c(\beta) + \\ c(\gamma)(s(\sigma 4)pa1\,(x4\,s(\alpha) - y4\,c(\alpha))s(\beta) + c(\delta)c(\sigma 4)pa4\,(x4\,c(\alpha) + s(\alpha)y4))) \end{aligned} \tag{A.35}$$

$$Dr_{a_{14}} = (|(c(\alpha)(c(\gamma)s(\sigma4)pa1 + (da24\,s(\delta) + pa4\,c(\delta)c(\sigma4))s(\gamma))s(\beta) - (da24\,s(\delta)+ pa4\,c(\delta)c(\sigma4))s(\alpha)c(\gamma) + c(\alpha)c(\beta)(la1 + da24\,c(\delta) - pa4\,c(\sigma4)s(\delta))+ s(\alpha)s(\gamma)s(\sigma4)pa1 - x4)|^2 + |(-(c(\gamma)s(\sigma4)pa1 + (da24\,s(\delta)+ pa4\,c(\delta)c(\sigma4))s(\gamma))s(\alpha)s(\beta) - c(\alpha)(da24\,s(\delta) + pa4\,c(\delta)c(\sigma4))c(\gamma)- c(\beta)s(\alpha)(la1 + da24\,c(\delta) - pa4\,c(\sigma4)s(\delta)) + c(\alpha)s(\gamma)s(\sigma4)pa1+ y4)|^2 + |((-c(\delta)s(\gamma)c(\sigma4)pa4 - c(\gamma)s(\sigma4)pa1 - s(\gamma)da24\,s(\delta))c(\beta)+ s(\beta)(la1 + da24\,c(\delta) - pa4\,c(\sigma4)s(\delta)) + z4)|^2)^{\frac{1}{2}} \tag{A.36}$$

$$Nr_{a_{15}} = ((s(\beta)da25(x5\,s(\alpha) - y5\,c(\alpha))s(\gamma) - pa5\,c(\sigma5)(x5\,s(\alpha)- y5\,c(\alpha))c(\beta) + c(\gamma)da25(x5\,c(\alpha) + s(\alpha)y5))s(\delta)+ (c(\delta)c(\sigma5)pa5(x5\,s(\alpha) - y5\,c(\alpha))s(\beta) - s(\sigma5)pa1(x5\,c(\alpha) + s(\alpha)y5))s(\gamma)+ (da25\,c(\delta) + la1)(x5\,s(\alpha) - y5\,c(\alpha))c(\beta) + c(\gamma)(s(\sigma5)pa1(x5\,s(\alpha)- y5\,c(\alpha))s(\beta) + c(\delta)c(\sigma5)pa5(x5\,c(\alpha) + s(\alpha)y5))) \tag{A.37}$$

$$Dr_{a_{15}} = (|(c(\alpha)(c(\gamma)s(\sigma5)pa1 + (da25\,s(\delta) + pa5\,c(\delta)c(\sigma5))s(\gamma))s(\beta)- (da25\,s(\delta) + pa5\,c(\delta)c(\sigma5))s(\alpha)c(\gamma) + c(\alpha)c(\beta)(la1 + da25\,c(\delta)- pa5\,c(\sigma5)s(\delta)) + s(\alpha)s(\gamma)s(\sigma5)pa1 - x5)|^2 + |(-(c(\gamma)s(\sigma5)pa1+ (da25\,s(\delta) + pa5\,c(\delta)c(sigma5))s(\gamma))s(\alpha)s(\beta) - c(\alpha)(da25\,s(\delta) + pa5\,c(\delta)c(\sigma5))c(\gamma) -c(\beta)s(\alpha)(la1 + da25\,c(\delta) - pa5\,c(\sigma5)s(\delta)) + c(\alpha)s(\gamma)s(\sigma5)pa1+ y5)|^2 + |((-c(\delta)s(\gamma)c(\sigma5)pa5 - c(\gamma)s(\sigma5)pa1 - s(\gamma)da25\,s(\delta))c(\beta)+ s(\beta)(la1 + da25\,c(\delta) - pa5\,c(\sigma5)s(\delta)) + z5)|^2)^{\frac{1}{2}} \tag{A.38}$$

$$a_{11} = \frac{Nr_{a_{11}}}{Dr_{a_{11}}}, a_{12} = \frac{Nr_{a_{12}}}{Dr_{a_{12}}}, a_{13} = \frac{Nr_{a_{13}}}{Dr_{a_{13}}}, a_{14} = \frac{Nr_{a_{14}}}{Dr_{a_{14}}}, a_{15} = \frac{Nr_{a_{15}}}{Dr_{a_{15}}} \tag{A.39}$$

$$Nr_{a_{21}} = -((s(\gamma)pa1(x1\,c(\alpha) + y1\,s(\alpha))c(\sigma1)+ c(\gamma)pa1(x1\,c(\alpha) + y1\,s(\alpha))s(\sigma1) - z1\,da11)c(\beta)- (s(\gamma)z1\,pa1\,c(\sigma1) + c(\gamma)s(\sigma1)z1\,pa1+ da11(x1\,c(\alpha) + y1\,s(\alpha)))s(\beta)) \tag{A.40}$$

$$Dr_{a_{21}} = (|(pa1(c(\alpha)s(\beta)s(\gamma) - c(\gamma)s(\alpha))c(\sigma1) + pa1\,s(\sigma1)(s(\alpha)s(\gamma)+ c(\alpha)c(\gamma)s(\beta)) + da11\,c(\alpha)c(\beta) - x1)|^2+ |((c(\gamma)s(\sigma1)pa1\,s(\beta) + s(\gamma)pa1\,s(\beta)c(\sigma1) + da11\,c(\beta))s(\alpha)+ pa1(c(\gamma)c(\sigma1) - s(\gamma)s(\sigma1))c(\alpha) - y1)|^2+ |(da11\,s(\beta) - c(\beta)(c(\sigma1)s(\gamma) + s(\sigma1)c(\gamma))pa1 + z1)|^2)^{\frac{1}{2}} \tag{A.41}$$

$$Nr_{a_{22}} = -((s(\gamma)pa2(x2c(\alpha) + s(\alpha)y2)c(\sigma2) + c(\gamma)pa2(x2c(\alpha)+ s(\alpha)y2)s(\sigma2) - da12\,z2)c(\beta) - (s(\gamma)z2\,pa2c(\sigma2) + c(\gamma)s(\sigma2)z2\,pa2+ da12(x2c(\alpha) + s(\alpha)y2))s(\beta)) \tag{A.42}$$

$$Dr_{a_{22}} = (|(pa2(c(\alpha)s(\beta)s(\gamma) - c(\gamma)s(\alpha))c(\sigma2) + pa2\,s(\sigma2)(s(\alpha)s(\gamma)+ c(\alpha)c(\gamma)s(\beta)) + da12c(\alpha)c(\beta) - x2)|^2 + |((da12c(\beta) + pa2c(\gamma)s(\beta)s(\sigma2)+ pa2\,s(\beta)c(\sigma2)s(\gamma))s(\alpha) + pa2(c(\gamma)c(\sigma2) - s(\gamma)s(\sigma2))c(\alpha) - y2)|^2+ |(da12\,s(\beta) - c(\beta)(c(\gamma)s(\sigma2) + s(\gamma)c(\sigma2))pa2 + z2)|^2)^{\frac{1}{2}} \tag{A.43}$$

$$Nr_{a_{23}} = -((s(\gamma)pa3(x3c(\alpha) + s(\alpha)y3)c(\sigma3) + c(\gamma)pa3(x3c(\alpha)+ s(\alpha)y3)s(\sigma3) - da13\,z3)c(\beta) - (s(\gamma)z3\,pa3c(\sigma3) + c(\gamma)s(\sigma3)z3\,pa3+ da13(x3c(\alpha) + s(\alpha)y3))s(\beta)) \tag{A.44}$$

$$Dr_{a_{23}} = (|(pa3(c(\alpha)s(\beta)s(\gamma) - c(\gamma)s(\alpha))c(\sigma3) + pa3\,s(\sigma3)(s(\alpha)s(\gamma)+ c(\alpha)c(\gamma)s(\beta)) + da13c(\alpha)c(\beta) - x3)|^2 + |((c(\gamma)s(\sigma3)pa3\,s(\beta) + s(\gamma)pa3\,s(\beta)c(\sigma3)+ da13c(\beta))s(\alpha) + pa3(c(\gamma)c(\sigma3) - s(\gamma)s(\sigma3))c(\alpha) - y3)|^2 + |(da13\,s(\beta)- c(\beta)(c(\gamma)s(\sigma3) + s(\gamma)c(\sigma3))pa3 + z3)|^2)^{\frac{1}{2}} \tag{A.45}$$

$$Nr_{a_{24}} = -((pa4\,(x4\,c(\alpha)c(\delta)s(\gamma) + c(\delta)s(\alpha)y4\,s(\gamma) + s(\delta)z4\,)c(\sigma4)+ x4\,(c(\gamma)s(\sigma4)pa1 + s(\gamma)da24\,s(\delta))c(\alpha) - c(\delta)z4\,da24 + y4\,(c(\gamma)s(\sigma4)pa1+ s(\gamma)da24\,s(\delta))s(\alpha) - z4\,la1)c(\beta) - (-pa4\,(x4\,c(\alpha)s(\delta) - c(\delta)s(\gamma)z4+ s(\alpha)s(\delta)y4\,)c(\sigma4) + x4\,(da24\,c(\delta) + la1)c(\alpha) + c(\delta)s(\alpha)y4\,da24+ y4\,la1\,s(\alpha) + z4\,(c(\gamma)s(\sigma4)pa1 + s(\gamma)da24\,s(\delta)))s(\beta)) \tag{A.46}$$

$$Dr_{a_{24}} = (|(c(\alpha)(c(\gamma)s(\sigma4)pa1 + (da24\,s(\delta) + pa4\,c(\delta)c(\sigma4))s(\gamma))s(\beta)- (da24\,s(\delta) + pa4\,c(\delta)c(\sigma4))s(\alpha)c(\gamma) + c(\alpha)c(\beta)(la1 + da24\,c(\delta)- pa4\,c(\sigma4)s(\delta)) + s(\alpha)s(\gamma)s(\sigma4)pa1 - x4\,)|^2 + |(-(c(\gamma)s(\sigma4)pa1 + (da24\,s(\delta)+ pa4\,c(\delta)c(\sigma4))s(\gamma))s(\alpha)s(\beta) - c(\alpha)(da24\,s(\delta) + pa4\,c(\delta)c(\sigma4))c(\gamma) - c(\beta)s(\alpha)(la1+ da24\,c(\delta) - pa4\,c(\sigma4)s(\delta)) + c(\alpha)s(\gamma)s(\sigma4)pa1 + y4\,)|^2 + |((-c(\delta)s(\gamma)c(\sigma4)pa4- c(\gamma)s(\sigma4)pa1 - s(\gamma)da24\,s(\delta))c(\beta) + s(\beta)(la1 + da24\,c(\delta) - pa4\,c(\sigma4)s(\delta)) + z4\,)|^2)^{\frac{1}{2}} \tag{A.47}$$

$$\begin{aligned} Nr_{a_{25}} = -((pa5(x5c(\alpha)c(\delta)s(\gamma) + c(\delta)s(\alpha)y5s(\gamma) + s(\delta)z5)c(\sigma5)+ \\ x5(c(\gamma)s(\sigma5)pa1 + s(\gamma)da25s(\delta))c(\alpha) - c(\delta)z5\,da25 + y5(c(\gamma)s(\sigma5)pa1+ \\ s(\gamma)da25s(\delta))s(\alpha) - z5la1)c(\beta) - (-pa5(x5c(\alpha)s(\delta) - c(\delta)s(\gamma)z5+ \\ s(\alpha)s(\delta)y5)c(\sigma5) + x5(da25c(\delta) + la1)c(\alpha) + c(\delta)s(\alpha)y5\,da25 + y5la1s(\alpha)+ \\ z5(c(\gamma)s(\sigma5)pa1 + s(\gamma)da25s(\delta)))s(\beta)) \end{aligned} \tag{A.48}$$

$$\begin{aligned} Dr_{a_{25}} = (|(c(\alpha)(c(\gamma)s(\sigma5)pa1 + (da25s(\delta) + pa5c(\delta)c(\sigma5))s(\gamma))s(\beta)- \\ (da25s(\delta) + pa5c(\delta)c(\sigma5))s(\alpha)c(\gamma) + c(\alpha)c(\beta)(la1 + da25c(\delta) - pa5c(\sigma5)s(\delta))+ \\ s(\alpha)s(\gamma)s(\sigma5)pa1 - x5)|^2 + |(-(c(\gamma)s(\sigma5)pa1 + (da25s(\delta)+ \\ pa5c(\delta)c(\sigma5))s(\gamma))s(\alpha)s(\beta) - c(\alpha)(da25s(\delta)+ \\ pa5c(\delta)c(\sigma5))c(\gamma) - c(\beta)s(\alpha)(la1 + da25c(\delta) - pa5c(\sigma5)s(\delta))+ \\ c(\alpha)s(\gamma)s(\sigma5)pa1 + y5)|^2 + |((-c(\delta)s(\gamma)c(\sigma5)pa5- \\ c(\gamma)s(\sigma5)pa1 - s(\gamma)da25s(\delta))c(\beta) + s(\beta)(la1 + da25c(\delta) - pa5c(\sigma5)s(\delta)) + z5)|^2)^{\frac{1}{2}} \end{aligned} \tag{A.49}$$

$$a_{21} = \frac{Nr_{a_{21}}}{Dr_{a_{21}}}, a_{22} = \frac{Nr_{a_{22}}}{Dr_{a_{22}}}, a_{23} = \frac{Nr_{a_{23}}}{Dr_{a_{23}}}, a_{24} = \frac{Nr_{a_{24}}}{Dr_{a_{24}}}, a_{25} = \frac{Nr_{a_{25}}}{Dr_{a_{25}}} \tag{A.50}$$

$$\begin{aligned} Nr_{a_{31}} = -pa1(((x1s(\beta)c(\alpha) + s(\beta)s(\alpha)y1 + c(\beta)z1)c(\gamma)+ \\ s(\gamma)(x1s(\alpha) - c(\alpha)y1))c(\sigma1) - s(\sigma1)((-x1s(\alpha) + c(\alpha)y1)c(\gamma)+ \\ s(\gamma)(x1s(\beta)c(\alpha) + s(\beta)s(\alpha)y1 + c(\beta)z1))) \end{aligned} \tag{A.51}$$

$$\begin{aligned} Dr_{a_{31}} = (|(pa1(c(\alpha)s(\beta)s(\gamma) - c(\gamma)s(\alpha))c(\sigma1) + pa1s(\sigma1)(s(\alpha)s(\gamma) + c(\alpha)c(\gamma)s(\beta)) \\ +da11c(\alpha)c(\beta) - x1)|^2 + |((c(\gamma)s(\sigma1)pa1s(\beta) + s(\gamma)pa1s(\beta)c(\sigma1)+ \\ da11c(\beta))s(\alpha) + pa1(c(\gamma)c(\sigma1) - s(\gamma)s(\sigma1))c(\alpha) - y1)|^2 + |(da11s(\beta)- \\ c(\beta)(c(\sigma1)s(\gamma) + s(\sigma1)c(\gamma))pa1 + z1)|^2)^{\frac{1}{2}} \end{aligned} \tag{A.52}$$

$$\begin{aligned} Nr_{a_{32}} = -pa2(((x2s(\beta)c(\alpha) + s(\beta)s(\alpha)y2 + c(\beta)z2)c(\gamma) + s(\gamma)(x2s(\alpha)- \\ y2c(\alpha)))c(\sigma2) - s(\sigma2)((-x2s(\alpha) + y2c(\alpha))c(\gamma) + s(\gamma)(x2s(\beta)c(\alpha)+ \\ s(\beta)s(\alpha)y2 + c(\beta)z2))) \end{aligned} \tag{A.53}$$

$$\begin{aligned} Dr_{a_{32}} = (|(pa2(c(\alpha)s(\beta)s(\gamma) - c(\gamma)s(\alpha))c(\sigma2) + pa2s(\sigma2)(s(\alpha)s(\gamma) + c(\alpha)c(\gamma)s(\beta))+ \\ da12c(\alpha)c(\beta) - x2)|^2 + |((da12c(\beta) + pa2c(\gamma)s(\beta)s(\sigma2)+ \\ pa2s(\beta)c(\sigma2)s(\gamma))s(\alpha) + pa2(c(\gamma)c(\sigma2) - s(\gamma)s(\sigma2))c(\alpha) - y2)|^2+ \\ |(da12s(\beta) - c(\beta)(c(\gamma)s(\sigma2) + s(\gamma)c(\sigma2))pa2 + z2)|^2)^{\frac{1}{2}} \end{aligned} \tag{A.54}$$

$$\begin{aligned} Nr_{a_{33}} = -pa3(((x3\,s(\beta)c(\alpha) + s(\beta)s(\alpha)y3 + c(\beta)z3)c(\gamma) + s(\gamma)(x3\,s(\alpha)- \\ y3\,c(\alpha)))c(\sigma 3) - s(\sigma 3)((-x3\,s(\alpha) + y3\,c(\alpha))c(\gamma) + s(\gamma)(x3\,s(\beta)c(\alpha)+ \\ s(\beta)s(\alpha)y3 + c(\beta)z3))) \end{aligned} \tag{A.55}$$

$$\begin{aligned} Dr_{a_{33}} = (|(pa3(c(\alpha)s(\beta)s(\gamma) - c(\gamma)s(\alpha))c(\sigma 3) + pa3\,s(\sigma 3)(s(\alpha)s(\gamma) + c(\alpha)c(\gamma)s(\beta))+ \\ da13\,c(\alpha)c(\beta) - x3)|^2 + |((c(\gamma)s(\sigma 3)pa3\,s(\beta) + s(\gamma)pa3\,s(\beta)c(\sigma 3)+ \\ da13\,c(\beta))s(\alpha) + pa3(c(\gamma)c(\sigma 3) - s(\gamma)s(\sigma 3))c(\alpha) - y3)|^2 + |(da13\,s(\beta)- \\ c(\beta)(c(\gamma)s(\sigma 3) + s(\gamma)c(\sigma 3))pa3 + z3)|^2)^{\frac{1}{2}} \end{aligned} \tag{A.56}$$

$$\begin{aligned} Nr_{a_{34}} = (-(c(\gamma)(x4\,c(\alpha) + s(\alpha)y4)s(\beta) + x4\,s(\alpha)s(\gamma) + c(\beta)c(\gamma)z4 - \\ y4\,s(\gamma)c(\alpha))c(\delta)pa4\,c(\sigma 4) + (s(\gamma)(x4\,c(\alpha) + s(\alpha)y4)s(\beta) - x4\,c(\gamma)s(\alpha)+ \\ c(\beta)s(\gamma)z4 + c(\gamma)y4\,c(\alpha))pa1 s(\sigma 4) - da24\,s(\delta)(c(\gamma)(x4\,c(\alpha) + s(\alpha)y4)s(\beta)+ \\ x4\,s(\alpha)s(\gamma) + c(\beta)c(\gamma)z4 - y4\,s(\gamma)c(\alpha))) \end{aligned} \tag{A.57}$$

$$\begin{aligned} Dr_{a_{34}} = (|(c(\alpha)(c(\gamma)s(\sigma 4)pa1 + (da24\,s(\delta) + pa4\,c(\delta)c(\sigma 4))s(\gamma))s(\beta) - (da24\,s(\delta)+ \\ pa4\,c(\delta)c(\sigma 4))s(\alpha)c(\gamma) + c(\alpha)c(\beta)(la1 + da24\,c(\delta) - pa4\,c(\sigma 4)s(\delta))+ \\ s(\alpha)s(\gamma)s(\sigma 4)pa1 - x4)|^2 + |(-(c(\gamma)s(\sigma 4)pa1 + (da24\,s(\delta)+ \\ pa4\,c(\delta)c(\sigma 4))s(\gamma))s(\alpha)s(\beta) - c(\alpha)(da24\,s(\delta) + pa4\,c(\delta)c(\sigma 4))c(\gamma) - c(\beta)s(\alpha)(la1+ \\ da24\,c(\delta) - pa4\,c(\sigma 4)s(\delta)) + c(\alpha)s(\gamma)s(\sigma 4)pa1 + y4)|^2+ \\ |((-c(\delta)s(\gamma)c(\sigma 4)pa4 - c(\gamma)s(\sigma 4)pa1 - s(\gamma)da24\,s(\delta))c(\beta) + s(\beta)(la1 + da24\,c(\delta)- \\ pa4\,c(\sigma 4)s(\delta)) + z4)|^2)^{\frac{1}{2}} \end{aligned} \tag{A.58}$$

$$\begin{aligned} Nr_{a_{35}} = (-(c(\gamma)(x5\,c(\alpha) + s(\alpha)y5)s(\beta) + x5\,s(\alpha)s(\gamma) + c(\beta)c(\gamma)z5 - \\ y5\,s(\gamma)c(\alpha))c(\delta)pa5\,c(\sigma 5) + (s(\gamma)(x5\,c(\alpha) + s(\alpha)y5)s(\beta) - x5\,c(\gamma)s(\alpha)+ \\ c(\beta)s(\gamma)z5 + c(\gamma)y5\,c(\alpha))pa1\,s(\sigma 5) - da25\,s(\delta)(c(\gamma)(x5\,c(\alpha) + s(\alpha)y5)s(\beta)+ \\ x5\,s(\alpha)s(\gamma) + c(\beta)c(\gamma)z5 - y5\,s(\gamma)c(\alpha))) \end{aligned} \tag{A.59}$$

$$\begin{aligned} Dr_{a_{35}} = (|(c(\alpha)(c(\gamma)s(\sigma 5)pa1 + (da25\,s(\delta) + pa5\,c(\delta)c(\sigma 5))s(\gamma))s(\beta) - (da25\,s(\delta)+ \\ pa5\,c(\delta)c(\sigma 5))s(\alpha)c(\gamma) + c(\alpha)c(\beta)(la1 + da25\,c(\delta) - pa5\,c(\sigma 5)s(\delta))+ \\ s(\alpha)s(\gamma)s(\sigma 5)pa1 - x5)|^2 + |(-(c(\gamma)s(\sigma 5)pa1 + (da25\,s(\delta)+ \\ pa5\,c(\delta)c(\sigma 5))s(\gamma))s(\alpha)s(\beta) - c(\alpha)(da25\,s(\delta) + pa5\,c(\delta)c(\sigma 5))c(\gamma) - c(\beta)s(\alpha)(la1+ \\ da25\,c(\delta) - pa5\,c(\sigma 5)s(\delta)) + c(\alpha)s(\gamma)s(\sigma 5)pa1 + y5)|^2+ \\ |((-c(\delta)s(\gamma)c(\sigma 5)pa5 - c(\gamma)s(\sigma 5)pa1 - s(\gamma)da25\,s(\delta))c(\beta) + s(\beta)(la1 + da25\,c(\delta)- \\ pa5\,c(\sigma 5)s(\delta)) + z5)|^2)^{\frac{1}{2}} \end{aligned} \tag{A.60}$$

$$a_{31} = \frac{Nr_{a_{31}}}{Dr_{a_{31}}}, a_{32} = \frac{Nr_{a_{32}}}{Dr_{a_{32}}}, a_{33} = \frac{Nr_{a_{33}}}{Dr_{a_{33}}}, a_{34} = \frac{Nr_{a_{34}}}{Dr_{a_{34}}}, a_{35} = \frac{Nr_{a_{35}}}{Dr_{a_{35}}} \tag{A.61}$$

$$a_{41} = 0, a_{42} = 0, a_{43} = 0 \tag{A.62}$$

$$\begin{aligned} Nr_{a_{44}} = (-(c(\beta)z4 + s(\beta)(x4\,c(\alpha) + s(\alpha)y4))(da24\,c(\delta) - pa4\,c(\sigma4)s(\delta))s(\gamma) + \\ (da24\,s(\delta) + pa4\,c(\delta)c(\sigma4))(x4\,c(\alpha) + s(\alpha)y4)c(\beta) - z4\,(da24\,s(\delta) + \\ pa4\,c(\delta)c(\sigma4))s(\beta) - c(\gamma)y4\,(da24\,c(\delta) - pa4\,c(\sigma4)s(\delta))c(\alpha) + x4\,s(\alpha)(da24\,c(\delta) - \\ pa4\,c(\sigma4)s(\delta))c(\gamma) - la1\,(da24\,s(\delta) + pa4\,c(\delta)c(\sigma4))) \end{aligned} \tag{A.63}$$

$$\begin{aligned} Dr_{a_{44}} = (|(c(\alpha)(c(\gamma)s(\sigma4)pa1 + (da24\,s(\delta) + pa4\,c(\delta)c(\sigma4))s(\gamma))s(\beta) - (da24\,s(\delta) + \\ pa4\,c(\delta)c(\sigma4))s(\alpha)c(\gamma) + c(\alpha)c(\beta)(la1 + da24\,c(\delta) - pa4\,c(\sigma4)s(\delta)) + \\ s(\alpha)s(\gamma)s(\sigma4)pa1 - x4)|^2 + |(-(c(\gamma)s(\sigma4)pa1 + (da24\,s(\delta) + \\ pa4\,c(\delta)c(\sigma4))s(\gamma))s(\alpha)s(\beta) - c(\alpha)(da24\,s(\delta) + pa4\,c(\delta)c(\sigma4))c(\gamma) - c(\beta)s(\alpha)(la1 + \\ da24\,c(\delta) - pa4\,c(\sigma4)s(\delta)) + c(\alpha)s(\gamma)s(\sigma4)pa1 + y4)|^2 + \\ |((-c(\delta)s(\gamma)c(\sigma4)pa4 - c(\gamma)s(\sigma4)pa1 - s(\gamma)da24\,s(\delta))c(\beta) + s(\beta)(la1 + \\ da24\,c(\delta) - pa4\,c(\sigma4)s(\delta)) + z4)|^2)^{\frac{1}{2}} \end{aligned} \tag{A.64}$$

$$\begin{aligned} Nr_{a_{45}} = (-(c(\beta)z4 + s(\beta)(x4\,c(\alpha) + s(\alpha)y4))(da24\,c(\delta) - pa4\,c(\sigma4)s(\delta))s(\gamma) + \\ (da24\,s(\delta) + pa4\,c(\delta)c(\sigma4))(x4\,c(\alpha) + s(\alpha)y4)c(\beta) - z4\,(da24\,s(\delta) + \\ pa4\,c(\delta)c(\sigma4))s(\beta) - c(\gamma)y4\,(da24\,c(\delta) - pa4\,c(\sigma4)s(\delta))c(\alpha) + x4\,s(\alpha)(da24\,c(\delta) - \\ pa4\,c(\sigma4)s(\delta))c(\gamma) - la1\,(da24\,s(\delta) + pa4\,c(\delta)c(\sigma4))) \end{aligned} \tag{A.65}$$

$$\begin{aligned} Dr_{a_{45}} = (|(c(\alpha)(c(\gamma)s(\sigma4)pa1 + (da24\,s(\delta) + pa4\,c(\delta)c(\sigma4))s(\gamma))s(\beta) - (da24\,s(\delta) + \\ pa4\,c(\delta)c(\sigma4))s(\alpha)c(\gamma) + c(\alpha)c(\beta)(la1 + da24\,c(\delta) - pa4\,c(\sigma4)s(\delta)) + \\ s(\alpha)s(\gamma)s(\sigma4)pa1 - x4)|^2 + |(-(c(\gamma)s(\sigma4)pa1 + (da24\,s(\delta) + \\ pa4\,c(\delta)c(\sigma4))s(\gamma))s(\alpha)s(\beta) - c(\alpha)(da24\,s(\delta) + pa4\,c(\delta)c(\sigma4))c(\gamma) - c(\beta)s(\alpha)(la1 + \\ da24\,c(\delta) - pa4\,c(\sigma4)s(\delta)) + c(\alpha)s(\gamma)s(\sigma4)pa1 + y4)|^2 + |((-c(\delta)s(\gamma)c(\sigma4)pa4 - \\ c(\gamma)s(\sigma4)pa1 - s(\gamma)da24\,s(\delta))c(\beta) + s(\beta)(la1 + da24\,c(\delta) - pa4\,c(\sigma4)s(\delta)) + z4)|^2)^{\frac{1}{2}} \end{aligned} \tag{A.66}$$

$$a_{44} = \frac{Nr_{a_{44}}}{Dr_{a_{44}}}, a_{45} = \frac{Nr_{a_{45}}}{Dr_{a_{45}}} \tag{A.67}$$

A.5 2-Link spherical-spherical CDSKC

The two link double joint (spherical-spherical) arm parameters are given in Table A.5.

	Link 0	Link 1		Link 2
Cable 1	$[-0.141, -0.141, 0]^\mathsf{T}$	$[-0.01, 0, 0.04]^\mathsf{T}$		
Cable 2	$[-0.141, 0.141, 0]^\mathsf{T}$	$[-0.01, 0, 0.08]^\mathsf{T}$		
Cable 3	$[0.141, -0.141, 0]^\mathsf{T}$	$[0.01, 0, 0.04]^\mathsf{T}$		
Cable 4	$[0.28, -0.28, 0]^\mathsf{T}$	$[-0.04, 0, 0.06]^\mathsf{T}$	$[-0.08, 0, 0.08]^\mathsf{T}$	$[0, -0.01, 0.04]^\mathsf{T}$
Cable 5	$[-0.28, -0.27, 0]^\mathsf{T}$	$[-0.04, 0, 0.06]^\mathsf{T}$	$[-0.08, 0, 0.08]^\mathsf{T}$	$[0, 0.01, 0.08]^\mathsf{T}$
Cable 6	$[-0.28, -0.27, 0]^\mathsf{T}$	$[0.04, 0, 0.06]^\mathsf{T}$	$[0.08, 0, 0.08]^\mathsf{T}$	$[0, -0.01, 0.04]^\mathsf{T}$
Cable 7	$[0.28, 0.28, 0]^\mathsf{T}$	$[0.04, 0, 0.06]^\mathsf{T}$	$[0.07, 0, 0.08]^\mathsf{T}$	$[0, 0.01, 0.08]^\mathsf{T}$

Table A.5: Cable configuration (in m) for 2-link CDSKC with $n + 1$ actuated cables with internal routing scheme

Appendix B

Prototype components

A reconfigurable and modular robot was designed tailoring the needs and requirements of testing different routing topologies. The key hardware components are the muscle actuators, NEMA 17 stepper motors with drive pulleys (a winding device) that allows the easy control of the robot motion, the tendon material is 0.48 mm 80lbs braided fishing line selected according to the task requirements. The body of the robot is made of 3D-printed thermoplastic Polylactic acid(PLA) and a variable spacer is employed to facilitate multiple routing configurations. The tendon pulling force is applied to the mounting point on the robot's body rather than generating torques directly between two rigid bodies. The slider based routing holes are 1.3mm in diameter and the distance between the holes are 2mm. The base slider can be shifted thereby changing the distance of the routing point and modifying parameter vaues in the tendon space Jacobian. This allows the user to reconfigure the robot into a new configuration and checking the wrench-feasible workspace. The number of routing holes are 12 at the base and 30 at the mounting parts. The length of fabricated links are 234mm and 315mm including the end effector. There are a total of 30 routing points. The two links are cylindrical and hollow that simplifies the internal routing, bundling and cross routing actuation schemes. The CAD model of the proposed experimental setup is shown in Fig. B.1. The wrench feasible motion generation for different topologies is explained in the following section.

Figure B.1: CAD Model

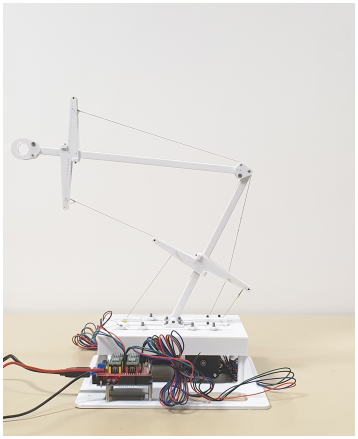

Figure B.2: Pose not satisfying force-closure

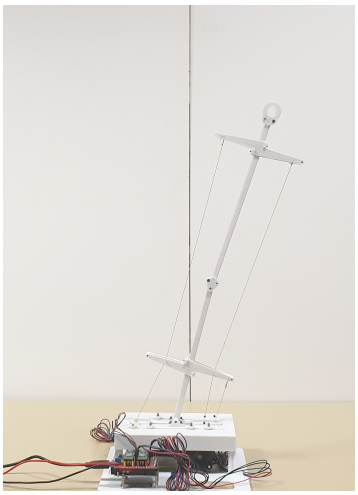

Figure B.3: Feasible pose satisfying force-closure

Figure B.4: Non-feasible pose, third cable is slack

Appendix C

Publications and related work

C.1 Kinematic and Workspace Analysis of Minimally Routed Cable Driven Open Chains

- **Authors:** Vishal Ramadoss, Dimiter Zlatanov, Matteo Zoppi
- **Type of publication:** Conference Article, *International Federation for the Promotion of Mechanism and Machine Science(IFToMM).*
- **Place and date:** Presented at *2019-15th IFToMM World Congress*, Krakow, Poland, on June 30, 2019.
- **Abstract:** This paper presents the kineto-static analysis of cable-driven serial kinematic chains (CDSKCs). The CDSKC are typically open-chain structures with complex cable routing and multiple links. By using cable routing between links, re-routing within links and cable bundles, any serial chain with n degrees of freedom can be controlled with $n+1$ cables. A generalized model that allows minimal and fully actuated cable routing for planar and spatial kinematic chain needs to be formulated. The analyses for CDSKCs require extensions from cable driven parallel manipulators (CDPMs) to consider the different types of cable routing. The workspace analysis of a

single and multi-link CDSKC is performed. The effects of changing cable configuration on the feasible workspace for such multilink unilateral manipulators are explored and the configurations of largest reachable workspace are determined.

C.2 Modeling and Design of an Active Assistive Exoskeletal Robot for Upper Limb Rehabilitation.

- **Authors:** Vishal Ramadoss, Dimiter Zlatanov, Matteo Zoppi
- **Type of publication:** Conference Extended Abstract, *CRAS 2019*.
- **Place and date:** Presented at *2019 Joint Workshop on New Technologies for Computer Robot Assisted Surgery (CRAS)*, Genoa, Italy, on March, 2019.
- **Abstract:** Wearable robotics is a fast growing field with assistive exoskeletons being developed for medical and purposes. These exoskeletons can be used for gait rehabilitation of patients, arm rehabilitation and provide body support during training. These exoskeletal systems are anthropomorphically structured mechanisms where the rigid links form a serial kinematic chain and the cables are attached in a parallel configuration. Cable-driven system eliminates the need of rigid links and mechanical joints, making the system lightweight. Due to the serial unilateral constraints, it has to be ensured that all cables remain in tension at any point of time for system functionality. This results in redundancy in the actuation system. The aim of this paper is to provide the kinematic analysis of these multilink cable-driven robots (MCDRs) with fully routed cable bundles.

C.3 Workspace Analysis of Fully Routed Two-Link Tendon Driven Manipulators

- **Authors:** Vishal Ramadoss*, Keerthi Sagar*, Rezia Molfino, Dimiter Zlatanov, Matteo Zoppi
- **Type of publication:** Conference Poster and Article in *IRIM 2019*.
- **Place and date:** Presented at *2019 1st Conferenza Italiana di Robotica e Macchine Intelligenti (IRIM)*, Roma, Italy, on October 26, 2019.
- **Abstract:** This paper presents workspace analysis of tendon-driven planar serial kinematic chains which allows single-point and multi-point routing with bundling per rigid link. Targeting a musculoskeletal two-link system with different tendon arrangements as a case study, the wrench-closure and wrench-feasible workspace are evaluated for different configurations. It is observed that, the single-point internally routed chain has more feasible workspace than the externally routed robot with 3 tendons.

C.4 Analysis of Planar Multilink Cable Driven Robots Using Internal Routing Scheme

- **Authors:** Vishal Ramadoss, Darwin Lau, Dimiter Zlatanov, Matteo Zoppi.
- **Type of publication:** Conference Article to be published in *ASME 2020*.
- **Place and date:** ASME IDETC CIE, USA, on August, 2020.
- **Abstract:**The multilink cable driven robot (MCDR) is an extension of the cable robots where the moving platform is replaced by a multibody chain. It is typically an open-chain structure with multiple links and complex cable routing. This design introduces the advantages of having a serial kinematic structure and preserves the benefits associated with cable-driven

parallel mechanism. To achieve a minimum number of actuating cables while possessing a large workspace region, a novel internal cable routing scheme is proposed. It is shown that by incorporating internal routing with multi-segment cables, any serial chain with n degrees of freedom can be controlled with n + 1 cables. In this work, through studying the kinematics and dynamics, we demonstrate how internally-routed cable actuation of multilink manipulators have an increased workspace and reduced cable forces to execute trajectories.

C.5 Design Of Serial Link Structure-Parallel Wire System For Virtual Reality Rehabilitation and Assessment

- **Authors:** Vishal Ramadoss, Mohamed Sadiq Ikbal, Dimiter Zlatanov, Matteo Zoppi.
- **Type of publication:** Conference Article to be published in *RAAD 2020*.
- **Place and date:** 29th International Conference on Robotics in Alpe-Adria Danube Region, Poitiers, France on June 17-19, 2020.

C.6 Modeling of a Cable-Based Revolute Joint Using Biphasic Media Variable Stiffness Actuation

- **Authors:** Jesus Hiram Lugo Calles, Vishal Ramadoss, Giorgio Cannata, Matteo Zoppi, Rezia Molfino
- **Type of publication:** Conference Article in *IEEE IRC 2019*.

- **Place and date:** IEEE Robotic Computing, Napoli, on February, 2019.
- **Abstract:** In recent times, safe interactions between humans and robots are required for innumerable tasks and environments. This safety can be achieved using compliance design and control of mechanisms. Cable-driven mechanisms are used when applications need to have light structures, meaning that their actuators must be relocated to ground and forces are transferred along tensioned cables. This paper presents a compliant cable-driven revolute joint using biphasic media variable stiffness actuators. Actuator's stiffness is controlled by changing pressure of control fluid into distribution lines. The used control fluid is biphasic, composed of separated gas and liquid fractions with predefined ratio. The mathematical model of the actuator is presented along with its position and stiffness model-based control, then,equations relating to the dynamics of the mechanism are provided with a joint stiffness and orientation controller. Results from simulations are discussed.

C.7 Design, Construction and Control of Curves and Surfaces via Deployable Mechanisms

- **Authors:** Vishal Ramadoss, Shengnan Lyu, Dimiter Zlatanov, Xilun Ding, Matteo Zoppi
- **Type of publication:** Journal Article in *JMR 2019*.
- **Place and date:** Journal of Mechanisms and Robotics, October, 2019.
- **Abstract:** There has been an increasing interest in design and construction of deployable mechanisms (DMs) with multiple degrees of freedom (DOFs). This paper summarizes a family of deployable mechanisms that approximates a series of curves and surfaces using the polygonal approximation technique. These mechanisms are obtained by linking the two- and three-dimensional deployable units, which are constitutive of Sarrus and scissor linkages. Multiple unit mechanisms with varying sizes are assembled and alter their shape

within a different family of parameterized curves and surfaces. A systematic methodology for polygonal approximation method is presented. Quadratic, semi-cubic, cubic, quartic and sextic curve boundaries, and quadric surfaces are approximated and controlled. Computer-aided design (CAD) models and kinematic simulations elucidate the mechanism's ability to approximate a set of curves and surfaces.

References

[1] S. K. Mustafa and S. K. Agrawal, "On the force-closure analysis of n-dof cable-driven open chains based on reciprocal screw theory," *IEEE Transactions on Robotics*, vol. 28, no. 1, pp. 22–31, 2011. viii, 1, 2, 3

[2] T. Rasheed, P. Long, D. Marquez-Gamez, and S. Caro, "Kinematic modeling and twist feasibility of mobile cable-driven parallel robots," in *International Symposium on Advances in Robot Kinematics*. Springer, 2018, pp. 410–418. viii, 13, 14

[3] J. M. Friesen, P. Glick, M. Fanton, P. Manovi, A. Xydes, T. Bewley, and V. Sunspiral, "The second generation prototype of a duct climbing tensegrity robot, ducttv2," in *2016 IEEE International Conference on Robotics and Automation (ICRA)*. IEEE, 2016, pp. 2123–2128. viii, 17

[4] D. Zlatanov, S. Agrawal, and C. M. Gosselin, "Convex cones in screw spaces," *Mechanism and machine theory*, vol. 40, no. 6, pp. 710–727, 2005. viii, 2, 3, 25, 26, 27, 28, 35, 61, 72

[5] N. G. D. James S. Albus, Roger V. Bostelman, "The nist robocrane," *Journal of Robotics Systems*, 1993. 1, 10, 11

[6] D. Lau, D. Oetomo, and S. K. Halgamuge, "Generalized modeling of multilink cable-driven manipulators with arbitrary routing using the cable-routing matrix," *IEEE Transactions on Robotics*, vol. 29, no. 5, pp. 1102–1113, 2013. 1, 13

[7] Y. Wu, H. H. Cheng, A. Fingrut, K. Crolla, Y. Yam, and D. Lau, "Cu-brick cable-driven robot for automated construction of complex brick structures: From simulation to hardware realisation," in *2018 IEEE International Conference on Simulation, Modeling, and Programming for Autonomous Robots (SIMPAR)*. IEEE, 2018, pp. 166–173. 1, 11

[8] Y. Mao and S. K. Agrawal, "Design of a cable-driven arm exoskeleton (carex) for neural rehabilitation," *IEEE Transactions on Robotics*, vol. 28, no. 4, pp. 922–931, 2012. 1, 12

[9] D. Surdilovic, J. Zhang, and R. Bernhardt, "String-man: Wire-robot technology for safe, flexible and human-friendly gait rehabilitation," in *2007 IEEE 10th International Conference on Rehabilitation Robotics*. IEEE, 2007, pp. 446–453. 1

[10] L.-W. Tsai, "Design of tendon-driven manipulators," *Journal of Mechanical Design*, 1995. 1, 2

[11] J.-P. Merlet, "Parallel robots: Open problems," in *Robotics research*. Springer, 2000, pp. 27–32. 1

[12] X. Cui, W. Chen, X. Jin, and S. K. Agrawal, "Design of a 7-dof cable-driven arm exoskeleton (carex-7) and a controller for dexterous motion training or assistance," *IEEE/ASME Transactions on Mechatronics*, vol. 22, no. 1, pp. 161–172, 2016. 1

[13] X. Cui, W. Chen, S. K. Agrawa, and J. Wang, "A novel customized cable-driven robot for 3-dof wrist and forearm motion training," in *2014 IEEE/RSJ International Conference on Intelligent Robots and Systems*. IEEE, 2014, pp. 3579–3584. 1

[14] S. Rezazadeh and S. Behzadipour, "Tensionability of an arbitrary two-link multibody," in *ASME 2009 International Design Engineering Technical Conferences and Computers and Information in Engineering Conference*. American Society of Mechanical Engineers Digital Collection, 2009, pp. 75–81. 2, 3, 12

[15] D. Zlatanov, "Serial kinematic chains with unilateral external force constraints," in *IFToMM World Congress in Mechanism and Machine Science, Guanajuato, Mexico*, 2011. 2, 12, 22, 24, 25, 29, 30, 72, 73, 106

[16] A. Ming and T. Higuchi, "Study on multiple degree-of-freedom positioning mechanism using wires (part 1) – concept, design and control," *International Journal of Japan Social Engineering*, vol. 28, no. 2, pp. 131—-138, 1994. 3, 11, 12

[17] S. Rezazadeh and S. Behzadipour, "Workspace analysis of multibody cable-driven mechanisms," *Journal of Mechanisms and Robotics*, vol. 3, no. 2, p. 021005, 2011. 3, 12

[18] G. Abbasnejad, J. Eden, and D. Lau, "Generalized ray-based lattice generation and graph representation of wrench-closure workspace for arbitrary cable-driven robots," *IEEE Transactions on Robotics*, vol. 35, no. 1, pp. 147–161, 2018. 3, 13

[19] P. H. Borgstrom, B. L. Jordan, B. J. Borgstrom, M. J. Stealey, G. S. Sukhatme, M. A. Batalin, and W. J. Kaiser, "Nims-pl: A cable-driven robot with self-calibration capabilities," *IEEE Transactions on Robotics*, vol. 25, no. 5, pp. 1005–1015, 2009. 10

[20] A. B. Alp and S. K. Agrawal, "Cable suspended robots: design, planning and control," in *Proceedings 2002 IEEE International Conference on Robotics and Automation (Cat. No. 02CH37292)*, vol. 4. IEEE, 2002, pp. 4275–4280. 10

[21] J.-p. Merlet and D. Daney, "A portable, modular parallel wire crane for rescue operations," in *2010 IEEE International Conference on Robotics and Automation*. IEEE, 2010, pp. 2834–2839. 10

[22] L. L. Cone, "Skycam-an aerial robotic camera system," *Byte*, vol. 10, no. 10, p. 122, 1985. 10, 11

[23] H. Kino, S. Yabe, and S. Kawamura, "A force display system using a serial-link structure driven by a parallel-wire mechanism," *Advanced Robotics*, vol. 19, no. 1, pp. 21–37, 2005. 10, 12

[24] J. Lamaury and M. Gouttefarde, "Control of a large redundantly actuated cable-suspended parallel robot," in *2013 IEEE International Conference on Robotics and Automation*. IEEE, 2013, pp. 4659–4664. 10

[25] N. Pedemonte, T. Rasheed, D. Marquez-Gamez, P. Long, É. Hocquard, F. Babin, C. Fouché, G. Caverot, A. Girin, and S. Caro, "Fastkit: A mobile cable-driven parallel robot for logistics," in *Advances in Robotics Research: From Lab to Market*. Springer, 2020, pp. 141–163. 11

[26] L. Gagliardini, S. Caro, M. Gouttefarde, P. Wenger, and A. Girin, "A reconfigurable cable-driven parallel robot for sandblasting and painting of large structures," in *Cable-Driven Parallel Robots*. Springer, 2015, pp. 275–291. 11

[27] J. P. Eden, "Modelling, analysis and control of multi-link cable-driven manipulators," Ph.D. dissertation, 2018. 12

[28] J. T. Bryson, "The optimal design of cable-driven robots," Ph.D. dissertation, University of Delaware, 2016. 13

[29] D. Lau, T. Hawke, L. Kempton, D. Oetomo, and S. Halgamuge, "Design and analysis of 4-dof cable-driven parallel mechanism," in *Proceedings of the Australasian conference on robotics and automation*, 2010. 13

[30] V. Ramadoss, D. Zlatanov, and M. Zoppi, "Kinematic and workspace analysis of minimally routed cable driven open chains," in *IFToMM World Congress on Mechanism and Machine Science*. Springer, 2019, pp. 2841–2851. 13, 78

[31] V. Ramadoss, D. Lau, D. Zlatanov, and M. Zoppi, "Analysis of Planar Multilink Cable Driven Robots Using Internal Routing Scheme," submitted for publication. 13

[32] V. Ramadoss, K. Sagar, S. Ikbal, M. Jilich, D. Zlatanov, and M. Zoppi, "Design and Analysis of Fully Routed and Bundled Unilaterally Actuated Serial Kinematic Chains," submitted for publication. 13

[33] D. Zlatanov, X. Jin, and S. K. Agrawal, "Minimal Fully-Routed Cable Actuation of Serial Kinematic Chains," 2015. 13, 101, 106

[34] J. Starke, E. Amanov, M. T. Chikhaoui, and J. Burgner-Kahrs, "On the merits of helical tendon routing in continuum robots," in *2017 IEEE/RSJ International Conference on Intelligent Robots and Systems (IROS)*, Sep. 2017, pp. 6470–6476. 13

[35] J. C. Case, E. L. White, V. SunSpiral, and R. Kramer-Bottiglio, "Reducing actuator requirements in continuum robots through optimized cable routing." *Soft robotics*, vol. 5 1, pp. 109–118, 2018. 13

[36] K. Moored and H. Bart-Smith, "Investigation of clustered actuation in tensegrity structures," *International Journal of Solids and Structures*, vol. 46, no. 17, pp. 3272 – 3281, 2009. [Online]. Available: http://www.sciencedirect.com/science/article/pii/S0020768309001826 13

[37] L. Barbieri and M. Bergamasco, "Nets of tendons and actuators: an anthropomorphic model for the actuation system of dexterous robot hands," in *Fifth International Conference on Advanced Robotics 'Robots in Unstructured Environments*, June 1991, pp. 357–362 vol.1. 13

[38] R. Qi, "Redundant hybrid cable-driven robots: Modeling, control, and analysis," 2019. 13

[39] M. Gouttefarde, "Analysis and synthesis of large-dimension cabledriven parallel robots," 2016. 14

[40] "Cuhk c3 robotics laboratory. spiderarm robot: Hybrid cable-driven robot with serial manipulator," https://www.youtube.com/watch?v=rf4Zpf˙MxrA, accessed: 2019-11-28. 14

[41] F. Trautwein, P. Tempel, and A. Pott, "A symbolic-numeric method to capture the impact of varied geometrical parameters on the translational workspace of a planar cable-driven parallel robot," in *2018 International Conference on Reconfigurable Mechanisms and Robots (ReMAR)*, June 2018, pp. 1–7. 13, 33

[42] N. Sanjeevi and V. Vashista, "On the stiffness analysis of a cable driven leg exoskeleton," in *2017 International Conference on Rehabilitation Robotics (ICORR)*. IEEE, 2017, pp. 455–460. 14

[43] ——, "Workspace analysis of a cable driven leg exoskeleton," in *Proceedings of the Advances in Robotics*. ACM, 2017, p. 47. 14

[44] N. Panchal, N. S. S. Sanjeevi, and V. Vashista, "Lower limb musculoskeletal stiffness analysis during swing phase as a cable-driven serial chain system," in *2018 7th IEEE International Conference on Biomedical Robotics and Biomechatronics (Biorob)*, Aug 2018, pp. 934–939. 14

[45] A. Alamdari and V. Krovi, "Robotic physical exercise and system (ropes): A cable-driven robotic rehabilitation system for lower-extremity motor therapy," in *ASME 2015 International Design Engineering Technical Conferences and Computers and Information in Engineering Conference*. American Society of Mechanical Engineers Digital Collection, 2015. 14

[46] A. Alamdari, R. Haghighi, and V. Krovi, "Stiffness modulation in an elastic articulated-cable leg-orthosis emulator: Theory and experiment," *IEEE Transactions on Robotics*, vol. 34, no. 5, pp. 1266–1279, 2018. 14

[47] F. E. Zajac, "Muscle and tendon: properties, models, scaling, and application to biomechanics and motor control." *Critical reviews in biomedical engineering*, vol. 17, no. 4, pp. 359–411, 1989. 15

[48] S. L. Delp and J. P. Loan, "A computational framework for simulating and analyzing human and animal movement," *Computing in Science & Engineering*, vol. 2, no. 5, pp. 46–55, 2000. 15

[49] S. L. Delp, F. C. Anderson, A. S. Arnold, P. Loan, A. Habib, C. T. John, E. Guendelman, and D. G. Thelen, "Opensim: open-source software to create and analyze dynamic simulations of movement," *IEEE transactions on biomedical engineering*, vol. 54, no. 11, pp. 1940–1950, 2007. 15

[50] S. L. Delp, J. P. Loan, M. G. Hoy, F. E. Zajac, E. Topp, and J. M. Rosen, "An interactive graphics-based model of the lower extremity to study orthopaedic surgical procedures," *IEEE Transactions on Biomedical Engineering*, vol. 37, pp. 757–767, 1990. 15

[51] W. Wu, P. V. Lee, A. L. Bryant, M. Galea, and D. C. Ackland, "Subject-specific musculoskeletal modeling in the evaluation of shoulder muscle and joint function," *Journal of biomechanics*, vol. 49, no. 15, pp. 3626–3634, 2016. 15

[52] D. Lau, J. Eden, D. Oetomo, and S. K. Halgamuge, "Musculoskeletal static workspace analysis of the human shoulder as a cable-driven robot," *IEEE/ASME Transactions on Mechatronics*, vol. 20, no. 2, pp. 978–984, 2014. 16

[53] R. E. Skelton and M. C. de Oliveira, *Tensegrity systems*. Springer, 2009, vol. 1. 16

[54] A. Pugh, *An introduction to tensegrity*. Univ of California Press, 1976. 16

[55] G. Scarr, *Biotensegrity*. Handspring Publishing, United Kingdom, 2014. 16, 17

[56] S. M. Levin, "The tensegrity-truss as a model for spine mechanics: biotensegrity," *Journal of mechanics in medicine and biology*, vol. 2, no. 03n04, pp. 375–388, 2002. 16

[57] R. B. Fuller, *Synergetics: explorations in the geometry of thinking*. Estate of R. Buckminster Fuller, 1982. 16

[58] C. Paul, F. J. Valero-Cuevas, and H. Lipson, "Design and control of tensegrity robots for locomotion," *IEEE Transactions on Robotics*, vol. 22, no. 5, pp. 944–957, 2006. 16

[59] J. Bruce, K. Caluwaerts, A. Iscen, A. P. Sabelhaus, and V. SunSpiral, "Design and evolution of a modular tensegrity robot platform," in *2014 IEEE International Conference on Robotics and Automation (ICRA)*. IEEE, 2014, pp. 3483–3489. 16

[60] J. Bruce, A. P. Sabelhaus, Y. Chen, D. Lu, K. Morse, S. Milam, K. Caluwaerts, A. M. Agogino, and V. SunSpiral, "Superball: Exploring tensegrities for planetary probes," 2014. 16

[61] K. Snelson, "Snelson on the tensegrity invention," *International Journal of Space Structures*, vol. 11, no. 1-2, pp. 43–48, 1996. 17

[62] Q. Boehler, I. Charpentier, M. S. Vedrines, and P. Renaud, "Definition and computation of tensegrity mechanism workspace," *Journal of Mechanisms and Robotics*, vol. 7, no. 4, p. 044502, 2015. 17

[63] M. Arsenault and C. M. Gosselin, "Kinematic, static and dynamic analysis of a planar 2-dof tensegrity mechanism," *Mechanism and Machine Theory*, vol. 41, no. 9, pp. 1072–1089, 2006. 17

[64] ——, "Kinematic, static, and dynamic analysis of a spatial three-degree-of-freedom tensegrity mechanism," *Journal of Mechanical Design*, vol. 128, no. 5, pp. 1061–1069, 2006. 17

[65] S. Chen and M. Arsenault, "Analytical computation of the actuator and cartesian workspace boundaries for a planar 2-degree-of-freedom translational tensegrity mechanism," *Journal of Mechanisms and Robotics*, vol. 4, no. 1, p. 011010, 2012. 17

[66] M. Furet and P. Wenger, "Workspace and cuspidality analysis of a 2-x planar manipulator," in *IFToMM Symposium on Mechanism Design for Robotics*. Springer, 2018, pp. 110–117. 17

[67] A. P. Sabelhaus, H. Ji, P. Hylton, Y. Madaan, C. Yang, A. M. Agogino, J. Friesen, and V. SunSpiral, "Mechanism design and simulation of the ultra spine: a tensegrity robot," in *ASME 2015 International Design Engineering Technical Conferences and Computers and Information in Engineering*

Conference. American Society of Mechanical Engineers Digital Collection, 2015. 17

[68] B. R. Tietz, R. W. Carnahan, R. J. Bachmann, R. D. Quinn, and V. SunSpiral, "Tetraspine: Robust terrain handling on a tensegrity robot using central pattern generators," in *2013 IEEE/ASME International Conference on Advanced Intelligent Mechatronics*. IEEE, 2013, pp. 261–267. 17

[69] M. Vespignani, J. M. Friesen, V. SunSpiral, and J. Bruce, "Design of superball v2, a compliant tensegrity robot for absorbing large impacts," in *2018 IEEE/RSJ International Conference on Intelligent Robots and Systems (IROS)*. IEEE, 2018, pp. 2865–2871. 17

[70] S. Lessard, D. Castro, W. Asper, S. D. Chopra, L. B. Baltaxe-Admony, M. Teodorescu, V. SunSpiral, and A. Agogino, "A bio-inspired tensegrity manipulator with multi-dof, structurally compliant joints," in *2016 IEEE/RSJ International Conference on Intelligent Robots and Systems (IROS)*. IEEE, 2016, pp. 5515–5520. 17

[71] L. B. Baltaxe-Admony, A. S. Robbins, E. A. Jung, S. Lessard, M. Teodorescu, V. SunSpiral, and A. Agogino, "Simulating the human shoulder through active tensegrity structures," in *ASME 2016 International Design Engineering Technical Conferences and Computers and Information in Engineering Conference*. American Society of Mechanical Engineers, 2016, pp. V006T09A027–V006T09A027. 17

[72] J. M. Friesen, J. L. Dean, T. Bewley, and V. Sunspiral, "A tensegrity-inspired compliant 3-dof compliant joint," in *2018 IEEE International Conference on Robotics and Automation (ICRA)*. IEEE, 2018, pp. 1–9. 17

[73] S. Venkateswaran, M. Furet, D. Chablat, and P. Wenger, "Design and analysis of a tensegrity mechanism for a bio-inspired robot," in *ASME 2019 International Design Engineering Technical Conferences and Computers and Information in Engineering Conference*. American Society of Mechanical Engineers Digital Collection, 2019. 17

[74] J. Friesen, A. Pogue, T. Bewley, M. de Oliveira, R. Skelton, and V. Sunspiral, "Ductt: A tensegrity robot for exploring duct systems," in *2014 IEEE International Conference on Robotics and Automation (ICRA)*. IEEE, 2014, pp. 4222–4228. 17

[75] "Vector spaces, twists and wrenches - dimec," http://www.dimec.unige.it/summer˙screws/SS09/PDF/Part1/SS09-Zlatanov.pdf, accessed: 2019-01-30. 18, 19, 20

[76] K. H. Hunt, *Kinematic geometry of mechanisms*. Oxford University Press, USA, 1978, vol. 7. 19, 20

[77] I. Ebert-Uphoff and P. A. Voglewede, "On the connections between cable-driven robots, parallel manipulators and grasping," in *IEEE International Conference on Robotics and Automation, 2004. Proceedings. ICRA'04. 2004*, vol. 5. IEEE, 2004, pp. 4521–4526. 31

[78] D. McColl and L. Notash, "Extension of antipodal theorem to workspace analysis of planar wire-actuated manipulators," in *Computational Kinematics*. Springer, 2009, pp. 9–16. 31

[79] P. A. Voglewede and I. Ebert-Uphoff, "Application of the antipodal grasp theorem to cable-driven robots," *IEEE Transactions on Robotics*, vol. 21, no. 4, pp. 713–718, 2005. 31

[80] P. H. Borgstrom, B. L. Jordan, G. S. Sukhatme, M. A. Batalin, and W. J. Kaiser, "Rapid computation of optimally safe tension distributions for parallel cable-driven robots," *IEEE Transactions on Robotics*, vol. 25, no. 6, pp. 1271–1281, 2009. 31

[81] S.-R. Oh and S. K. Agrawal, "Cable suspended planar robots with redundant cables: Controllers with positive tensions," *IEEE Transactions on Robotics*, vol. 21, no. 3, pp. 457–465, 2005. 32

[82] C. B. Pham, G. Yang, and S. H. Yeo, "Dynamic analysis of cable-driven parallel mechanisms," in *Proceedings, 2005 IEEE/ASME International Con-*

ference on Advanced Intelligent Mechatronics. IEEE, 2005, pp. 612–617. 32

[83] H. D. Taghirad and Y. B. Bedoustani, "An analytic-iterative redundancy resolution scheme for cable-driven redundant parallel manipulators," *IEEE Transactions on Robotics*, vol. 27, no. 6, pp. 1137–1143, 2011. 32

[84] M. Hassan and A. Khajepour, "Optimization of actuator forces in cable-based parallel manipulators using convex analysis," *IEEE Transactions on Robotics*, vol. 24, no. 3, pp. 736–740, 2008. 32

[85] S. Kawamura, H. Kino, and C. Won, "High-speed manipulation by using parallel wire-driven robots," *Robotica*, vol. 18, no. 1, pp. 13–21, 2000. 32

[86] J. Li, S. Andrews, K. G. Birkas, and P. G. Kry, "Task-based design of cable-driven articulated mechanisms," in *Proceedings of the 1st Annual ACM Symposium on Computational Fabrication.* ACM, 2017, p. 6. 33

[87] C. W. Wampler, "Manipulator inverse kinematic solutions based on vector formulations and damped least-squares methods," *IEEE Transactions on Systems, Man, and Cybernetics*, vol. 16, no. 1, pp. 93–101, 1986. 33

[88] L.-C. Wang and C.-C. Chen, "A combined optimization method for solving the inverse kinematics problems of mechanical manipulators," *IEEE Transactions on Robotics and Automation*, vol. 7, no. 4, pp. 489–499, 1991. 33

[89] C. Gosselin and J. Angeles, "Singularity analysis of closed-loop kinematic chains," *IEEE transactions on robotics and automation*, vol. 6, no. 3, pp. 281–290, 1990. 33

[90] D. Zlatanov, "Generalized singularity analysis," in *Singular Configurations of Mechanisms and Manipulators.* Springer, 2019, pp. 1–38. 33

[91] Z. Sheng, J.-H. Park, P. Stegall, and S. K. Agrawal, "Analytic determination of wrench closure workspace of spatial cable driven parallel mechanisms," in *ASME 2015 International Design Engineering Technical Conferences and*

Computers and Information in Engineering Conference. American Society of Mechanical Engineers Digital Collection, 2015. 33

[92] D. Lau, J. Eden, Y. Tan, and D. Oetomo, "Caspr: A comprehensive cable-robot analysis and simulation platform for the research of cable-driven parallel robots," in *2016 IEEE/RSJ International Conference on Intelligent Robots and Systems (IROS)*. IEEE, 2016, pp. 3004–3011. 33

[93] J. Eden, C. Song, Y. Tan, D. Oetomo, and D. Lau, "Caspr-ros: A generalised cable robot software in ros for hardware," in *Cable-Driven Parallel Robots*. Springer, 2018, pp. 50–61. 33

[94] A. Pott, "Efficient computation of the workspace boundary, its properties and derivatives for cable-driven parallel robots," in *Computational Kinematics*. Springer, 2018, pp. 190–197. 33

[95] Y. Wang, G. Yang, T. Zheng, K. Yang, and D. Lau, "Force-closure workspace analysis for modular cable-driven manipulators with co-shared driving cables," in *2018 13th IEEE Conference on Industrial Electronics and Applications (ICIEA)*. IEEE, 2018, pp. 1504–1509. 33

[96] E. Stump and R. V. Kumar, "Workspace delineation of cable-actuated parallel manipulators," *Departmental Papers (MEAM)*, p. 55, 2004. 33

[97] J.-P. Merlet, "Kinematics of the wire-driven parallel robot marionet using linear actuators," in *2008 IEEE International Conference on Robotics and Automation*. IEEE, 2008, pp. 3857–3862. 33

[98] A. Berti, J.-P. Merlet, and M. Carricato, "Workspace analysis of redundant cable-suspended parallel robots," in *Cable-Driven Parallel Robots*. Springer, 2015, pp. 41–53. 33

[99] D. Lau, D. Oetomo, and S. K. Halgamuge, "Wrench-closure workspace generation for cable driven parallel manipulators using a hybrid analytical-numerical approach," *Journal of Mechanical Design*, vol. 133, no. 7, p. 071004, 2011. 33

[100] P. Bosscher, A. T. Riechel, and I. Ebert-Uphoff, "Wrench-feasible workspace generation for cable-driven robots," *IEEE Transactions on Robotics*, vol. 22, no. 5, pp. 890–902, 2006. 33

[101] M. Gouttefarde and C. M. Gosselin, "Analysis of the wrench-closure workspace of planar parallel cable-driven mechanisms," *IEEE Transactions on Robotics*, vol. 22, no. 3, pp. 434–445, 2006. 33, 34, 35

[102] Q. Duan and X. Duan, "Workspace classification and quantification calculations of cable-driven parallel robots," *Advances in Mechanical Engineering*, vol. 6, p. 358727, 2014. 33

[103] M. Gouttefarde, J.-P. Merlet, and D. Daney, "Wrench-feasible workspace of parallel cable-driven mechanisms," in *Proceedings 2007 IEEE International Conference on Robotics and Automation*. IEEE, 2007, pp. 1492–1497. 33

[104] M. Gouttefarde, D. Daney, and J.-P. Merlet, "Interval-analysis-based determination of the wrench-feasible workspace of parallel cable-driven robots," *IEEE Transactions on Robotics*, vol. 27, no. 1, pp. 1–13, 2010. 33

[105] T. Bruckmann, L. Mikelsons, T. Brandt, M. Hiller, and D. Schramm, "Wire robots part i: Kinematics, analysis & design," 2008. 33

[106] A. T. Riechel and I. Ebert-Uphoff, "Force-feasible workspace analysis for underconstrained, point-mass cable robots," in *IEEE International Conference on Robotics and Automation, 2004. Proceedings. ICRA'04. 2004*, vol. 5. IEEE, 2004, pp. 4956–4962. 33

[107] C. B. Pham, S. H. Yeo, G. Yang, M. S. Kurbanhusen, and I.-M. Chen, "Force-closure workspace analysis of cable-driven parallel mechanisms," *Mechanism and Machine Theory*, vol. 41, no. 1, pp. 53–69, 2006. 34

[108] E. Stump and V. Kumar, "Workspaces of cable-actuated parallel manipulators," *Journal of Mechanical Design*, vol. 128, no. 1, pp. 159–167, 2006. 35

[109] G. Yang, C. B. Pham, and S. H. Yeo, "Workspace performance optimization of fully restrained cable-driven parallel manipulators," in *2006 IEEE/RSJ International Conference on Intelligent Robots and Systems*. IEEE, 2006, pp. 85–90. 35

[110] R. Kurtz and V. Hayward, "Dexterity measures with unilateral actuation constraints: the n+ 1 case," *Advanced robotics*, vol. 9, no. 5, pp. 561–577, 1994. 35, 36, 37

[111] J. Eden, D. Lau, Y. Tan, and D. Oetomo, "Unilateral manipulability quality indices: Generalised manipulability measures for unilaterally actuated robots," *Journal of Mechanical Design*, pp. 1–13, 2019. 37

[112] S. Bouchard, C. Gosselin, and B. Moore, "On the ability of a cable-driven robot to generate a prescribed set of wrenches," *Journal of Mechanisms and Robotics*, vol. 2, no. 1, p. 011010, 2010. 37, 94

[113] A. L. C. Ruiz, S. Caro, P. Cardou, and F. Guay, "Arachnis: Analysis of robots actuated by cables with handy and neat interface software," in *Cable-Driven Parallel Robots*. Springer, 2015, pp. 293–305. 37

[114] L. Gagliardini, S. Caro, and M. Gouttefarde, "Dimensioning of cable-driven parallel robot actuators, gearboxes and winches according to the twist feasible workspace," in *2015 IEEE International Conference on Automation Science and Engineering (CASE)*. IEEE, 2015, pp. 99–105. 37

[115] S. Lessanibahri, M. Gouttefarde, S. Caro, and P. Cardou, "Twist feasibility analysis of cable-driven parallel robots," in *Cable-Driven Parallel Robots*. Springer, 2018, pp. 128–139. 37

[116] G. Boschetti and A. Trevisani, "Cable robot performance evaluation by wrench exertion capability," *Robotics*, vol. 7, no. 2, p. 15, 2018. 37

[117] J.-P. Merlet, "On the real-time calculation of the forward kinematics of suspended cable-driven parallel robots," in *14th IFToMM World Congress on the Theory of Machines and Mechanisms*, Taipei, Taiwan, Oct. 2015. [Online]. Available: https://hal.inria.fr/hal-01259243 40

[118] J. Merlet, "The kinematics of cable-driven parallel robots with sagging cables: preliminary results," in *2015 IEEE International Conference on Robotics and Automation (ICRA)*, May 2015, pp. 1593–1598. 40

[119] D. Lau, D. Oetomo, and S. K. Halgamuge, "Inverse dynamics of multilink cable-driven manipulators with the consideration of joint interaction forces and moments," *IEEE Transactions on Robotics*, vol. 31, no. 2, pp. 479–488, April 2015. 41

[120] C. Ferraresi, C. D. Benedictis, and F. Pescarmona, "Development of a Haptic Device with Wire-Driven Parallel Structure," *International Journal of Automation Technology*, vol. 11, no. 3, pp. 385–395, 2017. 56

[121] S. Behzadipour and A. Khajepour, "Stiffness of cable-based parallel manipulators with application to stability analysis," *Journal of mechanical design*, vol. 128, no. 1, pp. 303–310, 2006. 68, 69

[122] A. Khan and A. Nayak, "Force closure analysis and modelling of cable driven serial kinematic chains," 2014. 73

[123] Q. Duan, X. Jin, and S. K. Agrawal, "Addition of springs and its impact on cable-driven serial manipulators," in *ASME 2014 International Design Engineering Technical Conferences and Computers and Information in Engineering Conference*. American Society of Mechanical Engineers, 2014, pp. V05AT08A086–V05AT08A086. 78, 91

[124] Y. Wang, C. Song, T. Zheng, D. Lau, K. Yang, and G. Yang, "Cable routing design and performance evaluation for multi-link cable-driven robots with minimal number of actuating cables," *IEEE Access*, vol. 7, pp. 135 790–135 800, 2019. 78

[125] S. Rezazadeh and S. Behzadipour, "Tensionability conditions of a multibody system driven by cables," in *ASME 2007 International Mechanical Engineering Congress and Exposition*. American Society of Mechanical Engineers Digital Collection, 2007, pp. 1369–1375. 83

[126] J. S. Dai and J. R. Jones, "Null–space construction using cofactors from a screw–algebra context," *Proceedings of the Royal Society of London. Series A: Mathematical, Physical and Engineering Sciences*, vol. 458, no. 2024, pp. 1845–1866, 2002. 89

[127] S. K. Mustafa and S. K. Agrawal, "Force-closure of spring-loaded cable-driven open chains: Minimum number of cables required influence of spring placements," in *2012 IEEE International Conference on Robotics and Automation*, May 2012, pp. 1482–1487. 91

[128] A. Taghavi, S. Behzadipour, N. Khalilinasab, and H. Zohoor, "Workspace improvement of two-link cable-driven mechanisms with spring cable," in *Cable-Driven Parallel Robots*. Springer, 2013, pp. 201–213. 91

[129] D. T. M. Lau, "Modelling and analysis of anthropomorphic cable-driven robots," Ph.D. dissertation, 2014. 94, 95

[130] V. Megaro, E. Knoop, A. Spielberg, D. I. Levin, W. Matusik, M. Gross, B. Thomaszewski, and M. Bächer, "Designing cable-driven actuation networks for kinematic chains and trees," in *Proceedings of the ACM SIGGRAPH/Eurographics Symposium on Computer Animation*. ACM, 2017, p. 15. 104

[131] J. M. Inouye and F. J. Valero-Cuevas, "Anthropomorphic tendon-driven robotic hands can exceed human grasping capabilities following optimization," *The International Journal of Robotics Research*, vol. 33, no. 5, pp. 694–705, 2014. 106

[132] G. Yang, W. Lin, M. S. Kurbanhusen, C. B. Pham, and S. H. Yeo, "Kinematic design of a 7-dof cable-driven humanoid arm: a solution-in-nature approach," in *IEEE/ASME International Conference on Advanced Intelligent Mechatronics (AIM), Monterey, CA, July*, 2005, pp. 24–28.

[133] S. Rezazadeh, "Dynamics and control of multibody cable-driven mechanisms with application in rehabilitation robotics," 2012.

[134] A. Alamdari and V. Krovi, "Design and analysis of a cable-driven articulated rehabilitation system for gait training," *Journal of Mechanisms and Robotics*, vol. 8, no. 5, p. 051018, 2016.